Dissertation

Regulation of Arginine Methylation in Health and Disease

Regulierung der Arginin-Methylierung in Krankheit und Gesundheit

submitted by

Fangrong ZHANG

for the Academic Degree of
Doctor of Philosophy (PhD)

at the
Medical University of Graz

Gottfried Schatz Research Center for Cell Signaling, Metabolism & Aging

Molecular Biology & Biochemistry

under the supervision of

Assoc. Prof. Dr. Tobias MADL

2021

Statutory Declaration

I hereby declare that this thesis is my own original work and that I have fully acknowledged by name all of those individuals and organizations that have contributed to the research for this thesis. Due acknowledgement has been made in the text to all other material used. Throughout this thesis and in all related publications I followed the "Standards of Good Scientific Practice and Ombuds Committee at the Medical University of Graz".

Graz, April 26th, 2021

Sign:

Disclosures

Parts of this thesis have been published in:

Fangrong Zhang, Jakob Kerbl-Knapp, Maria J. Rodriguez Colman, Andreas Meinitzer, Therese Macher, Nemanja Vujić, Sandra Fasching, Evelyne Jany-Luig, Melanie Korbelius, Katharina B. Kuentzel, Maximilian Mack, Alena Akhmetshina, Anita Pirchheim, Margret Paar, Beate Rinner, Gerd Hörl, Ernst Steyrer, Ulrich Stelzl, Boudewijn Burgering, Tobias Eisenberg, Brigitte Pertschy, Dagmar Kratky, Tobias Madl. *Global analysis of protein arginine methylation.* **Cell Reports Methods**, doi: 10.1016/j.crmeth.2021.100016 (2021)

Fangrong Zhang, Yingchao Wang, Geng Chen, Zhenli Li, Xiaohua Xing, Csilla Putz-Bankuti, Rudolf E. Stauber, Xiaolong Liu, Tobias Madl. *Growing human hepatocellular tumors undergo a global metabolic reprogramming.* **Cancers**, doi: 10.3390/cancers1308198 (2021)

Fangrong Zhang, Jakob Kerbl-Knapp, Alena Akhmetshina, Melanie Korbelius, Katharina Barbara Kuentzel, Nemanja Vujić, Gerd Hörl, Margret Paar, Dagmar Kratky, Ernst Steyrer, Tobias Madl. *Tissue-specific landscape of metabolic dysregulation during ageing.* **Biomolecules**, doi: 10.3390/biom11020235 (2021)

Co-authors that contributed to the thesis and the publications:

Jakob Kerbl-Knapp

Gottfried Schatz Center for Cell Signaling, Metabolism and Aging, Molecular Biology and Biochemistry, Medical University of Graz

Maria J. Rodriguez Colman

Oncode Institute and Department of Molecular Cancer Research, Center for Molecular Medicine, University Medical Center Utrecht

Andreas Meinitzer

Clinical Institute of Medical and Chemical Laboratory Diagnostics, Medical University of Graz

Therese Macher

Gottfried Schatz Center for Cell Signaling, Metabolism and Aging, Molecular Biology and Biochemistry, Medical University of Graz

Nemanja Vujić

Gottfried Schatz Center for Cell Signaling, Metabolism and Aging, Molecular Biology and Biochemistry, Medical University of Graz

Sandra Fasching

Institute of Pharmaceutical Sciences, University of Graz

Evelyne Jany-Luig

Institute of Pharmaceutical Sciences, University of Graz

Melanie Korbelius

Gottfried Schatz Center for Cell Signaling, Metabolism and Aging, Molecular Biology and Biochemistry, Medical University of Graz

Katharina B. Kuentzel

Gottfried Schatz Center for Cell Signaling, Metabolism and Aging, Molecular Biology and Biochemistry, Medical University of Graz

Maximilian Mack

Institute of Molecular Biosciences, NAWI Graz, University of Graz

Alena Akhmetshina

Gottfried Schatz Center for Cell Signaling, Metabolism and Aging, Molecular Biology and Biochemistry, Medical University of Graz

Anita Pirchheim

Gottfried Schatz Center for Cell Signaling, Metabolism and Aging, Molecular Biology and Biochemistry, Medical University of Graz

Margret Paar

Otto-Loewi Research Center, Physiological Chemistry, Medical University of Graz

Beate Rinner

Division of Biomedical Research, Medical University of Graz

Gerd Hörl

Otto-Loewi Research Center, Physiological Chemistry, Medical University of Graz

Ernst Steyrer

Gottfried Schatz Center for Cell Signaling, Metabolism and Aging, Molecular Biology and Biochemistry, Medical University of Graz

Ulrich Stelzl

Institute of Pharmaceutical Sciences, University of Graz

Boudewijn Burgering

Oncode Institute and Department of Molecular Cancer Research, Center for Molecular Medicine, University Medical Center Utrecht

Tobias Eisenberg

Institute of Molecular Biosciences, NAWI Graz, University of Graz

Brigitte Pertschy

Institute of Molecular Biosciences, NAWI Graz, University of Graz

Dagmar Kratky

Gottfried Schatz Center for Cell Signaling, Metabolism and Aging, Molecular Biology and Biochemistry, Medical University of Graz

Yingchao Wang

The United Innovation of Mengchao Hepatobiliary Technology Key Laboratory of Fujian Province, Mengchao Hepatobiliary Hospital of Fujian Medical University

Geng Chen

The United Innovation of Mengchao Hepatobiliary Technology Key Laboratory of Fujian Province, Mengchao Hepatobiliary Hospital of Fujian Medical University

Zhenli Li

The United Innovation of Mengchao Hepatobiliary Technology Key Laboratory of Fujian Province, Mengchao Hepatobiliary Hospital of Fujian Medical University

Xiaohua Xing

The United Innovation of Mengchao Hepatobiliary Technology Key Laboratory of Fujian Province, Mengchao Hepatobiliary Hospital of Fujian Medical University

Csilla Putz-Bankuti

Department of Internal Medicine, Division of Gastroenterology and Hepatology, Medical University of Graz

Rudolf E. Stauber

Department of Internal Medicine, Division of Gastroenterology and Hepatology, Medical University of Graz

Xiaolong Liu

The United Innovation of Mengchao Hepatobiliary Technology Key Laboratory of Fujian Province, Mengchao Hepatobiliary Hospital of Fujian Medical University

Tobias Madl

Gottfried Schatz Center for Cell Signaling, Metabolism and Aging, Molecular Biology and Biochemistry, Medical University of Graz

During my PhD thesis I also contributed to the following publications:

Irene Schilcher, Gerhard Ledinski, Snježana Radulović, Seth Hallström, Thomas Eichmann, Tobias Madl, Fangrong Zhang, Gerd Leitinger, Dagmar Kolb-Lenz, Barbara Darnhofer, Ruth Birner-Gruenberger, Christian Wadsack, Dagmar Kratky, Gunther Marsche, Saša Frank, Gerhard Cvirn. *Endothelial Lipase Increases Antioxidative Capacity of High-density Lipoprotein,* **Biochimica et Biophysica Acta (BBA)-Molecular and Cell Biology of Lipids**. doi: 10.1016/j.bbalip.2019.06.011.

Junpeng Shi, Xia Sun, Shenghui Zheng, Liang Song, Fangrong Zhang, Tobias Madl, Yun Zhang, Hongwu Zhang, and Maochun Hong, *Tin-Doped Near-Infrared Persistent Luminescence Nanoparticles with Considerable Improvement of Biological Window Activation for Deep Tumor Photodynamic Therapy*, **ACS Applied Bio Materials**, doi: 10.1021/acsabm.0c00644

Qishun Zhou, Sinem Usluer, Fangrong Zhang, Aneta J. Lenard, Benjamin M. R. Bourgeois, Tobias Madl, *ATP regulates RNA-driven CIRBP phase separation*, **Protein Science**. doi: 10.1002/pro.4123

Acknowledgements

Fangrong Zhang was trained within the frame of the PhD program in Molecular Medicine, Medical University of Graz.

I would like to thank:

Tobias Madl, **Roland Malli** and **Klaus Zangger** for being part of my thesis committee, for valuable and insightful comments and for supervising/discussing my project in our meetings.

Tobias Madl for the opportunity to do my PhD studies in his group, supervising this PhD project, providing his great scientific inputs for planning projects and writing papers. His way of accompanying me all along with the thesis, and guided me toward the path whenever he thought I needed it.

All the people that contributed to the work described in this thesis:
At Medical University of Graz, the Graier group, namely **Benjamin Gottschalk, Zhanat Koshenov**, the Malli group**, Helmut Bischof, Sandra Burgstaller** helped with their expertise in 2-photon microscopy to visualization of intracellular arginine methylation level. The Kratky group (**Nemanja Vujić**, **Melanie Korbelius**, **Katharina B. Kuentzel**, **Alena Akhmetshina**, **Anita Pirchheim, Dagmar Kratky**) helped a lot by mice dissection and real time-PCR**. Ernst Steyrer**, **Margret Paar** and **Gerd Hörl** provided mice and helped with maintaining of mice. **Jakob Kerbl-Knapp** helped a lot with metabolic sample preparation. **Therese Macher** helped with western blotting. **Csilla Putz-Bankuti** and **Rudolf E. Stauber** provided hepatocellular carcinoma patient plasma.
At University of Graz, **Sandra Fasching, Evelyne Jany-Luig, Ulrich Stelzl, Maximilian Mack, Tobias Eisenberg and Brigitte Pertschy** provided different yeast strains.
At Center for Molecular Medicine of University Medical Center Utrecht, **Maria J. Rodriguez Colman** and **Boudewijn Burgering** provided mouse intestinal organoids and helped with single cell sequencing.

At Mengchao Hepatobiliary Hospital of Fujian Medical University, Liu Group (**Xiaolong Liu**, **Yingchao Wang, Geng Chen, Zhenli Li**, **Xiaohua Xing**) provided hepatocellular carcinoma patient serum and tissues, helped a lot with building predictive model to discriminate against patients with different recurrence risks.

The whole MADL group (**Tobias Madl**, **Benjamin Bourgeois**, **Gesa Lucia Richter**, **Sarah Stryeck**, **Emil Spreitzer**, **Sinem Usluer**, **Qishun Zhou**, **Hermann Hans Habacher**, **Aneta Lenard**, **Bernhard_Sailer**, **Therese Macher**, **Anna Maria Springer**, **Denise Nadja Prietl, Jakob Kerbl-Knapp**, **Vivian Eber, Hansjörg Habisch**) for the great working atmosphere and all supports, for the thrilling discussions and out of work activities.

I am so grateful to my family and friends for their love and encouraging words. This memorable time would not have been possible without your great supports.

Table of contents

Abbreviations and Definitions

Acronym	Term
ADMA	N^G, N^G-dimethyl-L-arginine (asymmetric dimethylarginine)
Ado-Met/ SAM	S-Adenosyl-L-methionine
AFP	α-fetoprotein
AHCY	S-adenosylhomocysteine hydrolase
ALDOA	aldolase A
ALS	amyotrophic lateral sclerosis
ALT	alanine transaminase
APOA4	apolipoprotein A4
ArgMet	protein arginine methylation
AST	glutamic-oxaloacetic transaminase
AUC	area under the curve
BCAAs	branched chain amino acids
BCLC	barcelona clinic liver cancer
CIRBP	cold-inducible RNA-binding protein
CPMG	car-purcell-meiboom-grill
CT	carcinoma tissues
CTPS2	CTP synthase 2
DHODH	dihydroorotate dehydrogenase
FUS	fused-in-sarcoma
GABA	4-aminobutyrate
GAPDH	glyceraldehyde 3-phosphate dehydrogenase
GC-MS	gas chromatography-mass spectrometry
GLUD1	glutamate dehydrogenases
GO	gene ontology
GOT1	glutamic-oxaloacetic transaminases
GPI	glucose-6-phosphate isomerase
GPT	glutamic-pyruvate transaminases
HBV	chronic hepatitis B virus
HCC	hepatocellular carcinomas
HCV	chronic hepatitis C virus
HK2	hexokinase 2
HPLC	high-performance liquid chromatography
HSQC	heteronuclear single-quantum correlation
IDPs	intrinsically disordered proteins
IDRs	intrinsically disordered regions
IVD	*in vitro* diagnostic
JMJD6	jumonji domain-containing 6
JRES	2D homo-nuclear J-resolved experiments
LC-MS	liquid chromatography-mass spectrometry
LLPS	liquid-liquid phase seperations

MAT2A	methionine adenosyltransferase 2A
MDH1	malate dehydrogenase
MMA	N^G-monomethyl-L-arginine
MS	mass-spectrometry
MVI	microvascular invasion
N/A	not available
NASH	non-alcoholic steatohepatitis
ND	not determine
NME1	nucleoside diphosphate kinase A
NMR	nuclear magnetic resonance
ODC	ornithine decarboxylase
O-PLS-DA	orthogonal partial least squares discriminant analysis
PCA	principal component analysis
PGK1	phosphoglycerate kinase
PLG	plasminogen protein
PLS-DA	partial least squares-discriminant analysis
PRMT	protein arginine methyltransferase
PRMT1	protein arginine methyltransferase 1
PT	peritumoral tissue
PTMs	post-translational modifications
RFS	recurrence-free survival
RG/RGG	arginine-glycine(-glycine)
ROC	receiver operating characteristic
SAH	S-adenosylhomocysteine
SD	standard deviation
SDMA	N^G, N'^G-dimethyl-L-arginine (symmetric dimethylarginine)
SLICER	Singapore liver cancer recurrence
SPE	solid phase extraction
SS-CLIP	surgery-specific cancer of the liver italian program
STOCSY	statistical total correlation spectroscopy
TCA	tricarboxylic acid
THF	tetrahydrofolic acid
UMPS	uridine 5'-monophosphate synthase
γ-GT	gamma-glutamyltransferase

Zusammenfassung

Posttranslationale Arginin-Methylierung ist wichtig für eine vielzahl zellulärer Prozesse und biologischer Funktionen, einschließlich der metabolischen Homöostase. Die Rolle der Arginin-Methylierung in der (Patho)Physiologie ist aufgrund des Mangels an adäquaten Nachweismethoden immer noch ungenügend verstanden. Wir haben hierfür ein einfaches, schnelles und robustes Protokoll zur absoluten Quantifizierung der globalen Protein-Arginin-Methylierung auf Basis der Kernspinresonanz (NMR)-Spektroskopie entwickelt. Dieser Ansatz ermöglicht den quantitativen Nachweis von Veränderungen der Arginin-Methylierung, zusammen mit der Analyse von Stoffwechselprofilen in einer nahezu unbegrenzten Anzahl von biologischen Matrizen, einschließlich, aber nicht nur beschränkt auf Zellen, biologische Flüssigkeiten und Gewebe. In unserer Studie stellt die Rolle der Arginin-Methylierung bei post-translationalen Modifikation als weit verbreitet dar. Arginin-Methylierung ist eng mit dem Stoffwechselzyklus gekoppelt und kann durch kleine Moleküle und Metaboliten moduliert werden. Veränderungen der Arginin-Methylierung sind auch an Krebsbildung und Alterung beteiligt. Es wurde berichtet, dass Methionin-Restriktion die Lebensspanne verlängert und das Tumorwachstum unterdrückt, abhängig vom Fluss im Ein-Kohlenstoff-Stoffwechsel. Angesichts der Tatsache, dass ArgMet stark von der essentiellen Aminosäure Methionin abhängig ist, die ein Vorläufer von S-Adenosyl-L-Methionin ist, stellen wir die Hypothese auf, dass ArgMet stark an den Stoffwechsel gekoppelt ist. Metabolische Veränderungen sind ein Markenzeichen von Krebs und Alterung. Wir haben wir eine umfangreiche Kombination aus Proteomik- und Metabolomik-Analysen von Serum, Krebsgewebe und peritumoralem Gewebe von 200 Patienten mit hepatozellulärem Karzinom durchgeführt, die eine größenabhängige metabolische Umprogrammierung zeigt. Wir fanden hier Enzyme und Metabolite, die mit der Glykolyse, dem Tricarbonsäurezyklus und der Pyrimidin-Synthese verknüpft sind, und mit zunehmender Tumorgröße zunehmend einer Dysregulation unterliegen. Mehrere Metabolit-Biomarker boten prognostische Informationen für PatientInnen und konnten mit klinisch-pathologischen Daten kombiniert werden. Somit erstellten und validierten wir ein integriertes klinisch-pathologisches und metabolomisches Modell zur Vorhersage des 5-Jahres-Rezidivs. Angesichts des hohen therapeutischen Potenzials wird es interessant sein, Metaboliten und ArgMet-Inhibitoren über die Umprogrammierung des Ein-Kohlenstoff-Stoffwechsels zu kombinieren. Insgesamt unterstreichen unsere Daten, dass die gezielte Manipulation des

Krebsstoffwechsels/ArgMet zukünftig neue Wege für effektive Therapien von hepatozellulären Karzinomen ermöglichen wird. Wir haben auch eine metabolomische Analyse von alterndem Gewebe auf der Basis von NMR-Spektroskopie integriert. In den Geweben wurden durch das Altern erstaunlich unterschiedliche Metaboliten-profile verändert, und mehrere universelle metabolische Marker des Alterns identifiziert. Die bei den alten Mäusen gestörten Stoffwechselwege zeigen organspezifische und globalere Effekte des Alterns und weisen auf Mechanismen hin, denen man möglicherweise pharmakologisch entgegenwirken könnte, um Alterung und altersassoziierte Krankheiten zu behandeln. Zusätzlich können die identifizierten Metabolit-Biomarker zur Beurteilung der Qualität von alternden Geweben oder Organmodellen hergenommen werden und stellen einen Indikator zur Bewertung senolytischer Medikamentenkandidaten dar. Das signifikant verringerte ArgMet könnte auf die Verringerung des Methioninspiegels in der gealterten Milz zurückzuführen sein. Es wird interessant sein, nach Medikamenten zu suchen, die die Lebensspanne durch die Kombination von metabolomischen und ArgMet-Zielen verlängern. Zusammenfassend lässt sich sagen, dass unsere Methode neue robust Werkzeuge liefern, um die wichtigen (patho)physiologische Rollen der Protein-Arginin-Methylierung zu untersuchen.

Abstract

Post translational arginine methylation (ArgMet) is important for many cellular processes and biological functions including metabolic homeostasis. The role of ArgMet in (patho)physiology still remains poor understood due to the lack of applicable detection methods. Here, we developed a simple, fast and robust protocol for absolute quantification of global protein arginine methylation based on Nuclear Magnetic Resonance (NMR) spectroscopy. This approach enables the detection of ArgMet, together with the analyses of metabolic profiles in an almost unlimited number of biological matrices, including, but not limited to, cells, biological fluids and tissues. In our study, arginine methylation represents a high prevalent post-translational modification. Besides, arginine methylation is coupled with the metabolic cycle and can be modulated by small molecules and metabolites. Arginine methylation regulation also involved into cancers, differentiation and ageing. Methionine restriction has been reported to extend lifespan and suppress tumor growth depending on flux in the one carbon metabolism. Given that ArgMet is strongly dependent on the essential amino acid methionine, which is a precursor to S-Adenosyl-L-methionine, we hypothesize that ArgMet is strongly coupled to metabolism. Metabolic reprogramming is a hallmark of cancer and ageing. We undertook an extensive combined proteomics and metabolomics analysis of serum, cancer tissues and peritumoral tissue from 200 hepatocellular carcinoma patients demonstrating sized-dependent metabolic reprogramming. We found dysregulated enzyme and metabolites related with glycolysis, the tricarboxylic acid cycle and pyrimidine synthesis with increased tumor size. Several metabolite biomarkers offered prognostic information for patients and they can be combined with clinical pathological data. We built and validated the integrated clinicopathological and metabolomic model to predict the 5-year recurrence. Given the high therapeutic potential, it will be interesting to combine metabolites and ArgMet inhibitors via reprogramming of one carbon metabolism. Altogether, our data emphasize that targeting cancer metabolism/ArgMet will open new avenues for effective therapies for hepatocellular carcinoma in future. We also integrated a metabolomic analyses of ageing tissues based on NMR spectroscopy. Greatly different metabolic profiles of tissues were regulated by ageing and several universal metabolic biomarkers of ageing were identified. The pathways perturbed in ageing demonstrate organ-specific and more-global effects of ageing and point to mechanisms that could potentially be counter-regulated pharmacologically to treat ageing and age-associated diseases. Besides, identified metabolite

biomarkers can be evaluated for the effectiveness of ageing tissues or organs model and provide an assessable indicator for senolytic drug candidates. The significant decreased ArgMet might be due to reduction of methionine level in aged spleen. It will be interesting to search drugs to extend lifespan through combining metabolomic and ArgMet targets. In summary, our method provides new tools to study the important (patho)physiological role of protein arginine methylation.

1 Introduction

1.1 Physiology of arginine methylation

Protein arginine methylation (ArgMet) represents an abundant posttranslational modification of both nuclear and cytoplasmic proteins (1). ArgMet is involved in numerous cellular processes, including signal transduction cascades, transcriptional regulation (2), RNA metabolism and DNA damage repair (3), playing a significant biological role (3, 4). Recent research has identified ArgMet in (patho)physiology roles linked to diseases such as cancer, metabolism and neurodegeneration (5). However, reliable detection and absolute quantification of arginine and its methylated derivatives in diverse matrices, such as cells, body fluids, and tissues, remain challenging because of the lack of suitable detection techniques. Hence, the development of suitable quantitative methods of ArgMet is of great interest in the cell biology and pathology (physiology) fields.

1.1.1 RG/RGG proteome

Arginine-glycine/arginine-glycine-glycine (RG/RGG) is highly abundant in RNA-binding proteins, including more than 1000 proteins containing tri-RGG or di-RGG (**Figure 1**) (1). Intrinsically disordered proteins (IDPs) or intrinsically disordered regions (IDRs) often contain RGG repeat sequences (6). Proteins harbouring RG/RGG regions are involved in essential processes, including translational repression, transcriptional regulation, DNA damage repair, pre-mRNA splicing and regulation of apoptosis (**Figure 2**). Moreover, arginine is extensively methylated in many repetitive RG/RGG regions. Indeed, the RG/RGG regions is strongly favoured by PRMTs (7, 8). The physiological pertinence of RG/RGG regions is highlighted by their association with several diseases (1). In addition, RG/RGG regions are implicated in regulating the cellular localization and binding affinities of proteins under normal conditions and cellular stress conditions. Identifying the mechanism of action of RG/RGG regions and of interacting partners and developing a protocol for distinguishing regulatory effects induced by arginine methylation are ongoing challenges in the field.

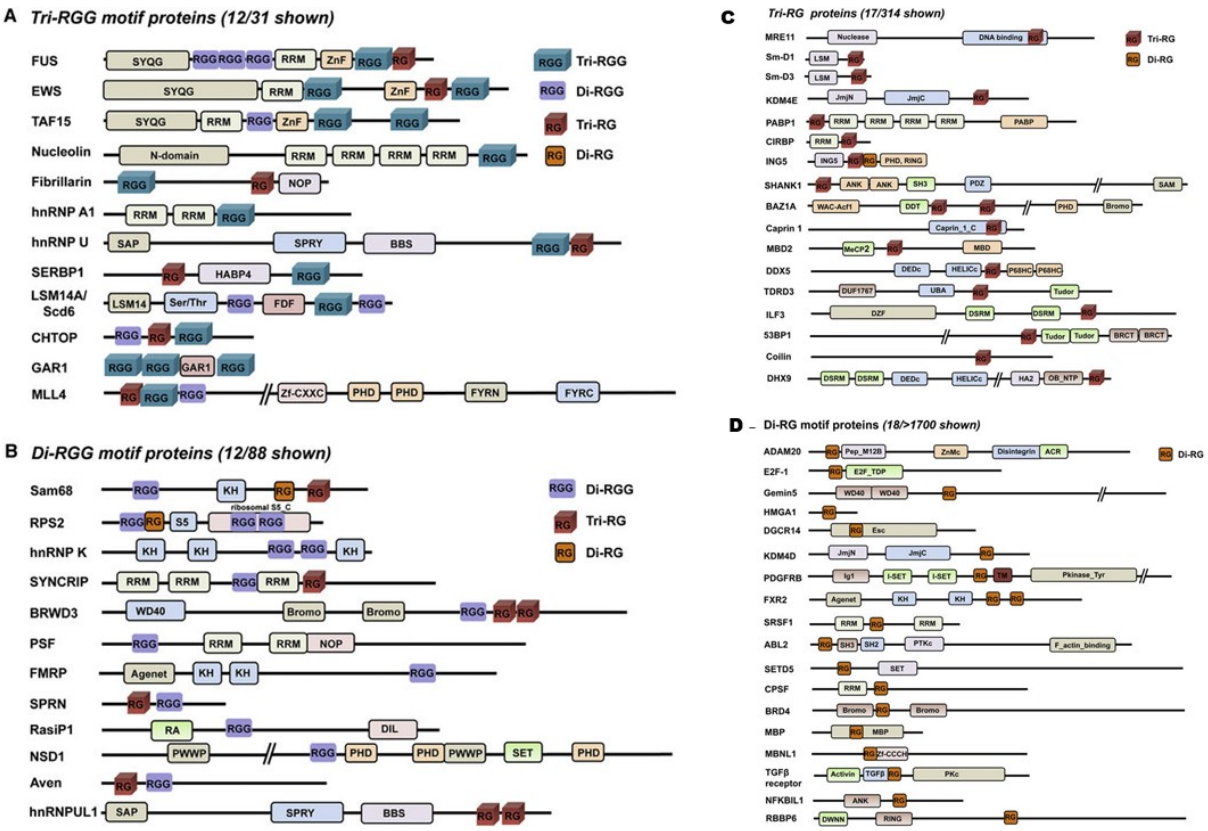

Figure 1. RG/RGG regions containing proteins in human proteome. Figure adapted from Thandapani. *et al* (1).

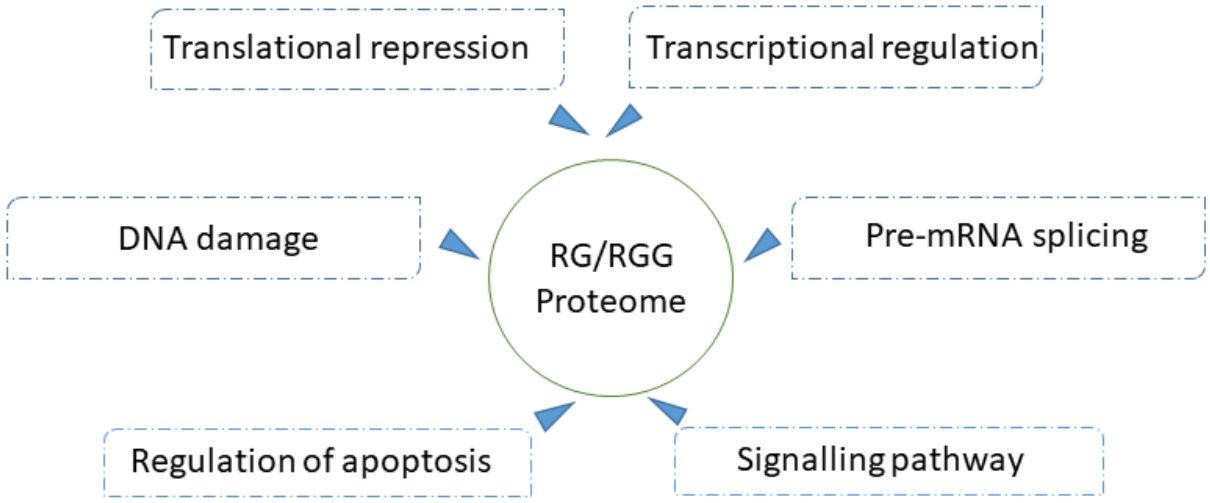

Figure 2. Functions of RG/RGG proteome

1.1.2 PRMT enzymes and arginine methylation

In recent studies, researchers have found that methyl groups play significant roles in protein function by serving as major controlling elements. Different methylation reactions are observed at the side chains of amino acid residues or at the N-terminus or C-terminus of proteins (9, 10). The most frequent protein methylation reaction is the modification of the guanidino group of the arginine side chain. Arginine methylation is catalysed by arginine methyltransferase (PRMT) proteins, and it is a common posttranslational modification in eukaryotic cells. In the reaction, a methyl group on the methyl donor S-adenosyl-L-methionine (Ado-Met, SAM) is transferred to the guanidinium nitrogen of an arginine residue. Three distinct types of arginine residue methylation in mammalian cells generate the following products: N^G-monomethyl-L-arginine (MMA), N^G,N^G-dimethyl-L-arginine (asymmetric dimethylarginine, ADMA) and N^G,N'^G-dimethyl-L-arginine (symmetric dimethylarginine, SDMA) (4). ADMA is the most prevalent modification, and MMA and SDMA occur at levels between 20 and 50% that of ADMA (9). At least nine different PRMT enzymes utilize SAM as a cofactor for the mono- and dimethylation of arginine in human. Type I PRMTs catalyse the formation of ADMA by PRMT1, PRMT2, PRMT3, PRMT4, PRMT6 and PRMT8, while type II PRMTs (PRMT5 and PRMT9) are critical for the catalysis of the SDMA. In addition, all PRMTs in mammalian cells can catalyse monomethylation to form MMA (**Figure 3**). In yeast cells, two main methyltransferases have been identified (HMT1/RMT1 and HSL7) (11). Some potential arginine methyltransferases have also been identified, but their biochemical functions remain to be investigated (12). Overall, of all the known protein substrates for arginine methylation, only a small proportion are clearly assigned to a unique PRMT. Therefore, the extent of methylated substrates and the functional importance of arginine methylation on many proteins remain to be discovered.

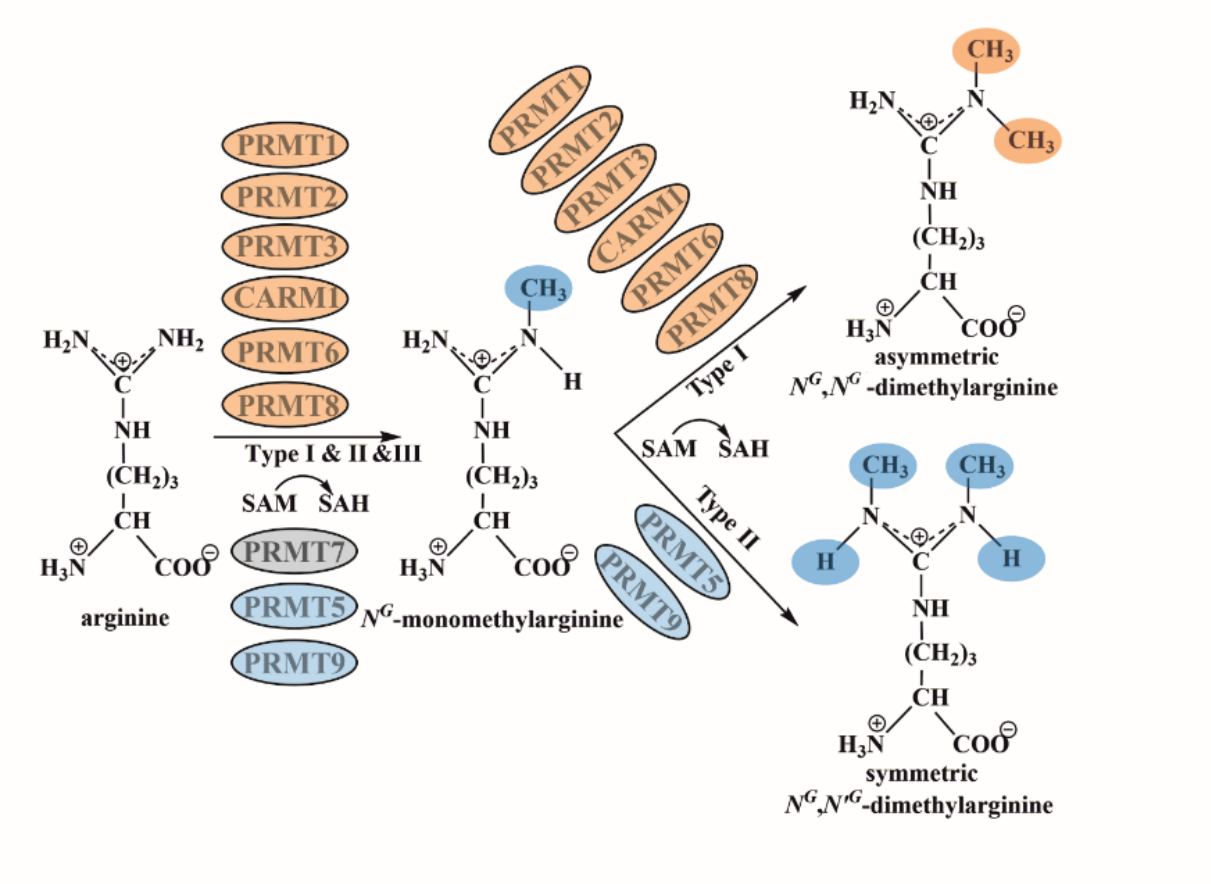

Figure 3. Methylation of the arginine side chain in proteins by PRMT enzymes.

1.1.3 PRMT substrates

There are more than 4000 reported ArgMet proteins, and 1.7% of all arginine residues in human proteins are methylated according to the PhosphoSite database (13). The estimation here for 1.7% methylated arginines assumes that all proteins show similar expression levels in the cell. The signatures of PRMT catalytic sites are similar within different sequences (14). Most PRMT enzymes methylate proteins containing RG/RGG regions (15-17). However, the glycine residue immediately adjacent to the target arginine is not essential for ArgMet, as indicated by studies showing that RXG regions can be methylated by PRMT1. In this region, lysine, phenylalanine, threonine or leucine are suitable amino acids in the variable position (18, 19). In addition, RPAAPR- or APR-regions can be sites of ArgMet (20). The PRMT2 substrate belongs to the serine/arginine-rich protein family (21). PRMT4/CARM1 has been found to methylate arginine residues in proline-, glycine-, and methionine-rich regions, which are found in more than 130

PRMT4 protein substrates (22, 23). Many PRMT5 targets recognized by mass spectrometry (MS) revealed that this enzyme preferentially methylates an arginine situated between two adjoining glycine residues (GRGs) (24). PRMT6 preferentially methylates arginine residues in positively charged regions and disfavours target arginine residues surrounded by acidic residues (17). Within proteins, IDRs regularly display ArgMet, but they are not exclusive sites of methylation (25). The modulation of methylation in these regions involves nucleic acid binding, protein-protein interactions, liquid liquid phase separation (LLPS), and protein localization at the molecular level (12).

1.2 Arginine methylation in diseases and ageing

ArgMet has been identified in many diseases. In recent studies focusing on the RNA-binding protein fused-in-sarcoma (FUS), we found that protein arginine methyltransferase 1 (PRMT1)-mediates arginine methylation within a disordered RG/RGG repeat region regulated FUS localization (26), liquid-liquid phase separation (27), and disease development (28). Interestingly, many human diseases show alterations in PRMT1 expression levels and/or arginine methylation, which in turn might affect the intracellular localization and phase separation of the RG/RGG proteome (29). Moreover, certain pathologies, such as human cancers, cardiovascular diseases, diabetes mellitus, leukaemia, multiple myeloma, sclerosis, spinal muscular atrophy, and viral pathogenesis, have been reported to involve arginine methylation (28, 30-36). Several recent studies have suggested that arginine methylation is a key regulator that ensures the survival of cancer cells (37). Although mutations in PRMT enzymes are uncommon, a strong association between PRMT overexpression and poor prognosis has been investigated (38). Overexpression of PRMT1 has been revealed in breast, bladder, and colon cancers (39-42). Increased PRMT4 expression has also been found in prostate cancer, colorectal cancer and non-small cell lung carcinomas (43-45). Upregulated PRMT5 has been shown in lung, gastric, bladder, breast, epithelial ovarian and colon cancer (46-49). Overexpression of PRMT enzymes may trigger hypermethylation of protein substrates, accelerating tumorigenesis (50). In addition, elevated ADMA plasma levels are typically observed in renal failure, pulmonary disease, hypertension, and atherosclerosis and may constitute a hallmark of cardiovascular disease (51). Accumulation of aggregated proteins containing ribonucleoproteins has been found in neurodegenerative diseases,

which can be regulated by ArgMet (52). Kensuke Ikenaka *et al.* found that patients with amyotrophic lateral sclerosis (ALS) presented with a high ADMA/L-arginine ratio, which predicted a poor prognosis (53).

Besides, PRMT6 and PRMT7 have been involved in cellular senescence modulation and cell proliferation (54). Ablation of PRMT6 and PRMT7 exhibited cellular senescence phenotypes. Abrogation of PRMT1 mediating senescence was accompanied by degradation of histone H4. Methylated FoxO by PRMT1 blocks its phosphorylation to prevent FoxO protein degradation contributing to lifespan extension (55). Significant decreased ADMA and PRMT1 have been revealed during senescence in WI-38 fibroblasts (56). Deprivation of PRMT1 induces breast cancer cellular senescence (56).

1.2.1 inhibitors

ArgMet is an understudied modification that is progressively increased in cancer growth. Therefore, targeting PRMT enzymes as therapeutic prospects has gained increasing interest. Multiple PRMT inhibitors have been studied and developed (**Table 1**), many of which have recently entered or soon will be entered into clinical trials of cancer therapy (https://clinicaltrials.gov) (37). However, how ArgMet levels are affected by small-molecule inhibitors remains to be investigated.

(i) Type I preclinical compounds				
Compound	**PRMT enzymes inhibited**	**Mode of action**	**Disease type(s) tested**	**Refs**
Allantodapsone	PRMT1 (IC_{50} 1.7 μM *in vitro*)	Competitive (substrate)	N/A	(57)
AMI-1	PRMT1 (IC_{50} 8.8 μM *in vitro)* PRMT3 (ND) CARM1 (IC_{50} 169.8 μM *in vitro*) PRMT6 (ND)	Competitive (substrate)	N/A	(58, 59)
AMI-408	PRMT1 (ND)	N/A	MLL-GAS7 leukaemia (mouse xenografts)	(60)
MS023	PRMT1 (IC_{50} 9 nM cell assay) PRMT3 (IC_{50} 119 nM cell assay) PRMT6 (IC_{50} 56 nM cell assay)	Noncompetitive (SAM and substrate)	N/A	(61)

MS049	CARM1 (IC_{50} 34 nM *in vitro*, 1.4 μM cell assay) PRMT6 (IC_{50} 43 nM *in vitro*, 0.97 μM cell assay)	Noncompetitive	N/A	(62)
E84	PRMT1 (IC_{50} 3.38 μM *in vitro*) CARM1 (IC_{50} 21.5 μM *in vitro*) PRMT5 (IC_{50} 35.4 μM *in vitro*) PRMT8 (IC_{50} 84.9 μM *in vitro*)	N/A	N/A	(63)
Furamidine (DB75)	PRMT1 (IC_{50} 9.4 μM *in vitro*) CARM1 (IC_{50} >400 μM *in vitro*) PRMT5 (IC_{50} 166 μM *in vitro*) PRMT6 (IC_{50} 283 μM *in vitro*)	Competitive (substrate)	N/A	(64)
GMS	PRMT1 (IC_{50} 500 nM *in vitro*) PRMT3 (IC_{50} 700 nM *in vitro*) CARM1 (IC_{50} <15 nM *in vitro*) PRMT5 (IC_{50} 300 nM *in vitro*) PRMT6 (IC_{50} 90 nM *in vitro*) PRMT8 (IC_{50} 11 nM *in vitro*)	Competitive (SAM and substrate)	N/A	(65)
PT1001B (DCPR049_12)	PRMT1 (IC_{50} 1.1 nM *in vitro*) PRMT3 (IC_{50} 22 nM *in vitro*) CARM1 (IC_{50} 63 nM *in vitro*) PRMT5 (IC_{50} >100 μM *in vitro*) PRMT6 (IC_{50} 1.2 nM *in vitro*) PRMT8 (IC_{50} 1.1 nM *in vitro*)	Noncompetitive	CKD (chronic kidney disease, mouse model)	(66)
SGC707	PRMT3 (IC_{50} 31 nM *in vitro*, 91–225 nM cell assay)	Noncompetitive	N/A	(67)
SGC2085	CARM1 (IC_{50} 50 nM *in vitro*) PRMT6 (IC_{50} 5.2 μM *in vitro*) PRMT8 (IC_{50} >50 μM *in vitro*)	Noncompetitive	N/A (cell-impermeable)	(68)
EPZ020411	PRMT1 (IC_{50} 0.119 μM *in vitro*) PRMT6 (IC_{50} 0.010 μM *in vitro*, 0.637 μM cell assay) PRMT8 (IC_{50} 0.223 μM *in vitro*)	Competitive (substrate)	N/A	(69, 70)
EPZ0025654 (GSK3536023)	CARM1 (IC_{50} 3 nM *in vitro*)	Competitive (substrate)	N/A	(71)

EZM2302 (GSK3359088)	CARM1 (IC50 6 nM *in vitro*, 0.015- >10 μM cell assay)	Competitive (substrate), synergistic with SAH	Multiple myeloma (mouse xenografts)	(71)
TP-064	PRMT1 (IC50 >10 μM *in vitro*) PRMT3 (IC50 >10 μM *in vitro*) CARM1 (IC50 <10 nM *in vitro*, 400–716 nM cell assay) PRMT5 (IC50 >10 μM *in vitro*) PRMT6 (IC50 1.6 μM *in vitro*) PRMT7 (IC50 >10 μM *in vitro*) PRMT8 (IC50 8.1 μM *in vitro*) PRMT9 (IC50 >10 μM *in vitro*)	Competitive (substrate)	N/A	(72)
(ii) Type II and III preclinical compounds				
Compound	**PRMT enzymes inhibited**	**Mode of action**	**Disease type(s) tested**	**Refs**
EPZ015666 GSK3235025)	PRMT5 (IC50 22 nM *in vitro*,) 64–904 nM cell assay)	Competitive (substrate	Mantle cell lymphoma (mouse xenografts)	(73)
EPZ015866 (GSK591)	PRMT5 (IC50 4 nM *in vitro*)	Competitive (substrate	N/A	(74, 75)
EPZ004777	PRMT5 (IC50 30 μM *in vitro*) PRMT7 (IC50 7.5 μM *in vitro*)	Competitive (SAM)	N/A	(76)
LLY-283	PRMT5 (IC50 22 nM *in vitro*, 25 nM cell assay)	Competitive (SAM)	Melanoma (mouse xenografts)	(77)
HLCL-61	PRMT5 (ND)	N/A	N/A	(78)
DS-437	PRMT5 (IC50 5.9 μM *in vitro*) PRMT7 (IC50 6 μM *in vitro*)	Competitive (SAM)	Breast cancer (mouse xenografts)	(76, 79)
SGC3027	PRMT7 (IC50 2.4 μM cell assay)	Cell-permeable prodrug; converted to the active form (SGC8158) in the cell	N/A	(80)
SGC8158	PRMT7 (IC50 <2.5 nM *in vitro*)	Competitive (SAM)	N/A	(80)
(iii) Inhibitors in Phase I clinical trials				
Compound	**PRMT enzymes inhibited**	**Mode of action**	**Disease type(s) tested**	**tested Trial**

				number
GSK3368715	PRMT1		Diffuse large B cell lymphoma (DLBCL) and refractory solid tumours (pancreatic, bladder, non-small cell lung cancer).	NCT03666988
EPZ015938 (GSK3326595)	PRMT5 (IC50 3–9.9 nM *in vitro*) PRMT9 (IC50 >40 μM *in vitro*)	Competitive (substrate)	MDS and AML solid tumours and non-Hodgkin's lymphoma	NCT02783300 NCT03614728
JNJ-64619178	PRMT5	N/A	PRMT5 B cell non-Hodgkin's lymphoma (NHL) or advanced solid tumours	
PF-06939999	PRMT5	N/A	Advanced or metastatic solid tumours (non-small cell lung cancer, head and neck squamous cell carcinoma, oesophageal cancer, endometrial cancer, cervical cancer, and bladder cancer).	NCT03854227
PRT811	PRMT5	N/A	advanced solid tumor, recurrent glioma, CNS lymphoma	NCT04089449

Table 1. Tool Compounds and Clinical Inhibitors of PRMTs. Table adapted from Jarrold *et. al.* (37) and have been updated.

[a]Abbreviations: N/A, not available; ND, not determined; SAH, S-adenosylhomocysteine; SAM, S-adenosyl methionine

1.3 One-carbon metabolism and arginine methylation

Metabolism plays a central role in all areas of biology, from ecology to bioengineering to diseases, and is interlaced with cellular signalling pathways and the posttranslational modification state of proteins. One carbon pool is the pool of methyl groups that are accessible for methylation reactions (81). Methionine is an essential amino acid involved in one-carbon metabolism that serves as the substrate for SAM, which provides a methyl group for methylation. PRMT enzymes catalyse methylated arginines and produce SAH as a side-product. SAH is hydrolysed by S-adenosylhomocysteine hydrolase to generate homocysteine and then contributes to re-synthesis of methionine. SAM additionally can be utilized for polyamine metabolism by producing spermidine, spermine and methylthioadenosine. Serine is considered to be the primary methyl provider, transferring methyl groups to tetrahydrofolic acid (THF) to form glycine, N^5-N^{10} methylene THF and 5-methyl THF. A methyl group from 5-methyl THF can be transferred to homocysteine by methionine synthase. The interaction between the folate cycle and the methionine cycle in one carbon metabolism refers to the methyl transfer. One carbon metabolism is not only a process that redistributes methyl groups but also provides additional energy. Glutamine can provide energy through TCA cycle and contributes one carbon building block through gluconeogenesis. Glutamine deprivation has been investigated to affect one carbon metabolism by changing serine level (82). Thus, glutamine, serine, glycine, spermidine and methionine are also involved in one-carbon metabolism (**Figure 4**). Recent publications have reported changes in threonine and methionine metabolism that affect histone methylation (83, 84). Threonine deprivation decreases accumulation of SAM and histone H3 lysine 4 methylations and methionine deleption reduces histone and DNA methylations (83, 84). However, it is unclear whether the regulation of the conditional metabolites involved in the one-carbon pathway can be directly sensed by cells to trigger a change in protein arginine methylation.

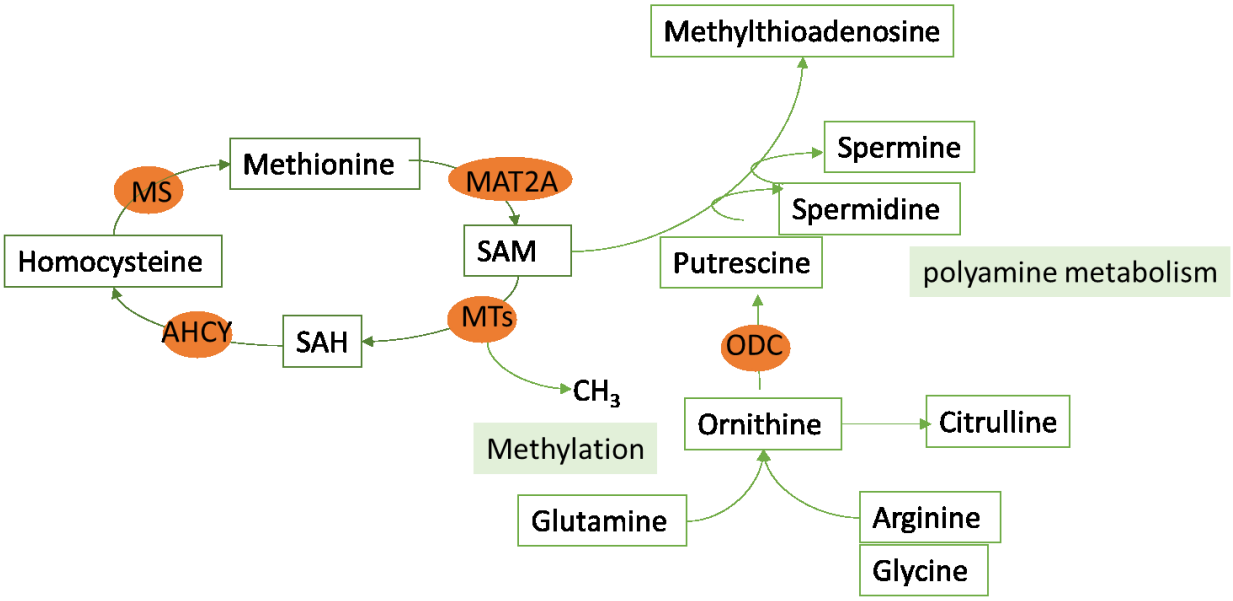

Figure 4. One-carbon metabolism and associates pathways. Methionine synthase (MS), Ornithine decarboxylase (ODC), S-adenosylhomocysteine hydrolase (AHCY), Methionine adenosyltransferase 2A (MAT2A), Methyltransferases (MTs), S-adenosylmethionine (SAM), S-adenosyl homocysteine (SAH).

ArgMet involves the metabolic process and *vice versa.* SAM metabolism is essentially entwined with PRMT enzymes. Metabolites and metabolic processes regulate PRMT enzyme activity, function and abundance. Methylome analyses have recognized that 3% of metabolic enzymes are arginine methylated, suggesting that PRMT enzymes could regulate metabolic pathways during tumorigenesis and ageing (15, 85-87). For example, NAUFAF7, a mitochondrial PRMT, regulates neuronal energy metabolism (88, 89). ArgMet of malate dehydrogenase (MDH1) by PRMT4 inhibits glutamine metabolism and suppresses pancreatic cancer cell growth (90). The dynamics of the ArgMet process and its relationship to cellular metabolism remain elusive. It is crucial to consider whether there are generic methods to unravel the relationship between ArgMet and metabolism.

1.4 Global analysis of protein arginine methylation

It has been difficult to understand precisely how ArgMet controls metabolism, cellular processes, and the mechanism remains elusive. The challenge in understanding how methylation affects (patho)physiological processes is identifying and quantifying protein arginine methylation (91).

Reliable detection and absolute quantification of arginine and its methylated derivatives in diverse matrices, such as cells, bodily fluids, and tissues, remain challenging because of the lack of suitable techniques. For instance, mass spectrometry (MS)-based approaches suffer from the lack of generally applicable methods to enrich the sample for methylated peptides, incomplete sequence coverage, and incorrect identification of methylation sites (92). The limitation of high-performance liquid chromatography (HPLC) relates to nonspecific and unstable derivatization and methylated arginine residues that are not effectively resolved under certain chromatographic conditions (**Table 2**) (93, 94). Most profiling studies of ArgMet are based on antibodies used for detection because they can be used for preferentially identifying specific and short target sequences, such as RG/RGG (1). The abundance of substrate sequences limits the application of immunoaffinity methods of ArgMet quantification.

	NMR	HPLC	MS	antibody
Sample preparation	simple	simple	extensive	simple
Sensitivity	μM	nM	only for peptide so far (not global)	not global/quantitative
Analysis	fast	slow	slow	fast
Dynamics	yes	no	technically possible, but haven't been tested	no
Advantage	dynamic study unlimited samples	high sensitivity,	site information	visualized
Limitations	less sensitivity no site information	slow analysis time, unstable derivatization	incomplete sequence coverage, lack of techniques for methyl peptide enrichment, limited target sequences, false positive	limited target sequences

Table 2. Comparison of MS, HPLC, antibody and NMR for ArgMet measurements

NMR based quantitative analysis of ArgMet has not been covered until so far. Compared to other methods, NMR is robust, highly reproducible, and quantitative over a wide dynamic range and are unmatched for determining structures of unknowns. NMR is adept at tracing metabolic fluxes and dynamics using isotope labels. Moreover, NMR is non-destructive and requires simpler sample preparation and faster analysis

1.5 NMR based metabolomics

Metabolomics is one of the core disciplines of systems biology (95). It focuses on the study of the changes of all metabolites produced by genetic alterations, in diseases and in response to environmental factors (96). Untargeted metabolomics has been established as a key technique for

the investigation of metabolic alterations in carcinogenesis (97, 98), microbiology (99, 100), precision medicine (101), biomarker discovery (102), chronic disease (103) and neurodegenerative disease (104). It can be used for quantitatively measuring dynamic multiple parameters of the metabolic response of the life system to pathophysiological stimuli or genetic modifications (105, 106). Moreover, metabolomics can be used to integrate and analyse metabolic information with biochemical and physiological changes in pathophysiological processes by tracking and detecting changes in metabolite levels and their dynamic transformations, and then, it can be used to determine relevant biomarkers (96). Therefore, metabolomics has been widely applied in many fields, such as to the diagnosis of diseases, exploration of pathogenesis, study of drug action mechanisms and search for new drug targets (105, 107). Untargeted metabolomic evaluation of arginine methylation might help us to understand the relationships between arginine methylation and metabolic pathways.

Currently, the main analytical techniques of metabolomics include chromatography, mass spectrometry, nuclear magnetic resonance (NMR) spectrometry, liquid chromatography-mass spectrometry (LC-MS) and gas chromatography-mass spectrometry (GC-MS) (50, 108, 109), each of which has its own advantages and scope of application. To achieve the goal of separating and analysing metabolites without bias, in a wide-ranging and high-throughput manner with high sensitivity and high precision, various spectral techniques combined with comprehensive analysis methods are increasingly being used in metabolomic research, showing the inevitable trend of the development of metabolomic analysis technology in the future. NMR spectroscopy is well suited and not destructive in the quantification of metabolites in complex mixtures of samples with minimal preparation (110). NMR spectroscopy has a lower sensitivity than LC-MS, but it shows high reproducibility and can be used for many matrices. In summary, NMR-based metabolomic analysis is mostly used in untargeted metabolomic studies and provides an abundance of metabolite information.

1.5.1 Metabolic alterations in hepatocellular carcinoma

Hepatocellular carcinoma (HCC) is one of the most lethal and prevalent cancers worldwide, accounting for between 85% and 95% of primary liver cancers (111, 112). HCC is a pathology process with multiple aetiologies that are dynamic consisting of multiple stages (113). The

observed variations in the age-, sex- and race-specific distribution of HCC in geographic regions are related to different types of hepatitis virus infection, alcohol abuse, aflatoxins and the subsequent cirrhosis (114-116). Common diagnostic tools include biopsy sampling and radiographic imaging; however, early diagnosis requires the impetus to conduct such testing. The serum marker alpha-fetoprotein (AFP), used as the only regular means of surveillance for early detection, is controversial due to false positives and its limited sensitivity. The development of clinical biomarkers for HCC in the early stage remains poor due to the lack of typical symptoms in the early stage and methodologic challenges, including incomplete characterization of patient cohorts. Most HCCs are found when the disease is in the advanced stage; therefore, only 30% of HCCs are suitable for resection, and up to 80% of patients present with underlying cirrhosis (117). Recurrent HCC is the rate-limiting factor of long-term survival. Although surgical resection, targeted drug therapies, local ablation and liver transplantation are well-developed strategies and are routinely used in the clinic, high mortality is related to a lack of effective timely diagnosis, systemic therapy resistance, poor prognosis and high postoperative recurrence (118, 119). HCC with rapid growth and vascular invasion depends on the formation of new blood vessels, which induce an abnormal microenvironment characterized by low oxygen tension. Recently, antiangiogenic strategies have been developed as therapies, i.e., sorafenib for advanced-stage HCC (120). Unfortunately, the limited number of studies focused on the angiogenic microenvironment has made it difficult to find prognostic biomarkers, similar to the situation of recurrence prediction. Limited resources have hampered clinical trials of incorporating biomarker studies in HCC for the following reasons: first, modelling HCC in mice has been difficult; second, HCC is a highly heterogeneous disease for which thorough mechanistic studies with relevant clinical models are needed. In this respect, the challenge of exploring predictive biomarkers (early stage or prognostic) or promising treatment options needs to improve our understanding of HCC carcinogenesis, the angiogenic microenvironment, rapid recurrence and metastasis.

The molecular mechanism of hepatocarcinogenesis is related to intracellular signalling pathways such as the Wnt/β-catenin, Ras/Raf/Mek/Erk, hedgehog, MAPK, AKT, ERK, VEGF, PI3k/Akt/mTOR and hypoxia-inducible factor pathways (121, 122). ArgMet also involves in hepatocarcinogenesis and enhances hepatitis virus replications (123, 124). Methylation of the core protein of HBV by PRMT5 induces its accumulation (125). In HCC, PRMT5 promotes cell

proliferation through ERK signalling pathway and enhances metastasis through Wnt/ß-catenin signalling pathway (126, 127). PRMT6 regulates Ras/Raf/Mek/Erk-mediate cancer stemness activity. These roles include regulation of cellular oxidative stress, and cell proliferation, differentiation and apoptosis, which in turn control hepatic growth, protein expression/post-translational modifications, xenobiotic metabolism and metabolic reprogramming to mediate an increase in glucose uptake, glycolysis, angiogenesis, and stress resistance. In this context, the variation in protein expression or post-translational modifications and metabolite levels induced by signalling pathways needs to be clarified to shed light on metabolic reprogramming and carcinogenesis.

First metablic data were obtained on HCC (128). For instance, Hao W *et al.* (129) used gas chromatography-mass spectrometry (GC-MS) to compare urine metabolite profiles of HCC patients and healthy individuals and were able to identify 18 biomarker candidates that could discriminate HCC patients from healthy individuals. Currently, the major analytical techniques of metabolomics include chromatography, mass spectrometry, NMR, liquid chromatography-mass spectrometry (LC-MS) and GC-MS (130). ^{1}H NMR spectroscopy has been successfully employed in metabolomic studies, producing a large amount of information on metabolites in biological matrices (131). However, the investigation of useful biomarkers for HCC, focused solely on metabolomics, has been difficult. Multiple complementary analytical platforms are required as profiling tools to help with metabolic visualization. Proteomic and metabolomic analyses with high-throughput platforms offer simultaneous readouts of hundreds of proteins and metabolites for us in gaining insight into cell signalling pathways. Integrating multiple omics techniques in a single study is not easy because each omics technique has its own degree of specialization and relevant analysis. Most studies have applied proteomic analysis to identify metabolic pathways for one or two metabolites (132) or used metabolic labelling for quantitative proteomic analysis (133). However, use of single omics does not allow comprehensive interpretation, as it is focused on the technical and analytical aspects of the process not necessarily the overall biological interpretation of the results; e.g., the number of proteins identified by proteomics is not indicative of protein activity or the factors critical for its activity. A few combined metabolomic and proteomic analyses, such as in cardiovascular diseases (134, 135), kidney cancer (136), atrial fibrillation (137), gestational diabetes mellitus (138) provide opportunities to bridge the gap between molecular and

systems biology and eliminate some of the bias inherent in single omics studies. Metabolic/proteomic adaptation should be assessed not only in terms of cancer cells but also in consideration of the contribution of normal (noncancerous) cells in the same tissues. Metabolomics and proteomics share an intracellular network that induces metabolic/proteomic dynamics through various chemical reactions and extracellular organic and signalling molecules that supplement and mediate stimuli.

1.5.2 The metabolic regulation of ageing

Ageing is an important contributor to energy metabolism. Ageing affects cellular function, including body homeostasis, DNA damage and oxidative stress (139). Several metabolic cellular ageing mechanisms have been implicated on the basis of studies across a range of species (140), including AMPK, IGF-1, transcriptional regulation, sirtuins, endoplasmic reticulum stress, autophagy, oxidative stress and mTOR (141, 142). Autophagy declines with increasing age leading to the accumulation of the damaged proteins and organelles (143). Autophagy-proteasomal degradation can be controlled by PRMT enzymes and ArgMet (144, 145). Consistently, methylation alterations in histones, DNA and chromatin-associated proteins prompt epigenetic changes that affect cellular senescence (140). As mentioned above, some PRMT enzymes affect cellular apoptosis or senescence (54-56).

The inability to maintain homeostasis can be observed both within cells and during intercellular communication. Researchers have found disturbances in different compartments of the cell, suggesting that ageing is not the result of a single process but is a result of multiple pathway interactions. Furthermore, researchers have proposed that the accumulation of senescent cells over time may contribute to the course of ageing and age-related disease. These alterations are common in ageing tissues and are associated with age-related pathologies, such as hypertension, Parkinson's disease, diabetes mellitus type 2, diabetes mellitus, multiple chronica condition, Alzheimer's disease, atherosclerosis and obesity (146-151). Whereas these conditions differ greatly in their manifestations, they share characteristic that they are accompanied with alterations in metabolism. For example, in diabetes mellitus type 2, blood levels of branched chain amino acids, low-carbon lipids or sugar metabolites are increased (152, 153), whereas in Alzheimer's disease, methionine, histidine, lysine and phosphatidylethanolamine can be detected at abnormal levels in plasma (154).

Moreover, there is increasing evidence showing that metabolic changes are not only a consequence of ageing processes but are also potential causes of ageing. Distinct physiological processes are controlled by tissues, substantially overlapping transcriptomes, proteomes and metabolomics. Whether different tissues age in the same way is an open question. For instance, muscle cells, among others, can utilize fatty acids for producing energy, whereas fatty acids cannot cross the blood-brain barrier, making the brain dependent on glucose for the same purpose. The levels of certain metabolites can therefore enable researchers to distinguish between the origins of single specimens and characterize them in ageing manner (155). Furthermore, distinct changes in the metabolic profile of organs in different states of health seems to be a reasonable supposition. This presumption was validated by Houtkooper *et al.*, who investigated changes in the metabolic profiles of muscle and liver tissue associated with ageing (156). As expected, when comparing the tissues of old and young mice, the activity of different pathways seemed to differ in those two tissue types. A sharp increase in metabolites associated with starch and sucrose metabolism, glycerolipid metabolism or phospholipid biosynthesis was seen in the livers with increasing age, where in muscles, the alterations mainly affected starch and glucose metabolism, galactose metabolism and polyunsaturated fatty acid metabolism (157). Consequently, the discovery of both ageing- and tissue-specific biomarkers seems a reasonable and desirable goal in the continuous search for reliable universal biomarkers of ageing. Several studies have revealed molecular effects of ageing on genomic instability, epigenetic alterations and metabolome levels. However, a comprehensive overview of metabolic changes in healthy ageing is lacking, especially in relation to post-translational modifications.

In addition to the potential use of metabolomics in the search for new biomarkers, identifying which metabolites are altered in different states of pathophysiological status or healthspan can help trace the primary interfering pathway(s) that play roles under the investigated conditions. Following this approach and assuming that the state of ageing differs from the state of health, identifying metabolites that change significantly with ageing seems important in classifying pathways that are closely connected to senescence. Moreover, a potential therapeutic approach targeting one carbon metabolism may be valuable by integrating arginine methylation and metabolomic correlations.

2 Motivation and Aims

ArgMet represents an abundant posttranslational modification regulating numerous cellular processes and biological functions. Given that ArgMet is strongly dependent on the essential amino acid methionine, which is a precursor to SAM, we hypothesize that ArgMet is strongly coupled to metabolism. Understanding alterations of ArgMet in fundamental processes, especially in metabolic contexts, has provided the rationale for targeting ArgMet in differentiation, ageing and oncology. However, due to the lack of appropriate tools for the quantitative analysis of global level of protein arginine methylation, we aim

1) To develop a novel, simple and fast protocol for absolute quantification of protein arginine methylation, including:

   i. Apply our methods in unlimited biological matrices, i.e. serum, urine, cell, organoid and tissue.

   ii. Validate whether ArgMet represents highly abundant post-translational modification and determine ArgMet levels in biological samples.

   iii. Apply our methods for characterizing PRMT enzymatic specificities and understand substrates specificity of PRMT enzymes.

   iv. Evaluate how ArgMet is modulated by metabolites.

   v. Evaluate the effectiveness of PRMT inhibitors to suppress ArgMet levels.

   vi. Understand dynamics and turnover of ArgMet, including the existence of an efficient arginine demethylase

2) To converge on ArgMet as a metabolic master switch for biological processes, including:

   i. Differentiation

   ii. Carcinogenesis

   iii. Ageing

3) To integrate with metabolomic data to analyse the relationship between ArgMet and metabolism.

i. Hepatocarcinogenesis, to merge the proteomic and metabolomic datasets derived from experiments on HCC (n=200) serum, carcinoma tissues and peritumoural tissue of distinct tumour sizes for understanding the signalling pathways and underlying mechanisms.

ii. Ageing, to study metabolic changes in the brain, heart, kidney, liver, lung and spleen in young (9-10 weeks) and old (96-104 weeks) mice.

3 Publication I

Global analysis of protein arginine methylation

Fangrong Zhang[1], Jakob Kerbl-Knapp[1], Maria J. Rodriguez Colman[2], Andreas Meinitzer[3], Therese Macher[1], Nemanja Vujić[1,4], Sandra Fasching[5], Evelyne Jany-Luig[5], Melanie Korbelius[1], Katharina B. Kuentzel[1], Maximilian Mack[4,6], Alena Akhmetshina[1], Anita Pirchheim[1], Margret Paar[7], Beate Rinner[8], Gerd Hörl[7], Ernst Steyrer[1], Ulrich Stelzl[4,5], Boudewijn Burgering[2], Tobias Eisenberg[4,6,9], Brigitte Pertschy[4,6], Dagmar Kratky[1,4], Tobias Madl*[1,4,10]

[1]Gottfried Schatz Research Center for Cell Signaling, Metabolism and Aging, Molecular Biology and Biochemistry, Medical University of Graz, 8010 Graz, Austria

[2]Oncode Institute and Department of Molecular Cancer Research, Center for Molecular Medicine, University Medical Center Utrecht, 3584 CX, Utrecht, The Netherlands

[3]Clinical Institute of Medical and Chemical Laboratory Diagnostics, Medical University of Graz, 8010 Graz, Austria

[4]BioTechMed-Graz, 8010 Graz, Austria

[5]Institute of Pharmaceutical Sciences, University of Graz, 8010 Graz, Austria

[6]Institute of Molecular Biosciences, NAWI Graz, University of Graz, 8010 Graz, Austria

[7]Otto-Loewi Research Center, Physiological Chemistry, Medical University of Graz, 8010 Graz, Austria

[8]Division of Biomedical Research, Medical University of Graz, 8036 Graz, Austria

[9]Field of Excellence BioHealth – University of Graz, Graz, Austria

[10]Lead contact

*Correspondence:

Tobias Madl

Gottfried Schatz Research Center, Molecular Biology and Biochemistry, Medical University of Graz, Neue Stiftingtalstraße 6/6, 8010 Graz, Austria

Phone: (+43-316) 385-71972
Fax: (+43-316) 385-79615
Email: tobias.madl@medunigraz.at

3.1 Highlights

- NMR enables robust quantification of (methylated) arginines in biological matrices
- Arginine methylation represents a highly abundant post-translational modification
- Arginine methylation can be modulated by small-molecule inhibitors and metabolites
- Alterations provide insights into phenotypes of cancer, differentiation and ageing

3.2 Motivation

Protein arginine methylation (ArgMet) is of high current and increasing interest due to its fundamental role in regulation of cellular processes, including transcription, RNA processing, signal transduction cascades, the DNA damage response and liquid–liquid phase separation. However, due to the lack of methods for global analysis of ArgMet, the mechanistic link between ArgMet levels, dynamics and (patho)physiology remain largely unknown. Here, we took advantage of the high sensitivity and robustness of Nuclear Magnetic Resonance spectroscopy and developed and applied a general method for quantification of global protein ArgMet.

3.3 Summary

Quantitative information about the levels and dynamics of post-translational modifications (PTMs) is critical for an understanding of cellular functions. Protein arginine methylation (ArgMet) is an important subclass of PTMs and is involved in a plethora of (patho)physiological processes. However, due to the lack of methods for global analysis of ArgMet, the link between ArgMet levels, dynamics and (patho)physiology remains largely unknown. We utilized the high sensitivity and robustness of Nuclear Magnetic Resonance (NMR) spectroscopy to develop a general method for the quantification of global protein ArgMet. Our NMR-based approach enables the detection of protein ArgMet in purified proteins, cells, organoids, and mouse tissues. We demonstrate that the process of ArgMet is a highly prevalent PTM and can be modulated by small-molecule inhibitors and metabolites and changes in cancer and during ageing. Thus, our approach enables to address a wide range of biological questions related to ArgMet in health and disease.

Graphical Abstract

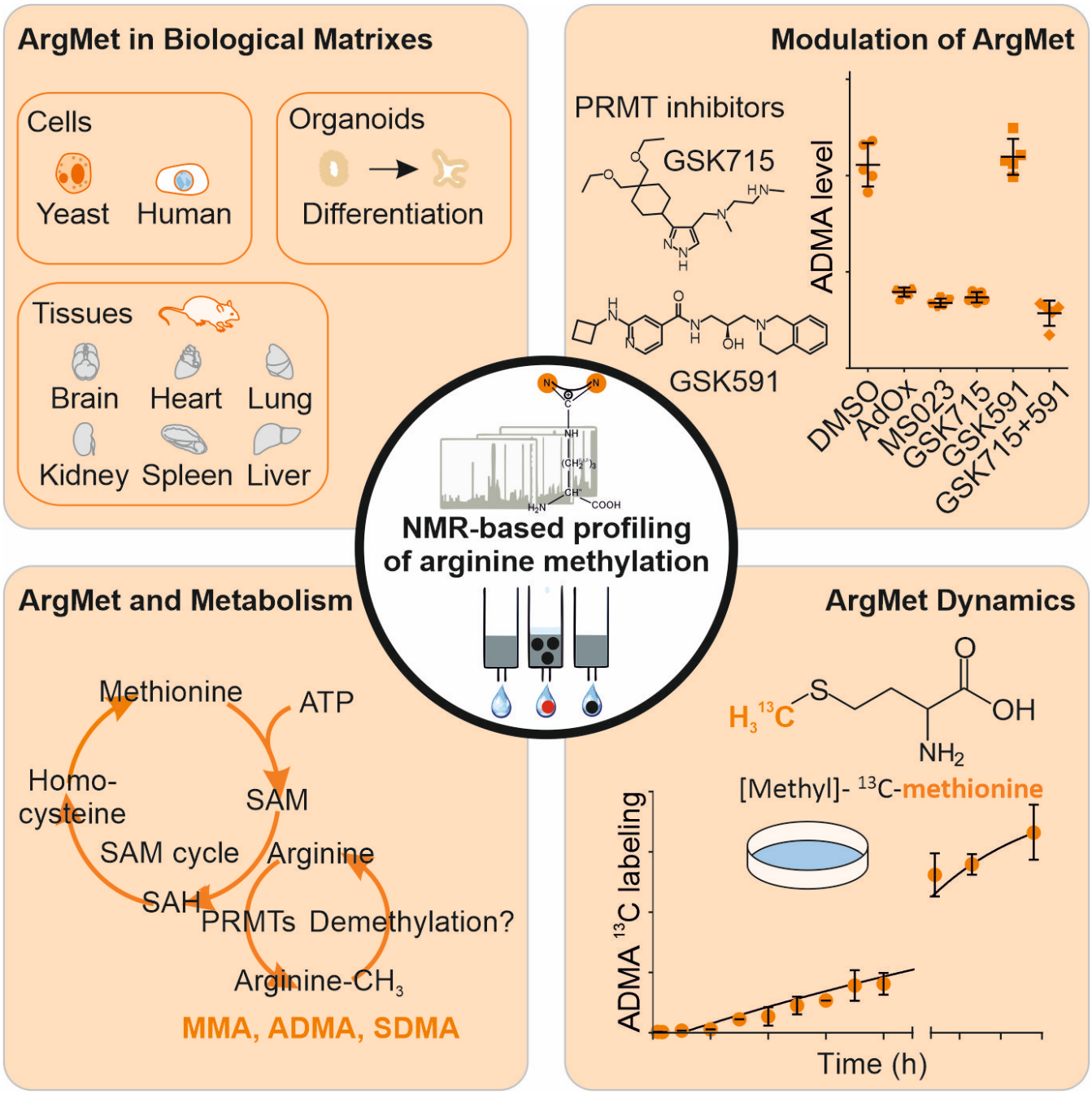

Keywords: arginine methylation, NMR spectroscopy, protein arginine methyltransferases, mouse models, organoids, yeast, cancer, cell differentiation, ageing

3.4 Introduction

Arginine methylation (ArgMet) is a prevalent post-translational modification (PTM) evolutionary conserved from unicellular eukaryotes to humans. It regulates a plethora of fundamental biological processes, such as transcription, translation, RNA metabolism, signal transduction, DNA damage response, apoptosis, and liquid-liquid phase separation (LLPS) (3, 4, 9, 10, 158)

Three main types of methylated arginine residues are present in cells, including ω-N^G-monomethylarginine (MMA), ω-N^G, N^G-asymmetric dimethylarginine (ADMA) and ω-N^G-N'^G-symmetric dimethylarginine (SDMA). Formation of MMA, SDMA and ADMA is catalysed by a broad spectrum of protein arginine methyltransferases (PRMTs). The number of PRMTs varies from unicellular eukaryotes to humans, with yeast having at least one or two main PRMTs (HMT1/RMT1 and HSL7) and a family of nine PRMTs being present in mammals (9, 10). Depending on the type of methylated arginine they produce, PRMTs are categorized into four main classes (10, 12). Type I PRMTs, including PRMT1, 2, 3, 4 (also called CARM1), 6, and 8 catalyse the formation of MMA/ADMA, whereas type II PRMTs, including PRMT5 and 9, catalyse the formation of MMA/SDMA (**Figure S1A**). Type III PRMTs such as PRMT7 catalyse the formation of MMA. In yeast, only the type IV PRMT RMT2 has so far been reported (11) to methylate the delta (δ) nitrogen atom of arginine residues (159). Additional potential arginine methyltransferases have been identified, but remain to be biochemically validated (NDUFAF7, METTL23) (12).

Most PRMTs methylate glycine- and arginine-rich, so-called arginine-glycine-glycine (RG/RGG), protein regions (15-17). More than 1000 human (in particular RNA-binding) proteins contain RG/RGG regions (1, 8). However, adjacent glycine residues are not a prerequisite for the ArgMet as it has been shown that RXG motifs can be methylated by PRMT1, where X is preferably lysine, phenylalanine, threonine or leucine (18, 19). Moreover, RPAAPR- or APR-motifs have been identified as sites of ArgMet (20). PRMT4/CARM1 has been reported to methylate arginines within proline-, glycine-, and methionine-rich regions (22, 23). A set of PRMT5 targets identified by mass spectrometry revealed the enzyme's preference for methylating arginine located between two neighbouring glycines (GRG) (24). PRMT6 prefers arginines in positively charged regions and disfavours acidic residues at essentially any position around the target arginines (17). Within

proteins, intrinsically disordered regions regularly display ArgMet, but are not exclusive sites (25). On a molecular level, methylation of these regions regulates nucleic acid binding, protein-protein-interactions, LLPS, and protein localization (12).

PRMTs are ubiquitously expressed in human tissues (160), with the exception of PRMT8, mainly expressed in the brain (158), and regulate important cellular processes that affect cell growth, proliferation and differentiation (5). Embryonic loss of most of these PRMTs results in pre- and perinatal lethality in mice (161, 162). Dysregulation of PRMTs has been implicated in the pathogenesis of several diseases, including cardiovascular, metabolic, and neurodegenerative diseases, viral infections, and various types of cancer (5). Since PRMTs tend to be upregulated in cancer malignancies (31, 37) they represent a promising target in cancer therapy and are currently being investigated in several clinical studies with PRMT inhibitors. Moreover, loss of PRMTs has been linked to cellular senescence and ageing in mice (5).

Despite the biological significance of ArgMet, several key questions are still elusive: (i) The global levels of ArgMet are largely unknown. Pioneering studies indicated that ArgMet might be as abundant as phosphorylation, with around 0.5 - 2% of arginine residues being methylated in mammalian cells and tissues (163-166). Although more than 1000 ArgMet-sites have already been identified by immunoaffinity purification and liquid chromatography–tandem mass spectrometry (LC-MS/MS) (15, 167), specific concentrations of ArgMet in cells and tissues, including the coupling of ArgMet and metabolism, have so far not been comprehensively studied by Nuclear Magnetic Resonance (NMR). The methyl group for protein ArgMet is provided by the universal methyl-donor S-adenosyl methionine (SAM), which is synthesized from methionine and ATP by SAM synthase. One carbon metabolism is required for recycling of the essential amino acid methionine (168, 169). How metabolism regulates ArgMet needs to be determined. (ii) Dynamics and turnover of ArgMet, including the existence of an efficient arginine demethylase, are controversial issues and still largely unexplored (12). (iii) Regulators of PRMTs (e.g. BTG1, TIS21/BTG2, or NR4A1) were proposed in the last years, but their impact on PRMT activity and, in turn, their contribution to global ArgMet concentrations remain enigmatic (3, 31). (iv) Small-molecule inhibitors of PRMTs have been discovered, yet their influence on the extent of ArgMet and how ArgMet levels are affected *in vivo* is currently unknown.

Addressing these questions is challenging, in part due to the lack of robust methods for (absolute) quantification of global ArgMet values and dynamics in cells and tissues. Most of the current approaches use antibodies to detect and distinguish differentially methylated arginines. These methods successfully track and annotate these PTMs (170). However, these antibodies are still only raised against specific, short target sequences (e.g. RGG) and mixtures of selected motifs, but fail to recognize or enrich the entire pool of arginine methylated proteins. This limits their use in quantifying of global ArgMet levels due to the large sequence diversities found around these sites (171, 172).

We therefore developed a general method for absolute, label-free quantification of (methylated) arginines in cells, organoids and tissues by using the high sensitivity and robustness of NMR spectroscopy. We demonstrate that ArgMet is a highly abundant PTM, whereas cellular dynamic changes of protein ArgMet occur at a slow rate. Our study provides a strong methodological development for the quantification of ArgMet levels and their dynamic changes, that also conceptually advances our understanding of the importance of ArgMet in biology and medicine. Moreover, we offer ways to study the modulation of protein ArgMet by inhibitors, metabolites and biological processes such as differentiation and ageing, enabling future studies from basic to translational research and drug discovery/development far beyond the current state of the art.

3.5 Results

3.5.1 NMR enables quantification of global protein arginine methylation

NMR spectroscopy enables robust quantification of metabolites in complex mixtures paired with simple and fast sample preparation, measurement and analysis (173). We built on previous chromatography-based approaches to analyse (methylated) arginines in protein hydrolysates (174, 175) and developed a NMR-based protocol for absolute quantification of protein ArgMet. A schematic representation of the workflow is shown in **Figure 5A.** Proteins were extracted from biological matrices, hydrolysed using hydrochloric acid, and delipidated. Basic/hydrophobic amino acids, including arginine and its derivatives, were purified by solid phase extraction (SPE) and analysed by NMR spectroscopy. NMR analysis of arginine, ADMA, MMA and SDMA standards revealed good separation of their ^{1}H signals, both in 1D Car-Purcell-Meiboom-Grill (CPMG) as well as in 2D homo-nuclear J-resolved experiments (JRES) (**Figure 5B**, **Figure 5C a**nd **Figure S1B**). The CPMG pulse sequence is routinely employed removing the residual broad signals from macromolecules (such as lipids) to avoid the signals from compounds with low molecular weight are overshadowed by signals of macromolecules (176, 177). The JRES approach separates the chemical shift and J-couplings into two different spectral dimensions. To minimise signal overlap with other metabolites present in biological materials, ^{1}H 1D projections of 2D J-resolved, virtually decoupled NMR spectra are recommended strategies for quantify ArgMet. We used the ^{1}H 1D projections of 2D J-resolved, virtually decoupled NMR spectra for all follow-up analyses, facilitating assignments and quantifications (173, 178-180). ^{1}H-methyl signals of MMA and SDMA overlapped in ^{1}H spectra when recorded in buffer, but could be resolved in d_6-DMSO as solvent (**Figure 5D**).

To validate the robustness of our workflow, we first evaluated stability and recovery of ADMA, MMA and SDMA signals in diverse biological matrices. All compounds were highly stable during hydrolysis and showed high recovery both from a protein matrix containing lysozyme and a methylation-free *Escherichia coli* cell matrix (**Figure 5E**, **Figure 5F**, **Figures S1E-G**). Protein-unbound free methyl arginines did not contribute to the detected protein ArgMet (**Figures S1C**, **S1D**). A quantitation limit for ADMA of 100 nM was determined (**Figure S1H**). Concentrations remained linear over a wide concentration range of 4 orders of magnitude up to the SPE column

saturation limit of 3 mM, as shown for arginine (**Figures S1I**). In summary, our NMR approach offers a simple, rapid and highly reproducible workflow for arginine and ArgMet quantification. Compared to HPLC-based quantification, NMR is label-free, does not require chromatographic separation or standards for quantification. Moreover, it enables detection of yet unknown arginine derivatives and can be combined with isotope labelling.

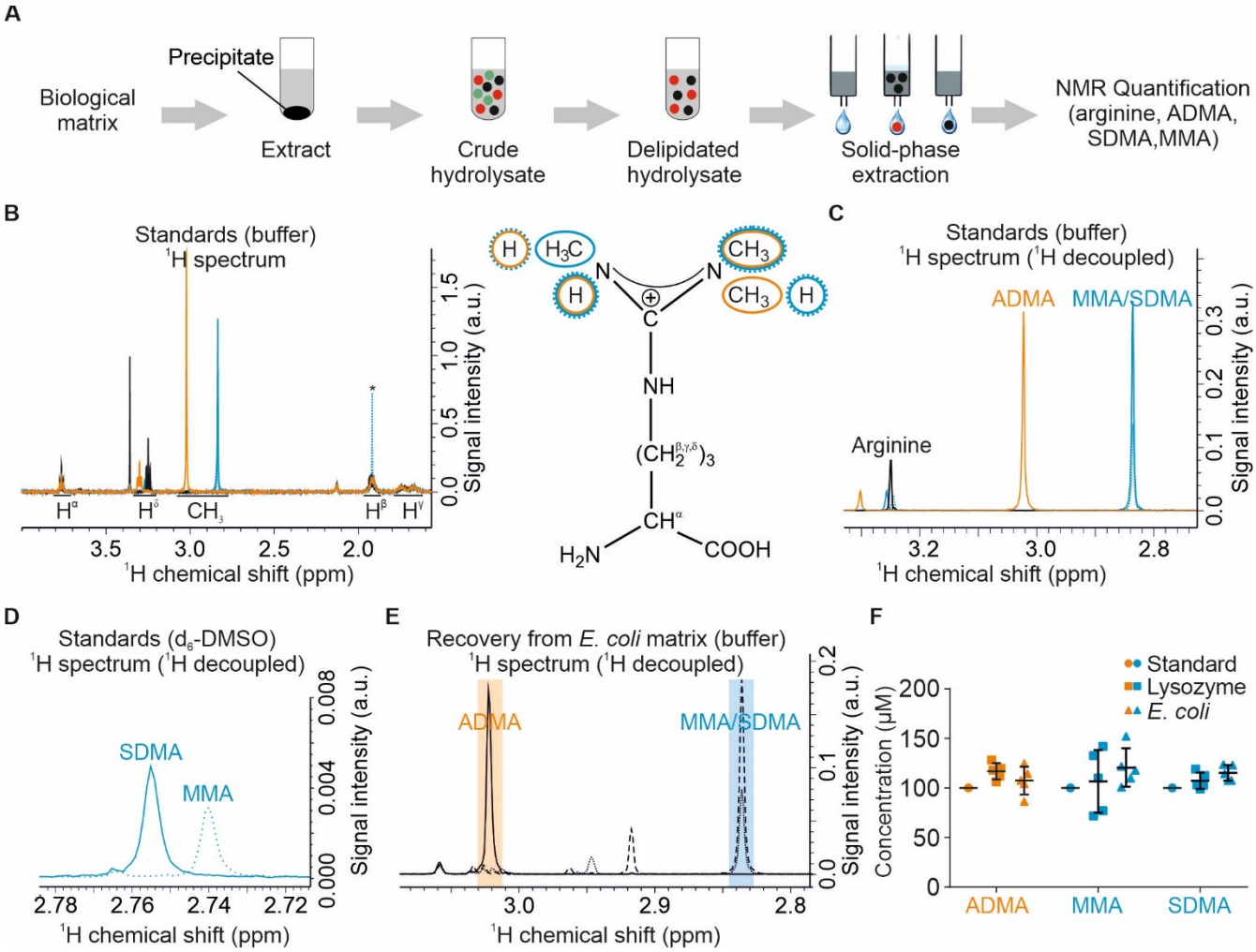

Figure 5. Absolute quantification of protein ArgMet by NMR.

(A) Schematic workflow depicting steps for protein arginine and ArgMet quantification. Biological matrices are extracted with water/methanol. Protein precipitate containing protein arginine and ArgMet is hydrolysed, lipids are removed with chloroform, and solid phase extraction (SPE) is used to isolate positively charged amino acids, including (methylated) arginine(s). The eluate is analysed by NMR spectroscopy.

(B) Overlay of ^{1}H 1D-CPMG NMR spectra of 100 µM arginine (black), ADMA (orange), MMA (blue, dashed line) and SDMA (blue, solid line). Chemical shift ranges for characteristic ^{1}H signals are shown in the spectra. Positions of the corresponding protons are labelled in the structure formula (ADMA - orange, MMA - blue, dashed line, SDMA-blue, solid line; an acetate impurity is labelled with an asterisk).

(C) Overlay of ^{1}H 1D projections of 2D J-resolved, virtually decoupled NMR spectra of the samples shown in (B). Characteristic regions of ADMA, MMA and SDMA methyl groups are indicated (arginine, black; ADMA, orange; MMA, blue, dashed line; and SDMA, blue, solid line).

(D) Overlay of ^{1}H 1D projections of 2D J-resolved NMR spectra of 100 µM MMA (blue, dashed line) and SDMA (blue, solid line) recorded in DMSO-d_6 show the resolution of methyl resonances.

(E) Overlay of representative recovery experiments of ^{1}H 1D projections of 2D J-resolved NMR spectra recovery experiments from *E. coli* lysates spiked with ADMA (solid line), MMA (dashed line) or SDMA (dotted line), respectively. Shaded regions represent characteristic regions of ADMA (orange), MMA and SDMA (blue) methyl groups.

(F) Statistical analysis of ADMA, MMA, SDMA recovery from lysozyme (square, n=5; mean ± SD) (0.34 mM) and *E. coli* lysates (triangle, n=5, mean ± SD). Samples were spiked with 100 µM ADMA (orange), MMA (blue), SDMA (blue) and prepared according to the workflow shown in (A).

3.5.2 NMR-based protein ArgMet profiling in vitro and in cells

To identify the proportion of ArgMet in protein and cell samples of unknown methylation status, we determined levels of arginine, ADMA, MMA and SDMA in recombinant proteins, yeast cell cultures and mammalian cell lines. Levels of ADMA, MMA and SDMA are presented normalised to the total arginine content to allow a direct comparison of ArgMet concentrations between different biological matrices. Alternatively, and because NMR is completely quantitative, absolute concentrations can be displayed, normalised to either cell number, tissue mass or protein content.

Methylation by PRMTs occurs preferentially within RG/RGG-rich and proline-glycine-methionine-rich regions **(5)**. In mammals, PRMT1 is the most abundant methyl transferase and catalyses formation of both ADMA and MMA. As expected, NMR analysis of the methylation-free recombinant RG/RGG model proteins cold-inducible RNA-binding protein (CIRBP) and RNA-binding protein fused in sarcoma (FUS) revealed that ADMA and MMA are detectable in

recombinant proteins after incubation with PRMT1 and the methyl-donor SAM (**Figure 6A**). Both model proteins are suitable as *in vitro* substrates for PRMT1, with 12% and 5% of all arginine residues being asymmetrically dimethylated in CIRBP and FUS, respectively. Interestingly, the levels of ADMA and MMA varied between CIRBP and FUS, with CIRBP lacking MMA/SDMA and FUS showing MMA (**Figure S2A**). The increased content of MMA in FUS might be due to the presence of two RGGY motifs in FUS. A preference for tyrosine in the +3 position was observed for PRMT1 MMA target sites (181).We cannot rule out the possibility that *in vitro* methylation might lead high MMA levels. These data indicated that PRMT1 selectively recognizes amino acid sequences in substrate (15) and that ArgMet-NMR is well-applicable to study levels and kinetics of ArgMet in purified protein substrates.

First HPLC-based studies estimated 0.5 - 2% of arginine residues to be methylated in mammalian cells and tissues (163-166). In yeast, four PRMTs (HMT1/RMT1 (182, 183), RMT2 (159), HSL7 (184) and SFM1(185)) have been described. Additionally, a large number of methylation sites and their associated proteins have been identified by mass spectrometry (186, 187), suggesting that ArgMet may represent an important mechanism in yeast. Of these PRMTs, HMT1/RMT1 has already been identified as a PRMT1 homologue in 1996 (182, 183). Analysis of wild-type and HMT1 or HSL7 knockout yeast strains, assessed in two distinct but related genetic backgrounds (BY4741 and BY4742) showed that on average more than 0.25% of all arginines are methylated in S. cerevisiae (**Figure 6B**). MMA was detectable in wild-type yeast (BY4741 and BY4742), albeit at low levels (~20% of ADMA), whereas SDMA was undetectable (**Figure 6C** and **Figure S2B**). Deletion of HMT1 essentially abolished ADMA and MMA levels in both backgrounds, consistent with an HPLC-based validation experiment (**Figure S2B**), suggesting that none of the other PRMTs contributed significantly to the global ArgMet levels. In line with these results, only very few substrates of RMT2, HSL7 and SFM1 have been reported so far (11, 185, 188). In contrast to HMT1 deletion, deletion of HSL7 showed no significant impact on global ADMA and MMA levels in BY4741 and BY4742 (**Figure 6B**), probably because HSL7 only recognizes a small subset of potential substrate proteins in yeast (188). Indirect effects associated with the loss of HMT1 are unlikely as the expression of other PRMTs is not affected by HMT1 knockout (189)

Our approach offers an excellent opportunity to characterise ArgMet in a variety of commonly used human cell lines. ArgMet-NMR analysis of nine human cells lines showed that ADMA and MMA/SDMA concentrations differ significantly, with primary fibroblasts showing the lowest and A375 malignant melanoma cells showing the highest levels of both ADMA and MMA/SDMA, respectively (**Figure 6D**). In all cell lines tested, ADMA was the predominant ArgMet species with more than 3% of all arginine residues being methylated in A375 cells. SDMA/MMA levels were significantly lower (**Figures 6D** and **E**). This finding is in line with previous studies estimating MMA and SDMA at levels of 20-50% of ADMA (9), although the MMA/SDMA values detected by NMR are consistently lower (~10% of ADMA). The significantly increased concentrations of ArgMet in A375 cells compared to all other cell lines is in agreement with a recent study showing overexpression of PRMT1 in these cells (190). In contrast, HPLC-based methods detected 0.8% of all arginine residues in A375 cells being asymmetrically dimethylated, which is lower than the 3.4% of ADMA we found (191). The increase of ADMA in all investigated cell lines is correlated with a concomitant increase in MMA and SDMA, indicating that the corresponding enzymes may be co-regulated (**Figure S2C**). Nevertheless, we cannot exclude, that the level of substrate proteins and PRMTs might also affect the ArgMet levels. PRMTs are constitutively active and localised in the nucleus and cytoplasm (192, 193). In the nucleus, histone ArgMet is an important modulator of dynamic chromatin regulation and transcriptional controls (194). We therefore analysed the ArgMet levels of chromatin and cytoplasm in A375 and HeLa cells and observed a significant increase of ArgMet in the chromatin fractions compared to the cytoplasmic fractions or whole-cell lysates (**Figures S2D** and **S2E**). This is in agreement with a previous study identifying lower PRMT1 protein levels in the chromatin fractions compared to the cytoplasm in HeLa cells (195). The higher levels of ArgMet observed in chromatin maybe due to a higher proportion of well-established PRMT substrates, such as histone proteins, which can be methylated by multiple PRMTs **(29)**. Our observation that ArgMet levels in the cytoplasm are similar to ArgMet levels in whole cells confirmed that the high ArgMet content in whole cells is not due to the chromatin compartment but to an overall high ArgMet level.

Generally, non-cancer cell lines such as primary fibroblasts show a tendency to lower concentrations of ArgMet compared to cancer cell lines such as HeLa, A375 or MDA-MB-231. Although HaCaT cells, an immortalized human keratinocyte line, exhibit also higher ArgMet levels,

the values are still lower than in cancer cell lines. In summary, our approach provides a direct read-out of protein ArgMet in cell lines.

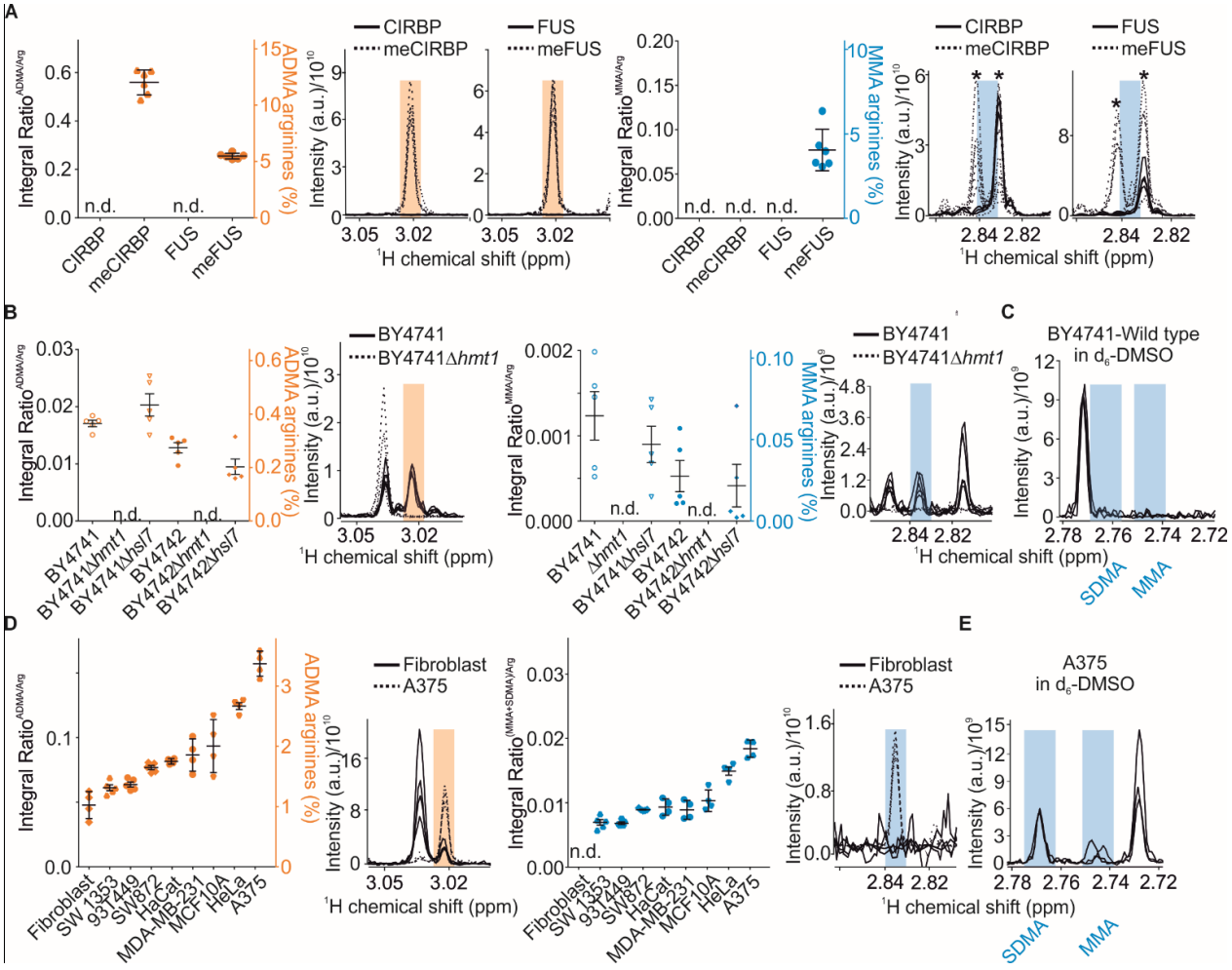

Figure 6. Characterisation of ArgMet in purified proteins, yeast and mammalian cell lysates.

(A) ArgMet quantification of recombinant CIRBP (triangle) and FUS (circle) peptides without methylation or *in vitro* methylated by recombinant PRMT1, respectively (n=6; mean ± SD; n.d. - not detectable; Tris buffer impurities are labelled with asterisks).

(B) Protein ArgMet quantification of yeast lysates (n=4; mean ± SD; n.d. - not detectable).

(C) Spectral overlays of characteristic MMA and SDMA NMR methyl signals in d_6-DMSO show that MMA and SDMA methyl resonances can be resolved (n=3).

(D) Protein ArgMet quantification of human cell lysates (n=4-5; mean ± SD; n.d. - not detectable). ADMA levels in relation to the total amount of arginine are indicated. Spectral overlays of characteristic ADMA and MMA/SDMA NMR methyl signals are shown (n=4).

(E) Spectral overlays of characteristic MMA and SDMA NMR methyl signals in d_6-DMSO show that MMA and SDMA methyl resonances can be resolved (n=3). In A, B and D, the ADMA concentrations are indicated relative to the total amount of arginine. Spectral overlays of characteristic ADMA (orange) and MMA/SDMA (blue) NMR methyl signals are shown as shaded regions (n=4-5).

3.5.3 NMR reveals modulation and dynamics of protein ArgMet

Although it has taken 50 years to acknowledge the significance of PRMTs in cancer, the pace at which major discoveries have been made in recent years is phenomenal. Disruption of ADMA modification at key substrates decreases the metastatic and proliferative ability of cancer cells (190), suggesting that PRMT inhibitors may be an effective strategy to combat different types of cancer. Several PRMT inhibitors have entered or are on the verge of entering the clinic, but how they alter global protein ArgMet levels remains to be uncovered.

Since our method provides a direct read-out of ArgMet modulation by PRMT inhibitors, we characterized ArgMet concentrations under distinct conditions of PRMT inhibition (**Figures 7A** and **B**). We first tested the impact of the commonly used general ArgMet inhibitor adenosine dialdehyde (AdOx) and the type I PRMT inhibitor MS023 (12, 73, 196). In line with our hypothesis, AdOx unselectively, though incompletely, reduced any kind of protein ArgMet significantly by ~60% ($p<0.0001$). As expected for a selective type I PRMT inhibitor, MS023 inhibited mostly ADMA, but not SDMA formation. PRMT5, the major enzyme catalysing the formation of SDMA, has been implicated in cancer biology, and controls expression of both tumour-suppressive and tumour-promoting genes (12). Inhibition of PRMT5 by the small-molecule compounds GSK3203591 or GSK3326595 has been reported to act anti-proliferatively on mantle cell lymphoma, both *in vivo* and *in vitro* (73, 74). Moreover, GSK3368715, a reversible type I PRMT inhibitor, exhibited anti-tumour effects in human cancer models and is currently in phase I clinical trials **(12)**. GSK3203591 and GSK3368715 have been reported to synergistically inhibit tumour growth *in vivo*, possibly through a tumour-specific accumulation of 2-methylthioadenosine, an endogenous inhibitor of PRMT5, which correlates with sensitivity to GSK3368715 in cell lines **(197)**. In agreement, GSK3368715 inhibited formation of ADMA, but not SDMA formation (**Figure S3A**), whereas GSK3203591 inhibited generation of MMA/SDMA but not of ADMA. These results were further validated by reverse-HPLC (**Figure S3B**). Compared to all other conditions tested, a combination of GSK3203591 and GSK3368715 showed the strongest inhibition of any type of ArgMet in HeLa cells. Interestingly, inhibition of type I PRMTs by MS023 or GSK3368715 doubled the levels of SDMA/MMA, suggesting that, on a global scale, several type I PRMT targets become symmetrically instead of asymmetrically dimethylated. Accordingly,

recent Western blotting experiments resulted in increased MMA/SDMA levels after treatment with PRMT1 inhibitors (61, 197, 198). Comparable results in other cell lines demonstrated that the mechanisms of ArgMet inhibition are independent of the cell line (**Figures S3C** and **D**).

One of the main goals of current ArgMet research is to further refine our mechanistic understanding of ArgMet and how this process is coupled with metabolism. PRMTs add methyl groups to arginine residues using the universal methyl-donor SAM, which is recycled through one-carbon metabolism (168, 199). Methionine is a key substrate for SAM production. Beyond the single-carbon metabolic pathway, additional metabolites can alter global cellular ArgMet by modulating the SAM levels and recycling. Indeed, considering that methionine is an essential amino acid and its recycling can therefore only partly contribute to the methionine pool required for SAM generation, deprivation of methionine strongly reduced the concentrations of ADMA and MMA/SDMA in HeLa cells (**Figures 7C** and **D**). Production of SAM requires ATP, and its recycling via S-adenosyl-homocysteine depends on supply of the single-carbon building block from serine (168). In cancer cells, glutamine can provide both the single-carbon building block through gluconeogenesis and energy through the tricarboxylic acid cycle, respectively. Thus, we tested in HeLa cells if depletion of glutamine reduced the overall levels of protein ArgMet. In line with our hypothesis, concentrations of ADMA and SDMA/MMA were reduced, although not as profoundly as in the case of methionine withdrawal. Glycine supplementation has been proposed to mimic the effects of methionine deprivation through inhibition of the serine-to-glycine conversion that otherwise provides the single-carbon building block for SAM recycling (200). In contrast to these studies, we observed even an increase in ADMA when cells were incubated with 2 mM glycine (**Figure 7C**). Taken together, ArgMet-NMR provides a toolbox for future studies of protein ArgMet regulation by inhibitors and metabolites.

Dynamics of arginine methylation and demethylation is one of the yet unsolved and controversial questions in the field (12). Several enzymes have been reported to act as demethylases. Peptidylarginine deiminase 4 (PAD4) might ‘demethylate’ proteins by converting methylated arginine to citrulline (201). The Jumonji domain-containing 6 (JMJD6) protein has been reported to demethylate arginine in histone tails (202). Nevertheless, both demethylation pathways remain controversial.

We therefore addressed the dynamics of re-methylation in a low-ArgMet background. We treated cells with medium supplemented with AdOx to reduce ArgMet, then exchanged the medium to AdOx-free medium and collected cells at different time points. We found that levels of ArgMet recovered slowly after AdOx removal, with ADMA having a half-life of > 11 hours (**Figure 7E**). As this process might have been affected by the levels of AdOx decreasing slowly inside the cell, we further validated the changes in ArgMet concentrations using methionine deprivation. Under these conditions, levels of protein ArgMet decreased considerably (~60%), with half-lives of 45 and 40 hours for ADMA and MMA/SDMA, respectively (**Figure 7F**). Although these alterations are strongly coupled to the dynamics of the cellular pool of methionine, our results indicate that de-methylation of methylated arginine residues is a slow process and that the available levels of methionine are insufficient to maintain the methylation levels over a longer period of time.

To monitor the dynamics of ArgMet in the absence of any interferences due to the manipulation of metabolic pathways, we combined ArgMet-NMR with stable isotope tracing using ^{13}C-methyl-labelled methionine. With methionine being an essential substrate for SAM production, we next examined whether the methyl group crucial for ArgMet is donated by methionine and investigated the dynamics of the associated methylation reaction. To track and quantify *de novo* ArgMet, we pulsed HeLa cells in media with ^{13}C-methyl-labelled methionine and chased its appearance by the decay of the ^{12}C-methyl NMR signals upon exchange with media containing ^{13}C-methyl labelled methionine (**Figures 7G** and **H**). Coupled with the decrease of ^{12}C protein ArgMet, 'newly' synthesized and ^{13}C isotopically labelled protein ArgMet appears (**Figure 7H**). Fitted half-lives of de-methylation (^{12}C-decay) and *de novo* methylation (^{13}C-increase) were in excellent agreement and approximately 18-19 and 34-37 hours for ADMA and MMA/SDMA, respectively. In line with the AdOx removal and methionine deprivation changes, these data indicate that the overall dynamics of arginine demethylation are slow.

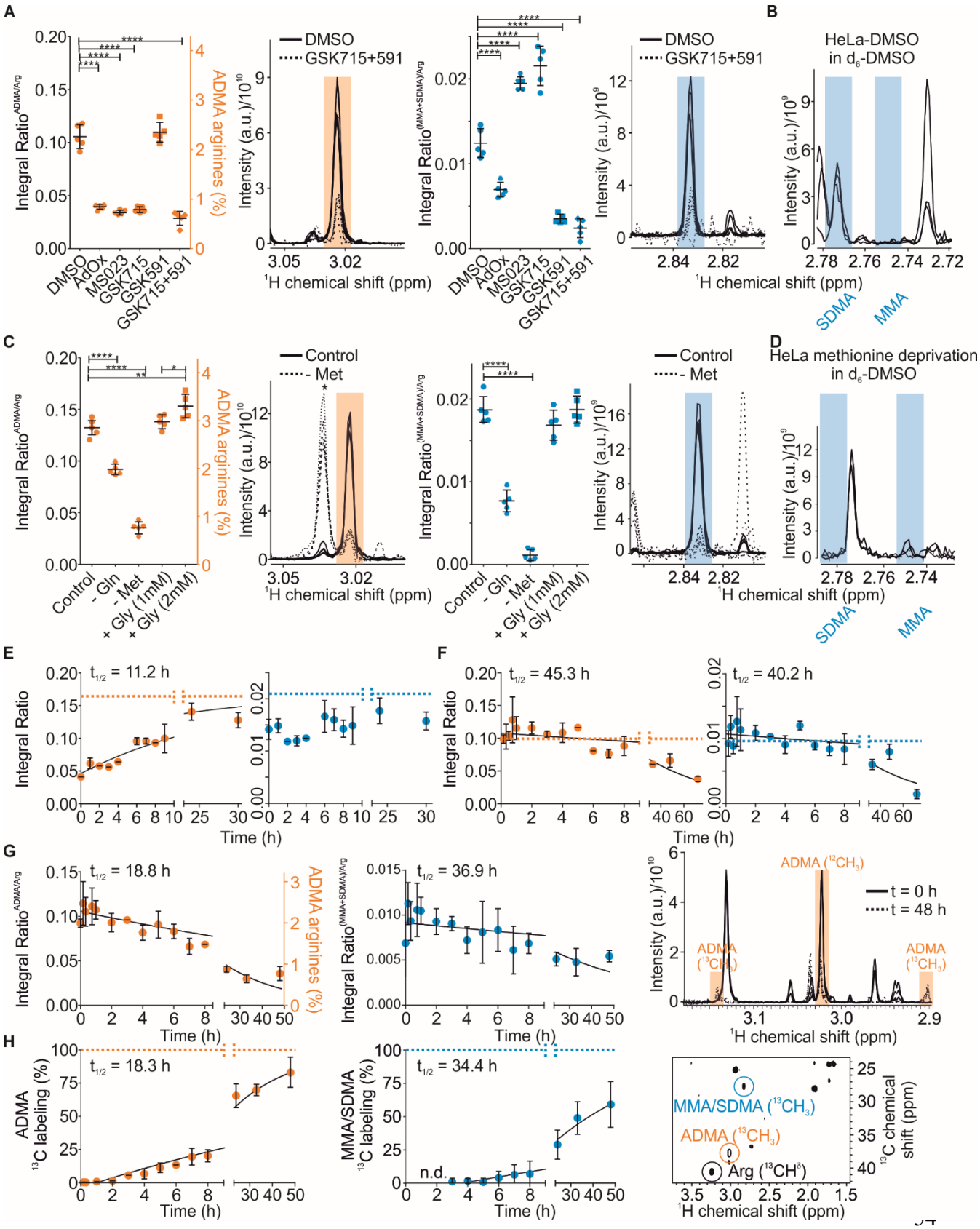
A
B
C
D
E
F
G
H
DMSO
GSK715+591
Control
- Met
HeLa-DMSO
in d6-DMSO
HeLa methionine deprivation
in d6-DMSO
SDMA
MMA
Integral Ratio ADMA/Arg
ADMA arginines (%)
Intensity (a.u.)/10^10
Intensity (a.u.)/10^9
1H chemical shift (ppm)
Integral Ratio (MMA+SDMA)/Arg
DMSO
AdOx
MS023
GSK715
GSK591
GSK715+591
Control
- Gln
- Met
+ Gly (1mM)
+ Gly (2mM)
t1/2 = 11.2 h
t1/2 = 45.3 h
t1/2 = 40.2 h
t1/2 = 18.8 h
t1/2 = 36.9 h
t1/2 = 18.3 h
t1/2 = 34.4 h
n.d.
Time (h)
ADMA (13CH3)
t = 0 h
t = 48 h
MMA/SDMA (13CH3)
Arg (13CH8)
13C chemical shift (ppm)
ADMA labeling (%)
MMA/SDMA labeling (%)

Figure 7. NMR enables quantification of protein ArgMet modulation and dynamics.

(A) Protein ArgMet quantification of HeLa cells treated for 3 days with either DMSO, 40 µM adenosine dialdehyde (AdOx), 10 µM MS023, 2 µM GSK3368715 (GSK715), 1 µM GSK3203591 (GSK591), or a combination of 2 µM GSK715 and 1 µM GSK591 (n=5; mean ± SD). ADMA levels in relation to the total amount of arginine are indicated. Spectral overlays of characteristic ADMA (orange) and MMA/SDMA (blue) NMR methyl signals are shown as shaded regions (n=5).

(B) Spectral overlays of characteristic MMA and SDMA NMR methyl signals in d_6-DMSO show that MMA and SDMA methyl resonances can be resolved (n=3). Shaded regions represent characteristic regions of MMA and SDMA (blue) methyl groups.

(C) Protein ArgMet quantification of HeLa cells cultured with or without 4 mM glutamine (Gln), 0.2 mM methionine (Met) or glycine (1 mM and 2 mM Gly) (n=5; mean ± SD). ADMA levels in relation to the total amount of arginine are shown. Spectral overlays of characteristic ADMA (orange) and MMA/SDMA (blue) NMR methyl signals are presented as shaded regions (n=5). (Unmethylated lysines are labelled with asterisks.)

(D) Spectral overlays of characteristic MMA and SDMA NMR methyl signals in d_6-DMSO show that SDMA levels strongly decrease upon methionine deprivation (n=3).

(E) Changes of ArgMet levels after removal of AdOx. Prior to removal of AdOx, HeLa cells were treated with AdOx for 3 days to reduce ArgMet. Integral ratios of ADMA/arginine (orange) and (SDMA+MMA)/arginine (blue) are plotted as mean ± standard error (n=3) for each time point. To estimate the half-life of ArgMet recovery ($t_{1/2}$) the data were fitted using a single exponential recovery function (95% CI: 7.5-19.9 h). Dotted lines indicate the level of methylation in the absence of AdOx.

(F) Changes of ArgMet levels after methionine removal. Integral ratios of ADMA/arginine (orange) and (SDMA+MMA)/arginine (blue) are plotted as mean ± standard error (n=3) for each time point. To estimate the half-life of ArgMet decay ($t_{1/2}$) the data were fitted using a single exponential decay function (ADMA/arginine - 95% CI: 34.0-62.7 h; (SDMA+MMA)/arginine - 95% CI: 27.8-61.1 h). Dotted lines indicate the level of methylation in the presence of methionine.

(G) Dynamics of *de novo* ArgMet via ^{13}C labelling are shown as decay of the ^{12}C-methyl NMR signals upon exchange of media containing ^{13}C-methyl-labelled methionine. Integral ratios of ADMA/arginine (orange) and (SDMA+MMA)/arginine (blue) are plotted as mean ± standard error (n=3) for each time point. To estimate the half-life of ArgMet ^{12}C-methyl signal decay ($t_{1/2}$), the data were fitted using a single exponential decay function (ADMA/arginine, 95% CI: 14.4-24.7; (SDMA+MMA)/arginine, 95% CI:21.9-73.8). Change of ADMA $^{12}C/^{13}C$-methyl signals at the beginning and after 48 h of cultivation in presence of ^{13}C-methyl-labelled methionine (^1H 1D projections of 2D J-resolved NMR spectra).

(H) Dynamics of *de novo* ArgMet via ^{13}C labelling are shown as increase of the ^{13}C-methyl NMR signals detected in $^{1}H,^{13}C$ HSQC NMR spectra upon exchange of media containing ^{13}C-methyl-labelled methionine. Fractions of ^{13}C-labeling are plotted as mean ± standard error (n=3) for each time point. To estimate the half-life of ArgMet ^{13}C-methyl labelling ($t_{1/2}$), the data were fitted using a one phase association function (ADMA/arginine, 95% CI: 16.4-21.2; (SDMA+MMA)/arginine, 95% CI:27.4-43.5). Arginine (black), ADMA (orange), MMA, and SDMA (blue) $^{1}H,^{13}C$ NMR signals are labelled in a representative $^{1}H,^{13}C$ HSQC NMR spectrum.

3.5.4 NMR provides insights into dynamics of ArgMet in organoids and tissues

Increasing evidence suggests that ArgMet is required to maintain cells in a proliferative state and plays a key role in the homeostasis of stem cell pools (5). In addition, the role of PRMTs has been associated with cell growth, differentiation, apoptosis and ageing (5, 12, 31). For example, depletion and exhaustion of muscle and hematopoietic stem cells in adulthood was linked to loss of ArgMet (54, 203). In addition, PRMTs play important regulatory roles in the differentiation of myeloid cells (204). To study the relationship of ArgMet and *in vitro* differentiation in a controlled manner, we generated cell type-enriched mouse small intestinal organoid cultures. We grew the organoids in complete ENR medium (EGF, Noggin, R-Spondin) as reference. In ENR medium, organoids contain stem cells, enterocytes and Paneth cells (roughly 15%, 80%, 5%, respectively). Stem cells, enterocytes and Paneth cells were enriched using media supplemented with Wnt-CM (conditioned medium)/valproic acid (VPA; stem cells enriched), removal of R-Spondin (EN; enterocytes enriched), or supplementation of Wnt-CM/N-[N-(3,5-difluorophenacetyl)-L-alanyl*]-S-phenylglycine t-butyl ester) (DAPT; Paneth cells enriched), respectively. Our data show alterations of ADMA and MMA/SDMA dependent on organoid composition (**Figure 8A**). In line with a high expression of PRMTs in stem cells found in single-cell mRNA sequencing of mouse small intestine (205-207) (**Figure S4A-C**, http://www.proteinatlas.org/), reference organoids (ENR) show higher ADMA and MMA/SDMA. Enrichment of Paneth cells in organoids (DAPT) results in a strong decrease in overall ArgMet, in line with a low expression of PRMTs in Paneth cells (**Figure S4A-C**). However, it remains to be investigated whether ArgMet is a cause or consequence of differentiation and to elucidate the key regulatory and metabolic mechanisms modulating ArgMet during differentiation.

Studying the global levels of ArgMet *in vivo* is the ultimate goal to reveal the mechanistic links between ArgMet and (patho)physiology. To demonstrate the feasibility of our approach for *in vivo* studies, we characterised ArgMet levels in commonly studied mouse tissues (brain, heart, kidney, liver, spleen and lung) in two groups of female wild-type mice (mixed background of 129/J and C57BL/6J) at young (9-11 weeks) and old (96-104 weeks) age. Strikingly, we observed varying levels of ADMA and MMA/SDMA among tissues, with highest levels of ArgMet in brain and spleen of young mice (**Figure 8B**). Recent studies revealed high expression of PRMT1 in the rat spleen and a high expression of PRMT5 in the rat brain (208), substantiating our findings of high ADMA in the spleen and high MMA/SDMA in the brain. Moreover, PRMT1 and PRMT8 expressions were elevated in mouse brain compared to liver (209). The PRMT7 mRNA expression in the spleen in old mice was markedly reduced (**Figure S4H**), consistent with the decreased ArgMet level in old mice. However, overall PRMT mRNA expression levels were not associated with protein ArgMet level in the tissues tested (**Figure S4D-I**). With the exception of brain and spleen, we observed no significant ageing-related changes in ArgMet levels in any other tissues. Expression and catalytic activity of PRMT1, PRMT4, PRMT5, and PRMT6 have been reported to be reduced in replicatively senescent cells relative to young cells (56, 210). In addition, senescent cells accumulate in tissues with age along with a decline in immune function (211). Although the underlying molecular mechanisms remain elusive, one might speculate that the changes in the aged spleen are caused by the accumulation of senescent cells.

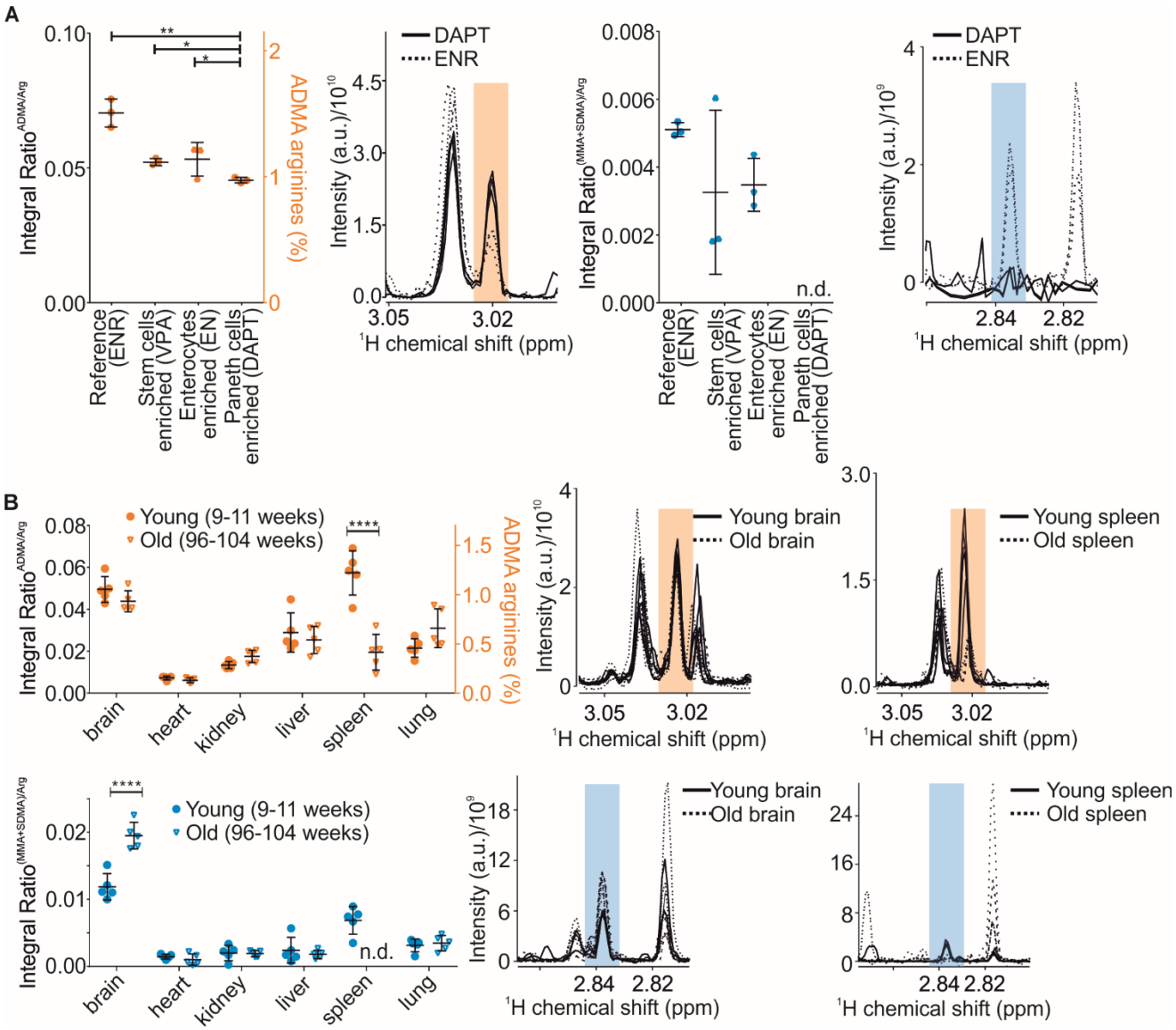

Figure 8. NMR enables characterization of ArgMet in cell differentiation and ageing *in vivo*.

(A) Protein ArgMet quantification of mouse small intestinal organoids cultured with EGF/Noggin/R-spondin1 (ENR), EGF/Noggin (EN), ENR plus valproic acid (VPA), or ENR plus Notch pathway inhibitor DAPT (N-[N-(3, 5-difluorophenacetyl)-L-alanyl*]-S-phenylglycine t-butyl ester) (n = 3; mean ± SD). ADMA levels are presented with respect to total amounts of arginine. Spectral overlays of characteristic ADMA (orange) and MMA/SDMA (blue) NMR methyl signals are shown as shaded regions (n=3).

(B) Quantification of protein ArgMet in mouse tissues collected from young (9-11 weeks, dots) and old mice (96-104 weeks, triangles) (n=5; mean ± SD). ADMA levels are presented with respect to total amounts of arginine.

Spectral overlays of characteristic ADMA (orange) and MMA/SDMA (blue) NMR methyl signals are shown as shaded regions (n=3).

3.6 Discussion

Protein ArgMet modulates the physicochemical properties of proteins and thus plays a major role in a multitude of regulatory pathways, including gene regulation, signal transduction, regulation of apoptosis and DNA repair (5, 12, 31). Although previous studies exist in this field, the lack of a reliable quantification of ArgMet is a restricting factor in elucidating the relevance of ArgMet in physiological and pathological processes. We have developed a simple, fast and robust protocol for NMR-based quantification of protein ArgMet levels and dynamics in purified proteins, cells, organoids and tissues. Our study reveals that NMR spectroscopy provides a sensitive read-out for detection and quantification of MMA, ADMA and SDMA in all matrices tested. We show that ArgMet-NMR enables detection of methylation patterns in purified proteins incubated with PRMT1. Methylation by PRMTs in the human proteome occurs preferentially (but not exclusively) within glycine-arginine- and proline-glycine-methionine-rich regions (1, 22, 212), but specific consensus sequences targeted by most of the human PRMTs remain to be identified. Our approach provides a toolbox for fast and label-free screening for PRMT selectivity in purified proteins/peptides, complementary to peptide arrays (213) and mass spectrometry (18). The limitations of our study are that distinguishing of MMA from SDMA requires an additional analysis step, and that our protocol does not provide site-specific information.

Although some of human PRMTs are well-studied, it is yet unknown for a plethora of PRMTs from other organisms whether they exhibit any enzymatic activity (214). For example, the main yeast methyltransferase is Hmt1, the presumable ortholog of human PRMT1. In addition, *in silico* studies have predicted 33 additional putative methyltransferases in *S. cerevisiae,* and it is likely that beside nucleic acid methyltransferases, and protein methyltransferases specific to other amino acids, also arginine methyltransferases are among them (215). We found that *S. cerevisiae* produces ADMA and MMA, but no SDMA, in line with a previous report (216). Strikingly, deletion of *Hmt1* led to a complete loss of ADMA and MMA, suggesting that the contribution of any other methyltransferase to global levels of ArgMet are negligible, at least in this yeast strain. However, we cannot exclude the possibility that the other putative methyltransferases methylate only a small subset of targets, resulting in low global ArgMet levels. Our proof-of-principle analysis in human cell lines identified a large fraction of arginine residues in a methylated state, ranging from 1 to

3.4%. In all cell lines tested, ADMA constituted the predominant methylated arginine species, followed by SDMA with about 10% and MMA with about 1% of ADMA. These ADMA levels are in agreement with the findings that PRMT1 is the predominant and most active PRMT present in mammalian cells (217). Screening the PhosphoSitePlus(R) database of PTMs for ArgMet revealed that for 1.7% of all arginines in human proteins methylation (ADMA, SDMA or MMA) has been reported. Given that we identified between a methylation status of 1 and 3.4% of arginines to be methylated indicates that most of the proteins for which ArgMet has been reported are entirely methylated. Note that this estimation assumes that all proteins are present at comparable levels inside the cell (13). Methylarginines are predominantly found in intrinsically disordered protein regions, e.g. RG/RGG regions, which are intimately connected to LLPS (8, 12, 212). A large proportion of the proteins implicated in LLPS are known targets for ArgMet, and therefore LLPS could be regulated by their ArgMet (8, 12, 25). Thus, it is conceivable that the global ArgMet levels regulate LLPS on a global scale *in vivo* by regulating fluidity and dynamics of membrane-less organelles containing e.g. RG/RGG proteins.

By comparing the methylation levels in cell lines, ArgMet were up to 3-fold higher in immortalized and cancer cells compared to primary cells. Strikingly, cells isolated from human metastases contained the highest levels of protein ArgMet. The increased ArgMet levels found in cancer cells are in line with overexpression of PRMT1 in human melanoma, breast and prostate cancer (29, 218). In addition, PRMT5 expression and activity seem to be important in tumorigenesis and are markers of poor clinical outcome (219). Based on the observation that increased PRMT expression is associated with tumour growth, inhibitors of protein arginine methyltransferases have been developed and showed promising results in clinical studies (https://clinicaltrials.gov). Our study demonstrates that ArgMet-NMR provides a precise and specific read-out for modulation of ArgMet levels in cells treated with distinct (specific) PRMT inhibitors. This suggests that ArgMet-NMR might be a valuable tool for ArgMet-based drug discovery, drug validation and patient stratification in the future.

By examining the modulation of ArgMet levels upon metabolite deprivation in cells, we detected a tight metabolic regulation of ArgMet levels by methionine, glutamine and glycine. Methionine is required for protein synthesis and its adenylation produces SAM, which serves in turn as a methyl

donor for methylation reactions (168, 169). Accordingly, we demonstrated that methionine deprivation had a strong impact on protein ArgMet by reducing ADMA, MMA and SDMA by more than 61%. Given that methionine is an essential amino acid whose levels are dictated by dietary factors (220), it is conceivable that nutrition and fasting could, in addition to protein synthesis, additionally affect protein ArgMet *in vivo*. Moreover, glutamine deprivation in HeLa cells culture reduced protein ArgMet by more than 30%, corroborating the observation that glutamine is a key energy source in cancer cells and can provide the single-carbon building block for SAM recycling through gluconeogenesis (221). Glutamine plays a pleiotropic role in cellular function and its consumption is elevated in proliferating cells not only due to increased DNA production (222, 223), but also for maintaining high ArgMet levels. Notably, ArgMet requires an energy demand of 12 molecules of ATP per methylation event (224). Thus, reduced energy supply by glutamine deprivation could be the major factor of the observed reduction in protein ArgMet. Glycine is an interesting metabolite due to its role in SAM recycling and methionine clearance. On the one hand, glycine can act as methyl group acceptor, leading to the formation of sarcosine (N-methylglycine) and S-adenosylhomocysteine. On the other hand, glycine is converted when the single-carbon block is transferred to tetrahydrofolate, which in turn is used to recycle SAM (168, 199, 225). Excess glycine has been proposed to reduce methionine levels and to mimic methionine deprivation (200). According to our findings but in contrast to previous studies, glycine supplementation failed to reduce global levels of protein ArgMet. The fact that glycine supplementation did not alter methionine levels in adult worms (226) suggests that under physiological conditions glycine supplementation is not generally applicable to mimic methionine deprivation in cancer cells. Our approach is expected to substantiate specific aspects of protein methylation research in the future. Moreover, it will be interesting to reveal whether lifespan extension via methionine restriction is mediated via modulation in ArgMet (227-229).

Dynamics of cellular protein ArgMet, the process of methylation and the process of ‘demethylation’, can also be easily examined by our methodology. The existence of an efficient arginine demethylase has not yet been proven and is a long-disputed question in this field (230). Our results obtained using different setups of re-methylation after treatment with the general methylation inhibitor AdOx and ‘demethylation’ upon methionine deprivation show that global arginine (de)methylation is a slowly developing process in a cellular context. We further

substantiated these findings by combining ArgMet-NMR with stable isotope tracing using ^{13}C-methyl-labelled methionine. A decrease of the NMR signal characteristic for unlabelled methylated arginine residues in combination with an increase of the NMR signal characteristic for ^{13}C-methylated arginines indicated that both *de novo* ArgMet and 'demethylation' are slow processes, especially in comparison to phosphorylation and de-phosphorylation. For example, global phosphorylation of the epidermal growth factor receptor occurs within 2–3 hours with a half-life of approximately 30 min, whereas its intracellular domain is dephosphorylated considerably faster ($t_{1/2}$ = 15 s) (231). We therefore conclude that no efficient demethylase exists that affects global methylation levels in HeLa cells. Whether demethylation affects specific targets rather than the global ArgMet levels remains to be investigated.

We observed even in mouse tissues a large fraction of arginines being methylated with brain and spleen showing the highest ArgMet levels. In line with the specific pattern of ADMA, SDMA and MMA observed in cells, ADMA was the most abundant methylated species, followed by SDMA and MMA. During ageing of mice, levels of protein ArgMet changed drastically in brain and spleen proteins, whereas other tissues, such as heart, liver and kidney, were less affected. The spleen is among the most affected organs during ageing, and a link to the accumulation of senescent cells has been hypothesised (56, 210). Thus, it is conceivable that the loss of protein ArgMet is associated with loss of PRMT1 expression/activity under physiological conditions, as demonstrated by a recent study linking PRMT1 downregulation with senescence of neuroblastoma cells (232). High levels of protein ArgMet in spleen and a strong reduction during ageing raises the question whether accelerated ageing of the spleen could be an inevitable side effect of the aforementioned protein arginine methyltransferase inhibitors. First links between ArgMet and neurodegenerative diseases have been suggested as hypomethylated RNA-binding proteins FUS and poly-GR dipeptide repeats were found to be enriched in patients with frontotemporal dementia or amyotrophic lateral sclerosis, respectively (233-235). Given the globally reduced levels of SDMA/MMA in the brain of old mice, it will be interesting to investigate whether ArgMet is associated with risks of neurodegenerative diseases, for example through modulation of LLPS of RNA-binding proteins.

Taken together, our findings support the idea that (i) protein ArgMet is a highly abundant PTM in cells and tissues, (ii) ArgMet and specific aspects of metabolism are tightly coupled, (iii) demethylation is a slow process, and (iv) cancer and ageing lead to substantial changes in global ArgMet levels. Given its relatively high proportion, we hypothesise that ArgMet plays a key role in maintaining cellular homeostasis, e.g. by regulating LLPS and formation of membrane-less organelles on a global scale. Concentrations of ADMA, SDMA and MMA in proteins might be used as biomarkers for drug discovery, treatment response and (potentially) for diagnosis of tumour susceptibility for arginine methyltransferase inhibitors. These findings could lead to the development of improved methods for basic research on ArgMet and implementing routine ArgMet-based screening in the clinic.

Limitations of the study

Despite the qualitative and quantitative information gathered by using our ArgMet-NMR protocol, some limitations to this study exist. With this assay, the detection limit for ADMA was approximately 100 nM (Figure S1H), and a saturation level of the SPE column of 3 mM arginine has been observed (Figure S1I). Thus, more material might be necessary for samples with low ArgMet content. Our method relies on sample clean-up by SPE using cation-exchange columns, which leads to a loss of some acidic and neutral amino acids and derivatives thereof. Distinguishing MMA from SDMA requires an additional analysis step using DMSO as solvent. In contrast to proteomics-based methods, our protocol does not provide site-specific ArgMet information. Nevertheless, our method could be combined with peptide-based libraries to evaluate sequence specific ArgMet mediated by PRMTs in vitro. Our protocol provides insight into changes in ArgMet levels related to cancers, cell differentiation, and aging. However, whether ArgMet is a cause or consequence in these contexts requires further studies in the future.

3.7 Acknowledgements

The work was supported by Austrian Science Fund (FWF) grants P28854, I3792, doc.funds BioMolStruct DOC 130 and DK-MCD W1226 to T.M. and FWF grant P30162 to U.S.; T.M. was supported by the Austrian Research Promotion Agency (FFG) Grants 864690 and 870454; the Integrative Metabolism Research Center Graz; Austrian Infrastructure Program 2016/2017, the Styrian Government (Zukunftsfonds), and BioTechMed-Graz (Flagship project DYNIMO). D.K.

was supported by the FWF (SFB F73, W1226, P32400, P30882, DP-iDP DOC 31), the BioTechMed-Graz flagship project “Lipases and Lipid Signaling”, the County of Styria, and the City of Graz. We thank the Center of Medical Research for access to cell culture facilities and Arno Absenger and Isabella Hindler for mouse care. F.Z. was trained within the frame of the PhD program Molecular Medicine, Medical University of Graz.

3.8 Contributions

Conceptualization, T.M.;

methodology, F.Z., J.K.K., A.A., M.K., A.M., A.P., K.B.K., N.V., S.F., E.J-L., G.H., M.P., M.R.C, M.P., E.J.L., M.M;

software, F.Z., T.M.;

validation, F.Z., T.M., A.M., A. P.;

formal analysis, F.Z., T.M.;

investigation, F.Z., T.M.;

resources, T.M., G.H., E.S., D.K., U.S.;

data curation, F.Z., T.M.;

writing—original draft preparation, F.Z., T.M.;

writing—review and editing, F.Z., J.K.K., A.A., M.K., K.B.K., N.V., T.M., N.V., E.S., G.H. D.K., U.S., M.R.C., B.B., T.E., B.R., B.P., M.P., M.M., A.M., A.P.;

visualization, T.M., F.Z.;

supervision, T.M.;

project administration, T.M.;

funding acquisition, T.M., D.K, U.S..

All authors have read and agreed to the published version of the manuscript.

Declaration of Interests

The authors declare no competing interests.

3.9 STAR METHODS

RESOURCE AVAILABILITY

Lead contact

Further information and requests for resources and reagents should be directed to and will be fulfilled by the Lead Contact, Tobias Madl (tobias.madl@medunigraz.at).

Materials availability

This study did not generate new unique reagents.

Data and code availability

This study did not generate computer algorithm or code.

EXPERIMENTAL MODEL AND SUBJECT DETAILS

Cell lines and culture conditions

MDA-MB-231 (Sigma Aldrich, Vienna, Austria), HaCat (ATCC, US), MCF10A (LGC Promochem, US), A375 (ATCC, US), SW-872 (ATCC, US), 93T449 (ATCC, US), SW1353 (CLS, Germany) and juvenile fibroblasts fresh established from foreskin samples were obtained from Division of Biomedical Research (BMF), Medical University of Graz, Austria. HeLa (ATCC®, Guernsey, UK), fibroblast, HaCat, SW1353 and A375 cells were cultured in DMEM supplemented with 2 mM glutamine, 1% PS (100 U/mL penicillin, 100 µg/mL streptomycin) and 10% fetal bovine serum (FBS). MCF10A were cultured in DMEM with single quot kit suppl. Gr, 5% Horse Serum, 20 ng/mL hEGF, 0.5 µg/ml hydrocortison, 100 ng/ml choleratoxin, 10 µg/ml insulin and 2 mM glutamine. MDA-MB-231 were maintained in DMEM Hams F12 with 10% FBS, 2 mM glutamine and 1% PS. SW872 were cultured in DMEM Hams F12 supplemented with 5% FBS, 2 mM glutamine and 1% PS. 93T449 were cultured with RPMI-1640 with 10% FBS, 2 mM glutamine, 10mM 4-(2-hydroxyethyl)-1-piperazineethanesulfonic acid (HEPES), 1mM sodium pyruvate and 1% PS.

Cells were maintained in a humidified incubator at 37°C with 5% CO_2. HeLa cells were treated for up to 3 days with AdOx (40 µM), MS023 (10 µM), GSK715 (2 µM), GSK591 (1 µM) and DMSO, before cell extracts were prepared.

Yeast strain and culture conditions

Yeast experiments were carried out in *S. cerevisiae* BY4741 (*MATa his3Δ-1 leu2 Δ -0 met15 Δ -0 ura3 Δ -0*) and BY4742 (*MATa his3Δ -1 leu2Δ -0 lys2Δ -0 ura3Δ-0*) wild type yeast (236) and the same strains carrying either an *HMT1*-knockout (*hmt1*:kanMX4), or *HSL7*-knockout (*hsl7*:kanMX4) all obtained from Euroscarf. Correct presence of respective gene knockouts was verified by PCR using forward primers 5'-TGAAGACATCCCATGTCCAG-3' (HMT1_up), 5'-TGAATGCTACTGATGTCTGC-3' (HSL7_up), and reverse primer 5'-CAAGACTGTCAAGGAGGG- 3' (KanR5b). Cells were grown to logarithmic phase in SC 2% glucose medium consisting of 0.14% yeast nitrogen base (BD Difco™, 233520), 5% $(NH_4)_2SO_4$ supplemented with 30 mg/L of all amino acids (except 80 mg/L histidine, 200 mg/L leucine, 120 mg/L lysine and 26 mg/L methionine), 30 mg/L adenine, and 320 mg/L uracil, allowing comparable growth of both BY4741 and BY4742 strains. Fresh overnight cultures were diluted to 0.1 OD600 (Genesys 10uv photometer, corresponds to ~2×10^6 cells/mL), incubated for 6 h at 28 °C, 145 rpm, to reach logarithmic growth phase at a culture density of ~0.6 OD600. 15 OD600 equivalents were harvested by centrifugation (1,700 g, 3 min, 4 °C), washed once with 10 ml ice-cold water, and the cell pellet was immediately snap frozen in liquid nitrogen and stored at -80 °C until processing for NMR analysis.

Organoid culture

Mouse small intestinal organoids were cultured as described previously (237). In short, the organoids were maintained using basic culture (ENR) medium, which contained advanced DMEM/F12 supplemented with penicillin/streptomycin (1%, 10 mM HEPES, 1× Glutamax, 1× B27 (all from Life Technologies) and 1 mM N-acetylcysteine (Sigma) supplemented with murine recombinant epidermal growth factor (Peprotech), R-spondin1-CM (5% v/v) and noggin-CM (10% v/v). A mycoplasma-free status was confirmed routinely. Organoids were split every 4–5 days by mechanical disruption and plated in Matrigel. Three days after splitting, stem cell-enriched organoid cultures (CV) were generated by supplementation of ENR with CHIR99021 (3 μM) and valproic acid (1 mM). Paneth cell-enriched organoids were generated by addition of Chir (3 μM) and DAPT (5 μM), stem cell-depleted organoid cultures (EN) were grown in ENR medium without R-Spondin-1. Organoids were harvested after 3 days by using mechanical dissociation of matrigel

followed by 3 washing steps with ice-cold PBS. Organoid pellets were immediately frozen at -80°C for further analysis.

Animals and diets

For all experiments, young (9-11 weeks) and old (96-104 weeks) female wild type mice (mixed genetic background of 129/J and C57BL/6J) were used (n=5). Mice were maintained in a clean, temperature-controlled (22 ± 1°C) environment with a regular light–dark cycle (12 h/12 h) and unlimited access to chow diet (Altromin 1324, Altromin Spezialfutter GmbH, Lage, Germany) and water. All experiments were performed in accordance with the European Directive 2010/63/EU and approved by the Austrian Federal Ministry of Education, Science and Research (GZ 66.010/0051-WF/V/3b/2015).

METHOD DETAILS

***In vitro* methylation assay**

The recombinant CIRBP-RGG and FUS-RGG-PY sequences were as follows: RSRGYRGGSAGGRGFFRGGRGRGRGFSRGGGDRGYGG and GPGGGPGGSHMGGNYGDDRRGGRGGYDRGGYRGRGGDRGGFRGGRGGGDRGGFGPG KMDSRGEHRQDRRERPY. Expression and purification of recombinant His_6-PRMT1, His_6-CIRBP-RGG and His_6-FUS-RGG-PY have been described in previous study (27, 238). Untagged CIRBP-RGG and FUS-RGG-PY recombinant proteins and His_6-PRMT1 were equilibrated in methylation buffer containing 50 mM Tris-HCl, 150 mM NaCl, and 2 mM Tris(2-carboxyethyl)phosphine, pH 7.5; 100 µM CIRBP-RGG or FUS-RGG-PY was incubated with 10 µM His_6-PRMT1 in the presence of 2 mM S-Adenosylmethionine (New England Biolabs) for 16 h at room temperature. Untagged methylated CIRBPRGG (meCIRBP) and FUS-RGG-PY (meFUS) were then isolated from PRMT1 performing a second affinity purification using Ni-NTA beads, and further analyzed using NMR**.**

Sample preparation

Cells (5 x 10^6) were plated onto 60 mm dishes and incubated under standard conditions as described above. To harvest the cells, medium was removed, cells were washed three times with 5 ml of cold phosphate-buffered saline (PBS, 137 mM NaCl, 2.7 mM KCl, 8 mM Na_2HPO_4, and 2 mM KH_2PO_4)

solution and collected using a cell scraper. A solution of 5×10^6 cells was centrifuged at 1,000 rpm for 1 min, the supernatant was discarded and the cell pellet was flash frozen in liquid nitrogen and stored at -80°C for the extraction step. The organs were isolated from sacrificed mice, divided into 20–30 mg and snap-frozen in liquid nitrogen for storage at -80°C until extraction. Cell pellets, tissues and mounse intestinal organoids were re-suspended in 400 µl ice-cold methanol (-20°C) and 200 µl MilliQ H_2O and transferred to a tube containing Precellys beads (1.4 mm zirconium oxide beads, Bertin Technologies, Villeurbanne, France) for homogenization on a Precellys 24 homogeniser for 2 cycles of 20 seconds with 5,000 rpm, 10-s breaks. Cell and tissues debris were pelleted by centrifugation at 13,000 rpm for 30 min (4°C) and the precipitate was used for hydrolysis. Supernatants were frozen at -80°C and be used for e.g. metabolite analysis.

The precipitates were hydrolysed with 500 µl 9 M HCl for 12 h at 110°C to obtain (modified) amino acids. The solution was lyophilised and resuspended in 900 µl of 0.1 M HCl and 100 µl chloroform to remove lipids, centrifuged (10 min, 13,000 rpm) and the supernatant subjected to i) solid-phase-extraction (SPE) using Waters™ cartridges (1 ml Oasis MCX 1 cc/30 mg, Waters™, Eschborn, Germany) containing a mixed-mode polymeric sorbent with both reverse phase and cation exchange functionalities. Each step was performed with 1 ml of solution and by centrifugation at room temperature (1,000 rpm for 1 min). ii) auto SPE using Gilson® GX-241 ASPEC system (Gilson Incorporated, Middleton, WI) and Waters™ cartridges. The flow rate for the injection of liquids was set to 2 ml/min for the sample, 7 ml/min for the replacement solution and the 0.1 M HCl, and to 10 ml/min for methanol, PBS and MilliQ-water. The cartridges were pre-conditioned with a detachment solution (2x 1 ml, 10% NH_3 saturated solution, 40 % MilliQ H_2O, 50 % methanol), methanol (1x 1 ml) and with PBS (2x 1 ml). After sample loading (1x 1 ml), cartridges were washed with MilliQ-water (3x 1 ml), 0.1 M HCl (5x 1 ml) and methanol (2x 1 ml,). The arginine and its derivatives were recovered with the replacement solution (2x 1 ml), lyophylized and dissolved in 500 µl NMR buffer [0.08 M Na_2HPO_4, 5 mM 3-(trimethylsilyl) propionic acid-2,2,3,3-d4 sodium salt (TSP), 0.04 (w/v) % NaN_3 in D_2O, pH adjusted to 7.4 with 8 M HCl and 5 M NaOH] for measuring. The Chromatin Extraction Kit (ab117152, Abcam) was used for HeLa/A375 chromatin and non-chromatin fractions extraction according to the manufacturer's instructions.

NMR measurements and spectral processing

All NMR experiments were acquired at 310 K using Bruker 600 MHz spectrometer equipped with a TXI probe head. The 1D CPMG (Carr–Purcell–Meiboom–Gill) pulse sequence (cpmgpr1d, 512 scans, size of fid 73728, 11904.76 Hz spectral width, recycle delay 4 s), with water signal suppression using presaturation, was recorded for ^{1}H 1D NMR experiments. ^{1}H-^{13}C HSQC (heteronuclear single quantum coherence spectroscopy) NMR spectra were recorded for 13C-methyl labelled methionine assays with a recycle delay of 1.0 s, spectral widths of 20.8228/83.8554 ppm, centered at 3.923/50 ppm in ^{1}H/^{13}C, with 2048 and 256 points, respectively, and 8 scans per increment. The 2D JRES (^{1}H homo-nuclear J-resolved spectroscopy) pulse sequence (jresgpprqf, 16 scans, size of fid 16384 (direct dimension F2)/256 (indirect dimension F1), 10000.00/78.042 Hz spectral width in F2 (chemical shift axis)/F1 (spin-spin coupling axis), recycle delay 2 s, Figure S1J) with presaturation during the relaxation delay was recorded to obtain virtually decoupled spectra (173, 178-180). In brief, data were processed in Bruker Topspin version 4.0.6 using one-dimensional exponential window multiplication of the FID, Fourier transformation and phase correction. Processing of 2D JRES was done using the SINE and QSINE window functions (SSB = 0) in F2/F1. Fourier transform was performed with 16384/256 F2/F1 points of the fid. 2D J-resolved experiments were processed using back prediction implemented in the Bruker au program proc_jres.be (173, 239-241). The JRES spectra were then projected along F2 and exported as 1D NMR spectra.

The ^{1}H 1D projections of 2D J-resolved, virtually decoupled NMR spectra data processing was carried out using MestReNova 12.0.4 software's automatic phase and baseline correction. Calibration was made by using tetramethylsilane (δH = 0). Quantification of arginine, MMA, ADMA and SDMA used integration of characteristic peaks. Calculation of absolute concentrations is based on known concentrations of external standards. The ADMA levels relative to total amounts of arginine are calculated by the formula: ADMA/arginine (%) = (integrals (ADMA)/integrals (arginine)) * (integrals (100µM arginine)/integrals (100µM ADMA)), MMA/arginine (%) = (integrals (MMA)/integrals (arginine)) * (integrals (100µM arginine)/integrals (100µM MMA)).

High performance liquid chromatography (HPLC) assay

To verify the accuracy of NMR results, cell hydrolysates were compared with an established chromatographic method with slight modifications (242). Samples were derivatized with an autosampler by mixing with o-phtalaldehyde solution (1mg/mL in 0.2 M borate puffer pH=9.5 with 0.5% mercaptopropionic acid). After a two-minute incubation, the mixture was injected. Arginine and metabolites were separated on a Chromolith® Performance RP-18e, column 100 x 4.6 mm (Merck, Darmstadt, Germany) with an isocratic mobile phase (flow 2.0 mL/min) consisting of 50 mM KH_2PO_4 pH=6.8 and 6% (v/v) acetonitrile. After 15 min, the column was regenerated for 2 min with a mixture of 50 mM KH_2PO_4 pH=6.5 and 50% (v/v) acetonitrile and reequilibrated before the next injection. The compounds were detected with a fluorescence detector (Agilent 1260 FLD, Santa Clara, CA, USA) at excitation 340 nm and emission 455 nm. Data were acquired on the Agilent Chemstation version B04.03. In contrast to the original protocol, no internal standard was used and the analysis was performed with the standard addition method. Defined concentrations of Arginine, ADMA, SDMA and MMA were added to the hydrolysates and analysed without and with the addition of pure substance. From the differences, the concentrations of the initial concentrations were calculated.

RNA isolation, reverse transcription and real-time PCR

RNA was isolated using TRIsureTM following the manufacturer's guidelines (Meridian BioscienceTM, Cincinatti, OH). Then 2 µg of RNA were reverse transcribed with the High Capacity cDNA Reverse Transcription Kit (Applied Biosystems, Carlsbad, CA) and quantitative real-time PCR was performed using the Bio Rad C1000 TouchTM Thermal Cycler combined with CFX96 Real Time SystemTM (Bio Rad Laboratories, Hercules, CA). For expression analyses, 6 ng cDNA were analysed in duplicate and normalised to the expression of the housekeeping gene cyclophilin A. Expression profiles were determined using the $2^{-\Delta\Delta CT}$ method.

QUANTIFICATION AND STATISTICAL ANALYSIS

Data are presented as mean ± standard deviation (SD). Statistical differences among multiple groups (one-way ANOVA) are indicated by multiplicity adjusted *P*-values of < 0.05 (*), < 0.01 (**), < 0.001 (***) or < 0.0001 (****). Statistical analyses and graphs were generated using Graph Pad Prism 5.01. software (GraphPad Software, La Jolla, CA, USA).

3.10 Supplemental Information

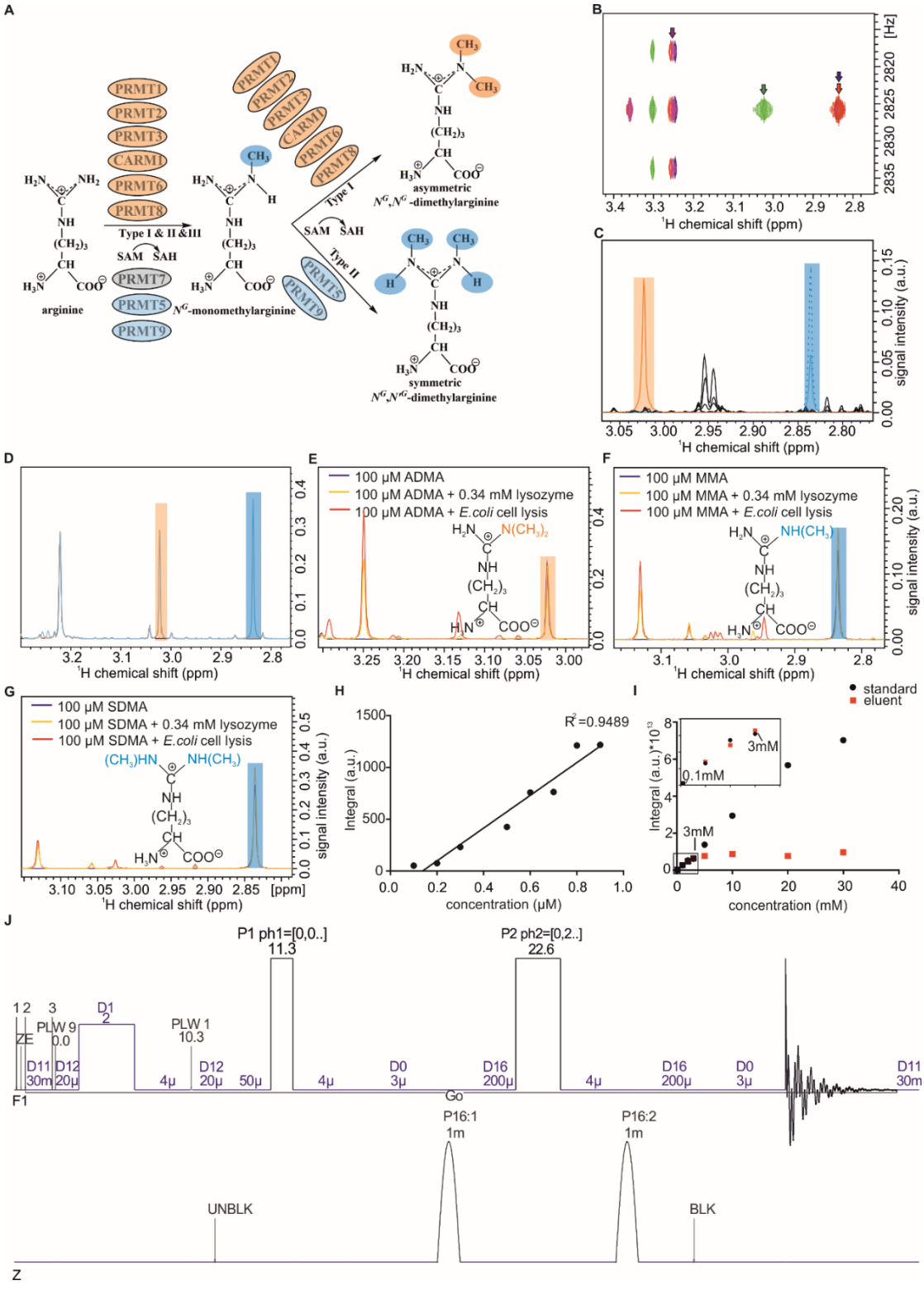

Figure S1. Related to Figure 1. Absolute quantification of protein arginine methylation by ArgMet-NMR.

(A) Arginine residues are methylated by the protein arginine methyltransferase (PRMT) (type I, orange; type II, blue; type III, grey) family members. PRMTs catalyze either the formation of monomethylarginine (MMA) (blue), asymmetric dimethylarginine (ADMA) (orange) or symmetric dimethylarginine (SDMA) (blue).

(B) Overlay of ^{1}H 2D J-resolved experiments of arginine (magenta), ADMA (green), MMA (purple) and SDMA (red), each 100 µM.

(C) Overlay of ^{1}H 1D projections of 2D J-resolved, virtually decoupled NMR spectra of *E. coli* lysates spiked with 100 µM ADMA, MMA and SDMA (black, solid line) before whole workflow, and 100 µM ADMA (orange, solid line), MMA (blue, dotted line) or SDMA (blue, dashed line), respectively, showing free methylarginines are negligible using our protocol.

(D) Overlay of 1H 1D projections of 2D J-resolved, virtually decoupled NMR spectra of metabolites extraction from HeLa cells (black), and then spiked with 100 µM ADMA (orange), MMA and SDMA (blue), respectively.

(E) Overlay of ^{1}H 1D projections of 2D J-resolved, virtually decoupled NMR spectra of ADMA recovery from lysozyme (yellow) and *E. coli* cell lysates (red). Shaded regions represent characteristic regions of ADMA (orange) methyl groups.

(F) Overlay of ^{1}H 1D projections of 2D J-resolved, virtually decoupled NMR spectra of MMA recovery from lysozyme (yellow) and *E. coli* cell lysates (red). Shaded regions represent characteristic regions of MMA (blue) methyl groups.

(G) Overlay of ^{1}H 1D projections of 2D J-resolved, virtually decoupled NMR spectra of SDMA recovery from lysozyme (yellow) and *E. coli* cell lysates (red). Shaded regions represent characteristic regions of SDMA (blue) methyl groups.

(H) Correlation between integrals and concentration changes of ADMA signal of ^{1}H 1D projections of 2D J-resolved spectra. Correlation coefficient (R^2 = 0. 9489, p = 0.033) was computed with the Pearson Product Moment statistic.

(I) Integrals of arginine (red, square) recovery from SPE compared to standard concentrations (black, circle).

(J) Pulse sequence of the 2D JRES NMR experiment.

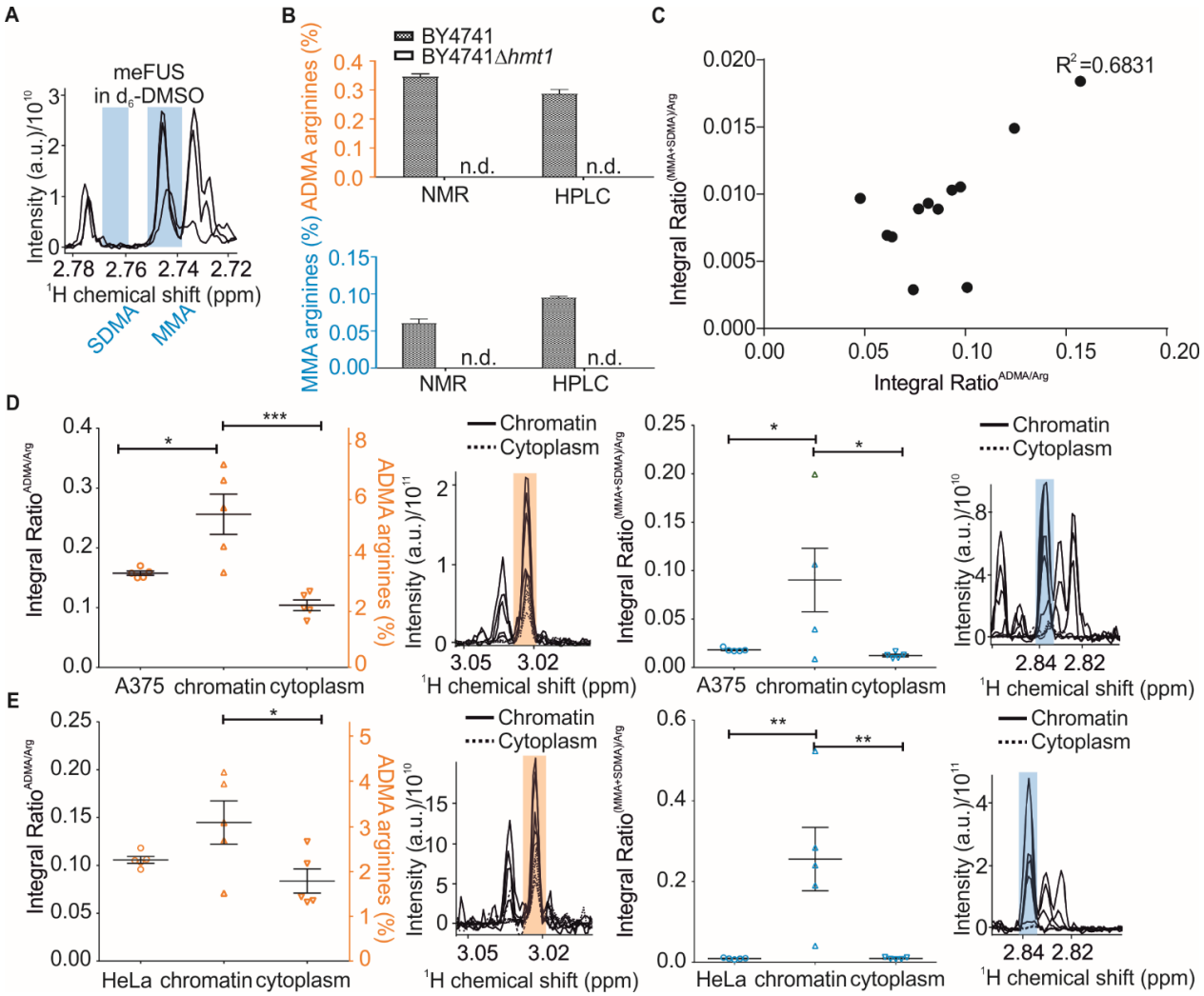

Figure S2. Related to Figure 2. Characterisation of ArgMet in purified proteins, yeast and mammalian cell lysates.

(A) Spectral overlays of characteristic MMA and SDMA NMR methyl signals in d_6-DMSO (n=3). Shaded regions represent characteristic regions of MMA and SDMA (blue) methyl groups.

(B) HPLC and NMR based protein ArgMet quantification of yeast lysates (n=3; mean ± SD; n.d. - not detectable). ADMA or MMA levels in relation to the total amount of arginine are indicated. The MMA peak obtained from HPLC showed spectral overlap interference.

(C) The correlation between integral ratios of ADMA/arginine and (SDMA/MMA)/arginine. Correlation coefficient (R^2 = 0. 6381, p = 0.0143) was computed with the Pearson Product Moment statistic.

(D) ArgMet quantification of chromatin and cytoplasm in A375 cells (n=5; mean ± SD). Spectral overlays of characteristic ADMA (orange) and MMA/SDMA (blue), NMR methyl signals are shown as shaded regions.

(E) ArgMet quantification of chromatin and cytoplasm in HeLa cells (n=5; mean ± SD). Spectral overlays of characteristic ADMA (orange) and MMA/SDMA (blue), NMR methyl signals are shown as shaded regions.

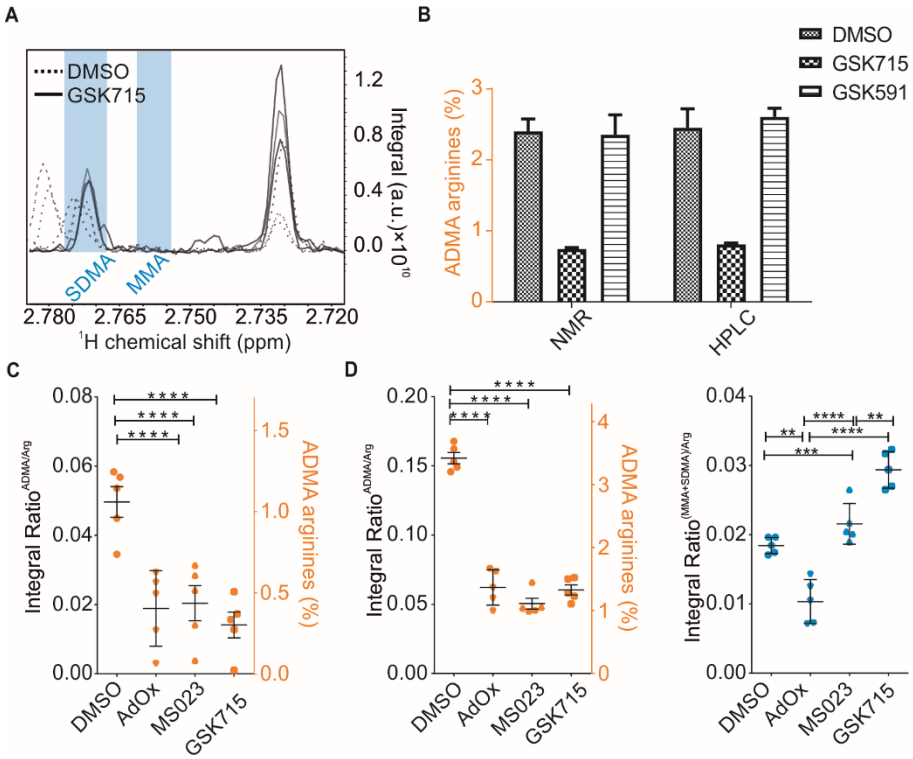

Figure S3. Related to Figure 3. ArgMet NMR enables quantification of protein ArgMet modulation and dynamics.

(A) Spectral overlays of characteristic MMA and SDMA NMR methyl signals in d_6-DMSO show that MMA and SDMA methyl resonances can be resolved (n=3), and higher SDMA represented in GSK715 than DMSO. Shaded regions represent characteristic regions of MMA and SDMA (blue) methyl groups.

(B) HPLC and NMR based protein ArgMet quantification of HeLa cells treated for 3 days with either DMSO, 2 µM GSK3368715 (GSK715) or 1 µM GSK3203591 (GSK591) (n=3; mean ± SD). ADMA levels in relation to the total amount of arginine are indicated.

(C) Protein ArgMet quantification of fibroblast cells treated for 3 days with either DMSO, 40 µM AdOx, 10 µM MS023, 2 µM GSK715 (n=5; mean ± SD). ADMA levels with respect to total amounts of arginine are shown. Both MMA and SDMA are non-detectable in these conditions.

(D) Protein ArgMet quantification of A375 cells treated for 3 days with either DMSO, 40 µM AdOx, 10 µM MS023, 2 µM GSK715 (n=5; mean ± SD). ADMA levels are presented with respect to total amounts of arginine.

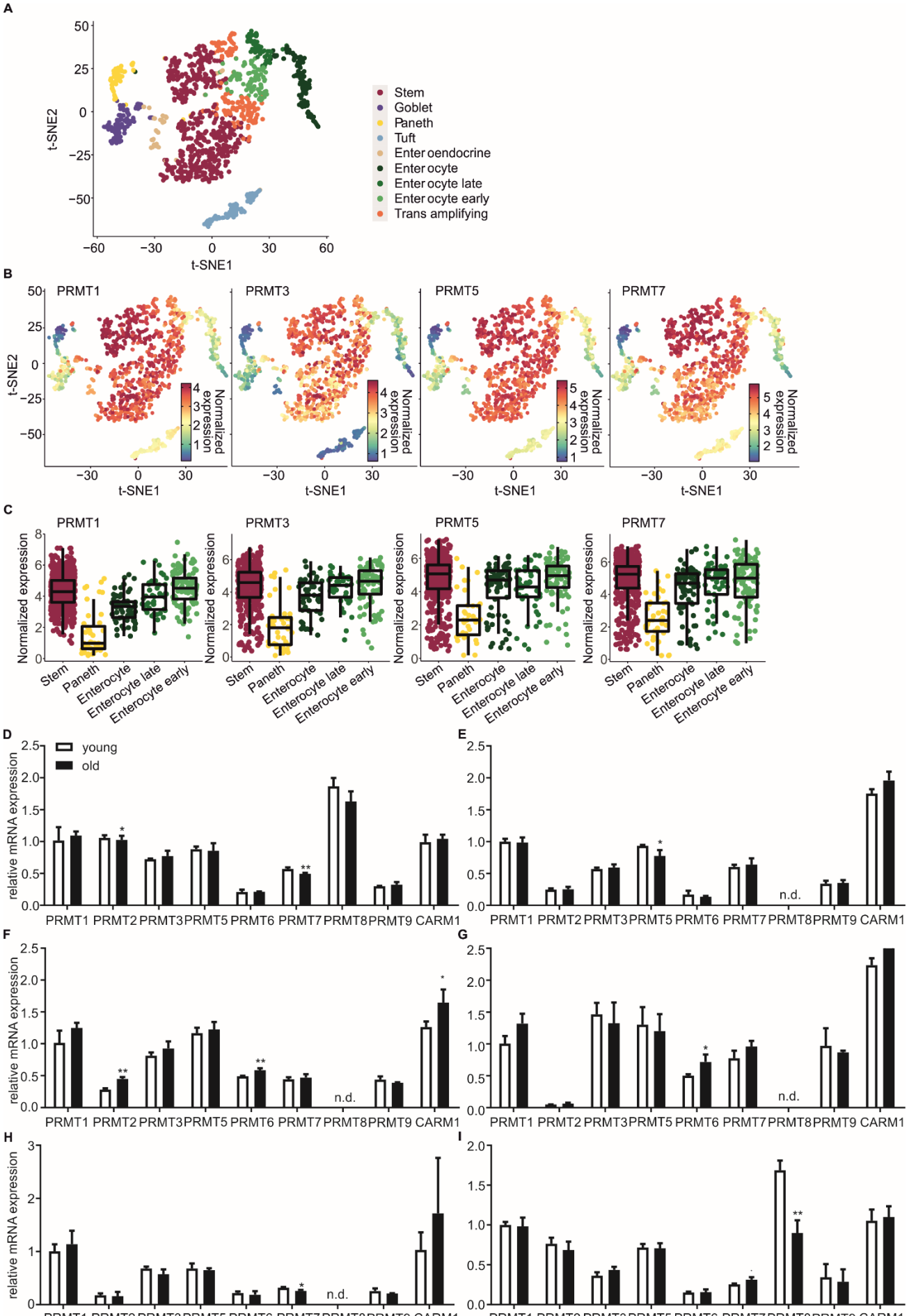
A
t-SNE2
t-SNE1
Stem
Goblet
Paneth
Tuft
Enter oendocrine
Enter ocyte
Enter ocyte late
Enter ocyte early
Trans amplifying
B
PRMT1
PRMT3
PRMT5
PRMT7
Normalized expression
C
Normalized expression
Stem
Paneth
Enterocyte
Enterocyte late
Enterocyte early
D
young
old
relative mRNA expression
PRMT1 PRMT2 PRMT3 PRMT5 PRMT6 PRMT7 PRMT8 PRMT9 CARM1
E
n.d.
F
G
H
I

Figure S4. Related to Figure 4. NMR enables characterization of ArgMet in cell differentiation and ageing *in vivo*.

(A) t-distributed stochastic neighbourhood embedding (t-SNE) visualization of 1,522 single-cell full-length sc-RNaseq data. Cluster annotation was done based on the expression of known cell type markers.

(B) PRMT1, 3, 5 and 7 gene expression levels are plotted on t-SNE plots.

(C) Boxplots represent the quantification of gene expression in each cluster gene (median values and 25th and 75th percentiles). The analysis was performed on mouse small intestine single cell RNAseq data set from Haber *et al.* (207) and the analysis was performed as described in Ludikhuize *et al.* (206).

(D-I) mRNA expression of PRMTs in (D) brain, (E) heart, (F) kidney, (G) liver, (H) spleen and (I) lung from young (9-11 weeks) and old mice (96-104 weeks) analysed by real-time PCR and normalized to cyclophilin A as reference gene. Expression profiles and associated statistical parameters were determined by the $2^{-\Delta\Delta Ct}$ method. Data represent means ± SD (n=3); *p < 0.05, **p < 0.01, ***p < 0.001.

4 Publication II

Publication II has been published in the open access journal Cancers with permission to reprint data under the terms of the Creative Commons CC BY license.

Growing Human Hepatocellular Tumors Undergo a Global Metabolic Reprogramming

Fangrong Zhang [1,2], Yingchao Wang [3], Geng Chen [3], Zhenli Li [3], Xiaohua Xing [3], Csilla Putz-Bankuti [4], Rudolf E. Stauber [4], Xiaolong Liu [3,5,*] and Tobias Madl [1,2,5,*]

[1] Gottfried Schatz Research Center, Molecular Biology and Biochemistry, Medical University of Graz, Neue Stiftingtalstraße 6/6, 8010 Graz, Austria; fangrong.zhang@medunigraz.at

[2] Department, BioTechMed-Graz, Mozartgasse 12/II, 8010 Graz, Austria

[3] The United Innovation of Mengchao Hepatobiliary Technology Key Laboratory of Fujian Province, Mengchao Hepatobiliary Hospital of Fujian Medical University, Fuzhou 350025, China; yingchaowang@fzu.edu.cn (Y.W.); thestaroceanster@bjmu.edu.cn (G.C.); 11218083@zju.edu.cn (Z.L.); xingxiaohua2006@fjmu.edu.cn (X.X.)

[4] Department of Internal Medicine, Division of Gastroenterology and Hepatology, Medical University of Graz, Auenbruggerplatz 15, 8036 Graz, Austria; ordination@pro-endo.at (C.P.-B.); rudolf.stauber@medunigraz.at (R.E.S.)

[5] Xiamen Institute of Rare Earth Materials, Fujian Institute of Research on the Structure of Matter, Chinese Academy of Sciences, Xiamen 361024, China

* Correspondence: **liuxl@fjirsm.ac.cn (X.L.);** tobias.madl@medunigraz.at (T.M.); Tel.: (+43-316) 385-71972 (T.M.); Fax: (+86-591) 8370-5927 (X.L.); (+43-316)-385-79615 (T.M.)

4.1 Simple Summary

Metabolic reprogramming is a hallmark of malignancy. Hepatocellular carcinoma (HCC) cancer cells alterations in metabolism are due to the adaption to hypoxia and hypo-nutrient conditions. Several proteins and metabolites associated with glycolysis, tricarboxylic acid cycle and pyrimidine synthesis were found to be differentially regulated in serum, tumor and peritumoral tissues with increased tumor size, suggesting that microenvironment and tumor cell cooperate to regulate metabolism. In this study, the metabolomic characterization of HCC using paired tumor and adjacent liver tissues indicated tumor size-dependent metabolic reprogramming. Targeting cancer metabolism provides potential diagnostic and prognostic metabolic biomarkers. Our study brings new insight into the potential therapeutic use of metabolic targets and a methodological framework and diagnostic and prognostic metabolic markers that may be used in a clinical setting. The stratification of future clinical trials based on these metabolic subsets should improve the development of effective therapies and more intensive surveillance.

4.2 Abstract

Hepatocellular carcinoma (HCC) is a common malignancy with poor prognosis, high morbidity and mortality concerning with lack of effective diagnosis and high postoperative recurrence. Similar with other cancers, HCC cancer cells have to alter their metabolism to adapt to the changing requirements imposed by the environment of the growing tumor. In less vascularized regions of tumor, cancer cells experience hypoxia and nutrient starvation. Here, we show that HCC undergoes a global metabolic reprogramming during tumor growth. A combined proteomics and metabolomics analysis of paired peritumoral and tumor tissues from 200 HCC patients revealed liver-specific metabolic reprogramming and metabolic alterations with increasing tumor sizes. Several proteins and metabolites associated with glycolysis, the tricarboxylic acid cycle and pyrimidine synthesis were found to be differentially regulated in serum, tumor and peritumoral tissue with increased tumor sizes. Several prognostic metabolite biomarkers involved in HCC metabolic reprogramming were identified and integrated with clinical and pathological data. We built and validated this combined model to discriminate against patients with different recurrence risks. An integrated and comprehensive metabolomic analysis of HCC is provided by our present

work. Metabolomic alterations associated with the advanced stage of the disease and poor clinical outcomes, were revealed. Targeting cancer metabolism may deliver effective therapies for HCC.

Keywords: hepatocellular carcinoma; metabolomics; proteomics; NMR spectroscopy; predictive model

4.3 Introduction

Hepatocellular carcinoma (HCC) is one of the most prevalent cancers around the world and the second-most common cause of cancer-related death (243). HCC is a pathology processed with multiple etiologies, which are dynamic and multi-staged (244). The observed variations in the age-, sex- and race-specific distributions of HCC in geographic regions are related to different abundance of risk factors, with chronic hepatitis B virus (HBV), chronic hepatitis C virus (HCV) infection and cirrhosis being the largest risk factors (245).

The high lethality (10-20/100,000, in East Asia) associated with HCC is mainly due to the late diagnosis and high post-operative recurrence, which is, in turn, due to the lack of symptoms at the early stage (246). Currently, there is no standard or routine screening test for liver cancer. Depending on the local guidelines, ultrasound, X-ray Computed Tomography scan and α-fetoprotein (AFP) are the typical tests being used to screen for liver cancer (247-249). The available tests have several limitations: for example, early/small tumors are difficult to be detected by ultrasound and computed tomography scan and often show negative AFP levels (250). In contrast, AFP levels are often elevated under certain conditions, including pregnancy, hepatitis, cirrhosis and other types of cancer, causing up to 20% false-positive results (249, 250). Furthermore, there is currently no consensus regarding the risk stratification. These limitations complicate the recurrence surveillance of high-risk patients. Recently, several models to evaluate postoperative recurrence have been developed—for example, the Korean model, the Singapore Liver Cancer Recurrence (SLICER) score and the Surgery-Specific Cancer of the Liver Italian Program (SS-CLIP) (251-253). However, the performance of these models is still not satisfactory for clinical practice, due to the lack of specific biomarker integration. Thus, novel biomarker candidates for

the early diagnosis of HCC and new approaches that allow clinicians to estimate the risk of recurrence in an individual patient are urgently required.

Recent studies based on mass spectrometry and next-generation sequencing unveiled the activation status of signaling pathways and reprogramming of liver-specific metabolism in HBV-related HCC on the genomic and the proteomic levels (254, 255). MS-based proteomics can provide measures of the global changes in protein abundance related to the deregulation of signaling and metabolic pathways in HCC. Nonetheless, how the cancer metabolic phenotypes are driven by proteomic alterations remains unexplained in HBV-related HCC. Moreover, the application of proteomics-based biomarkers for diagnosis and prognosis remains difficult in a clinical setting (256, 257). One of the reasons of these complications might be imposed by the observation that tumors can undergo re-programming during growth to allow the tumor to adapt to changing conditions and challenges, including, for example, limited access to nutrients and oxygen (258, 259). However, how proteomic and metabolomic signatures change upon tumor growth in HCC remains unknown.

Nuclear Magnetic Resonance (NMR) spectroscopy-based metabolomics can provide an untargeted, quantitative snapshot of global metabolite abundance to provide additional biological insights, which cannot be deciphered by proteomics alone (131). Compared to other “omics”, the metabolome provides the most direct snapshot of the actual functional and physiological state of biological networks (97). Related to HCC, metabolic fingerprints have the potential to capture metabolic changes, which could help clarifying the pathogenesis and changes in environmental or lifestyle factors (105). Untargeted metabolomics has been established as key technique for investigation of metabolic alterations in carcinogenesis (97, 98), and the first metabolites have been identified to be changed in HCC (260, 261). Metabolomic research associated with HCC allows an unparalleled opportunity to discover metabolites for early diagnosis candidates and to assess the progression of treatment. The combination with MS-based proteomics promises to fill the current knowledge gap between HCC cancer proteomic and metabolomic phenotypes and the underlying molecular mechanisms (262).

Here, we performed a metabolomic analysis of patient serum samples and integrative analyses of metabolomic and proteomic (257) data from tumor and matched peritumoral liver tissues. Significant alterations in crucial metabolic and signaling pathways were revealed by this analysis.

Strikingly, a comparison of the proteomic and metabolomic signatures obtained for different tumor sizes and their matched peritumoral tissues showed that both tumors and their surrounding tissues undergo proteomic and metabolic reprogramming during growth. Proteomic clustering resulted in a set of proteins that are differentially regulated in different-sized tumors. Several proteins, and metabolites involved in glycolysis, the tricarboxylic acid (TCA) cycle and pyrimidine synthesis were found to be differentially regulated with increased tumor sizes in serum, tumor and peritumoral tissues.

We further used our metabolomic data to develop a statistical model that can predict the risk of HCC recurrence based on clinical pathological data, metabolomics data and a combination thereof. This model will be valuable in predicting the clinical outcomes of the treatment, guiding follow-up surveillance or in the design of post-resection clinical strategies aiming to decrease the risk of recurrence. In conclusion, our study provides high-quality and high-content proteometabolomic resources of HBV-related HCC complementary to the sequencing-based data. Moreover, it highlights the therapeutic and prognostic implications and inherent regulatory mechanisms of metabolomic data benefiting clinical practice.

4.4 Materials and Methods

4.4.1 Patients

Tissues (carcinoma tissues (CT) and peritumoral tissues (PT)) and fasting sera were collected from 200 patients (male/female, 160/40) with HCC ranged from age 23 to 77 years. Several tumorous factors were collected, including tumor size, microvascular invasion, tumor lesion number, differentiation grade and portal vein tumor thrombus. According to the Barcelona Clinic Liver Cancer (BCLC) staging classification system (263) or TNM-based staging system (264), the tumor size is an important factor to grade HCC patients. In a number of more recent studies, the tumor size reflects changes in tumor growth, which were related with metastasis, microvascular invasion, operative complications and recurrence. Herein, serum, CT and PT were divided into 4 groups according to the tumor size (diameter $\leq$ 3 cm, grade I, n = 50; 3 cm < diameter $\leq$5 cm, grade II, n = 50; 5 cm < diameter $\leq$ 10 cm, grade III, n = 50; diameter > 10 cm, grade IV, n = 50). Serum and tissues were taken from each individual, i.e., serum, CT and PT were from the same patient. Intact encapsulation or distinct boundary tumors of patients through computed tomography scan were

selected as the clinical samples. Of these, 45 of grade I patients, 40 of grade II, 48 of grade III and 41of grade IV HCC patients were HBsAg-positive (Hepatitis B surface antigen) and one grade III patient with unknown HBsAg (all HCV (Hepatitis C virus) negative). All patients received the standard radical resection without any other therapies before surgery. The detailed clinical information is summarized in **Table S1**.

In addition, 42 HCC patients with cirrhosis and 23 cirrhosis controls without HCC enrolled at the Medical University of Graz were included. These patients were enrolled 2007–2009 in a biomarker study, and plasma samples stored at −70 °C were used for metabolomic analyses. In the HCC patients (male/female, 35/7; age range 54–83 years) all had underlying cirrhosis of different etiologies (alcohol, 13; NASH, 13; HCV, 12; other, 4). Cirrhosis controls without HCC were matched to age, sex and etiology.

This study was approved by the ethics committee of the Institution Review Board of Mengchao Hepatobiliary Hospital of Fujian Medical University, China (ethical code: 2018_067_01) and by the Ethics Committee of the Medical University of Graz (ethical code: 33-040 ex 20/21), respectively. Written informed consent was obtained from all patients.

4.4.2 MS Sample Preparation, Data Acquisition

In our previous study (265), CT and PT tissues were collected from 60 patients and were divided into 4 groups according to their tumor sizes, including small (n = 15), medium (n = 15), large (n = 15) and huge HCC groups (n = 15), respectively. The criteria for grouping was the same as in this study. After sample preparation, 5 individual samples with equal amounts from the same group were pooled together and were labeled using the iTRAQ kit, resulting in 3 biological repeats of each group, named as CT/PTI1, CT/PTI2, CT/PTI3, CT/PTII1, CT/PTII2, CT/PTII3, CT/PTIII1, CT/PTIII2, CT/PTIII3, CT/PTIV1, CT/PTIV2 and CT/PTIV3, respectively. Proteomic profiles of pooled samples were identified by 2D LC-MS/MS. Here, the raw data obtained in the previous study was used as input for the analysis.

4.4.3 NMR Sample Preparation, Data Acquisition and Analysis

Tissues samples were flash-frozen in liquid nitrogen and stored at −80°C until analysis. In each patient, approximately 9-mm^3 CT and PT was resected and 200-µL serum was used for the

metabolomics analysis. Serum and tissue sample preparation was conducted as described previously (266, 267). Tissuelyser-24 was used for homogenization at 60 Hz for 180 seconds (Lixin Co., Ltd, Shanghai, China). NMR measurements for ^{1}H NMR metabolic profiling and analyses were performed as described and using a Bruker Avance III HD 600-MHz NMR spectrometer equipped with a TXI probe head (267, 268). Chenomx NMR suite 8.4 and reference compounds were used to identify the metabolites in the serum and tissue during the analysis. A Receiver Operating Characteristic (ROC) analysis was done in MetaboAnalyst 5.0 to evaluate the specificity and sensitivity of each metabolite. GraphPad Prism 5.01 (GraphPad Software, La Jolla, CA, USA) was employed to perform a univariate statistical analysis where the data are represented as the mean +/− standard deviation (SD). Statistical differences among multiple groups (one-way ANOVA) are indicated by multiplicity adjusted P-values of < 0.05 (*), < 0.01 (**), < 0.001 (***) or < 0.0001 (****).

4.4.4 Multivariable Prediction Model

The model building and evaluation were performed by SPSS statistical software (V19.0, SPSS Inc., Chicago, IL, USA) or in R version 3.2.5 (R Foundation for Statistical Computing, Vienna, Austria). Two models to predict the recurrence of HCC were built using the derivation cohort. The difference between two models is whether the metabolites as a parameter are included in the model. Cox regression was conducted to evaluate the correlation between the clinicopathological parameters and metabolites. Univariable factors with $p < 0.05$ were incorporated into the multivariable cox regression analysis. Multivariate cox regression was then applied to establish the final model. As shown in **Table 3** and **Table S4**, two novel risk score formulae were developed, including or omitting metabolites, respectively. The risk score of enrolled HCC patients was calculated according to the aforementioned risk scoring formulae. The median risk score was subsequently used as cut-off to divide the patients into low- and high-risk groups. The survival differences between low- and high-risk groups were examined by a Kaplan–Meier analysis.

The sensitivity and specificity of this prognosis prediction model were assessed by the area under the time-dependent receiver operating characteristic (tdROC) curve (tdAUC), which was analyzed using the “tdROC” package of R software (4.0.3, R core Team, R Foundation for Statistical

Computing, Vienna, Austria). The discriminatory performance of the models was assessed by Harrell's c-index, Gönen & Heller's K, as previously described (269-271).

4.5 Results

4.5.1 Metabolic Serum Profiles Change during Tumor Progression

Given that metabolic reprogramming is a hallmark of cancer development (272), we hypothesized that tumors of HCC patients undergo metabolic changes upon growth. To this end, we carried out an in-depth analysis using recently published proteomic data (257). Proteomic clustering was performed based on differentially expressed proteins in different-size tumors, revealing 509 dysregulated proteins during tumor growth (**Figure 9A**). The proteins whose expression were altered the most significantly ($p < 0.01$), along with the increase in tumor size, are listed in **Figure 9A**. Among these differentially expressed proteins, many proteins have been demonstrated to be involved in glycometabolism, such as glyceraldehyde 3-phosphate dehydrogenase (GAPDH) (273) and phosphoglycerate kinase 1 (PGK1) (274), lipid metabolism such as apolipoprotein A4 (APOA4) (275) and protein synthesis or degradation such as plasminogen protein (PLG) (276) in cancer cells. Next, a Gene Ontology (GO) enrichment analysis identified the top terms (ranked by *p*-values) specific for the upregulated biological processes involving metabolic, mRNA, cellular metabolic, RNA, organic substances and catabolic processes (**Figure 9B**, upper panel). Tumors with larger sizes showed a decrease of mRNA processing related to the carboxylic acid, oxoacid, organic acid, small molecule and monocarboxylic acid metabolic processes (**Figure 9B**, lower panel). These results clearly indicate that metabolism undergoes tremendous change in tumors with different sizes. Therefore, we hypothesized that the metabolomic profile might consistently change in tumors with different sizes.

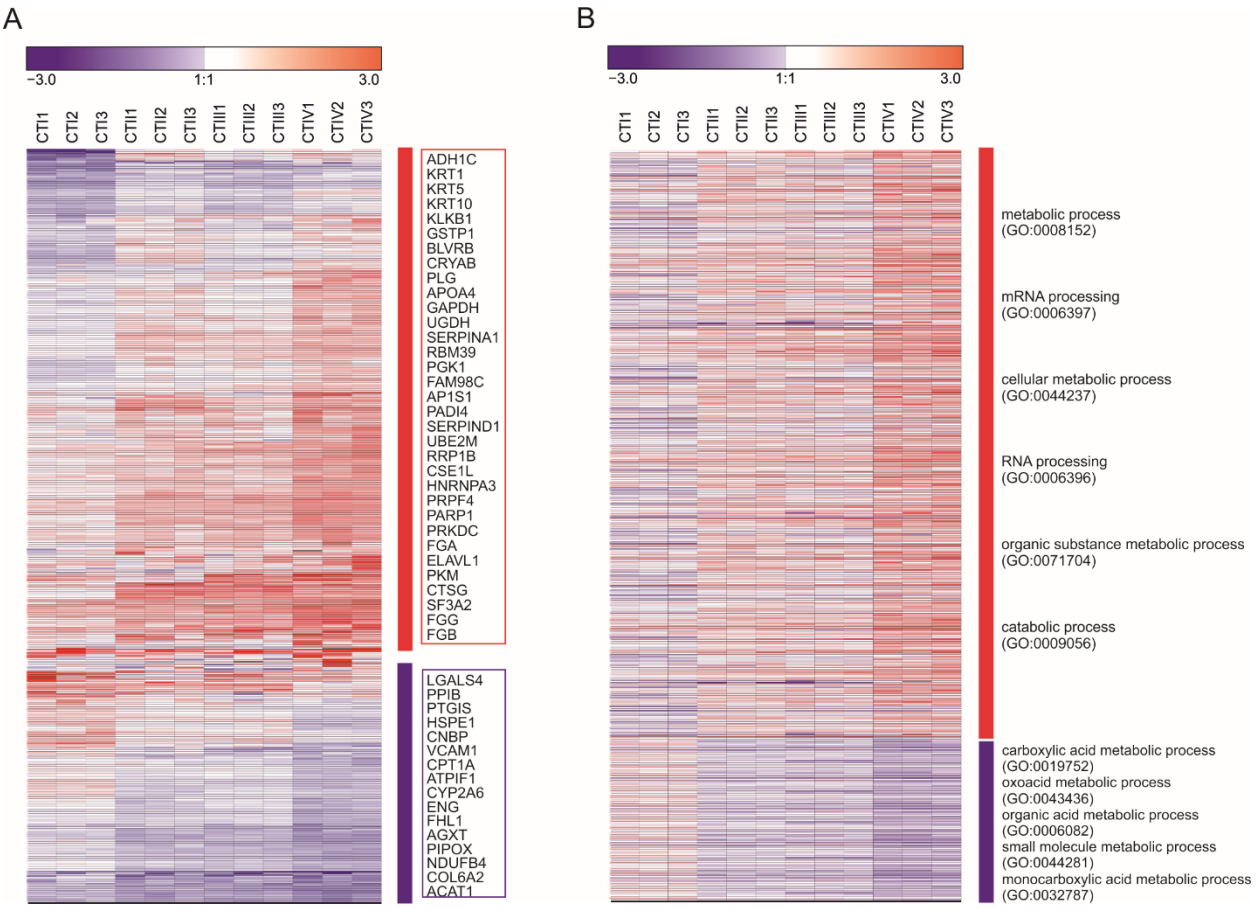

Figure 9. Proteome changes during tumor progression. (**A**) Hierarchal molecular clustering of 509 dysregulated (1.5-fold up or down regulation) proteins in tumors of different HCC subtypes. Each column represents a pool of patient samples, and rows indicate proteins. Up- and downregulated proteins were compared to the peritumoral tissue, respectively. The red frame surrounds the proteins whose upregulation was significantly associated with larger tumor sizes ($p < 0.001$), while the purple frame surrounds proteins whose downregulation was significantly associated with bigger tumor sizes ($p < 0.001$). (**B**) An enriched analysis of the Gene Ontology Biological Processes (GOBP) using protein panels based on upregulated and downregulated proteins to generate top-term significant biological process. Each column represents a pool of patient samples, and rows indicate proteins involved in that particular biological process. Cells are colored according to their Z-score (log2 of the relative protein abundance). The analysis was performed on the HCC cancer tissue proteome dataset from a previous work (257).

To obtain a comprehensive molecular understanding of the metabolic changes in HCC patients, tumor tissues, their paired peritumoral tissues and serum collected from 200 HCC patients were used for a metabolomic analysis based on stringent criteria (see Materials and Methods). The study

was designed to obtain samples of 50 HCC patients for each of the four groups defined according to a classification based on tumor size **(277, 278)**. To this end, the HCC patients were divided into four subtypes, including small HCC (diameter ≤ 3 cm, grade I), medium HCC (3 cm < diameter ≤ 5 cm, grade II), large HCC (5 cm < diameter ≤ 10 cm, grade III) and huge HCC (diameter > 10 cm, grade IV).

Using untargeted NMR spectroscopy, we determined the metabolic fingerprints of the serum and tissues. A Principal Component Analysis (PCA) and Partial Least Squares-Discriminant Analysis (PLS-DA) of the serum samples showed that the serum metabolic profiles of HCC patients gradually change with increasing the tumor size (**Figure 10A**). While the metabolic profiles of HCC patients with small tumors are more homogenous, the profiles become more heterogeneous with the increasing tumor size**.** An inspection of the PCA loading plot revealed a strong increase of several ^{1}H NMR signals between 3.5–4.0 ppm and between 5.4 and 5.7 ppm in a subset of patient samples with grade III and IV tumors. A statistical total correlation spectroscopy (STOCSY) (279) analysis confirmed that all the signals belong to the same group of metabolites (**Figure S5A**). Although the corresponding metabolites could not be assigned unambiguously, we suspect that this group of metabolites corresponds to circulating DNA. This is in line with previous works reporting high levels of circulating tumor and cell-free DNA in HCC (280, 281). When comparing the differences in the metabolic fingerprints between the serum samples of patients with different tumor sizes, O-PLS-DA revealed increasing correlation coefficients R^2Y up to 0.924 and a Q^2 of 0.714 ($p < 0.01$) (**Figure 10B, C**) with increased clustering of the patient samples. In patients with different tumor sizes, altered serum metabolites were indicated by the reduced NMR spectra (**Figure 10D**) and indicated that the serum levels of glucose, pyruvate, glutamine, succinate, valine and 3-hydroxyisovalerate significantly changed (**Figure 10E**). The results obtained for succinate and valine were in line with a recent study using gas chromatography-mass spectrometry (GC-MS) on a small HCC patient cohort (282) and indicated that metabolites are stable markers for HCC. In line, we also observed significantly decreased glutamine and increased 3-hydroxyisovalerate in plasma samples of HCC patients with cirrhosis compared to matched cirrhosis controls without HCC in the European cohort (Graz, Austria) (**Figure S5B**). We further analyzed HCC metabolomic results in subgroups (Asian vs. non-Asian and nonalcoholic steatohepatitis (NASH) vs. other etiologies). When comparing the metabolic fingerprints between serum/plasma from Asian

(Chinese cohort) and non-Asian (European cohort), the O-PLS-DA revealed distinct clustering with correlation coefficients R^2Y of up to 0.977 ($p < 0.01$) and a positive Q^2 of 0.942 ($p < 0.01$) (**Figure S5C**). We found significantly increased levels of branched-chain amino acids (BCAAs; valine, leucine and isoleucine) in the Asian group (**Figure S5D**), which demonstrated changes in the metabolites may be relevant to HCC in a population-specific manner. Lower valine levels in the non-Asian group are in agreement with a previous study (283). However, we cannot exclude the possibility that pre-analytics (plasma vs. serum), diet or lifestyle cause the differences. NASH is a common preneoplastic state of HCC (284). Emerging data has revealed excessive hepatic lipid accumulation as the major contributor for NASH that sensitizes the liver to oxidative stress, along with subsequent necroinflammation (285, 286). The distinguishing clustering of plasma samples (European cohort) from NASH and other etiologies is shown in the score and validation plots of the O-PLS-DA (**Figure S5F**) with a correlation coefficients R^2Y value of 0.936 ($p = 0.81$) and the Q^2 value of 0.217 ($p = 0.02$). We observed elevated concentrations of glucose in the NASH group (**Figure S5E**). Consistently, a global meta-analysis demonstrated that NASH patients have a higher prevalence of type 2 diabetes and obesity compared to patients having nonalcoholic fatty liver diseases (287). Glucose metabolism is complexly associated with other metabolic pathways (i.e., fatty acids metabolism), which will require further studies to obtain a deeper understanding (286).

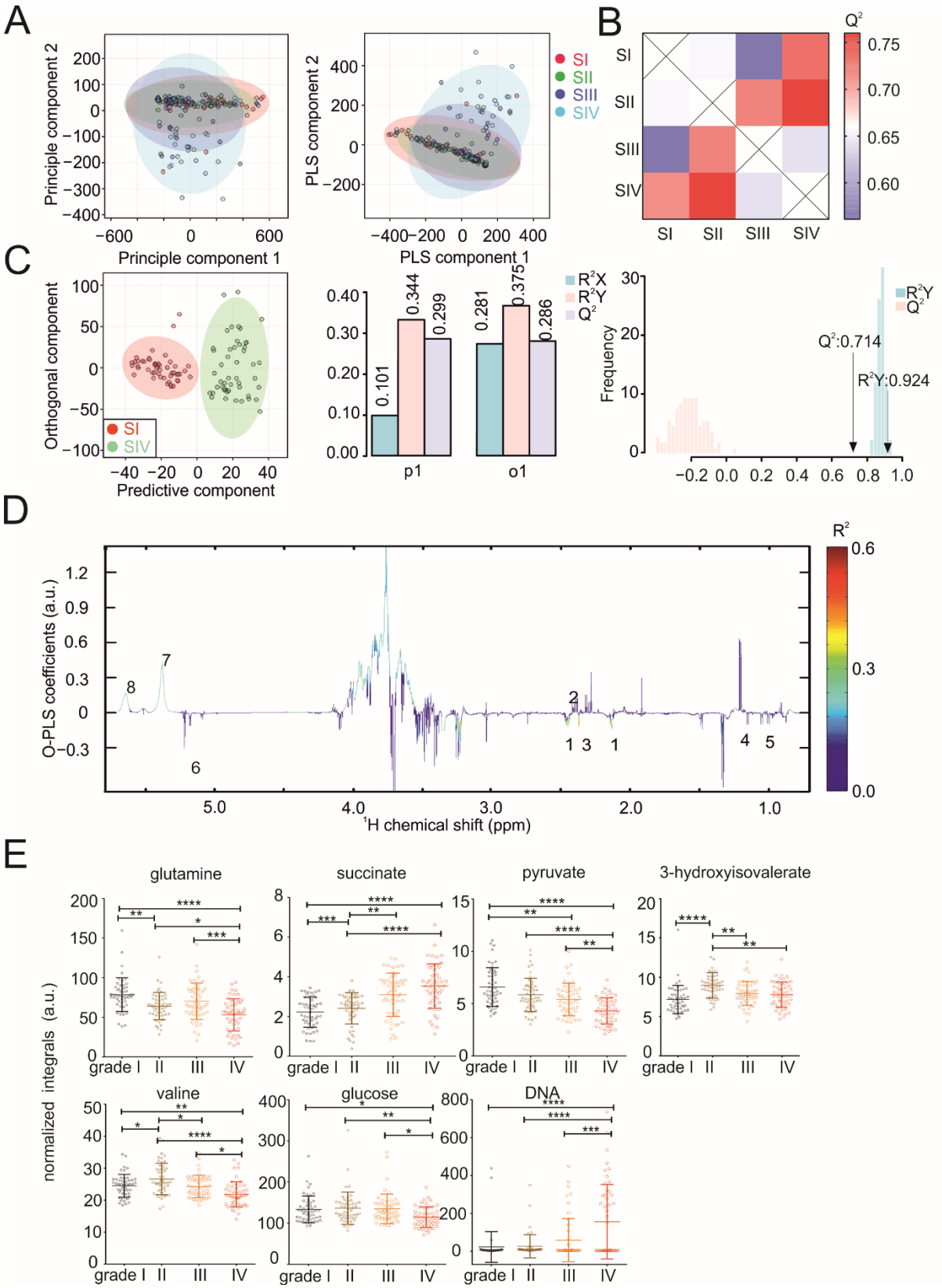
A
Principle component 2
Principle component 1
PLS component 2
PLS component 1
SI
SII
SIII
SIV
B
Q²
0.75
0.70
0.65
0.60
C
Orthogonal component
Predictive component
R²X
R²Y
Q²
0.101
0.344
0.299
0.281
0.375
0.286
p1
o1
Frequency
Q²:0.714
R²Y:0.924
D
O-PLS coefficients (a.u.)
¹H chemical shift (ppm)
R²
E
normalized integrals (a.u.)
glutamine
succinate
pyruvate
3-hydroxyisovalerate
valine
glucose
DNA
grade I
II
III
IV

Figure 10. NMR metabolomics analysis of serum samples. (**A**) PCA and PLS-DA plots of serum samples. (**B**) Heatmap showing O-PLS-DA-derived Q^2 for pairwise comparisons of the serum samples. (**C**) O-PLS-DA plot of the serum samples, including a cross-validation. (**D**) The reduced NMR spectrum reveals altered components in normalized serum samples. Positive covariance corresponds to the components present at increased concentrations, whereas negative covariance corresponds to decreased component concentrations. The predictivity of the model is represented by R^2. (1) glutamine, (2) succinate, (3) pyruvate, (4) 3-hydroxyisovalerate, (5) valine, (6) glucose and (7) and (8) DNA. (**E**) Statistical analysis of individual metabolites in serum samples. Statistical differences among multiple groups (one-way ANOVA) are indicated by *p*-values of < 0.05 (*), < 0.01 (**), < 0.001 (***) or < 0.0001 (****).

4.5.2. Metabolic Profiles of Tumor and Peritumoral Tissues Change duringTumor Progression

In line with the serum data, the PCA and PLS-DA of tumor and peritumoral tissue samples showed that the metabolic profiles of tumor and peritumoral tissues gradually changed with the increasing tumor size, with grade III and IV tumor tissues showing the largest metabolic heterogeneity (**Figure 11A**). Interestingly, about half of the peritumoral tissue samples show a metabolic profile more similar to cancer tissues, whereas the other half showed a distinct metabolic phenotype. We hypothesized that this could be due to increased metastasis in these patients. To test our hypothesis, we performed a PCA analysis dividing the NMR metabolomics datasets into three groups: (i) cancer tissue, (ii) peritumoral tissue without metastasis and (iii) peritumoral tissue with metastasis. In agreement with our hypothesis, peritumoral tissue samples without metastasis clustered with a distinct metabolic phenotype, whereas peritumoral tissue samples with metastasis showed a more cancer-like metabolic phenotype (**Figure S6A, B**). Reduced NMR spectra revealed glucose and succinate as the most significantly changed metabolites (**Figure S6C**). Given that many peritumoral tissue samples showed a cancer-like phenotype even without reported metastasis, metabolic biomarkers might help to detect metabolic reprogramming and early metastasis in peritumoral tissue in the future. O-PLS-DA of pairs of tumor–tumor, peritumoral–peritumoral and tumor–peritumoral tissue revealed an increased clustering of patient samples with different tumor sizes (**Figure 11B, C** and **Figure 12A, B, D, E)**. Strikingly, not only the metabolic profiles of tumors but, also, peritumoral liver tissues are affected, depending on the size of the tumors.

Reduced NMR spectra revealed altered metabolites under all conditions compared, i.e., between tumor and peritumoral tissue (**Figure 11D**), as well as between different grade tumors (**Figure S7B**) and peritumoral tissues (**Figure S7A**), respectively. The levels of glucose, lactate; succinate; 3-hydroxyisovalerate; glutamate; choline; fumarate; nucleotides (uridine and UDP sugars) and other amino acids (isoleucine, leucine, valine, phenylalanine, tyrosine and lysine) were changed in tumor tissues compared to peritumoral tissue (**Figure 11E**), with a largest difference observed for grade IV tumor–peritumoral tissue pairs (**Figure 11C**). Within the tumor, the levels of glucose; lactate; glutamine; fumarate; nucleotides (uridine and UDP sugars) and other amino acids (isoleucine, leucine, valine, phenylalanine, tyrosine and lysine) were affected (**Figure 12F**). Interestingly, most of these metabolites were affected similarly in peritumoral tissues—in particular, lactate; glutamine; nucleotides (uridine and UDP sugars) and several amino acids (isoleucine, leucine, valine and lysine) (**Figure 12C**). Glucose, lactate and leucine have been identified previously by solid-state ^{1}H NMR in HCC tumor tissues and are in line with our results (261). In summary, our results indicate that NMR metabolomics are well-suited to studying tumor metabolism and that metabolism of the tumor is strongly coupled to its environment (**Figure 12C**).

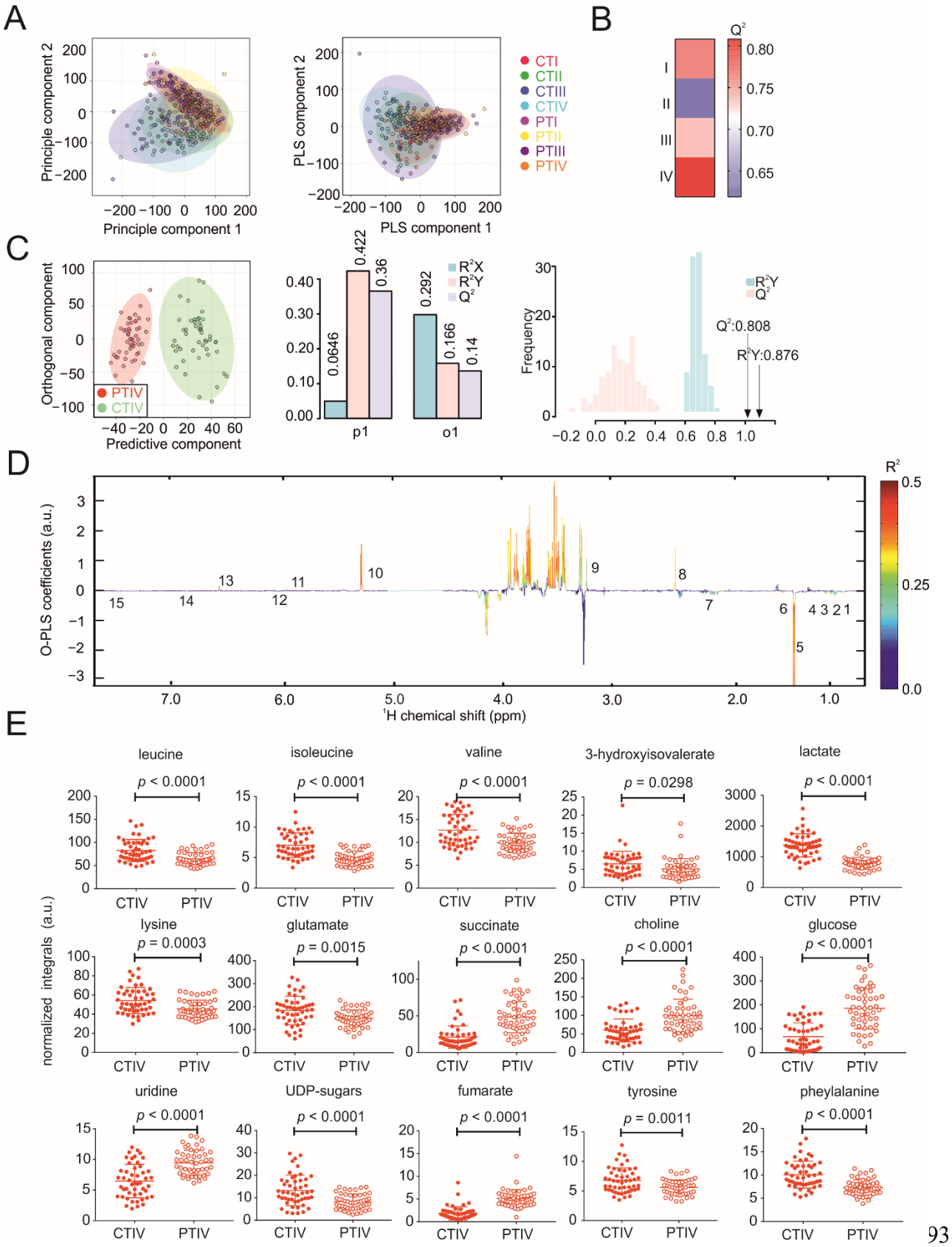
A
Principle component 2
Principle component 1
PLS component 2
PLS component 1
CTI
CTII
CTIII
CTIV
PTI
PTII
PTIII
PTIV
B
Q²
I
II
III
IV
C
Orthogonal component
Predictive component
PTIV
CTIV
R²X
R²Y
Q²
0.0646
0.422
0.36
0.292
0.166
0.14
p1
o1
Frequency
Q²:0.808
R²Y:0.876
D
O-PLS coefficients (a.u.)
¹H chemical shift (ppm)
R²
E
normalized integrals (a.u.)
leucine
p < 0.0001
isoleucine
p < 0.0001
valine
p < 0.0001
3-hydroxyisovalerate
p = 0.0298
lactate
p < 0.0001
lysine
p = 0.0003
glutamate
p = 0.0015
succinate
p < 0.0001
choline
p < 0.0001
glucose
p < 0.0001
uridine
p < 0.0001
UDP-sugars
p < 0.0001
fumarate
p < 0.0001
tyrosine
p = 0.0011
pheylalanine
p < 0.0001
CTIV
PTIV

Figure 11. NMR metabolomics analysis of the tissue samples. (**A**) PCA and PLS-DA plots of tissue samples (grade IV carcinoma tissues (CTIV) and peritumoral tissues (PTIV)). (**B**) Heatmap showing O-PLS-DA-derived Q^2 for pairwise comparisons of the tissue samples (same stage, carcinoma tissues vs. peritumoral tissues). (**C**) O-PLS-DA plot of the tissue samples, including a cross-validation. (**D**) The reduced NMR spectrum reveals altered components in the normalized tissue samples. Positive covariance corresponds to the components present in increased concentrations, whereas negative covariance corresponds to decreased component concentrations. The predictivity of the model is represented by R^2. (1) leucine, (2) isoleucine, (3) valine, (4) 3-hydroxyisovalerate, (5) lactate, (6) lysine, (7) glutamate, (8) succinate, (9) choline, (10) glucose, (11) uridine, (12) UDP sugars, (13) fumarate, (14) tyrosine and (15) phenylalanine. (**E**) Statistical analysis of the individual metabolites in the tissue samples.

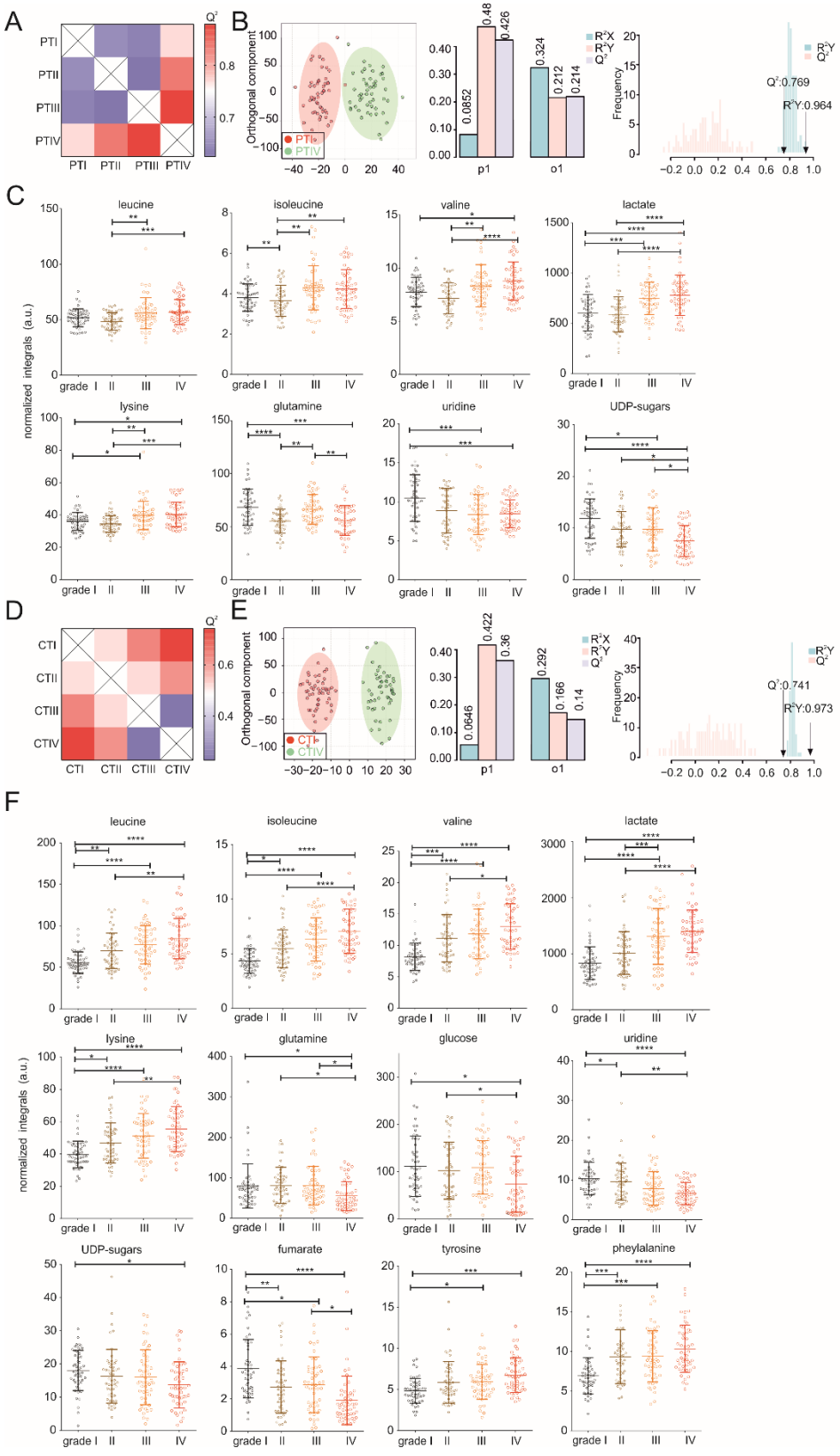
A
B
C
D
E
F
PTI
PTII
PTIII
PTIV
CTI
CTII
CTIII
CTIV
Orthogonal component
Frequency
Q²:0.769
R²Y:0.964
Q²:0.741
R²Y:0.973
normalized integrals (a.u.)
grade I II III IV
leucine
isoleucine
valine
lactate
lysine
glutamine
uridine
UDP-sugars
glucose
fumarate
tyrosine
pheylalanine

Figure 12. NMR metabolomics analysis of peritumoral and cancer tissue samples at different stages. (**A**) Heatmap showing O-PLS-DA-derived Q^2 for pairwise comparisons of peritumoral tissue samples. (**B**) O-PLS-DA plot of peritumoral samples, including a cross-validation. (**C**) Statistical analysis of individual metabolites in peritumoral tissue samples. (**D**) Heatmap showing O-PLS-DA-derived Q^2 for pairwise comparisons of cancer tissue samples. (**E**) O-PLS-DA plot of cancer tissue samples, including a cross-validation. (**F**) Statistical analysis of individual metabolites in cancer tissue samples. Statistical differences among multiple groups (one-way ANOVA) are indicated by *p*-values of < 0.05 (*), < 0.01 (**), < 0.001 (***) or < 0.0001 (****).

4.5.3. Metabolite Panels Enable Diagnosis and Prognosis Potential of HCC

We performed a supervised analysis to identify robust and representative metabolites for the serum-based discrimination against the tumor size and prognosis. In the serum, increased levels of succinate and decreased levels of glutamine and pyruvate were observed depending on the tumor grade (**Figure 10E**). To assess the specificity and sensitivity for each serum metabolite, an ROC analysis was applied. The highest predictivity associate with a tumor grade, as indicated by the highest values of the Area under the Curve (AUC), was obtained for pyruvate (AUC, 0.849), followed by glutamine (AUC, 0.84), and succinate (AUC, 0.809) (**Figure S8B**). Glutamine also exhibited a high diagnostic accuracy for the discrimination of HCC with underlying cirrhosis from cirrhosis without HCC in the European cohort (AUC, 0.787) (**Figure S8C**). These metabolites also showed an elevated response probability to the prognosis, which was consistent with the above order for pyruvate (AUC, 0.625) followed by glutamine (AUC, 0.621) and succinate (AUC, 0.583) (**Figure S8D**). Using a combination of these metabolites yielded a slightly higher AUC (~0.65) compared to the AUC using single metabolites (pyruvate of serum, 0~0.625), revealing an improved predictive estimate of recurrence (**Figure S8E**).

Surgical resection offers a potential curative treatment for HCC patients. Nonetheless, as a major cause of mortality, recurrence happens in around 50–70% of the patients within the 5 years' recurrence period (288, 289). Out of 200 patients of the Chinese cohort tested in this study, a total of 96 patients (48%) developed recurrence within 5 years of surgery.

We hypothesized that metabolites might assist to enable clinicians to determine the suitable therapy and surveillance of patients who were at higher risk of recurrence after surgery. Despite a lack of consensus regarding the optimal tool for stratification, Chan et al. recently proposed a prognostic

model called the Early Recurrence After Surgery for Liver tumor (ERASL) (290) for the surgical treatment of the patients with HCC according to the accessible pathological and clinical parameters. As described before, the tumor number and size, the preoperative alpha-fetoprotein (AFP) level, the preoperative albumin-bilirubin (ALBI) grade and gender were first combined as independent predictors to first validate the pre-ERASL model. In our cohort, 86 out of 184 patients (46.73%) developed recurrence within 5 years of surgery. An additional 16 patients with missing data in our cohort were excluded; in eight patients, no AFP could be detected, in six patients, no exact AFP value could be reported and, in two patients, no ALBI could be determined). We found that the ERASL model is suitable to predict the 5-year (preoperative) recurrence of HCC patients with our own data provided ($p = 0.03$) (**Figure S9**).

Among the 22 clinicopathological parameters analyzed, a univariate Cox regression analysis was performed, and tumor number, tumor size, TNM stage (8th version (264)), serum alanine transaminase (ALT), alkaline phosphatase (ALP), serum glutamic-oxaloacetic transaminase (AST), Gamma-glutamyltransferase (γ-GT) and tumor encapsulation were found to be potentially relevant with $p < 0.05$ (**Table S2** and **Table S3**). Here, in contrast to previous studies (291), we did not find microvascular invasion to improve the prediction of recurrence-free survival in our derivation cohort (100 randomly picked samples, $p = 0.377$), although it could improve the prediction in the entire cohort (200 samples, $p = 0.0041$). Patients were divided randomly into two groups of 100 patients each to generate a derivation and validation cohort, and the eight relevant parameters were used to build a modified and slightly improved preoperative model to predict the 5-year recurrence ($p = 0.006$ for the derivation and $p = 0.025$ for the validation cohort) (**Figure 13A, B**). The formula of the constructed preoperative model is shown in **Table S4**. Using 0.691 as the cut-off value for the clinicopathological preoperative model score, two prognostically distinct groups were stratified, a low risk (5-year recurrence-free survival, RFS = 64/37%) and a high-risk (5-year RFS = 33/0%) group in the derivation and validation groups, respectively.

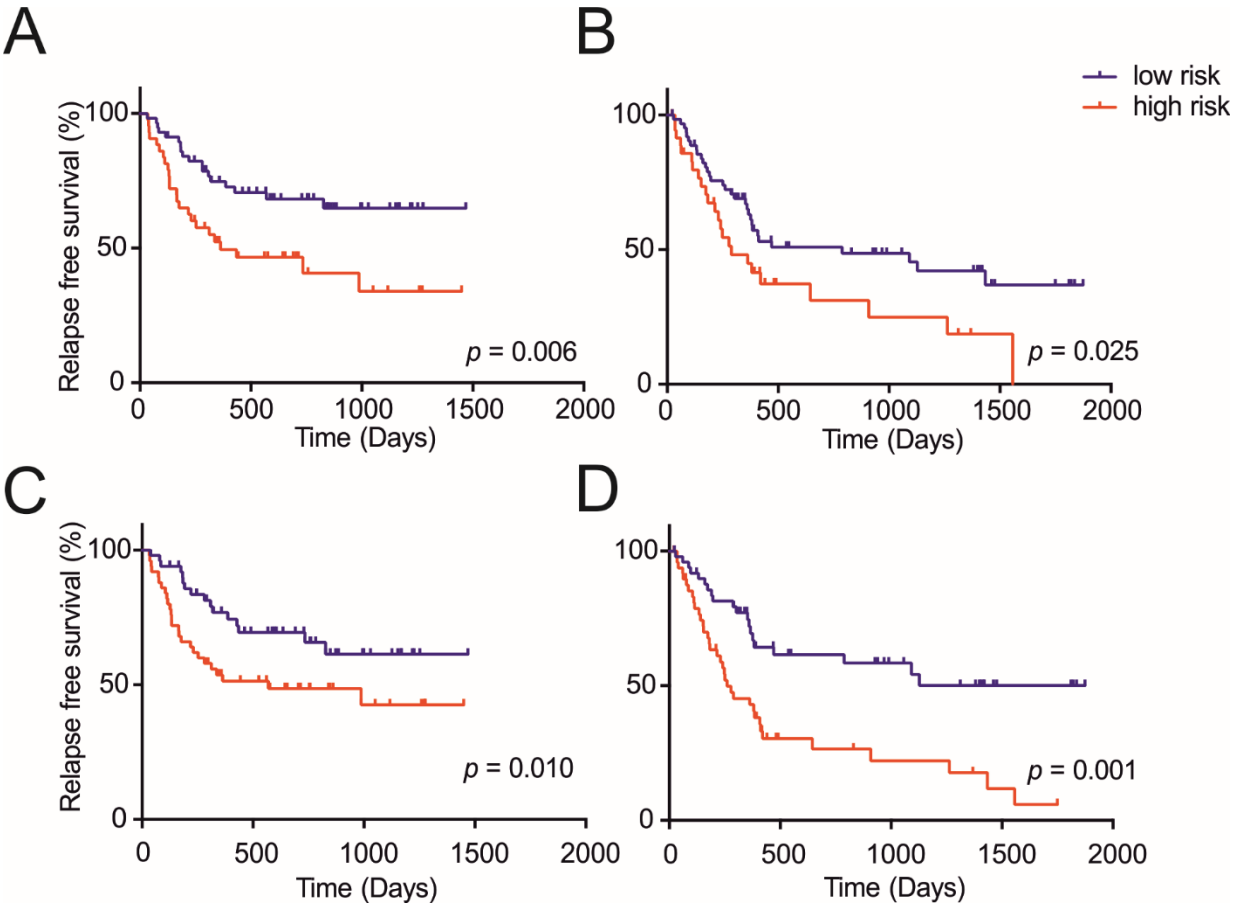

Figure 13. Recurrence-free survival (RFS) according to risk groups defined by the clinicopathological and metaboclinicopathological model. Clinicopathological model (**A**) derivation group and (**B**) validation group. Metaboclinicopathological model (**C**) derivation group and (**D**) validation group.

Next, we aimed to validate the suitability of metabolites to improve the preoperative model by using the same derivation and validation cohorts. To this end, all significantly changed serum and tissue metabolites and their ratios were subjected to a univariable Cox regression analysis. Several metabolites were found to be potentially relevant, with $p < 0.05$ in the univariable Cox regression analysis: serum succinate and glucose, CT lactate, PT lactate, isoleucine, glucose, UDP sugars and valine, as well as the ratios of serum pyruvate/PT valine, serum pyruvate/PT isoleucine, serum pyruvate/CT lactate, serum pyruvate/PT leucine and serum succinate/pyruvate (**Table S2** and **Table S3**). These 13 metabolite parameters were combined with the eight relevant clinicopathological parameters to build an integrated metaboclinicopathological model. The combination of parameters showed a comparable performance in the derivation group (from p =

0.006 to $p = 0.010$) and an improved performance in the validation group (from $p = 0.025$ to $p = 0.001$) (**Figure 13C, D**). The multivariable analysis identified the tumor number, alanine aminotransferase, succinate and pyruvate as the key parameters related to a poor prognosis. Using these variables, a metaboclinicopathological preoperative model was constructed, and the independent parameters and their formulae are shown in **Table 3**. Using 0.874 as the cut-off value, two prognostically distinct groups were stratified, a low-risk (5-year RFS = 61/50%) and high-risk (5-year RFS = 42/6%), in the derivation and validation groups, respectively. The discriminatory performance of the models was compared via Harrell's c-index, Gönen & Heller's K and tdAUC, as shown in **Table 4**. By including NMR metabolite data, the metaboclinicopathological preoperative model showed a better discriminatory performance compared to the clinicopathological preoperative model. Both models may help to design clinical guidelines trials.

Table 3. Multivariable Cox regression analyses of the prognostic factors in the derivation and validation groups of the Chinese cohort with metabolic factors.

Variable	**Derivation Group (*n* = 100)**			**Validation Group (*n* = 100)**		
	Hazard Ratio (95% CI)	**β-Estimate (95% CI)**	***p*-Value**	**Hazard Ratio (95% CI)**	**β-Estimate (95% CI)**	***p*-Value**
ALT						
<50	Ref	Ref		Ref	Ref	
>50	2.557 (1.191, 5.490)	2.552 (1.291, 5.046)	0.007	0.916 (0.473, 1.774)	−0.088 (−0.749, 0.573)	0.794
serum succinate/serum pyruvate	4.572 (1.360,15.372)	1.520 (0.307, 2.733)	0.014	1.968 (1.185,3.268)	0.677 (0.170, 1.184)	0.009

Tumor number	2.242	(1.540, 3.264)	0.807	(0.432, 1.183)	<0.0001	2.228	(1.614,3.075)	0.801	(0.479, 1.123)	<0.0001

Model score = tumor number * 0.807 + serum succinate / serum pyruvate * 1.52 + ALT (0, <50; 1, ≥50) * 0.937;

PI = e^ model score/(1 + e^model score); Cut-off to generate the risk groups: PI ≤ 0.874 (low) and PI > 0.874 (high).

ALT, Alanine aminotransferase.

Table 4. Prognostic performance of the models.

Measure of Discrimination	**With Metabolites**		**Without Metabolites**	
	Derivation (SE)	**Validation (SE)**	**Derivation (SE)**	**Validation (SE)**
Harrell's c-index	0.661 (0.047)	0.638 (0.041)	0.610 (0.045)	0.573 (0.040)
Gönen & Heller's K	0.658 (0.041)	0.619 (0.036)	0.669 (0.056)	0.637 (0.052)
tdAUC (5 years)	0.671 (0.059)	0.667 (0.060)	0.618 (0.055)	0.572 (0.052)

Standard errors (SE) were estimated from 200 bootstrap samples; tdAUC, areas under the time-dependent receiver operating characteristic curve.

4.6 Discussion

A comprehensive global genomic, transcriptomic, proteomic and phosphoproteomic analysis of HCC provided the first insights into the underlying molecular mechanisms and first insights into the biological understanding of HCC (254, 292). Herein, the global metabolomics data provided new insights into the biological understanding of HCC, with particular implications related to the clinical and therapeutic understanding of HCC. NMR spectroscopy is a powerful tool in this regard,

as it is characterized by its high reproducibility and outstanding suitability for *in vitro* diagnostics (IVD). The integrated metabolomic characterization of the serum and paired tumor and peritumoral liver tissue tumor samples at different grades of tumor growth revealed metabolic reprogramming, communication between tumor and peritumoral tissue and clinically and therapeutically relevant metabolite markers in HCC.

Our integrated analysis revealed alterations of the metabolic pathways in the serum, tumor tissue and peritumoral liver tissue. Moreover, we discovered that metastasis affects the metabolic profile of peritumoral tissue. The related metabolites can be used in follow-up studies as markers in a clinical setting for the early diagnosis of HCC and to detect metastasis in peritumoral tissue, which is a difficult task—in particular, for micrometastasis (293).In addition, we compared the metabolic changes of serum/plasma in subgroups (Asian vs. non-Asian and others vs. NASH). Our results showed that BCAAs may act as population-specific HCC metabolites and identified glucose as a plasma biomarker candidate for distinguishing NASH from other etiologies. A limitation of our analysis concerns the inability to subdivide HBV and HCV in the same population.

Strikingly, the metabolic phenotypes of the serum and tumor tissue, as well as peritumoral liver tissue, are shifted gradually with the increasing tumor size. Together with an alteration of the proteomics phenotype, this indicates that tumors undergo metabolic reprogramming with increasing size. Metabolic reprogramming is a hallmark of tumor growth, independent of their carcinogenetic origin (294). Our results in the serum and tissues of HCC patients show that the tumor shifts metabolic pathways and indicates that the resulting change in the nutrient supply is indispensable to overcome nutrient starvation and the changing environmental conditions. Notably, metabolites related with glycolysis, the tricarboxylic acid (TCA) cycle and pyrimidine synthesis were changed in tumor tissues of different stages. The increasing demand of growing tumors for glucose and glutamine is well-visible in the serum and both tumor and peritumoral tissues, respectively. In line with this, the lactate levels increased both in tumor and peritumoral tissues, as well as the expression of glutamine transporters (i.e., SLC1A5) and glycolytic enzymes, such as glucose-6-phosphate isomerase (GPI), phosphoglycerate kinase (PGK1), aldolase A (ALDOA) and hexokinase 2 (HK2) (**Figure 14**). Despite the increased glutamine uptake, enzymes involved in the conversion of glutamate to α-ketoglutarate are downregulated, such as glutamate dehydrogenases

(GLUD1), glutamic-oxaloacetic transaminases (GOT1) and glutamic-pyruvate transaminases (GPT). This might be coupled to the altered expression of downstream TCA enzymes. A prominent example is the drop in the tumor suppressor succinate dehydrogenase (SDHA and SDHB) with the increasing tumor size. Converting succinate to fumarate, the loss of this enzyme is in agreement with reduced levels of fumarate in tumors and increased levels of succinate in the serum. In addition to glutamine, other amino acids such as branched-chain amino acids (BCAAs; valine, leucine and isoleucine) can function as opportunistic fuel sources for cells. In line with this expression of related catabolic enzymes such as BCAT2 are increased in tumor tissues, although other enzymes are undetectable.

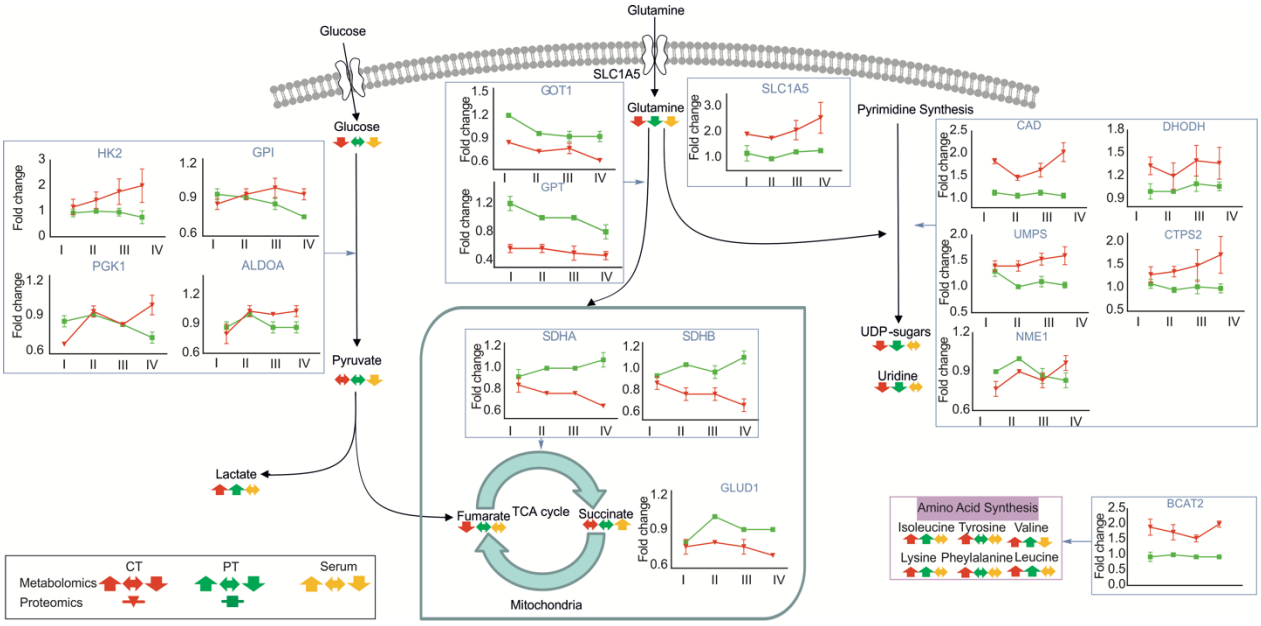

Figure 14. Schematic overview of growing human hepatocellular tumors undergoing a global metabolic reprogramming and proteomic changes. Metabolic genes and metabolites involved in glycolysis, the tricarboxylic acid (TCA) cycle and pyrimidine synthesis. Red line represents tumor tissues, and green line represents peritumoral tissues in proteomics. Red arrow represents tumor tissues, green arrow represents peritumoral tissues and yellow arrow represents the serum in the metabolism.

Strikingly, we observed large changes in the metabolites associated with pyrimidine synthesis (UDP sugars and uridine), which are in line with the recent proteogenomic analysis of HCC **(254)** and the upregulation of CAD protein (CAD), dihydroorotate dehydrogenase (DHODH), uridine 5'-

monophosphate synthase (UMPS), CTP synthase 2 (CTPS2) and nucleoside diphosphate kinase A (NME1). These findings suggested that pyrimidine synthesis pathways could be an alternative target for HCC therapy.

Encouraged by the large changes in HCC metabolic profiles, we validated and adapted a recently proposed a preoperative model that enables risk assessment of 5-year recurrence before resection for the inclusion of metabolomics data. Our validation shows that the recently proposed model can be applied to our setting and that it was capable of stratifying patients into two groups with discrete risk profiles. In the low-risk group comprising about 56.52% of patients among the entire cohort, only 34.61% developed 5-year recurrence, whereas in the intermediate-risk group of 42.39% patients, 61.53% developed 5-year recurrence (Figure S5). Although the metabolomics data on their own were not sufficient to predict the 5-year recurrence ($p = 0.000$ for the derivation and $p = 0.705$ for the validation cohort), the inclusion of metabolomics data improved the predictions of the clinical model. Currently, the serum AFP levels and ultrasonography are regarded as common means for the surveillance of HCC and the early detection of recurrence (295). Ultrasonography shows a low level of sensitivity for the surveillance of HCC, especially in patients with cirrhosis (295). Indeed, AFP leads to high rates of false negatives for HCC, both in the case of the Chinese (66/192) and the European cohorts (20/42). The ROC curve analysis and AUC revealed a higher diagnostic performance of our metaboclinicopathological model (AUC 0.669) than AFP (AUC 0.518) to predict the 5-year recurrence (Figure S4A). Our models are clinically relevant, as they enable the identification of a small, although potentially manageable group of patients with a high risk of recurrence for which an adjuvant therapy and more intensive surveillance could be provided. The benefit of adding metabolomics data to the set of clinicopathological parameters should be further validated in a multicenter study in the future.

In all, after the curative surgery for HCC, recurrence of the tumor is a common and potentially severe complication. Our combined clinicopathological and metabolomic model is a clinically relevant, validated and potent tool to predict the 5-year recurrence. Further prospective studies are needed to demonstrate the applicability of our model in patient allocation for adjuvant trails and more frequent follow-up.

4.7 Conclusions

An integrated and comprehensive metabolomic analysis of HCC is provided by our current work. It could be established that poor clinical outcomes, coupled with an advanced disease stage, were the key factors associated with metabolic alterations. Targeting cancer metabolism, especially purine metabolism, may offer a promising strategy for the effective treatment of HCC. The methodological framework, diagnostic and prognostic metabolic markers capable of being used in a clinical setting are provided by our study, besides generating a high-quality untargeted analysis of HCC metabolism, also benefitting the basic research.

Supplementary Materials: The following are available online at www.mdpi.com/xxx/s1, Figure S1: NMR metabolomics analysis of serum/plasma samples, Figure S2: NMR metabolomics analysis of metastasis, Figure S3: NMR metabolomics analysis of peritumoral and cancer tissue samples at different stages (grade IV vs. grade I), Figure S4: ROC analysis of AFP, metaboclinicopathological model and altered metabolites, Figure S5: Recurrence-free survival (RFS) according to risk groups defined by Early Recurrence After Surgery for Liver tumor (ERASL)-pre model, Table S1: Patient demographics and clinical characteristics (Chinese cohort), Table S2: Univariate and multivariate analysis of pre-operative factors, Table S3: Univariate analysis of other factors, Table S4: Multivariable Cox regression analyses of prognostic factors in the derivation and validation cohort without metabolic factors.

Author Contributions: Conceptualization, F.Z., X.L. and T.M.; Data curation, F.Z. and Y.W.; Formal analysis, F.Z., Y.W., G.C. and X.X.; Funding acquisition, T.M.; Methodology, F.Z., Y.W., Z.L., R.S., X.L. and T.M.; Project administration, X.L. and T.M.; Resources, C.P.-B, R.S. and X.L.; Software, F. Z., Y.W, G.C. and Z.L.; Supervision, X.L. and T.M.; Validation, R.S.; Visualization, F.Z. and T.M.; Writing—original draft, F.Z. and T.M. and Writing—review and editing, F.Z., Y.W, G.C., Z.L., X.X., C.P.-B., R.S., X.L. and T.M. All authors have read and agreed to the published version of the manuscript.

Funding: T.M. was supported by Austrian Science Foundation Grants P28854, I3792 and DK-MCD W1226; Austrian Research Promotion Agency (FFG) Grants 864690 and 870454; the Integrative Metabolism Research Center Graz; Austrian Infrastructure Program 2016/2017; the

Styrian Government (Zukunftsfonds) and BioTechMed-Graz (Flagship project). F.Z. was trained within the frame of the PhD program Molecular Medicine, Medical University of Graz.

Institutional Review Board Statement: This study was approved by ethics committee of Institution Review Board of Mengchao Hepatobiliary Hospital of Fujian Medical University (ethical code: 2018_067_01), China and by the Ethics Committee of the Medical University of Graz (ethical code: 33-040 ex 20/21), respectively.

Informed Consent Statement: Informed consent was obtained from all the subjects involved in the study.

Data Availability Statement: The data presented in this study are available on request from the corresponding author.

Acknowledgments: We thank Zhengxia Yang for assistance with the statistical analysis.

Conflicts of Interest: The authors have no competing financial interests to declare.

Abbreviations: hepatocellular carcinoma (HCC), chronic hepatitis B virus (HBV), chronic hepatitis C virus (HCV), α-fetoprotein (AFP), Surgery-Specific Cancer of the Liver Italian Program (SS-CLIP), Singapore Liver Cancer Recurrence (SLICER), mass-spectrometry (MS), Nuclear Magnetic Resonance (NMR), tricarboxylic acid (TCA), carcinoma tissues (CT), peritumoral tissue (PT), Barcelona Clinic Liver Cancer (BCLC), microvascular invasion (MVI), tricarboxylic acid (TCA), Principal component analysis (PCA), orthogonal partial least squares discriminant analysis (O-PLS-DA), partial least squares-discriminant analysis (PLS-DA), statistical total correlation spectroscopy (STOCSY), gas chromatography-mass spectrometry (GC-MS), Receiver Operating Characteristic (ROC), area under the curve (AUC), standard deviation (SD), glyceraldehyde 3-phosphate dehydrogenase (GAPDH), phosphoglycerate kinase 1 (PGK1), apolipoprotein A4 (APOA4), plasminogen protein (PLG), gene ontology (GO), alanine transaminase (ALT), glutamic-oxaloacetic transaminase (AST), Gamma-glutamyltransferase (γ-GT), recurrence-free survival (RFS), *in vitro* diagnostic (IVD), glucose-6-phosphate isomerase (GPI), phosphoglycerate kinase (PGK1), aldolase A (ALDOA), hexokinase 2 (HK2), glutamate dehydrogenases (GLUD1), glutamic-oxaloacetic transaminases (GOT1) and glutamic-pyruvate transaminases (GPT), branched-chain amino acids (BCAAs), CAD protein (CAD), dihydroorotate dehydrogenase

(DHODH), uridine 5'-monophosphate synthase (UMPS), CTP synthase 2 (CTPS2), nucleoside diphosphate kinase A (NME1), non-alcoholic steatohepatitis (NASH).

4.8 Supplemental information

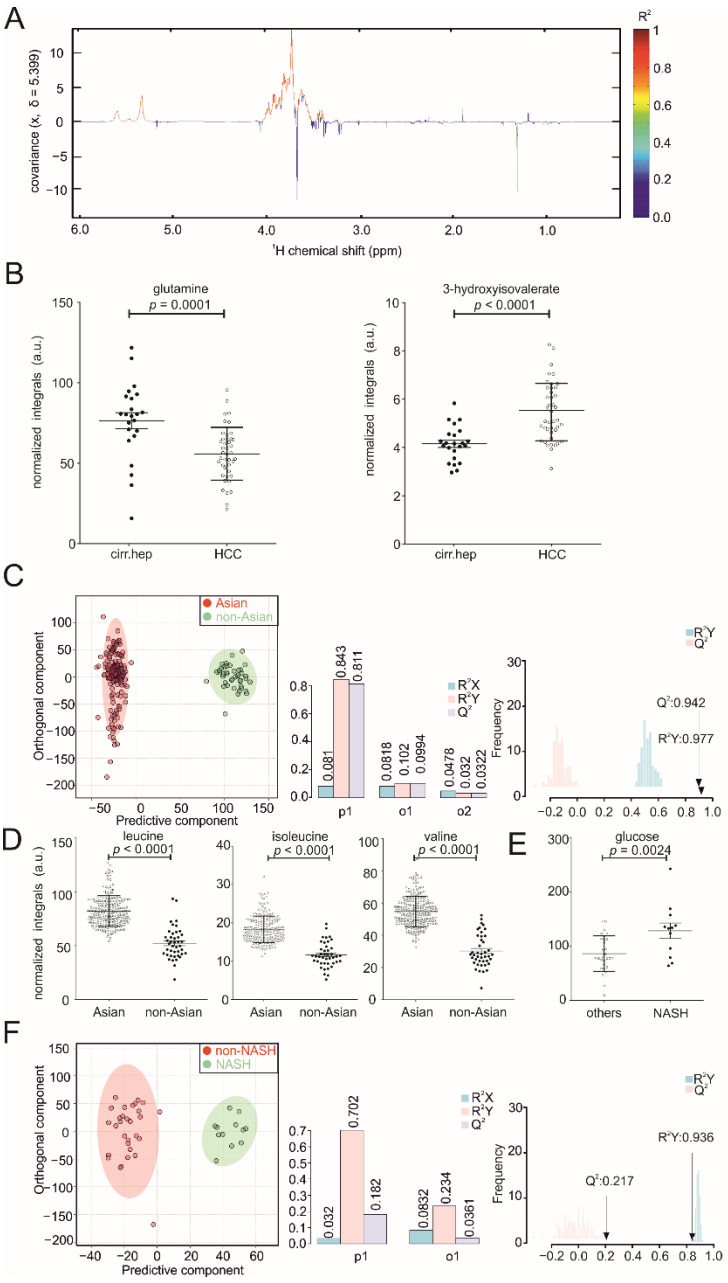

Figure S5. NMR metabolomics analysis of serum/plasma samples. (**A**) Statistical total correlation spectroscopy (STOCSY) analysis of NMR signals at 5.399 ppm. (**B**) Statistical analysis of individual metabolites in serum samples of European cohort. (**C**) O-PLS-DA plot of HCC serum/plasma samples, including cross validation

(Asian vs. non-Asian). (**D**) Statistical analysis of individual metabolites in serum/plasma samples (Asian vs. non-Asian). (**E**) Statistical analysis of individual metabolites in serum/plasma samples (others vs. NASH). (**F**) O-PLS-DA plot of HCC serum/plasma samples (European cohort), including cross validation (others vs. NASH).

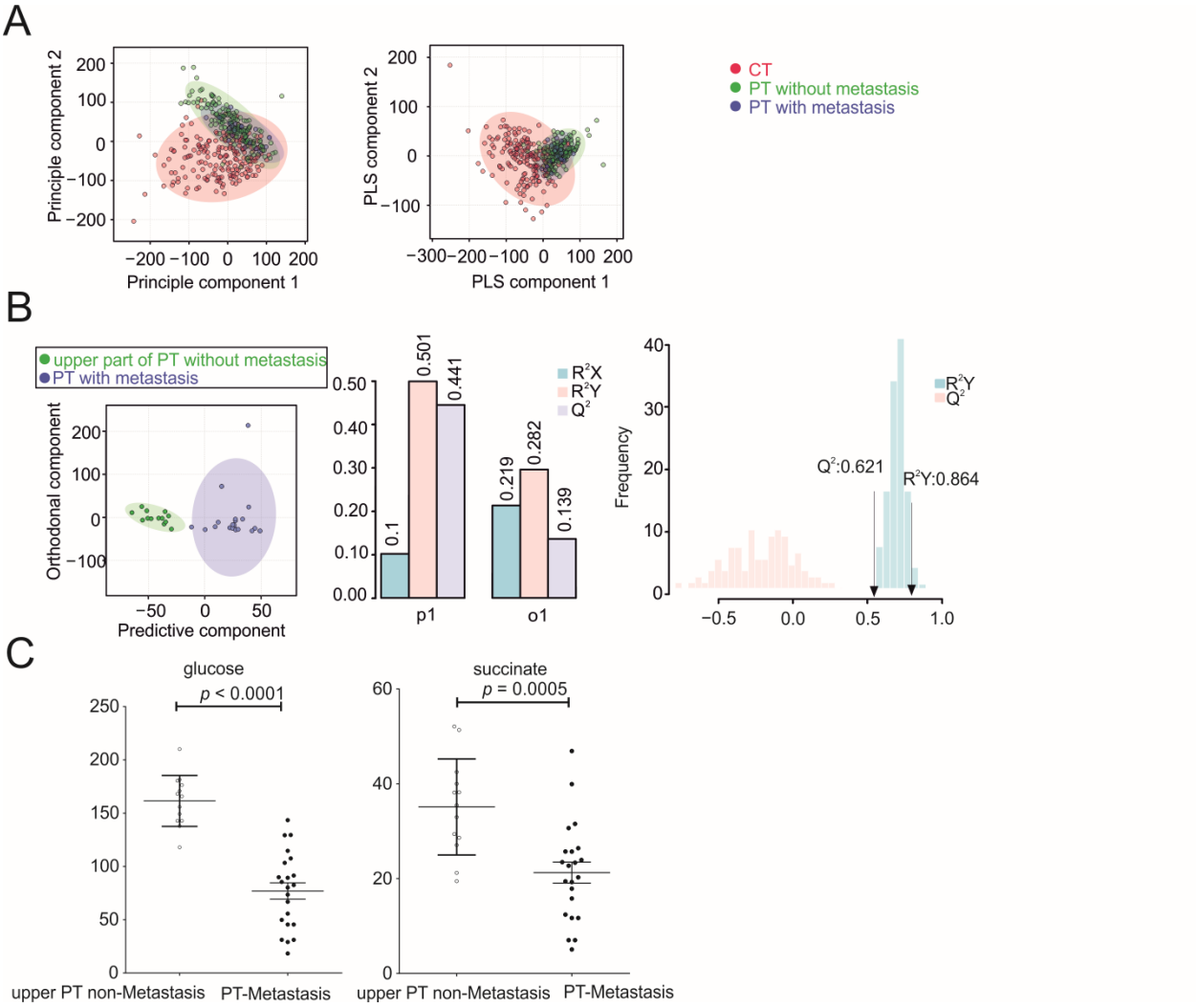

Figure S6. NMR metabolomics analysis of metastasis. (**A**) PCA and PLS-DA plots of tissue samples separated according to metastasis. (**B**) O-PLS-DA plot of peritumoral tissue samples with vs. without metastasis, including and cross validation. (**C**) Statistical analysis of individual metabolites in tissue samples.

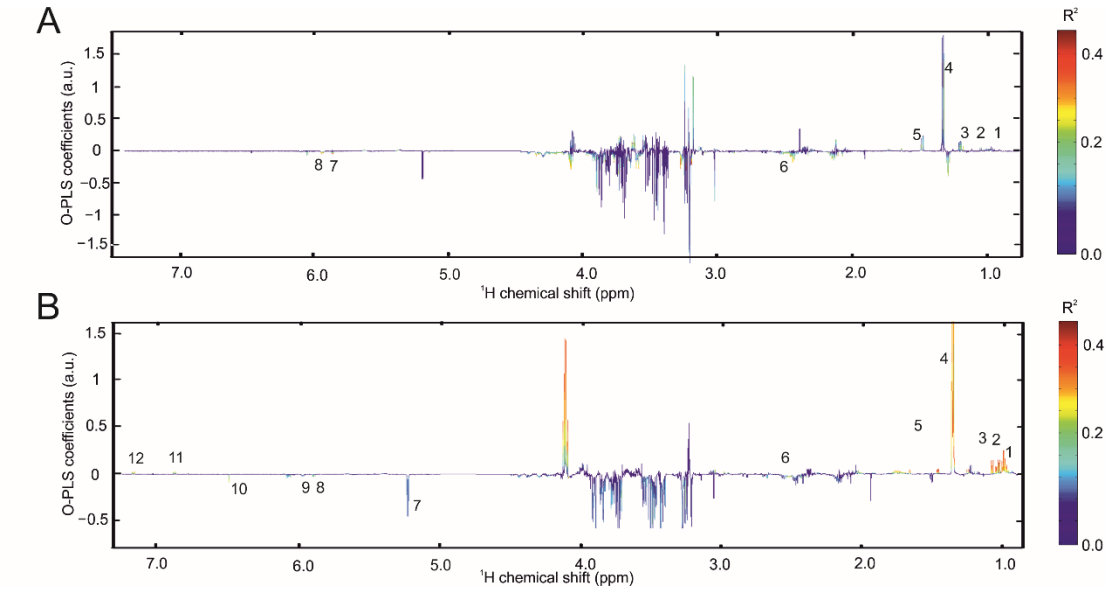

Figure S7. NMR metabolomics analysis of peritumoral and cancer tissue samples at different stages (grade IV vs. grade I). (**A**) The reduced NMR spectrum reveals altered components in normalized peritumoral tissue samples. Positive covariance corresponds to component present at increased concentrations, whereas negative covariance corresponds to decreased component concentration. Predictivity of the model is represented by R^2. 1…leucine, 2…isoleucine, 3…valine, 4…lactate, 5…lysine, 6…glutamine, 7…uridine, 8…UDP-sugars. (**B**) The reduced NMR spectrum reveals altered components in normalized cancer tissue samples. Positive covariance corresponds to component present at increased concentrations, whereas negative covariance corresponds to decreased component concentration. Predictivity of the model is represented by R^2. 1…leucine, 2…isoleucine, 3…valine, 4…lactate, 5…lysine, 6…glutamine, 7…glucose, 8…uridine, 9…UDP-sugars, 10…fumarate, 11…tyrosine, 12…phenylalanine.

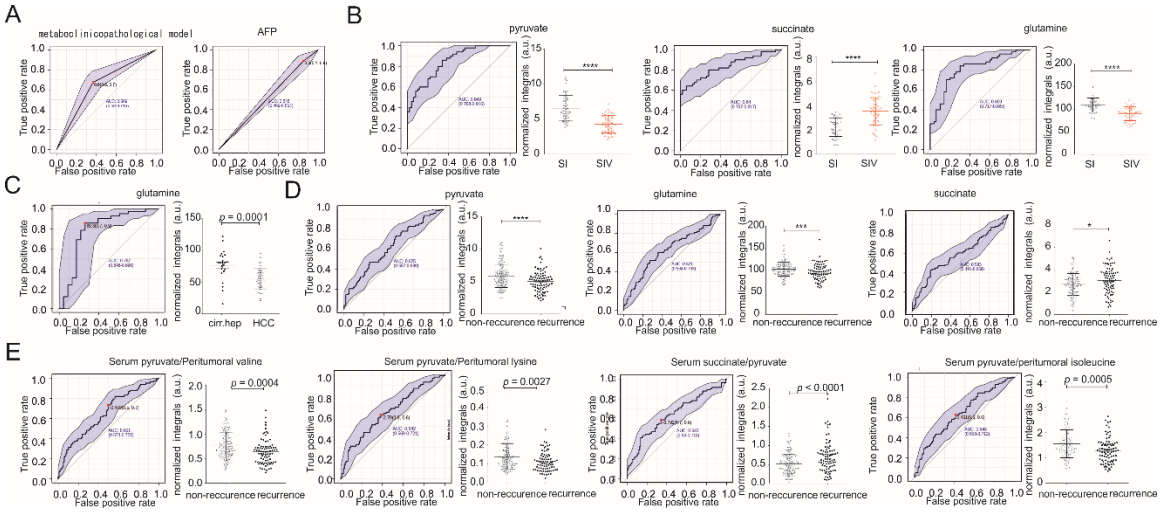

Figure S8. ROC analysis of AFP, metaboclinicopathological model and altered metabolites. (**A**) ROC curve of metaboclinicopathological model (high vs. low risk) and AFP (positive vs. negative) in HCC patients with recurrence versus non-recurrence. Absolute integrals were used to calculate ROC curves for distinct metabolites and to assess the prognostic value of the distinct metabolites of serum for tumor size (**B**), HCC (European cohort) (**C**) and recurrence (**D**). (**E**) Combination of all metabolites (serum and tissues) for ROC analysis. Statistically significant differences between groups (Student's t-test) are indicated by *p*-values of < 0.05 (*), < 0.01 (**), < 0.001 (***) or < 0.0001 (****).

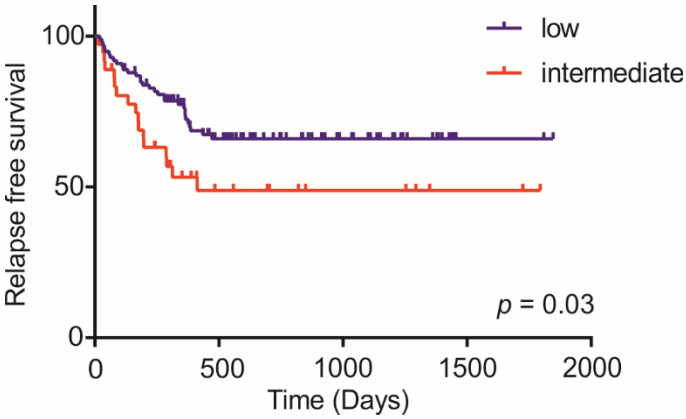

Figure S9. Recurrence-free survival (RFS) according to risk groups defined by Early Recurrence After Surgery for Liver tumor (ERASL)-pre model.

Table S1. Patient demographics and clinical characteristics (Chinese cohort).

Patient variables	All (*N*=200)	Grade I (*N*=50)	Grade II (*N*=50)	Grade III (*N*=50)	Grade IV (*N*=50)
Age (years)	54 (23–77)	64 (37–77)	56 (29–75)	54 (23–72)	52 (24–77)
Female, N (%)	40 (20%)	11 (22%)	8 (16%)	10 (20%)	11 (22%)
AFP[a]					
>10	126	27	25	35	39
≤10	66	21	24	13	8
ALT[b] U/L					
>50	38	10	10	18	0
≤50	162	40	40	32	50
Albumin (g/mL)	38.83±5.11	38.98±4.36	38.30±7.13	39.12±4.26	38.92±4.21
Bilirubin (mol/L)	18.32±14.36	17.58±7.31	22.46±26.90	15.91±5.90	17.42±8.22
Hepatitis B	174	45	40	48	41
Diameter of tumor	6.41±4.47	2.04±0.53	3.64±0.53	7.15±1.37	12.81±3.02
Cirrhosis					
N	70	7	11	20	32
Nodular	130	43	39	30	18
MVI[b]					

MV0	119	40	35	25	19
MV1	37	7	11	12	7
MV2	44	3	4	13	24

[a]AFP, alpha-fetoprotein, AFP value > 10 is positive through the manufacturer's introduction (8 patients did not receive AFP measurement). [b]ALT, Alanine aminotransferase. MVI, microvascular invasion, MV0 means the number of MV is 0, MV1 means the number of MV = 1–5, MV2 shows the number of MV > 5.

Table S2. Univariate and multivariate analysis of pre-operative factors.

Variables	Recurrence			
	Univariate Analysis		Multivariate Analysis	
	HR (95%)	*p* Value	HR (95%)	*p* Value
Gender (female vs male)	1.576 (0.663-3.743)	0.303		
Age (≥55 vs <55)	0.657 (0.355-1.216)	0.181		
Cirrhosis (yes vs no)	0.593 (0.324-1.085)	0.09		
Tumor number (single vs multiple)	2.045 (1.396-2.998)	**0.000**	2.242 (1.540-3.264)	**0.000**
AFP (≥10 vs <10)	1.315 (0.691-2.504)	0.405		
HBV (yes vs no)	0.903 (0.322-2.533)	0.847		
DCP (>40 vs ≤40)	1.610 (0.790-3.283)	0.190		
ϒ-GT (>60 vs ≤60)	2.501 (1.345-4.650)	**0.004**		
LDH (>245 vs ≤245)	1.866 (0.915-3.803)	0.086		
ALP (>125 vs ≤125)	2.285 (1.163-4.491)	**0.016**		
PT (>14.5 vs ≤14.5)	0.543 (0.193-1.527)	0.247		
ALB (>34 vs ≤34)	1.057 (0.376-2.967)	0.916		
ALT (≥50 vs <50)	2.003 (1.060-3.785)	**0.032**	2.552 (1.291-5.046)	**0.007**
AST (≥40 vs <40)	1.898 (1.028-3.507)	**0.041**		
TBIL (≥26 vs <26)	0.650 (0.157-2.696)	0.553		

TG (>1.7 vs ≤1.7)	1.250 (0.384-4.068)	0.771		
Platelet (>125 vs ≤125)	1.010 (0.524-1.946)	0.976		
No. of WBC (>9.5 vs ≤9.5)	0.858 (0.207-3.557)	0.833		
Serum succinate	1.393 (1.009-1.921)	**0.044**		
Serum glucose	0.987 (0.976-0.999)	**0.029**		
Serum succinate/serum pyruvate	3.941 (1.219-12.748)	**0.022**	4.572 (1.360-15.372)	**0.014**

AFP, alpha-fetoprotein; ALB, albumin; PT, prothrombin time; ALT, alanine aminotransferase; AST, aspartate aminotransferase; TBIL, total bilirubin; TG, triglyceride; WBC, white blood cell; DCP, abnormal prothrombin; ϒ-GT, glutamyltranspeptidase; LDH, lactate dehydrogenase; ALP, alkaline phosphatase; Significant *p*-values are indicated in bold (significance considered $p < 0.05$).

Table S3. Univariate analysis of other factors.

Variables	**Recurrence**	
	Univariate Analysis	
	HR (95%)	***p* Value**
Tumor size	1.120 (1.052-1.193)	**0.000**
Tumor encapsulation (present vs absent)	0.424 (0.244-0.736)	**0.002**
Microvascular invasion (yes vs no)	1.316 (0.715-2.420)	0.377
TNM stage	1.524 (1.102-2.106)	**0.011**
peritumoral isoleucine	1.450 (1.075-1.957)	**0.015**
peritumoral glucose	0.995 (0.991-1.000)	**0.042**

peritumoral valine	1.308 (1.110-1.541)	**0.001**
peritumoral UDP-sugars	0.894 (0.818-0.976)	**0.013**
cancers lactate	1.000 (1.000-1.000)	**0.005**
peritumoral lactate	1.000 (1.000-1.000)	**0.023**
serum pyruvate/peritumoral valine	0.177 (0.049-0.637)	**0.008**
serum pyruvate/peritumoral isoleucine	0.445 (0.239-0.829)	**0.011**
serum pyruvate/tumoral lactate	0.000 (0.000-0.000)	**0.033**
serum pyruvate/peritumoral leucine	0.000 (0.000-0.193)	**0.02**

Significant *p*-values are indicated in bold (significance considered $p < 0.05$).

Table S4. Multivariable Cox regression analyses of prognostic factors in the derivation and validation cohort without metabolic factors.

Variable	Derivation Group			Validation Group		
	Hazard Ratio (95% CI)	**β-Estimate (95% CI)**	***p* Value**	**Hazard Ratio (95% CI)**	**β-Estimate (95% CI)**	***p* Value**
ALT						
<50	Ref	Ref		Ref	Ref	
>50	2.424 (1.230, 4.778)	0.8850 (0.207, 1.564)	0.011	1.040 (0.546, 1.982)	0.039 (−0.606, 0.684)	0.905
Tumor number	2.241 (1.519, 3.305)	0.807 (0.418, 1.195)	<0.0001	2.074 (1.509, 2.850)	0.729 (0.411, 1.047)	<0.0001

Model score = tumor number * 0.807 + ALT * 0.885; PI = e^ model score/(1 + e^model score);

Cut-off to generate the risk groups: PI ≤ 0.691 (low), PI > 0.691 (high)

5 Publication III

Tissue-Specific Landscape of Metabolic Dysregulation During Ageing

Fangrong Zhang[1], Jakob Kerbl-Knapp[1], Alena Akhmetshina[1], Melanie Korbelius[1], Katharina B. Kuentzel[1], Nemanja Vujić[1], Gerd Hörl[2], Margret Paar[2], Dagmar Kratky[1,3], Ernst Steyrer[1], Tobias Madl[*1,3,4]

[1]Gottfried Schatz Research Center for Cell Signaling, Metabolism and Ageing, Molecular Biology and Biochemistry, Medical University of Graz, 8010 Graz, Austria

[2]Otto-Loewi Research Center, Physiological Chemistry, Medical University of Graz, 8010 Graz, Austria

[3]BioTechMed-Graz, 8010 Graz, Austria

[4]Lead contact

[*]Correspondence: Tobias Madl; Gottfried Schatz Research Center, Molecular Biology and Biochemistry, Medical University of Graz, Neue Stiftingtalstraße 6/6, 8010 Graz, Austria; Phone: (+43-316) 385-71972; Fax: (+43-316) 385-79615; e-mail: tobias.madl@medunigraz.at

5.1 Abstract

The dysregulation of cellular metabolism is a hallmark of ageing. To understand the metabolic changes that occur as a consequence of the ageing process and to find biomarkers for age-related diseases, we conducted a metabolomic analyses of brain, heart, kidney, liver, lung and spleen in young (9-10 weeks) and old (96-104 weeks) wild type mice [mixed genetic background of 129/J and C57BL/6] using NMR spectroscopy. We found differences in metabolic fingerprints of all tissues and distinguished several metabolites to be altered in most tissues, suggesting that they may be universal biomarkers of ageing. In addition, we found distinct tissue-clustered sets of metabolites throughout the organism. The associated metabolic changes may reveal novel

therapeutic targets for the treatment of ageing and age-related diseases. Moreover, the identified metabolite biomarkers could provide a sensitive molecular read-out to determine the age of biologic tissues and organs and to validate the effectiveness and potential off-target effects of senolytic drug candidates on both a systemic and tissue-specific level.

Keywords: ageing; tissues-specific; metabolomics; biomarker

5.2 Introduction

Ageing might be defined as the process by which structural and functional changes accumulate in an organism over time. Overall, ageing is characterized by a reduction in the ability to maintain metabolic and functional homeostasis in multiple tissues (140). This can occur at vastly different compartments within the cell, implying that ageing proceeds as a consequence of the interplay between a multitude of pathways, rather than from a single cause. Altogether, the following nine hallmarks are most frequently proposed to be epiphenomena of ageing: genomic instability, telomere attrition, epigenetic alterations, loss of proteostasis, deregulated nutrient-sensing, mitochondrial dysfunction, stem cell exhaustion, altered intercellular communication and cellular senescence (140). In particular, senescence has been suggested to contribute to the course of ageing and age-related diseases (296) by imbalanced cellular function, leading to increased DNA damage, generation of reactive metabolites, oxidative stress and inflammation (297-299). These changes can lead to pathophysiological manifestations like tissue atrophy and nerve loss, both of which are common in ageing tissues. In addition, they are associated with age-related pathologies, such as geriatric syndromes, Parkinson's and Alzheimer's disease, diabetes mellitus type 2, and atherosclerosis (146-151, 300, 301). Whereas these conditions differ greatly in their clinical manifestations, they share a common trait of dysregulated metabolism (152-154, 301-303). As an example, blood concentrations of branched chain amino acids (BCAAs), lipids with low carbon numbers, or sugar metabolites are increased in diabetes mellitus type 2 (152, 153), whereas methionine, histidine, lysine and phosphatidylethanolamine are increased in patients suffering from Alzheimer's disease (154). Moreover, there is increasing evidence that metabolic changes do not only occur as a consequence of ageing processes, but, vice versa, might be drivers thereof (302).

In each organism, tissues are combined in structural and functional units to form organs. Different organs are integrated and connected by blood and lymph vessels to form a whole organism. The

tissue conditions may affect basic vital functions and the health status of the entire organism and vice versa. With respect to age-related alterations in the metabolome at the tissue level, only few studies have been performed so far in mice, and even less in humans (157, 304-306). Mice are a key tool for ageing research due to their relatively short life span, which allows monitoring of the ageing process within a reasonable time frame, and due to the ability to perform genetic manipulations. Ageing research has so far mostly focused on genetically modified mice mimicking progeroid syndromes and not on animals that age by themselves. Therefore, aging mice under normal physiological condition are a highly valuable model to investigate the changes in metabolites and metabolic pathways as a consequence of the spontaneous deterioration of homeostatic balance over time. Metabolomics enables the capturing of the entire metabolic state of an organism, allows its temporal resolution at distinct time points during the ageing process, and helps to identify altered pathways and biomarkers during ageing and in disease (105, 106). Today´s biomarkers of ageing mainly include phenotypical read-outs such as frailty or grip-strength (307) and a small set of to-be-further-evaluated molecular markers, which provide a more general assessment of the physiological age (308). These biomarkers are an important tool to describe the physiological changes that occur with age, the process of ageing and the occurrence of age-related diseases.

Here, we aimed to provide a comprehensive set of ageing-related metabolic biomarkers in mouse tissues for the identification of tissue-specific and systemic metabolic changes in an ageing organism. To this end, we employed untargeted Nuclear Magnetic Resonance (NMR) spectroscopy and determined changes in polar metabolites in brain, heart, kidney, liver, lung and spleen of young (9-10 weeks) and aged (96-104 weeks) wild type mice (mixed genetic background of 129/J and C57BL/6J). We found alterations in the metabolic phenotypes of all tissues and identified sets of both tissue-specific and systemic metabolite biomarkers of ageing. We identified the following organ-specific biomarkers: i) BCAAs, uracil and glutamine in the brain, ii) leucine, isoleucine, valine and 4-aminobutyrate (GABA) in the heart, iii) succinate and choline in the kidney, iv) nicotinamide, glycerol and inosine in the liver, v) lysine, nicotinamide, aspartate and fumarate in the lung, and vi) taurine and uridine in the spleen. Uridine changed systemically in most tissues, indicating conserved mechanisms of ageing. Our comprehensive metabolic profiling of the key mouse tissues at different ages provides a robust set of metabolic biomarker candidates to study

the mechanisms of metabolic reprograming associated with ageing. A deeper understanding of the underlying processes might not only shed light onto the causes of age-related pathologies, but also help to discover novel targets for pharmacological interventions. These biomarker candidates could serve as a read-out of the biological age of tissues and may be utilized to validate the effectiveness of proposed senolytic therapies. Taken together, comprehensive analyses and utilization of metabolomics provide a useful tool to monitor changes of metabolites during ageing and degenerative process, respectively, and may eventually help to increase health span and, thus, the life quality of the aged population.

5.3 Materials and Methods

5.3.1 Animals and diets

For all experiments, organs were isolated from young (9-10 weeks) and old (96-104 weeks) female wild type mice (mixed genetic background of 129/J and C57BL/6J) were used (n=5). Mice were maintained in a clean, temperature-controlled (22 ± 1°C) environment with a regular light–dark cycle (12 h/12 h) and unlimited access to chow diet (Altromin 1324, Altromin Spezialfutter GmbH, Lage, Germany) and water. All experiments were performed in accordance with the European Directive 2010/63/EU and approved by the Austrian Federal Ministry of Education, Science and Research.

5.3.2 NMR sample preparation, data acquisition and analysis

Organ samples were snap frozen in liquid nitrogen and stored at -80°C until analysis. For NMR metabolomics analysis, 30-50 mg of each organ were resected. To extract metabolites, 400 µl of ice-cold methanol and 200 µl MilliQ H_2O were added and the samples transferred to a tube containing Precellys beads (1.4 mm zirconium oxide beads, Bertin Technologies, Villeurbanne, France) for homogenisation by Precellys24 tissue homogeniser (Bertin Technologies, Montigny-le-Bretonneux, France). After centrifugation at 13,000 rpm for 45 min (4°C), the supernatant was transferred to a fresh tube, and the samples were lyophilised at < 1 Torr, 850 rpm, 25 °C for 10 h in a vacuum drying chamber (Savant Speedvac SPD210 Vacuum Concentrator), with an attached cooling trap (Savant RVT450 Refrigerated Vapor Trap) and vacuum pump (VLP120 Vacuum pump) (Thermo Scientific, Waltham, MA). For NMR experiments, samples were re-dissolved in

500 µl of NMR buffer [0.08 M Na_2HPO_4, 5 mM TSP (3-(trimethylsilyl) propionic acid-2,2,3,3-d_4 sodium salt), 0.04 (w/v) % NaN_3 in D_2O, pH adjusted to 7.4 with 8 M HCl and 5 M NaOH].

Metabolic profiling analysis was conducted at 310 K using a 600 MHz Bruker Avance Neo NMR spectrometer equipped with a TXI 600S3 probe head. The Carr–Purcell–Meiboom–Gill (CPMG) pulse sequence was used to acquire ^1H 1D NMR spectra with a pre-saturation for water suppression (cpmgpr1d, 512 scans, 73728 points in F1, 12019.230 Hz spectral width, 1024 transients, recycle delay 4 s) (309). The $^1H–^{13}C$ heteronuclear single-quantum correlation (HSQC) spectra were recorded with a recycle delay of 1.0 s, spectral widths of 15.9/30 ppm, centered at 4.7/118.0 ppm in $^1H/^{13}C$, with 1024 and 256 points, respectively, and 16 scans per increment. NMR spectral data were processed as previously described (266). Briefly, data were processed in Bruker Topspin version 4.0.2 using one-dimensional exponential window multiplication of the FID, Fourier transformation, and phase correction. NMR data were then imported to Matlab2014b, TSP was used as internal standard for chemical shift referencing (set to 0 ppm), regions around the water, TSP and methanol signals were excluded, NMR spectra were aligned, and a probabilistic quotient normalization was performed. Principal component analysis (PCA), orthogonal partial least squares discriminant analysis (O-PLS-DA) and partial least squares-discriminant analysis (PLS-DA) were performed in Matlab2014b and MetaboAnalyst 4.0 (268) as well as all associated data consistency checks and cross-validation. The statistical significance of the determined differences is validated by the quality assessment statistic Q^2. This measure provides information about cross-validation and is a qualitative measure of consistency between the predicted and original data with a maximum value of 1. Metabolite identification was carried out using Chenomx NMR Suite 8.4 (Chenomx Inc., Edmonton, AB, Canada) and reference compounds. Quantification of metabolites was carried out by signal integration of normalized spectra. For each metabolite, a representative peak with no overlapping signals was identified, the start and end points of the integration were chosen to revolve around that peak, and the area of the peak was integrated by summing up the value for each point. For visualization of our integration approach, the characteristic peaks of selected metabolites are shown in **Figure S10**, with the area of integration indicated by the black bars. Univariate statistical analysis was carried out using GraphPad Prism 5.01 (GraphPad Software, La Jolla, CA). Data are represented as mean ± standard deviation (SD). P-values were

calculated using a two-tailed Student's t-test for pairwise comparison of variables and are only given for metabolites with $p < 0.05$.

5.4 Results

Our goal was to establish both tissue-specific profiles and systemic metabolic signatures of ageing, which could serve as a basis for understanding the overall ageing process. ^{1}H-NMR spectroscopy is a powerful technique capable of simultaneous identification and quantification of multiple metabolites in complex biological matrices (310). To better understand the systemic and tissue-specific ageing process and to identify metabolites influenced by age, we carried out metabolic profiling of brain, heart, kidney, liver, lung and spleen from young and aged mice using an untargeted NMR spectroscopy approach. Using this approach, we were able to plot all spectra of identifiable metabolites within one sample and allocated the particular peaks to the respective metabolites available in metabolite databases (311). The identified respective biomarker candidates will provide a valuable resource for a variety of applications in ageing research and drug discovery.

Using this method, we first determined the metabolic fingerprints of brain samples in young (9-10 weeks) and aged mice (96-104 weeks). Neurocognitive ageing is characterized by a reduction in the information processing time, an impaired long-term memory (312), both of which are related to an imbalance in energy metabolism and redox homeostasis (313).The discriminant clustering between brains from young and old mice shown in the Orthogonal-Partial Least Squares - Discriminant Analysis (O-PLS-DA) plot in **Figure 14A** indicates the underlying differences in the metabolome, supported by the correlation coefficients R^2Y up to 0. 997 ($p=0.02$) and a positive Q^2 of 0.727 ($p=0.03$), validating the significance of these results. Reduced NMR spectra revealed alterations in the levels of metabolites in mouse brains of different ages (**Figure 14B**), with decreased concentrations of lactate, methionine, N-acetylaspartate, uridine and inosine. In contrast, concentrations of leucine, isoleucine, valine, glutamine, allantoin, uracil, tyrosine and phenylalanine were increased in the aged mice (**Figure 14B** and **C**). 2D HSQC spectra of one brain sample further confirmed the assigned metabolites (**Figure S11A**).

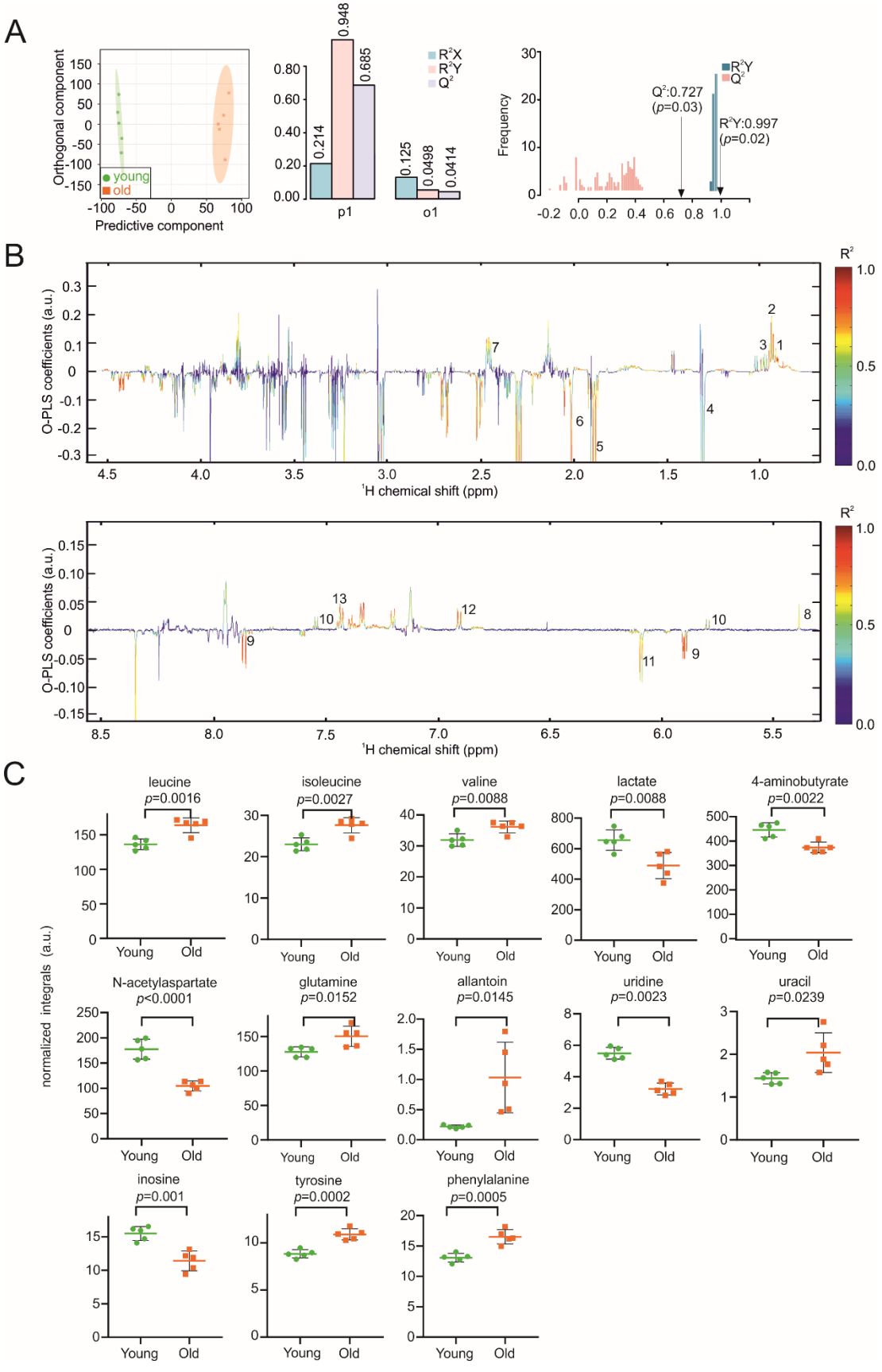
A
Orthogonal component
Predictive component
young
old
0.214
0.948
0.685
p1
0.125
0.0498
0.0414
o1
R²X
R²Y
Q²
Frequency
Q²:0.727
(p=0.03)
R²Y:0.997
(p=0.02)
B
O-PLS coefficients (a.u.)
¹H chemical shift (ppm)
R²
C
normalized integrals (a.u.)
leucine
p=0.0016
isoleucine
p=0.0027
valine
p=0.0088
lactate
p=0.0088
4-aminobutyrate
p=0.0022
N-acetylaspartate
p<0.0001
glutamine
p=0.0152
allantoin
p=0.0145
uridine
p=0.0023
uracil
p=0.0239
inosine
p=0.001
tyrosine
p=0.0002
phenylalanine
p=0.0005
Young
Old

Figure 14. NMR metabolomics analysis of mouse brain samples. (A) O-PLS-DA plot of brain samples, including cross validation. (B) The reduced NMR spectrum reveals altered components in normalized brain samples. Positive covariance corresponds to components present at increased concentrations, whereas negative covariance corresponds to decreased component concentration. Predictivity of the model is represented by R^2. 1. Leucine, 2. isoleucine, 3. valine, 4. lactate, 5. 4-aminobutyrate, 6. N-acetylaspartate, 7. glutamine, 8. allantoin, 9. uridine, 10. uracil, 11. inosine, 12. tyrosine, 13. phenylalanine. (C) Statistical analysis of altered metabolites in brain samples using Student's t-test. $p < 0.05$ was considered statistically significant.

Impaired metabolic flexibility is a hallmark of the ageing heart, with decreased capacity to oxidize fatty acids and increased glucose metabolism (314). When comparing the metabolic fingerprints between heart samples isolated from young and aged mice, O-PLS-DA revealed distinct clustering of respective heart samples with correlation coefficients R^2Y of up to 0.999 ($p=0.19$) and a Q^2 of 0.786 ($p = 0.02$) (**Figure 15A**). Reduced NMR spectra demonstrated altered abundance of metabolites in normalized heart samples (**Figure 15B**) and indicated decreased uridine concentrations in the hearts of aged mice, whereas the levels of leucine, isoleucine, valine, acetate, GABA, creatine, uracil, tyrosine and phenylalanine were increased (**Figures 15C**). 2D HSQC spectra of one heart sample is consistent with the assigned metabolites in **Figure S11B**.

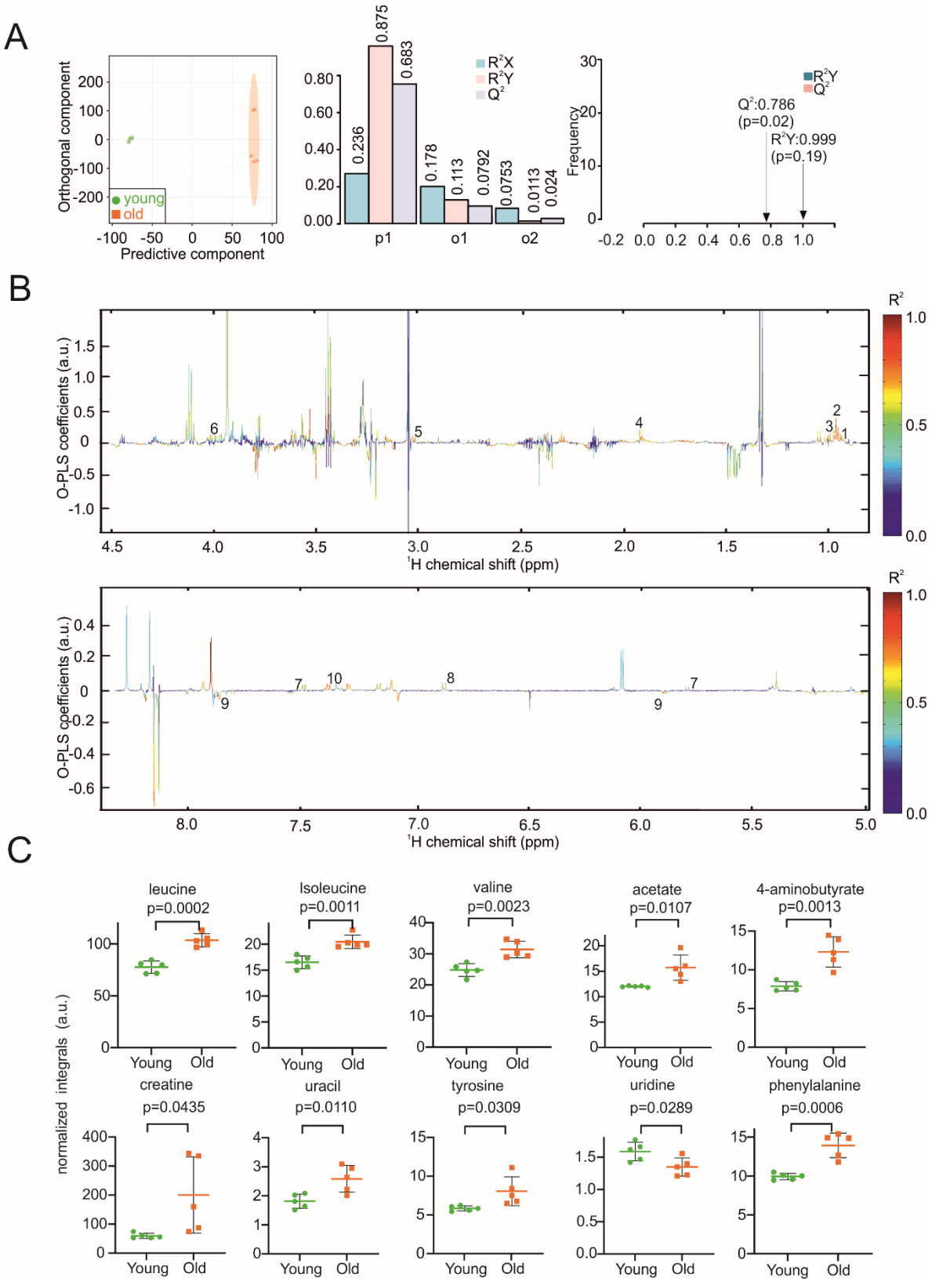
A
Orthogonal component
Predictive component
young
old
0.236
0.875
0.683
0.178
0.113
0.0792
0.0753
0.0113
0.024
p1
o1
o2
R²X
R²Y
Q²
Frequency
Q²:0.786
(p=0.02)
R²Y:0.999
(p=0.19)
B
O-PLS coefficients (a.u.)
¹H chemical shift (ppm)
R²
C
normalized integrals (a.u.)
leucine
p=0.0002
Isoleucine
p=0.0011
valine
p=0.0023
acetate
p=0.0107
4-aminobutyrate
p=0.0013
creatine
p=0.0435
uracil
p=0.0110
tyrosine
p=0.0309
uridine
p=0.0289
phenylalanine
p=0.0006
Young
Old

Figure 15. NMR metabolomics analysis of mouse heart samples. (A) O-PLS-DA plot of heart samples, including cross validation. (B) The reduced NMR spectrum reveals altered components in normalized heart samples. Positive covariance corresponds to component present at increased concentrations, whereas negative covariance corresponds to decreased component concentration. Predictivity of the model is represented by R2. 1. Leucine, 2. isoleucine, 3. valine, 4. acetate, 5. 4-aminobutyrate, 6. creatine, 7. uracil, 8. tyrosine, 9. uridine, 10. phenylalanine. (C) Statistical analysis of altered metabolites in heart samples using Student's t-test. $p < 0.05$ was considered statistically significant.

A plethora of abnormalities in kidney structure and function are positively correlated with advancing age (315). In the kidney, local immune responses induce cellular metabolic reprogramming that changes with ageing (316). The distinct clustering of kidney samples from young and old mice is shown in the score and validation plots of the O-PLS-DA (**Figure 16A**). The two clusters show correlation coefficients R^2Y of up to 0.997 ($p=0.03$) and Q^2 values of 0.898 ($p = 0.01$) (**Figure 16A**). In reduced NMR spectra, we found differences in the abundance of 23 age-dependent metabolites (**Figure 16B**). Leucine, isoleucine, valine, alanine, methionine, glutamate, succinate, aspartate, asparagine, lysine, ethanolamine, choline, glycerol, creatine, serine, uridine, inosine, tyrosine and nicotinamide were decreased in the cohort representing the older mice, whereas the levels of allantoin and uracil were increased (**Figures 16C**). 2D HSQC spectra of one kidney sample in **Figure S11C** also matched the assigned metabolites in 1D spectra.

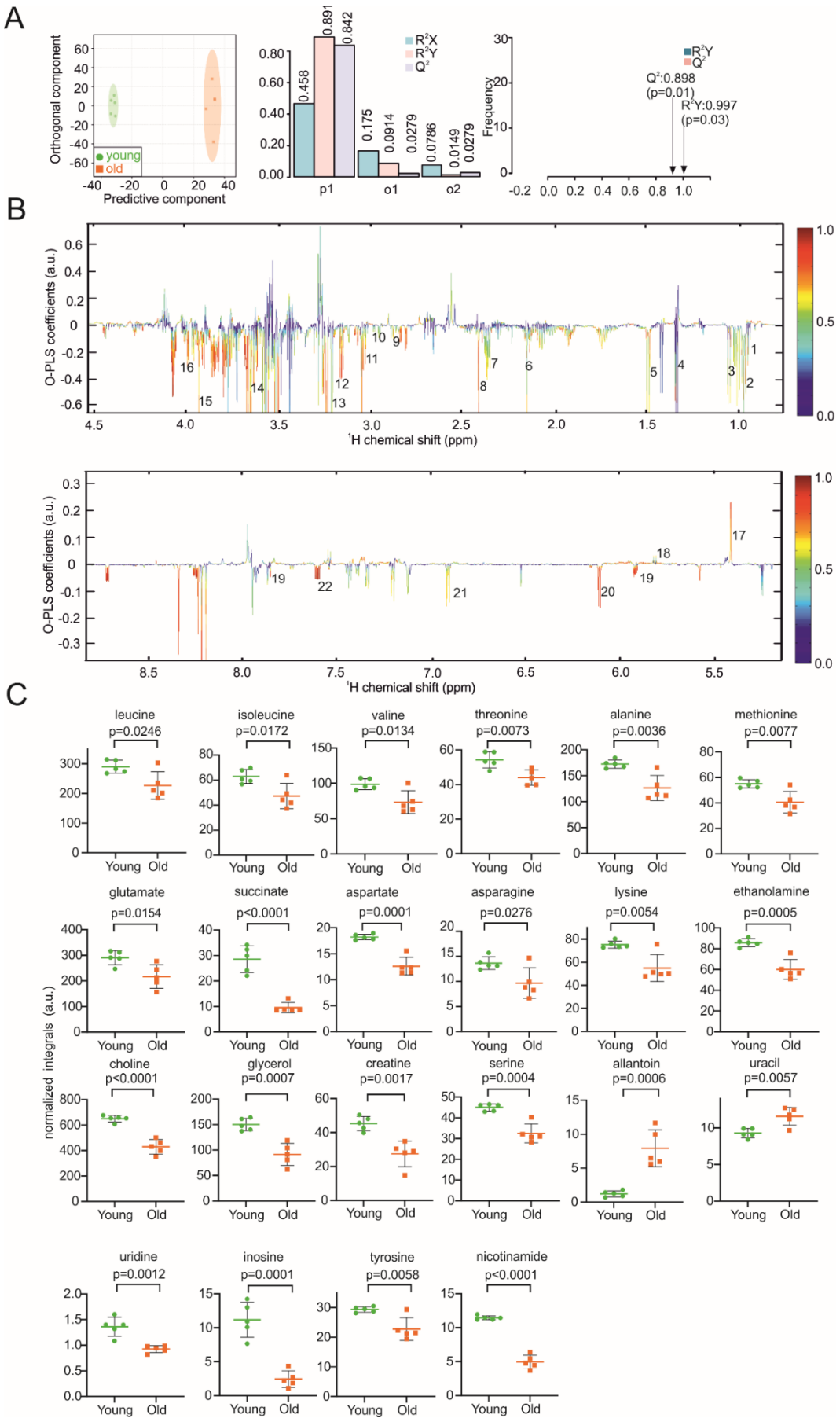
A
Orthogonal component
Predictive component
young
old
R²X
R²Y
Q²
0.458
0.891
0.842
0.175
0.0914
0.0279
0.0786
0.0149
0.0279
p1
o1
o2
Frequency
Q²:0.898
(p=0.01)
R²Y:0.997
(p=0.03)
B
O-PLS coefficients (a.u.)
¹H chemical shift (ppm)
C
normalized integrals (a.u.)
leucine p=0.0246
isoleucine p=0.0172
valine p=0.0134
threonine p=0.0073
alanine p=0.0036
methionine p=0.0077
glutamate p=0.0154
succinate p<0.0001
aspartate p=0.0001
asparagine p=0.0276
lysine p=0.0054
ethanolamine p=0.0005
choline p<0.0001
glycerol p=0.0007
creatine p=0.0017
serine p=0.0004
allantoin p=0.0006
uracil p=0.0057
uridine p=0.0012
inosine p=0.0001
tyrosine p=0.0058
nicotinamide p<0.0001
Young
Old

Figure 16. NMR metabolomics analysis of mouse kidney samples. (A) O-PLS-DA plot of kidney samples, including cross validation. (B) The reduced NMR spectrum reveals altered components in normalized kidney samples. Positive covariance corresponds to component present at increased concentrations, whereas negative covariance corresponds to decreased component concentration. Predictivity of the model is represented by R2. 1. Leucine, 2. isoleucine, 3. valine, 4. threonine 5. alanine, 6. methionine, 7. glutamate, 8. succinate, 9. aspartate, 10. asparagine, 11. lysine, 12. ethanolamine, 13. choline, 14. glycerol, 15. creatine, 16. serine, 17. allantoin, 18. uracil, 19. uridine, 20. inosine, 21. tyrosine, 22. nicotinamide. (C) Statistical analysis of altered metabolites in kidney samples using Student's t-test. $p < 0.05$ was considered statistically significant.

Impaired fatty acid oxidation and increased *de nov*o lipogenesis in the liver contribute to the risk for age-associated chronic liver disease (317). Comparable to other organs described above, we also identified two distinct metabolic clusters in livers of old and young mouse with correlation coefficients R^2Y of up to 0.997 ($p<0.01$) and a positive Q^2 of 0.842 ($p<0.01$) (**Figure 17A**). Reduced NMR spectra revealed nine metabolites with varying concentrations (**Figure 17B**). In old mice, the concentrations of lactate, alanine, glycerol, glucose, uridine, inosine, fumarate and nicotinamide were decreased, whereas aspartate was increased (**Figure 17C**). The assignment of metabolites was confirmed by 2D HSQC spectra of one liver sample in **Figure S11D**.

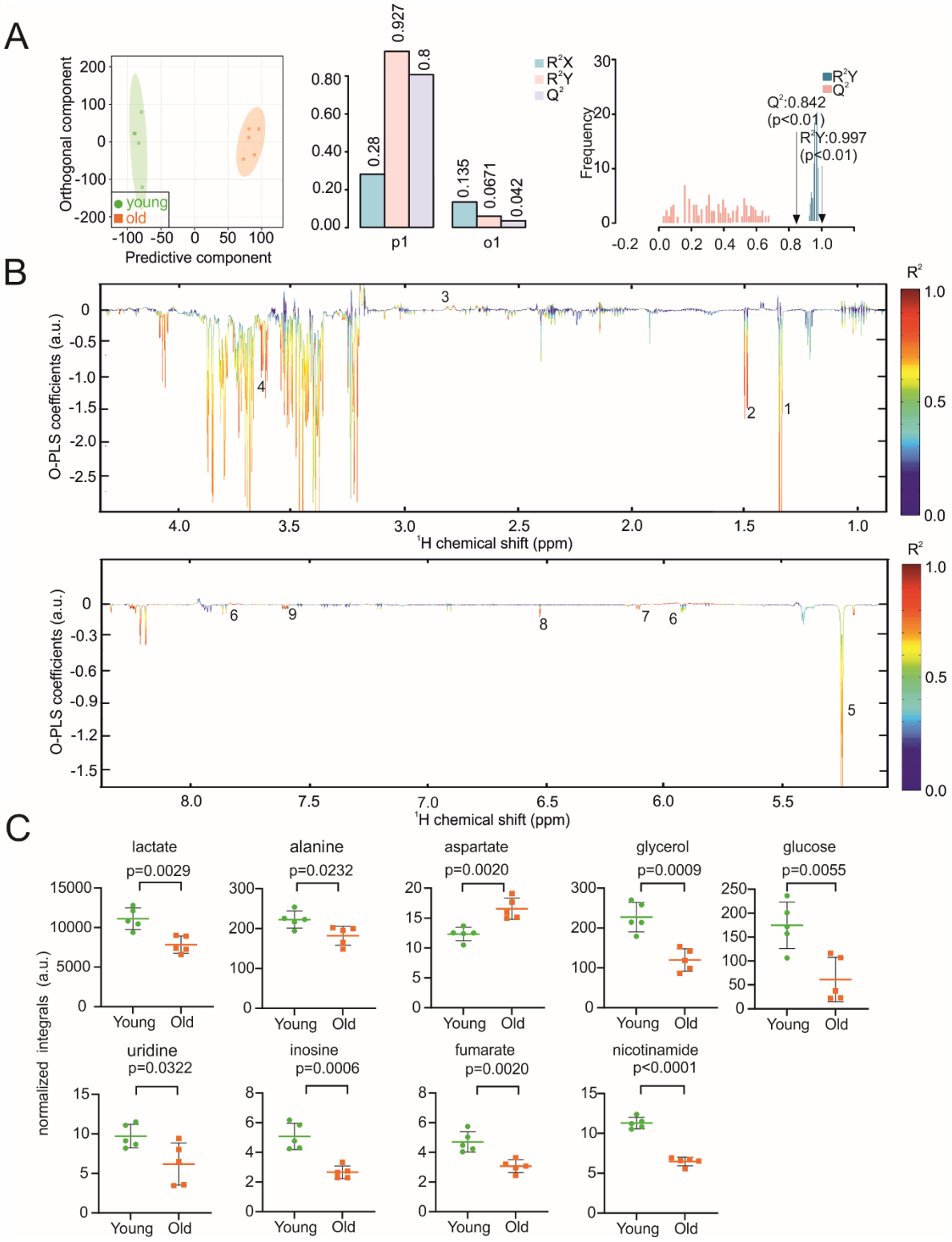

Figure 17. NMR metabolomics analysis of mouse liver samples. (A) O-PLS-DA plot of liver samples, including cross validation. (B) The reduced NMR spectrum reveals altered components in normalized liver samples. Positive

covariance corresponds to component present at increased concentrations, whereas negative covariance corresponds to decreased component concentration. Predictivity of the model is represented by R^2. 1. Lactate, 2. alanine, 3. aspartate, 4. glycerol, 5. glucose, 6. uridine, 7. inosine, 8. fumarate, 9. nicotinamide. (C) Statistical analysis of altered metabolites in liver samples using Student's t-test. $p < 0.05$ was considered statistically significant.

Lung ageing is related to structural remodeling, decreased respiratory function and chronic lung diseases, which are closely linked to the ageing process of the immune system (318). The hierarchical O-PLS-DA scores plots (**Figure 18A**) allowed a clear discrimination between lung samples from young and old mice with correlation coefficients R^2Y of up to 0.986 ($p=0.26$) and a positive Q^2 of 0.755 ($p=0.02$)). Malonate, fumarate, and nicotinamide were decreased in the old mice, whereas leucine, isoleucine, valine, threonine, methionine, aspartate, lysine, allantoin, tyrosine, and phenylalanine concentrations were increased (**Figures 18B** and **C**). Additional confirmation of assigned metabolites of lung sample was provided by 2D HSQC spectra in **Figure S11E**.

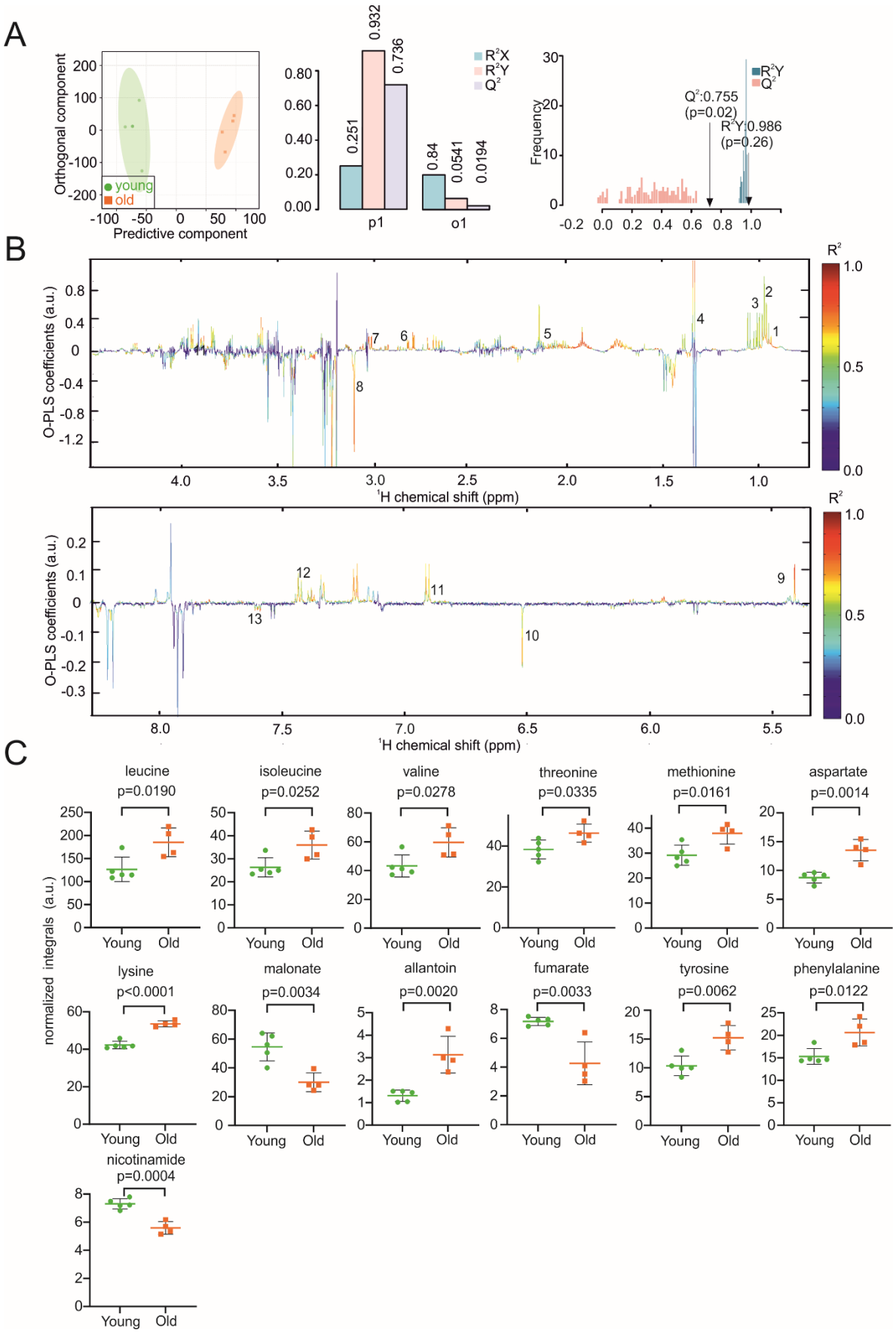
A
Orthogonal component
Predictive component
young
old
0.932
0.736
0.251
0.84
0.0541
0.0194
p1
o1
R²X
R²Y
Q²
Frequency
Q²:0.755
(p=0.02)
R²Y:0.986
(p=0.26)
B
O-PLS coefficients (a.u.)
¹H chemical shift (ppm)
R²
C
normalized integrals (a.u.)
leucine p=0.0190
isoleucine p=0.0252
valine p=0.0278
threonine p=0.0335
methionine p=0.0161
aspartate p=0.0014
lysine p<0.0001
malonate p=0.0034
allantoin p=0.0020
fumarate p=0.0033
tyrosine p=0.0062
phenylalanine p=0.0122
nicotinamide p=0.0004
Young
Old

Figure 18. NMR metabolomics analysis of mouse lung samples. (A) O-PLS-DA plot of lung samples, including and cross validation. (B) The reduced NMR spectrum reveals altered components in normalized lung samples. Positive covariance corresponds to component present at increased concentrations, whereas negative covariance corresponds to decreased component concentration. Predictivity of the model is represented by R^2. 1. Leucine, 2. isoleucine, 3. valine, 4. threonine, 5. methionine, 6. aspartate, 7. lysine, 8. malonate, 9. allantoin, 10. fumarate, 11. tyrosine, 12. phenylalanine, 13. nicotinamide. (C) Statistical analysis of altered metabolites in lung samples using Student's t-test. $p < 0.05$ was considered statistically significant.

The spleen plays an important role in the immune system. In aged mice, structural changes in the spleen result in a less effective or decreased immune response (319). O-PLS-DA models clearly discriminated NMR spectra of spleen samples from young and aged mice (**Figure 19A**). Reduced NMR spectra revealed decreased concentrations of alanine, methionine, glutamate, aspartate, asparagine, lysine, o-phosphocholine, taurine, glycine, uridine, fumarate, tyrosine, and phenylalanine in the aged mice, whereas lactate, glucose, and allantoin concentrations were increased (**Figures 19B, C**). The 2D HSQC spectra assignment of spleen sample was found to be consistent with the assigned metabolites in 1D spectra (**Figure S11F**).

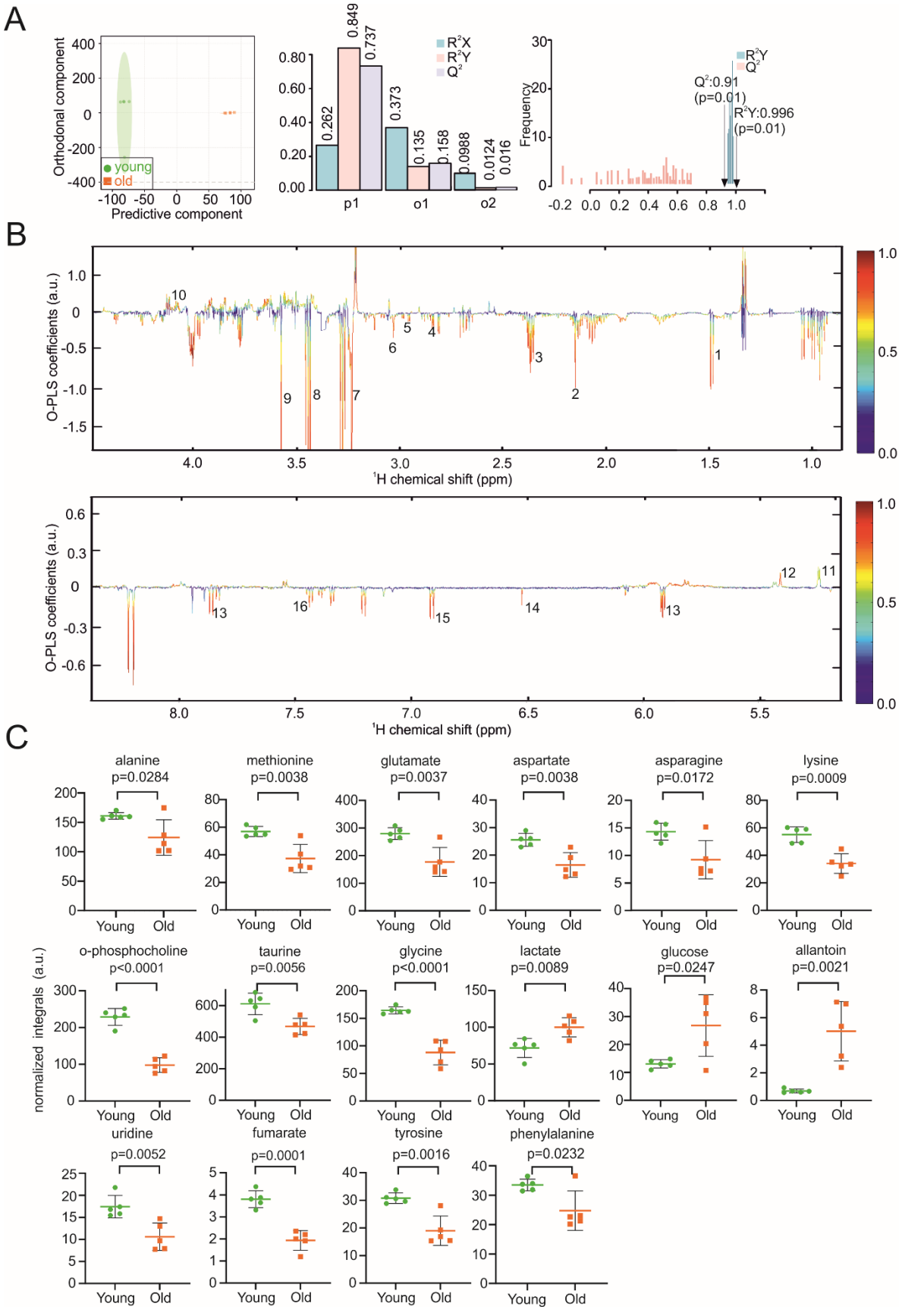
A
Orthodonal component
Predictive component
young
old
R²X
R²Y
Q²
0.262
0.849
0.737
0.373
0.135
0.158
0.0988
0.0124
0.016
p1
o1
o2
Frequency
Q²:0.91
(p=0.01)
R²Y:0.996
(p=0.01)
B
O-PLS coefficients (a.u.)
¹H chemical shift (ppm)
C
normalized integrals (a.u.)
alanine p=0.0284
methionine p=0.0038
glutamate p=0.0037
aspartate p=0.0038
asparagine p=0.0172
lysine p=0.0009
o-phosphocholine p<0.0001
taurine p=0.0056
glycine p<0.0001
lactate p=0.0089
glucose p=0.0247
allantoin p=0.0021
uridine p=0.0052
fumarate p=0.0001
tyrosine p=0.0016
phenylalanine p=0.0232
Young
Old

Figure 19. NMR metabolomics analysis of mouse spleen samples. (A) O-PLS-DA plot of spleen samples, including cross validation. (B) The reduced NMR spectrum reveals altered components in normalized spleen samples. Positive covariance corresponds to component present at increased concentrations, whereas negative covariance corresponds to decreased component concentration. Predictivity of the model is represented by R2. 1. Alanine, 2. methionine, 3. glutamate, 4. aspartate, 5. asparagine, 6. lysine, 7. o-phosphocholine, 8. taurine, 9. glycine, 10. lactate, 11. glucose, 12. allantoin, 13. uridine, 14. fumarate, 15. tyrosine, 16. phenylalanine. (C) Statistical analysis of altered metabolites in spleen samples using Student's t-test. $p < 0.05$ was considered statistically significant.

Finally, we compared the abundance of all metabolites between the organs of young and aged mice. **Figure 20** depicts a correlation heatmap of metabolites in the six investigated tissues from both young and old mice, which exhibited the different distribution patterns of metabolites between different age and organs.

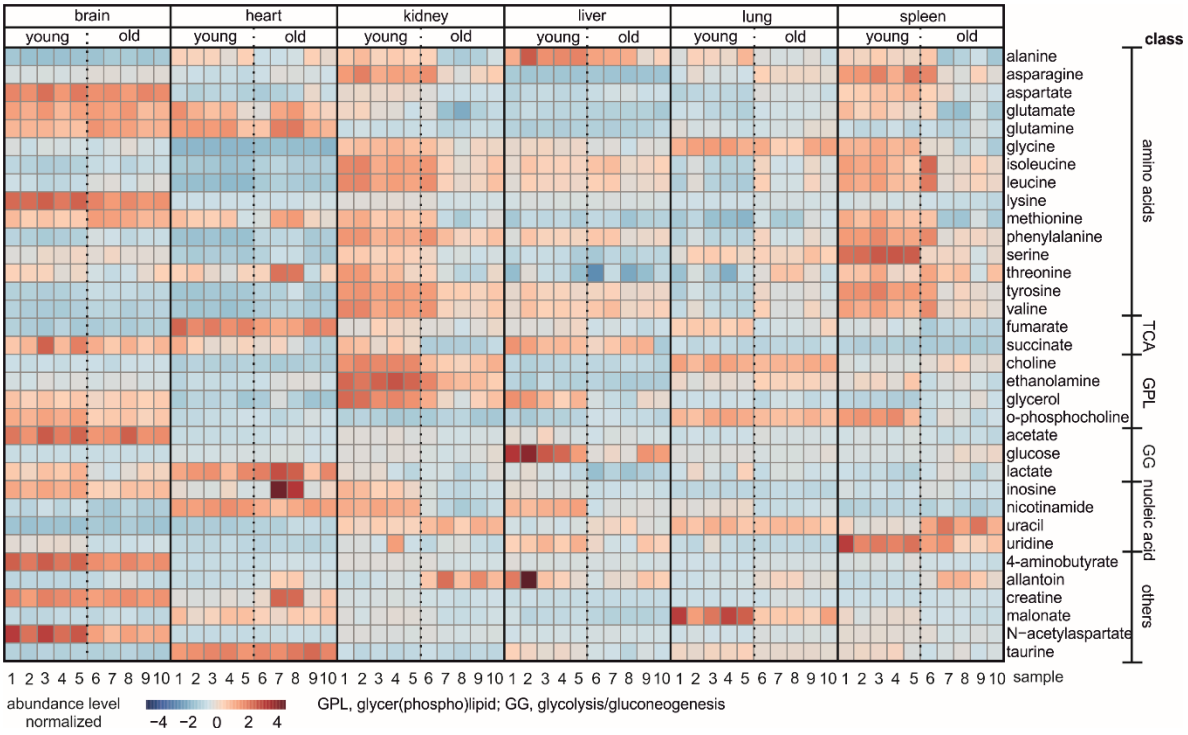

Figure 20. Heat map of NMR analyses showing the relative metabolite levels in organs from young and old mice. Each column represents one single sample, each row represents one distinct metabolite as indicated. Increased and decreased metabolites are given in red and blue, respectively. Metabolites are indicated and sorted according to different chemical classes or biomolecular pathways. Bioinformatic analysis of data was performed using the statistical package in MetaboAnalyst 5.0 **(**http://www.metaboanalyst.ca/MetaboAnalyst/**).**

5.5 Discussion

Ageing is a process that gradually increases the organism's vulnerability and affects multiple biological pathways, including metabolism. The health state of tissues plays a key role in ageing or *vice versa*, as age-associated organ failure, for example, can lead to the death of an organism. Therefore, revealing the consequences of ageing on specific metabolites in distinct tissues is essential to provide information of the underlying mechanisms as they explain the metabolic activity in various tissues and provide functional evidence for biochemical activity. By studying metabolic reprogramming in ageing mice using untargeted NMR-based metabolomics, we identified a set of robust biomarkers for ageing in several murine tissues. NMR spectroscopy is a powerful tool in this regard due to its high reproducibility and simple analysis.

For all six tissues studied, we identified sets of tissue-specific biomarkers of ageing. In the brain, we identified 13 metabolites comprising amino acids and their derivatives, such as tyrosine, phenylalanine and N-acetylaspartate. In addition to amino acid metabolism, the ageing metabolome of mouse brain is characterized by alterations in the purine and pyrimidine metabolism, with a significant increase in uracil (306). In line, we also observed increased uracil in aged mice. Larsson *et. al.* reported that the elevated plasma levels of BCAAs (isoleucine, leucine and valine) are associated with Alzheimer's disease (320). In line with this observation, we also found increased levels of BCAAs in brain lysates of old mice. This phenomenon may be related to the production of the neurotransmitter glutamate known to be altered in the nervous system during ageing (321). Additionally, our results on changes in glutamine concentrations, in line with a study that investigated metabolites of the motor cortex of the brain in humans of different age (24 to 68 years) by ^{1}H-NMR indicate that these metabolites represent stable ageing markers in the brain of both mice and humans (322). Thus, changes in BCAAs, uracil and glutamine are in accordance with recent studies of brain metabolites (320, 323).

With ageing, the heart exhibits alterations in amino acid and purine metabolism. Here we found a set of ten metabolites significantly changed in the ageing mouse heart. Downregulation of BCAA catabolism in cardiomyocytes has been previously reported to disrupt autophagy, which in turn may be associated with ageing (324, 325). Elevated BCAA levels can therefore be seen as detrimental, in line with large-scale human cohort studies, investigating heart failure (326) and

risks of cardiovascular disease (327). Thus, increased BCAA levels suggest an increased risk of cardiovascular disease in course of aging. Similarly, the neurotransmitter GABA has been proposed to interfere with cardiac function and was increased by ageing (328, 329). A direct association with cardiac function has previously been demonstrated (326, 328, 329), rendering leucine, isoleucine, valine and GABA particularly promising as aging-heart biomarkers.

In the kidney, we identified profound changes in metabolic profiles, with more than 20 metabolites differing between old and young mice. Most metabolic changes were associated with amino acid, purine/pyrimidine metabolism, and the tricarboxylic acid (TCA) cycle. Among additional metabolites, changes in the choline status might indicate kidney damage (330). Choline deficiency has been reported to cause kidney damage in rats due to a decrease in the formation of phospholipids, which in turn causes degeneration of the kidney structure (331). Thus, the decreased choline status in aged mice point to similar mechanisms (330). Succinate activates the longevity regulator DAF-16 C in *C. elegans*, which increases stress resistance and may extend lifespan (332). Decreased succinate levels in old mice suggest a more important role of this metabolite in age-related metabolic adaptations than previously assumed. The importance of glutamate is still investigated, but recent publications indicate a tight connection to cellular senescence (333, 334). Here, a decrease in glutamate seems to be linked to the avoidance cell death in senescent cells, mediated through the expression of glutaminases. We could observed lowered glutamate levels in the kidney and spleen of our old mice, supporting the theory that lowered glutamate levels are linked to senescence and ageing (334). Choline, succinate and glutamate might be used in the future as promising biomarkers to determine the health- and age-related status of the kidneys.

Metabolic profiles of mouse livers differ substantially in old compared to young mice with marked changes in the TCA cycle, as shown by the altered levels of alanine, aspartate and fumarate. Ageing reduces glycerol-3-phosphate acyltransferase activity (335) and glycerol (336), respectively, in rats, which is consistent with decreased glycerol concentrations in old mice. Nicotinamide, a poly ADP-ribose synthetase inhibitor, attenuated ischemia-induced liver injury with potent anti-inflammatory effects (337). Inosine also has an anti-inflammatory potential and has been shown to be decreased in 24 month- compared to 1.5 month-old rats (338). We also observed decreased nicotinamide and inosine levels in old mice, which may be related to chronic inflammation during

ageing (339). Due to the low variability within each group and the clear distinction between the groups, we propose nicotinamide, glycerol and inosine as potential biomarkers for differentiating between young and old liver tissues.

In the lung, a panel of 13 metabolites was identified and linked mostly to amino acid metabolism and the TCA cycle (alanine, aspartate and glutamine). The concentration of the two aromatic amino acids tyrosine and phenylalanine, all three BCAAs and methionine were increased. To date, few metabolome-wide analyses have been performed on lung tissues and no data at all are available for heathy lung tissue in context of ageing. Thus, our results could set the base for further investigations, focusing on the general protein biosynthesis activity and its alterations as potential cause or consequence of the ageing process. Compared to other organs, lung lysates showed smaller differences in their metabolic profiles between the two respective mouse groups. This may suggest that the change in the metabolic phenotype of the lung is a consequence of metabolic derailing in other organs which in turn affects the lung metabolome. Nevertheless, the levels of lysine, nicotinamide, aspartate and fumarate differ between the two groups, implying these metabolites as biomarkers for the assessment of ageing in lung tissue. In addition to amino acids and metabolites of purine/pyrimidine metabolism, glucose and lactate levels were changed, indicating derailing of the glucose metabolism with age. Altered levels of nicotinamide and inosine in lung and liver might be linked to the ability of both molecules in triggering inflammatory responses (337).

The results we obtained for the levels of the BCAAs (leucine, isoleucine and valine) are of special interest, since the catabolism of these amino acids does not occur in hepatic cells, but in non-hepatic cells like neurons, cardiomyocytes or the diaphragm (324). Usually, the degradation of BCAAs in mice is regulated by an enzyme called protein phosphatase 2Cm (PP2Cm), whose mRNA is particularly highly expressed in the brain and heart, indicating their primary sites of BCAA catabolism (340). In the context of diseases, BCAAs have been correlated with cardiac pathology, since the expression of their catabolism activator PP2Cm can be influenced by stress and was therefore decreased in conditions like hypertrophy or heart failure. *In vivo* studies in zebrafish with deficiency of PP2Cm led to a loss of cardiac contractility and premature death, further pointing out the potential role of a functioning BCAA catabolism on cardiac health (340). Since stress signals such as oxidation or genetic damage increase with age, these stress signals may affect the

expression of PP2Cm, and a defect in BCAA catabolism may have adverse health effects, possibly explaining the increase of these metabolites in the aged mice (324). In detail, the increased levels of the BCAAs (leucine, isoleucine and valine) were detected in the brain, heart and lung, whereas no significant changes were seen in the liver, which broadly fits to the hypothesis that accumulating stress signals may influence BCAA levels. Whether there is a causal or close relationship between these observations and ageing cannot be answered by our results. Nevertheless, the role of BCAAs in healthy ageing should be further investigated in the future, as this subset of amino acids represents promising biomarkers for the assessment of healthy ageing. mTOR signalling is active in all tissues particularly involved in cell growth, ageing and metabolism, which is presumably important in tissues with high metabolic rates, such as the liver (341). Here we found significant changes in glucose and glycerol, which are involved in glycolysis/gluconeogenesis, which in turn are downstream targets of the mTOR signalling pathway.

Sixteen metabolites have been found as biomarker candidates for the ageing spleen. Among them, metabolites emerge as components of metabolic pathways linked to amino acid, glucose and lipid metabolism. A decreased concentration of taurine, a sulfur-containing amino acid that augments the proliferative responses of T-cells, indicates defective proliferative response of T-cells in old mice (342) and point to a reduced potential for detoxification of reactive oxygen species (343). In line with previous results (344), we observed decreased uridine levels in the ageing spleen, suggesting uridine and taurine as robust spleen-specific biomarker candidates for the ageing process. Accordingly, reduced levels of uridine might be associated with increased cellular senescence in all tissues, as uridine has been shown to affect senescence in human mammary epithelial cells (345). During ageing, senescent cells stop producing nucleotides, the essential building blocks of DNA, implying that precursors like inosine, uridine, uracil and nicotinamide might also be found at abnormal levels (345). Taking all of this into account, decreased uridine concentrations in the brain, heart, kidney, liver and spleen of aged mice indicate that uridine may be a general biomarker for ageing.

5.6 Conclusions

Research desperately seeks for molecular markers of ageing (346). Our straightforward workflow of NMR-based untargeted metabolomics together with the identified metabolite biomarker panels

is well suited to study the effect of senolytic drug candidates such as dasatinib, quercetin (347), FOXO4-DRI peptide (348), Bcl-2 family inhibitors (349) and Hsp90 inhibitors (350) to increase overall health span and enable healthy ageing. Although experiments with mouse models have already been performed to test the efficacy of certain senolytics in the past, these investigations mostly focused on measuring motor activities, frailty or physical characteristics (308). The ageing-associated, tissue-specific metabolite biomarkers discovered in the current study should provide a novel molecular read-out for ageing-associated changes of an organism. Our results represent a powerful tool for future drug discovery projects to build a bridge between *in vitro* and *in vivo* studies, and to validate the molecular efficacy of investigated therapeutics.

Importantly, besides the power of metabolomics for biomarker discovery and validation, identification of metabolites altered in different states of health and disease can help tracing back the pathway(s) causing metabolic derailing during ageing. Following this approach, and assuming that ageing influences the health status, the identification of altered metabolites during ageing is crucial in classifying metabolic pathways closely linked to key ageing processes such as cellular senescence (351). Senescent cells are "hypermetabolic", a condition that could potentially be therapeutically targetable. As previously demonstrated, interventions such as rapamycin treatment and methionine restriction impact important aspects of metabolism and delay cellular senescence to extend cellular lifespan (352, 353). How metabolically targeted drugs can achieve sufficient specificity for senescent over non-senescent cells *in viv*o to allow successful translation remains an open question. Our study provides a protocol to evaluate these metabolism-targeting drugs *in vivo,* based on both universal and tissue-specific metabolite alterations that accompany the ageing process. In addition, our approach also depicts a metabolite panel for future *in vivo* NMR studies in living animals.

In this study, NMR-based untargeted metabolomics was applied to investigate the metabolic profile of key tissues in young and old mice. We revealed that ageing is associated with considerable metabolic alterations specifically in amino acids, neurotransmitters and other small molecules. Our study not only generated a high-quality untargeted analysis of ageing metabolism, but also provided a set of metabolic markers that may be used in further translational studies, such as the development

of senolytic compounds. Taken together, our approach brought up a metabolite panel for future *in vivo* magnetic resonance studies.

Patents

Not applicable.

5.7 Supplementary Materials

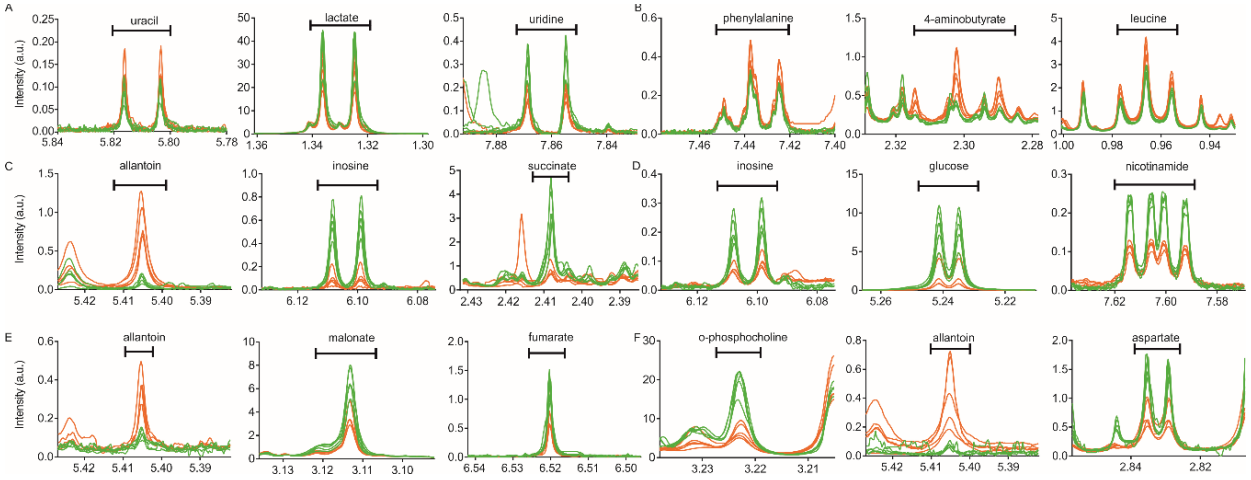

Figure S10. Overlapping signals of ^{1}H-NMR spectra of significantly different metabolites for each organ from young and old mice. The curves visualize the altered levels of metabolites between each group and/or organ. Signals originating from 9-10 weeks old mice are coloured in green, curves in orange represent samples from 96-104 weeks old mice. The black bars indicate the integrated area further used for statistical analysis. Three metabolites and their characteristic peak in the NMR spectra are shown in (A) brain, (B) heart, (C) kidney, (D) liver, (E) lung and (F) spleen.

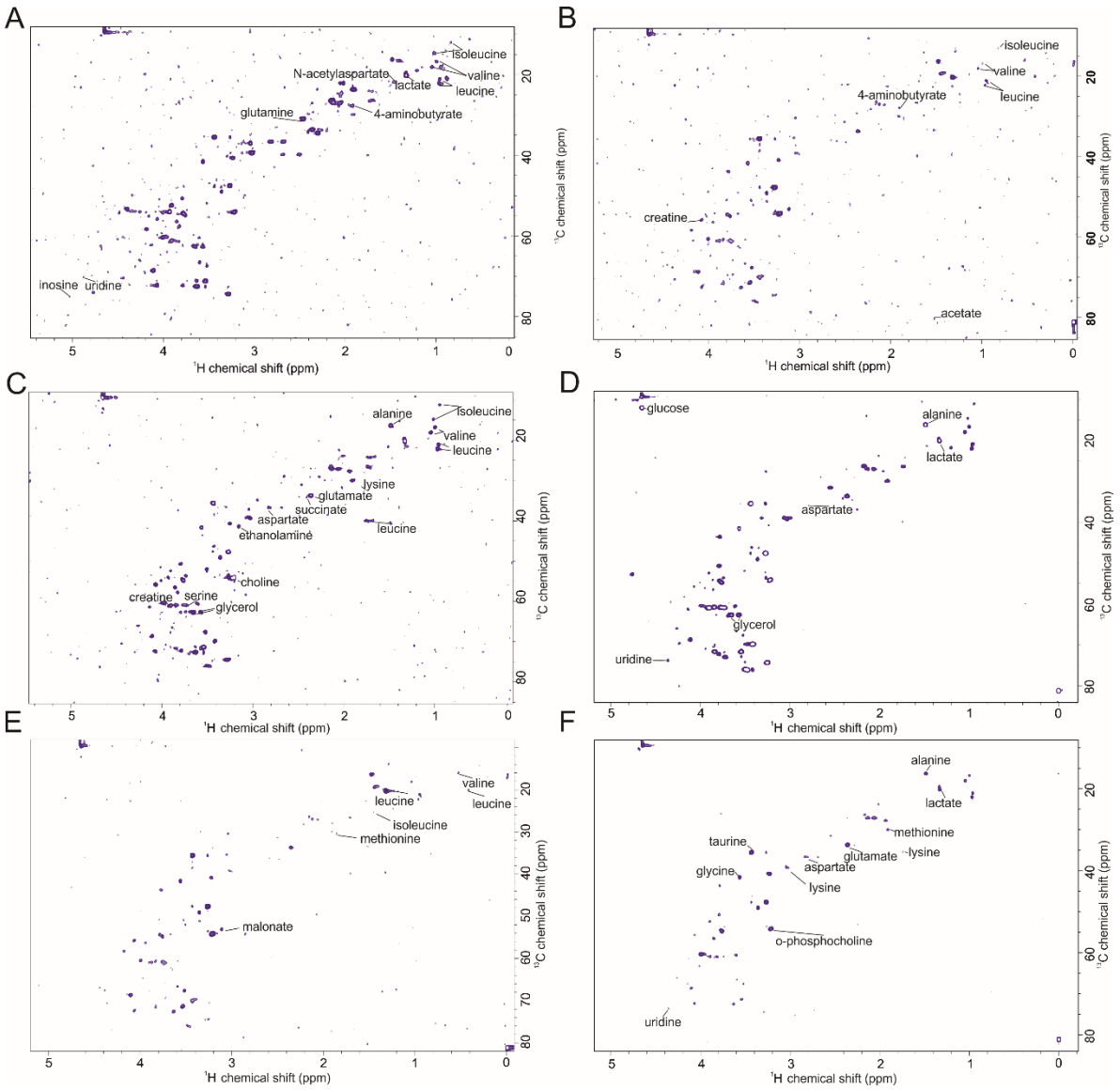

Figure S11. 2D ^{1}H, ^{13}C HSQC NMR spectra for the different organs with assigned and cross-validated metabolites for (A) brain, (B) heart, (C) kidney, (D) liver, (E) lung and (F) spleen.

Author Contributions: Conceptualization, T.M. and D.K.; methodology, F.Z., J.K.K., A.A., M.K., K.B.K., N.V., G.H., M.P.; software, F.Z and J.K.K..; validation, F.Z. and T.M.; formal analysis, F.Z. and J.K.K.; investigation, F.Z., J.K.K., T.M.; resources, T.M., G.H., E.S., D.K.; data curation, F.Z., J.K.K., T.M.; writing—original draft preparation, F.Z. and J.K.K.; writing—review and editing, F.Z., J.K.K., A.A., M.K., K.B.K., N.V., T.M., N.V., E.S., G.H. D.K..; visualization,

F.Z.; supervision, T.M.; project administration, T.M.; funding acquisition, T.M., D.K. All authors have read and agreed to the published version of the manuscript.

Funding: T.M. was supported by Austrian Science Fund (FWF) grants P28854, I3792, and DK-MCD W1226; Austrian Research Promotion Agency (FFG) Grants 864690 and 870454; the Integrative Metabolism Research Center Graz; Austrian Infrastructure Program 2016/2017, the Styrian Government (Zukunftsfonds), and BioTechMed-Graz (Flagship project). D.K. was supported by the FWF (SFB F73, W1226, P32400, P30882, DP-iDP DOC 31), the BioTechMed-Graz flagship project "Lipases and Lipid Signaling", the County of Styria, and the City of Graz. F.Z. was trained within the frame of the PhD program Molecular Medicine, Medical University of Graz.

Acknowledgments: The authors thank A. Absenger and I. Hindler (Medical University of Graz, Austria) for mice care.

Conflicts of Interest: The authors declare no conflict of interest.

6 Discussion

The protein ArgMet plays a significant role in regulating several signalling pathways. Gene regulation, DNA repair, signal transduction, metabolism and regulation of apoptosis have been involved in physicochemical processes shown to be modulated by ArgMet (5, 12, 31). ArgMet has been involved into metabolic dyregulation during tumorigenesis and ageing, but the molecular mechanism still remains unclear. Despite the existence of literature on this topic, insufficient and unreliable quantitative methods limit the interpretation of the significance of ArgMet in pathological and physiological processes. Here, a simple, robust and fast NMR-based quantification protocol was developed to quantify ArgMet levels and dynamics in purified proteins, cells, organoids and tissues. ADMA, MMA, and SDMA in all the tested biological samples can be quantified and detected by our NMR spectroscopy-based protocol. In the recovery experiments, methylated arginine residues were recovery at an average of approximately 100%. The levels of ArgMet obtained using our new NMR-based approach have been validated for a subset samples (**Figure S2B** and **Figure S3B**) by a reversed-phase HPLC method. Summarizing, we found that the results from NMR and HPLC are in good agreement. The MMA peak in BY4741 obtained from HPLC show spectral overlap interference (**Figure S2B**), suggesting that our method exhibits higher resolution of ArgMet in complex samples than HPLC. In addition, protein unbound arginine methylation and other metabolites can also be quantified in this protocol. A cold methanol extraction solvent is used to simultaneously extract metabolites and precipitate proteins/lipids in the same samples during sample preparation. Therefore, we can use the supernatant for untargeted metabolomics studies and the precipitated fraction is then analysed for protein arginine methylation. In the same approach, we can also perform untargeted metabolomic analysis to understand the metabolic profiles alongside the changes of arginine methylation., both relying on the robust analysis of NMR.

ArgMet-NMR proved to be useful for detecting methylation patterns in recombinant protein when PRMT1 was incubated with protein to induce *in vitro* methylation reactions. According to Cheng *et al.*, methylation motifs in PRMTs contain RG/RGG, RXG, RPAAPR or APR sites of ArgMet (1, 22, 212). However, the actual consensus patterns in the majority of human PRMTs are not yet

known. In the development of this method, we sought to devise a strategy to not only quantitate but also to understand how perturbations to the sequence/substrate alter ArgMet or PRMT specificity. Our protocol may help to determine arginine methylation of simple and repetitive AA sequence patterns. For example, different recombinant proteins or synthetic peptides can be further studied using our protocol using different PRMTs as basic ArgMet screening agents because it is based on label-free protein and requires only minimal sample preparation, i.e., for protein or peptide concentrations greater larger than 5 μM. Our protocol may help in understanding different PRMT MMA or ADMA/SDMA target sequences. This approach offers a quick platform for label-free screening for PRMTs in recombinant proteins, which may be a supplementary analysis for use with peptide arrays (213) or mass spectrometry (18).

Recent bioinformatic studies have predicted an additional 33 putative methyltransferases in *S. cerevisiae* (215). It is possible that some protein methyltransferases may have been misclassified because the prediction of putative methyltransferase function is imperfect. Our protocol may enable an effective evaluation of these methyltransferases. For example, we detected ArgMet in *S. cerevisiae* BY4741 and BY4742, strains that produce ADMA and MMA but not SDMA, yielding results consistent with those of previous publications (216). HMT1 is a major enzyme critical for most of the formation of ArgMet. Knocking out HMT1 in yeast abolished ADMA and MMA, suggesting that other methyltransferases do not affect global ArgMet levels. However, these results may have been obtained because other methyltransferases recognize only a small set of the specific substrates tested. Our method can be used to help explore which type of PRMT is crucial for hypomethylation or hypermethylation, the potential demethylase and the coupling metabolism in yeast. In addition, our protocol can be used to investigate the conservation of the biological functions of methylarginine residues in yeast and mammals.

Highly abundant arginine methylation has been found in up to 3.4% of cells, which required high levels of metabolism, with 12 molecules of ATP per methylation event (224). The cytoplasm of these cells showed lower levels of chromatin, but it was equal to that at whole-cell level, suggesting highly abundant ArgMet not of chromatin but at an overall level. We found that ADMA was the major methylated arginine species in all tested cell lines, followed by SDMA and MMA, with only approximately 10% and 1% in the form of ADMA, respectively. PRMT1 is the predominant

enzyme in mammalian cells (217), which is in line with our results. Consistent with our previous works, many of the enriched ArgMet proteins found in our latest study were involved in RNA-binding, associated with nuclear functions and embedded in intrinsically disordered proteins (8, 12, 25). Our group also found that ArgMet affected intrinsically disordered protein localization and LLPS but only in specific proteins, i.e., FUS or CIRBP. How the global ArgMet level regulates LLPS through fluidity and dynamics remains unknown. Our future study will be focused on this area.

Arginine methylation is a highly abundant posttranslational modification in different matrices. Given the high levels of ArgMet protein, we hypothesized that ArgMet plays a key role in maintaining cell homeostasis. High levels of the ArgMet protein in cancer cell lines are likely related to aberrant clinicopathological characteristics and poor prognosis. Interestingly, we found increased ADMA levels in cancer cells compared to primary cells, which is consistent with PRMT1 overexpression in human melanoma and breast and prostate cancer (29, 218). The increased PRMT expression in cancer has encouraged people to focus on PRMT-targeted inhibitors for tumour therapy. An increasing number of small-molecule ArgMet inhibitors are expected to be entered into the clinic. Our study provided a comprehensive understanding of the consequences of small-molecule ArgMet inhibitors. We tested the most commonly commercially available inhibitors. Our results showed that ArgMet-NMR is well suited to study differences in inhibitors of arginine methylation and provide guidance for synergistic drug screening with ArgMet targets. Other investigations can be evaluated with our protocol to dissect the role of PRMT inhibitors or metabolites on both cancer cells and immune cells, as the net balance of inhibiting both likely determines the long-term therapeutic efficacy of these compounds.

Our work shows the prevalent and dynamic occurrence of ArgMet in cancer cells. Given the strong relationship between arginine methylation and metabolism, both are involved in carcinogenesis. Here, HCC has been further investigated for metabolomic analysis. A comprehensive global proteomic, genomic, transcriptomic and phosphoproteomic analysis of HCC has been revealed as a strategy to better understand the molecular mechanism and biological functions of HCC. Metabolic pathways, including one carbon metabolism, free fatty acids, cellular energy metabolism, glutamine metabolism, amino acid metabolism and the TCA cycle, have been shown to be involved in HCC

(354, 355). These specific dysregulated metabolic pathways related to cancer may constitute novel biomarkers or targeted therapeutics. Metabolic reprogramming is now considered a hallmark of cancer (356). However, the metabolic changes are still not clear, especially during tumour growth.

Our work reveals the global metabolic landscape of HCC reprogramming, providing a clinical and therapeutic understanding of HCC. Interestingly, the metabolic phenotypes of serum, cancer tissues and peritumoural tissues show evidence of gradual metabolic changes with increasing tumour size. Our integrated analysis combining metabolomics and proteomics showed alterations during tumour growth, suggesting metabolic reprogramming with increasing size. Strikingly, metabolites related to glycolysis, the TCA cycle and pyrimidine synthesis were changed in the tumour tissues with increasing size. The increasing requirements of growing tumours for glucose and glutamine are obvious in serum and tissues (both tumour and peritumoural tissues). In previous work, elevated expression of glutamine synthetase (GS) has been shown to also be a marker of HCC (357). In tumour cells, both glutamine and glucose, acting as fuels, fulfil the requirements for energy and for the synthesis of macromolecules (358). Consistently, PRMT5 enhances tumorigenicity and glycolysis in pancreatic cancer (359). PRMT1 and PRMT6 increase hepatic gluconeogenesis (360, 361). PRMT4 regulated glucose metabolism through GAPDH methylation. ArgMet plays a crucial role in liver metabolism with regulating metabolic enzyme and one carbon cycle. We have not yet analysed ArgMet levels of HCC tissues and this will be the focus of our future work to explore the potential mechanism. In this study, we focused on the changes in metabolites during tumour growth. We also discussed changes in proteomic data regarding pathways influencing cell metabolism. Whether metabolic reprogramming in cancer is intrinsically different from the metabolic response to proliferative stimuli in peritumoural tumour cells is not clear. Cancer cells can take up exosomes secreted by surrounding cells and proteins from the microenvironment by endocytosis and micropinocytosis. Nutrients are delivered to lysosomes, which contain abundant enzymes that are metabolized into metabolic intermediates and small molecules (362). Our data suspect that there seem symbiotic bridges to support nutrient availability in cancer and/or that the same metabolic behaviours may induce tumour invasion. Metabolic reprogramming in HCC is a multifactor and multistep process. These data revealed markedly different biochemistry of larger tumours, which suggested that stratification may be advantageous in the clinic. As indicated by the current results,

these phenotypes can be utilized in cancer therapy based on the use of metabolite or enzyme inhibitors. In addition, we validated and adapted a recently proposed preoperative model for the evaluation of 5-year recurrence risks after resection **(290)**. Our metaboclinicalpathological model led a better prediction than that realized using clinicopathological parameters alone. Our predictive model is clinically relevant and enables the identification of patients at high risk. The benefit of including metabolites in the clinicopathological setup should be validated in future research. Further prospective studies are required to verify the applicability of our model in patient allocation for adjuvant trials and follow-up. In addition, the changes in metabolites have profound implications for designing new targets or biomarker candidates for HCC. Our predictive model offers a powerful approach for predicting 5-year recurrence.

ArgMet regulates metabolic processes, and we also found that the levels of protein ArgMet can be modulated (selectively) by metabolites. The link between metabolism and protein ArgMet level has been under discussion for a long time. The SAM-donated methyl groups modulate one-carbon metabolism. Methionine is the basis of SAM production through ATP-derived adenylation, and then, SAM provides methyl groups to substrates for use in methylation reactions (168, 169). In our study, methionine, glutamine and glycine were tested for their relationships with ArgMet. Given that methionine is used as an upstream substrate in SAM production, we first sought to determine whether methionine levels affect ArgMet level. As we expected, deletion of methionine led to the loss of 61% of the ArgMet. Methionine, as an essential amino acid, is mainly obtained from the diet. Therefore, both diet and fasting behaviour may affect ArgMet levels *in vivo*. Glutamine is a provider of fuel for cancer cells, and the glutamine requirement level is increased in proliferating cells. Deprivation of glutamine decreased ArgMet by approximately 30%, which may be due to the limited energy sources and the need for single-carbon building blocks for SAM recycling through gluconeogenesis because ArgMet is an energy-consuming event (221). Glycine supplementation, which has been reported to mimic methionine deprivation, prolongs lifespan but does not lead to reduction in the global levels of proteins ArgMet; in contrast, an increase in ArgMet has been observed (200). Glycine plays a role in methionine clearance due to its effects on the SAM production cycle. In addition, glycine can be used as a methyl group acceptor for the formation of sarcosine (N-methylglycine) and S-adenosylhomocysteine. We found that glycine supplementation

did not increase ArgMet levels, suggesting that the addition of glycine may not mimic methionine deprivation in cancer cells. Consistently, in adult worms, glycine supplementation did not change methionine levels (226). Our methods provide a better understanding of the regulation of arginine methylation by methionine. If prolonged lifespan through limited methionine is due to regulation of ArgMet, then further study is warranted (227-229).

The discussion thus far raises the follow-up long-disputed question in the entire field of biology: Does an efficient demethylase exists (230). Using our methodology, it will be possible to address this question. Our methods can provide a better understanding of whether a dedicated arginine demethylase that enables cycling of methylation and demethylation truly exists. Further understanding of dynamic changes in proteins with ArgMet may indicate opportunities for manipulating ArgMet levels in diseases. We used different setups to measure the ArgMet dynamics as regulated by inhibitors and metabolites. First, we utilized AdOx or methionine deprivation to inhibit ArgMet, and both treatments showed that the ArgMet demethylation process was slow. In addition, remethylation of arginine residues required hours. Our approach with stable isotope tracing obtained deeper insight into metabolic fluxes. For example, ^{13}C-methyl-labelled methionine was used to trace the dynamics of ArgMet. Loss of unlabelled methylated arginine and increases in ^{13}C-methyl-labelled methylated arginine were in sync, validating the finding that ArgMet and demethylation are slow. Therefore, we demonstrated that there is no efficient demethylase that affects global ArgMet levels. However, we cannot exclude the possibility that demethylases affect only a small set of protein substrates. Using our methodology, we expect to stimulate several paradigm shifts in the field of metabolism research.

How arginine methylation affects physiological or pathological processes is also a topic of interest. Our approach was also studied in mouse intestinal organoids and mouse tissues. For organoids at different levels of differentiation and enriched with different cell types, we found different arginine methylation levels. However, it remains to be confirmed that the arginine methylation levels were truly altered because of their differentiation levels. During the ageing of mice, we found significant changes in the spleen and brain. There were no changes in the heart, liver, lung or kidney. According to our hypothesis, the increase in ArgMet levels in the spleen is due to the accumulation of senescent cells. Increased atrophy of the spleen has been found in advanced age (56, 210). In a previous report,

downregulated PRMT1 was found in senescent neuroblastoma cells with senescence (232). The reduced arginine methylation in the spleen may be due to some methyltransferase inhibitors, thus accelerating the ageing of the spleen. ArgMet has been found to be related to neurodegenerative diseases. Hypomethylated RNA-binding protein FUS and poly-GR dipeptide repeat regions have been identified in frontotemporal dementia and in ALS (27). In line with this finding, we found decreased MMA/SDMA in the brains of old mice. Detection of arginine methylation in relation to neurodegenerative diseases has clinical significance.

In the same cohort of mouse tissues, we also integrated the metabolic analysis of ageing. Metabolites are key biological molecules and they indicate metabolic activity in cells and tissues by providing functional evidence of biochemical activity. However, in a state of stable growth arrest, senescent cells exhibit a highly active metabolism that may be essential to the senescent phenotype. Senescent cells accumulate in ageing tissues and contribute to age-related decline in tissue function (296, 363). By understanding metabolic reprogramming in the ageing process, we sought to identify appropriate biomarkers for ageing or lifespan stage. We have illustrated the use of metabolomics to identify differences in metabolite profiles in different tissues (liver, heart, lung, spleen, kidney, and brain) in young and old mice. We used NMR-based metabolomics to study metabolic reprogramming in ageing mice. Each of the organs on which we focused is involved in a major public health issue related to ageing: chronic kidney disease, heart dysfunction and neurodegenerative diseases, chronic lung diseases, fatty liver disease, and chronic spleen disease. Metabolomics offers potential in establishing tissue-specific biomarkers of ageing, and efforts are needed to provide a metabolite database for assessing a wide range of ageing markers in different tissues. NMR spectroscopy is a powerful tool in this regard because of its high reproducibility and simple analysis. Integrated metabolomic characterizations of different tissue samples at different ages revealed metabolic reprogramming at different ages and relevant metabolite markers during ageing.

Young mice have more DNA relative to RNA per organ, with kidney and spleen DNA decreasing between cell maturity and senescence (364). Uridine suppresses fatty liver in an age-related manner by modulating the liver protein acetylation profile. Decreased uptake of uridine was found in the brain, heart, kidney, liver and spleen of aged mice, which is in line with previous results suggesting that uridine could be a potential common biomarker for ageing (345). Minimal uracil levels in DNA

help to prevent genomic instability because repeated glycosylase cycles lead to risk of accumulating basic sites, subsequent DNA strand breaks and, ultimately, cell death. Accumulation of uracil was found in old mouse brain, heart and kidney tissues, suggesting that uracil could be a common biomarker for ageing may be induced by DNA damage (306). The methyl transfer (one carbon metabolism) plays an important role in the synthesis of purines and pyrimidines, DNA and RNA. Recent evidence demonstrates that ArgMet inhibition induces cell cycle-check point defects in response to DNA damage (365), which is consistent with hypomethylation in aged spleen. Deletion of PRMT enzymes in transgenic mice has been shown to be relevant for cellular senescence and premature ageing (366). Are PRMTs recruited to DNA damage sites and is their activity regulated by metabolites? Significant decreased methionine has been observed in aged spleen, which is consistent with low ArgMet induced by methionine restriction. Is hypomethylated aged spleen due to a harmful side effect of the aforementioned protein arginine methyltransferase inhibitors? Interestingly, increased methionine and glutamine have been observed in aged brain, in agreement with increased ArgMet. It remains to be investigated whether ArgMet is a cause or consequence of metabolic changes. These questions remain in-depth analyses and our study provides some clues to the relationship among ageing, ArgMet and metabolism. Metabolomics has revealed similar changes in the TCA cycle across multiple tissues, including the lung and liver. Our analysis revealed alterations in metabolic pathways in brain, heart, kidney, lung, liver and spleen tissues. The related metabolites can be used in follow-up studies as markers in ageing and lifespan. Our study provided metabolic profiles of key tissues in young and old mice. We demonstrated metabolic alterations in amino acids, neurotransmitters and other molecules during the ageing process. In this study, we not only provided a high-quality metabolic landscape of ageing but also generated a set of metabolic markers that may further benefit the study of senolytic compound development. In addition, our study may provide some clues to extend the cell lifespan. In summary, our study provides a metabolite panel for future studies on ageing in different tissues.

In addition, we also combined our method with a commercially available automated SPE system, which is suitable for large-scale disease studies and used to assess the relevance of arginine methylation. Untargeted metabolomics also can be analyses under same approach. Thus, this method

is suitable for highly accurate quantification of ArgMet, which can be utilized for further studies of metabolism, mechanisms and disease states that coincide with ArgMet.

In summary, our study not only provides a first general method for the quantification of ArgMet levels and dynamics but also highlights the importance of ArgMet in biology and medicine. Moreover, we provide new routes for studying the modulation of protein ArgMet by inhibitors, metabolites and biological processes, such as ageing, that will enable future studies, from basic to translational research and drug discovery/development. i) We found that the levels of protein ArgMet can be modulated (selectively) by inhibitors of protein arginine methyltransferases and by metabolites. The link between metabolism and protein ArgMet has been under discussion for a long time. Our method allows simultaneous quantification of arginine methylation and analyses of metabolic profiles. Overall, the lack of methods for the quantification of ArgMet levels and dynamics has created a bottleneck in the entire field, which we overcame with our novel approach. Confirming previous findings, we found that methionine deprivation has a strong impact on protein ArgMet. We extended and combined our approach with stable isotope tracing to obtain deeper insight into metabolic fluxes. We have also identified metabolites that change significantly with tumourigenesis and ageing, and deeper mechanistic study still need to be invesitigated. ii) The dynamics of protein ArgMet can be followed using our novel methodology. We show in cells that both the process of methylation and the process of "demethylation" (i.e., the loss of protein ArgMet) are slow. iii) Given the large differences in ArgMet observed in cells, we hypothesized that ArgMet might be changed during cell differentiation. Addressing the link between ArgMet and differentiation will be important for the entire field. Our technology will enable us to address this question. iv) Interestingly, we also identified high levels of protein ArgMet in tissues, with the brain and spleen showing the highest levels in young mice. We observed that with ageing, levels of protein ArgMet changed dramatically in these tissues, whereas other tissues, such as the heart, liver and kidney, were affected to a lesser extent. The spleen is among the most affected organs during ageing, and it has been hypothesized that these changes are linked to the accumulation of senescent cells. Our approach will enable the discover of a link between cellular senescence and ArgMet. Observations of high levels of protein ArgMet in the spleen and a great reduction of protein ArgMet during ageing raise the question of whether accelerated ageing of the spleen could be a harmful side effect of the aforementioned protein arginine methyltransferase inhibitors.

7 References

1. Thandapani P, O'Connor TR, Bailey TL, Richard S. Defining the RGG/RG motif. Molecular cell. 2013;50(5):613-23.
2. Lee DY, Teyssier C, Strahl BD, Stallcup MR. Role of protein methylation in regulation of transcription. Endocrine reviews. 2005;26(2):147-70.
3. Bedford MT, Richard S. Arginine methylation: an emerging regulatorof protein function. Molecular cell. 2005;18(3):263-72.
4. Pahlich S, Zakaryan RP, Gehring H. Protein arginine methylation: cellular functions and methods of analysis. Biochimica et Biophysica Acta (BBA)-Proteins and Proteomics. 2006;1764(12):1890-903.
5. Blanc RS, Richard S. Arginine Methylation: The Coming of Age. Mol Cell. 2017;65(1):8-24.
6. Van Der Lee R, Buljan M, Lang B, Weatheritt RJ, Daughdrill GW, Dunker AK, et al. Classification of intrinsically disordered regions and proteins. Chemical reviews. 2014;114(13):6589-631.
7. Wu Q, Schapira M, Arrowsmith CH, Barsyte-Lovejoy D. Protein arginine methylation: from enigmatic functions to therapeutic targeting. Nature Reviews Drug Discovery. 2021:1-22.
8. Chong PA, Vernon RM, Forman-Kay JD. RGG/RG motif regions in RNA binding and phase separation. Journal of molecular biology. 2018;430(23):4650-65.
9. Bedford MT, Clarke SG. Protein arginine methylation in mammals: who, what, and why. Molecular cell. 2009;33(1):1-13.
10. Bachand F. Protein arginine methyltransferases: from unicellular eukaryotes to humans. Eukaryotic cell. 2007;6(6):889-98.
11. Chern M-K, Chang K-N, Liu L-F, Tam T-CS, Liu Y-C, Liang Y-L, et al. Yeast ribosomal protein L12 is a substrate of protein-arginine methyltransferase 2. Journal of Biological Chemistry. 2002;277(18):15345-53.
12. Guccione E, Richard S. The regulation, functions and clinical relevance of arginine methylation. Nat Rev Mol Cell Biol. 2019;20(10):642-57.
13. Hornbeck PV, Zhang B, Murray B, Kornhauser JM, Latham V, Skrzypek E. PhosphoSitePlus, 2014: mutations, PTMs and recalibrations. Nucleic acids research. 2015;43(D1):D512-D20.
14. Tewary SK, Zheng YG, Ho M-C. Protein arginine methyltransferases: insights into the enzyme structure and mechanism at the atomic level. Cellular and Molecular Life Sciences. 2019;76(15):2917-32.
15. Guo A, Gu H, Zhou J, Mulhern D, Wang Y, Lee KA, et al. Immunoaffinity enrichment and mass spectrometry analysis of protein methylation. Molecular & Cellular Proteomics. 2014;13(1):372-87.
16. Feng Y, Maity R, Whitelegge JP, Hadjikyriacou A, Li Z, Zurita-Lopez C, et al. Mammalian protein arginine methyltransferase 7 (PRMT7) specifically targets RXR sites in lysine-and arginine-rich regions. Journal of Biological Chemistry. 2013;288(52):37010-25.
17. Hamey JJ, Rakow S, Bouchard C, Senst JM, Kolb P, Bauer U-M, et al. Systematic investigation of PRMT6 substrate recognition reveals broad specificity with a preference for an RG motif or basic and bulky residues. The FEBS Journal.n/a(n/a).

18. Uhlmann T, Geoghegan VL, Thomas B, Ridlova G, Trudgian DC, Acuto O. A method for large-scale identification of protein arginine methylation. Molecular & cellular proteomics. 2012;11(11):1489-99.
19. Wooderchak WL, Zang T, Zhou ZS, Acuna M, Tahara SM, Hevel JM. Substrate profiling of PRMT1 reveals amino acid sequences that extend beyond the "RGG" paradigm. Biochemistry. 2008;47(36):9456-66.
20. Lee J, Bedford MT. PABP1 identified as an arginine methyltransferase substrate using high-density protein arrays. EMBO reports. 2002;3(3):268-73.
21. Cura V, Marechal N, Troffer-Charlier N, Strub JM, van Haren MJ, Martin NI, et al. Structural studies of protein arginine methyltransferase 2 reveal its interactions with potential substrates and inhibitors. The FEBS journal. 2017;284(1):77-96.
22. Cheng D, Cote J, Shaaban S, Bedford MT. The arginine methyltransferase CARM1 regulates the coupling of transcription and mRNA processing. Mol Cell. 2007;25(1):71-83.
23. Shishkova E, Zeng H, Liu F, Kwiecien NW, Hebert AS, Coon JJ, et al. Global mapping of CARM1 substrates defines enzyme specificity and substrate recognition. Nature communications. 2017;8(1):1-13.
24. Musiani D, Bok J, Massignani E, Wu L, Tabaglio T, Ippolito MR, et al. Proteomics profiling of arginine methylation defines PRMT5 substrate specificity. Science signaling. 2019;12(575).
25. Lorton BM, Shechter D. Cellular consequences of arginine methylation. Cellular and Molecular Life Sciences. 2019:1-24.
26. Dormann D, Madl T, Valori CF, Bentmann E, Tahirovic S, Abou-Ajram C, et al. Arginine methylation next to the PY-NLS modulates Transportin binding and nuclear import of FUS. The EMBO journal. 2012;31(22):4258-75.
27. Hofweber M, Hutten S, Bourgeois B, Spreitzer E, Niedner-Boblenz A, Schifferer M, et al. Phase separation of FUS is suppressed by its nuclear import receptor and arginine methylation. Cell. 2018;173(3):706-19. e13.
28. Aletta JM, Hu JC. Protein arginine methylation in health and disease. Biotechnology annual review. 2008;14:203-24.
29. Bedford MT. Arginine methylation at a glance. Journal of cell science. 2007;120(24):4243-6.
30. Wang S-CM, Dowhan DH, Muscat GE. Epigenetic arginine methylation in breast cancer: emerging therapeutic strategies. Journal of molecular endocrinology. 2019;62(3):R223-R37.
31. Yang Y, Bedford MT. Protein arginine methyltransferases and cancer. Nature Reviews Cancer. 2013;13(1):37-50.
32. Zakrzewicz D, Eickelberg O. From arginine methylation to ADMA: a novel mechanism with therapeutic potential in chronic lung diseases. BMC pulmonary medicine. 2009;9(1):1-7.
33. Wang Z, Tang WW, Cho L, Brennan DM, Hazen SL. Targeted metabolomic evaluation of arginine methylation and cardiovascular risks: potential mechanisms beyond nitric oxide synthase inhibition. Arteriosclerosis, thrombosis, and vascular biology. 2009;29(9):1383-91.
34. Lee JH, Park GH, Lee YK, Park JH. Changes in the arginine methylation of organ proteins during the development of diabetes mellitus. Diabetes research and clinical practice. 2011;94(1):111-8.

35. Gullà A, Hideshima T, Bianchi G, Fulciniti M, Samur MK, Qi J, et al. Protein arginine methyltransferase 5 has prognostic relevance and is a druggable target in multiple myeloma. Leukemia. 2018;32(4):996-1002.
36. Friesen WJ, Massenet S, Paushkin S, Wyce A, Dreyfuss G. SMN, the product of the spinal muscular atrophy gene, binds preferentially to dimethylarginine-containing protein targets. Molecular cell. 2001;7(5):1111-7.
37. Jarrold J, Davies CC. PRMTs and arginine methylation: cancer's best-kept secret? Trends in molecular medicine. 2019;25(11):993-1009.
38. Chiang K, Zielinska AE, Shaaban AM, Sanchez-Bailon MP, Jarrold J, Clarke TL, et al. PRMT5 is a critical regulator of breast cancer stem cell function via histone methylation and FOXP1 expression. Cell reports. 2017;21(12):3498-513.
39. Mathioudaki K, Scorilas A, Ardavanis A, Lymberi P, Tsiambas E, Devetzi M, et al. Clinical evaluation of PRMT1 gene expression in breast cancer. Tumor Biology. 2011;32(3):575-82.
40. Baldwin RM, Morettin A, Paris G, Goulet I, Côté J. Alternatively spliced protein arginine methyltransferase 1 isoform PRMT1v2 promotes the survival and invasiveness of breast cancer cells. Cell cycle. 2012;11(24):4597-612.
41. Mathioudaki K, Papadokostopoulou A, Scorilas A, Xynopoulos D, Agnanti N, Talieri M. The PRMT1 gene expression pattern in colon cancer. British journal of cancer. 2008;99(12):2094-9.
42. Papadokostopoulou A, Mathioudaki K, Scorilas A, Xynopoulos D, Ardavanis A, Kouroumalis E, et al. Colon cancer and protein arginine methyltransferase 1 gene expression. Anticancer research. 2009;29(4):1361-6.
43. Elakoum R, Gauchotte G, Oussalah A, Wissler M-P, Clément-Duchêne C, Vignaud J-M, et al. CARM1 and PRMT1 are dysregulated in lung cancer without hierarchical features. Biochimie. 2014;97:210-8.
44. Hong H, Kao C, Jeng MH, Eble JN, Koch MO, Gardner TA, et al. Aberrant expression of CARM1, a transcriptional coactivator of androgen receptor, in the development of prostate carcinoma and androgen-independent status. Cancer: Interdisciplinary International Journal of the American Cancer Society. 2004;101(1):83-9.
45. Habashy HO, Rakha EA, Ellis IO, Powe DG. The oestrogen receptor coactivator CARM1 has an oncogenic effect and is associated with poor prognosis in breast cancer. Breast cancer research and treatment. 2013;140(2):307-16.
46. Bao X, Zhao S, Liu T, Liu Y, Liu Y, Yang X. Overexpression of PRMT5 promotes tumor cell growth and is associated with poor disease prognosis in epithelial ovarian cancer. Journal of Histochemistry & Cytochemistry. 2013;61(3):206-17.
47. Yang F, Wang J, Ren H-y, Jin J, Wang A-l, Sun L-l, et al. Proliferative role of TRAF4 in breast cancer by upregulating PRMT5 nuclear expression. Tumor Biology. 2015;36(8):5901-11.
48. Wang L, Pal S, Sif S. Protein arginine methyltransferase 5 suppresses the transcription of the RB family of tumor suppressors in leukemia and lymphoma cells. Molecular and cellular biology. 2008;28(20):6262-77.
49. Wei TYW, Juan CC, Hisa JY, Su LJ, Lee YCG, Chou HY, et al. Protein arginine methyltransferase 5 is a potential oncoprotein that upregulates G 1 cyclins/cyclin-dependent kinases and the phosphoinositide 3-kinase/AKT signaling cascade. Cancer science. 2012;103(9):1640-50.

50. Aliferis KA, Chrysayi-Tokousbalides M. Metabolomics in pesticide research and development: review and future perspectives. Metabolomics. 2011;7(1):35-53.
51. Be³towski J, Kêdra A. Asymmetric dimethylarginine (ADMA) as a target for pharmacotherapy. Pharmacological Reports. 2006;58(159):159-78.
52. Jucker M, Walker LC. Self-propagation of pathogenic protein aggregates in neurodegenerative diseases. Nature. 2013;501(7465):45-51.
53. Ikenaka K, Atsuta N, Maeda Y, Hotta Y, Nakamura R, Kawai K, et al. Increase of arginine dimethylation correlates with the progression and prognosis of ALS. Neurology. 2019:10.1212/WNL. 0000000000007311.
54. Blanc RS, Vogel G, Chen T, Crist C, Richard S. PRMT7 preserves satellite cell regenerative capacity. Cell reports. 2016;14(6):1528-39.
55. Zhang X-S, Wang T, Lin X-W, Denlinger DL, Xu W-H. Reactive oxygen species extend insect life span using components of the insulin-signaling pathway. Proceedings of the National Academy of Sciences. 2017;114(37):E7832-E40.
56. Lim Y, Lee E, Lee J, Oh S, Kim S. Down-regulation of asymmetric arginine methylation during replicative and H2O2-induced premature senescence in WI-38 human diploid fibroblasts. Journal of biochemistry. 2008;144(4):523-9.
57. Spannhoff A, Heinke R, Bauer I, Trojer P, Metzger E, Gust R, et al. Target-based approach to inhibitors of histone arginine methyltransferases. Journal of medicinal chemistry. 2007;50(10):2319-25.
58. Cheng D, Yadav N, King RW, Swanson MS, Weinstein EJ, Bedford MT. Small molecule regulators of protein arginine methyltransferases. Journal of Biological Chemistry. 2004;279(23):23892-9.
59. Bonham K, Hemmers S, Lim YH, Hill DM, Finn M, Mowen KA. Effects of a novel arginine methyltransferase inhibitor on T-helper cell cytokine production. The FEBS journal. 2010;277(9):2096-108.
60. Cheung N, Fung TK, Zeisig BB, Holmes K, Rane JK, Mowen KA, et al. Targeting aberrant epigenetic networks mediated by PRMT1 and KDM4C in acute myeloid leukemia. Cancer cell. 2016;29(1):32-48.
61. Eram MS, Shen Y, Szewczyk MM, Wu H, Senisterra G, Li F, et al. A potent, selective, and cell-active inhibitor of human type I protein arginine methyltransferases. ACS chemical biology. 2016;11(3):772-81.
62. Shen Y, Szewczyk MM, Eram MS, Smil D, Kaniskan HU, Ferreira de Freitas R, et al. Discovery of a potent, selective, and cell-active dual inhibitor of protein arginine methyltransferase 4 and protein arginine methyltransferase 6. Journal of medicinal chemistry. 2016;59(19):9124-39.
63. Hu H, Owens EA, Su H, Yan L, Levitz A, Zhao X, et al. Exploration of cyanine compounds as selective inhibitors of protein arginine methyltransferases: synthesis and biological evaluation. Journal of medicinal chemistry. 2015;58(3):1228-43.
64. Yan L, Yan C, Qian K, Su H, Kofsky-Wofford SA, Lee W-C, et al. Diamidine compounds for selective inhibition of protein arginine methyltransferase 1. Journal of medicinal chemistry. 2014;57(6):2611-22.
65. Wu H, Zheng W, Eram MS, Vhuiyan M, Dong A, Zeng H, et al. Structural basis of arginine asymmetrical dimethylation by PRMT6. Biochemical Journal. 2016;473(19):3049-63.

66. Wang C, Jiang H, Jin J, Xie Y, Chen Z, Zhang H, et al. Development of potent type I protein arginine methyltransferase (PRMT) inhibitors of leukemia cell proliferation. Journal of medicinal chemistry. 2017;60(21):8888-905.
67. Wu M, Lin P, Li L, Chen D, Yang X, Xu L, et al. Reduced asymmetric dimethylarginine accumulation through inhibition of the type I protein arginine methyltransferases promotes renal fibrosis in obstructed kidneys. The FASEB Journal. 2019;33(6):6948-56.
68. Kaniskan HÜ, Szewczyk MM, Yu Z, Eram MS, Yang X, Schmidt K, et al. A potent, selective and cell-active allosteric inhibitor of protein arginine methyltransferase 3 (PRMT3). Angewandte Chemie. 2015;127(17):5255-9.
69. Ferreira de Freitas R, Eram MS, Smil D, Szewczyk MM, Kennedy S, Brown PJ, et al. Discovery of a potent and selective coactivator associated arginine methyltransferase 1 (CARM1) inhibitor by virtual screening. Journal of medicinal chemistry. 2016;59(14):6838-47.
70. Mitchell LH, Drew AE, Ribich SA, Rioux N, Swinger KK, Jacques SL, et al. Aryl pyrazoles as potent inhibitors of arginine methyltransferases: identification of the first PRMT6 tool compound. ACS medicinal chemistry letters. 2015;6(6):655-9.
71. Drew AE, Moradei O, Jacques SL, Rioux N, Boriack-Sjodin AP, Allain C, et al. Identification of a CARM1 inhibitor with potent in vitro and in vivo activity in preclinical models of multiple myeloma. Scientific reports. 2017;7(1):1-13.
72. Nakayama K, Szewczyk MM, dela Sena C, Wu H, Dong A, Zeng H, et al. TP-064, a potent and selective small molecule inhibitor of PRMT4 for multiple myeloma. Oncotarget. 2018;9(26):18480.
73. Chan-Penebre E, Kuplast KG, Majer CR, Boriack-Sjodin PA, Wigle TJ, Johnston LD, et al. A selective inhibitor of PRMT5 with in vivo and in vitro potency in MCL models. Nature chemical biology. 2015;11(6):432.
74. Gerhart SV, Kellner WA, Thompson C, Pappalardi MB, Zhang X-P, de Oca RM, et al. Activation of the p53-MDM4 regulatory axis defines the anti-tumour response to PRMT5 inhibition through its role in regulating cellular splicing. Scientific reports. 2018;8(1):1-15.
75. Duncan KW, Rioux N, Boriack-Sjodin PA, Munchhof MJ, Reiter LA, Majer CR, et al. Structure and property guided design in the identification of PRMT5 tool compound EPZ015666. ACS medicinal chemistry letters. 2016;7(2):162-6.
76. Smil D, Eram MS, Li F, Kennedy S, Szewczyk MM, Brown PJ, et al. Discovery of a dual PRMT5–PRMT7 inhibitor. ACS medicinal chemistry letters. 2015;6(4):408-12.
77. Bonday ZQ, Cortez GS, Grogan MJ, Antonysamy S, Weichert K, Bocchinfuso WP, et al. LLY-283, a potent and selective inhibitor of arginine methyltransferase 5, PRMT5, with antitumor activity. ACS medicinal chemistry letters. 2018;9(7):612-7.
78. Tarighat SS, Santhanam R, Frankhouser D, Radomska HS, Lai H, Anghelina M, et al. The dual epigenetic role of PRMT5 in acute myeloid leukemia: gene activation and repression via histone arginine methylation. Leukemia. 2016;30(4):789-99.
79. Nagai Y, Ji MQ, Zhu F, Xiao Y, Tanaka Y, Kambayashi T, et al. PRMT5 associates with the FOXP3 homomer and when disabled enhances targeted p185erbB2/neu tumor immunotherapy. Frontiers in immunology. 2019;10:174.
80. Szewczyk MM, Ishikawa Y, Organ S, Sakai N, Li F, Halabelian L, et al. Pharmacological inhibition of PRMT7 links arginine monomethylation to the cellular stress response. Nature communications. 2020;11(1):1-15.

81. Kalhan SC. One-carbon metabolism, fetal growth and long-term consequences. Maternal and Child Nutrition: The First 1,000 Days. 2013;74:127-38.
82. Tanaka K, Sasayama T, Nagashima H, Irino Y, Takahashi M, Izumi Y, et al. Glioma cells require one-carbon metabolism to survive glutamine starvation. Acta neuropathologica communications. 2021;9(1):1-14.
83. Shyh-Chang N, Locasale JW, Lyssiotis CA, Zheng Y, Teo RY, Ratanasirintrawoot S, et al. Influence of threonine metabolism on S-adenosylmethionine and histone methylation. Science. 2013;339(6116):222-6.
84. Shiraki N, Shiraki Y, Tsuyama T, Obata F, Miura M, Nagae G, et al. Methionine metabolism regulates maintenance and differentiation of human pluripotent stem cells. Cell metabolism. 2014;19(5):780-94.
85. Gu H, Ren JM, Jia X, Levy T, Rikova K, Yang V, et al. Quantitative profiling of post-translational modifications by immunoaffinity enrichment and LC-MS/MS in cancer serum without immunodepletion. Molecular & Cellular Proteomics. 2016;15(2):692-702.
86. Lorton BM, Shechter D. Cellular consequences of arginine methylation. Cellular and Molecular Life Sciences. 2019;76(15):2933-56.
87. Zhang F, Kerbl-Knapp J, Rodriguez Colman MJ, Macher T, Vujić N, Fasching S, et al. Global analysis of protein arginine methylation. 2021.
88. Carilla-Latorre S, Gallardo ME, Annesley SJ, Calvo-Garrido J, Graña O, Accari SL, et al. MidA is a putative methyltransferase that is required for mitochondrial complex I function. Journal of Cell Science. 2010;123(10):1674-83.
89. Zurita Rendón O, Silva Neiva L, Sasarman F, Shoubridge EA. The arginine methyltransferase NDUFAF7 is essential for complex I assembly and early vertebrate embryogenesis. Human molecular genetics. 2014;23(19):5159-70.
90. Wang Y-P, Zhou W, Wang J, Huang X, Zuo Y, Wang T-S, et al. Arginine methylation of MDH1 by CARM1 inhibits glutamine metabolism and suppresses pancreatic cancer. Molecular cell. 2016;64(4):673-87.
91. Krause CD, Yang Z-H, Kim Y-S, Lee J-H, Cook JR, Pestka S. Protein arginine methyltransferases: evolution and assessment of their pharmacological and therapeutic potential. Pharmacology & therapeutics. 2007;113(1):50-87.
92. Martens-Lobenhoffer J, Bode-Böger SM. Measurement of asymmetric dimethylarginine (ADMA) in human plasma: from liquid chromatography estimation to liquid chromatography-mass spectrometry quantification. European Journal of Clinical Pharmacology. 2006;62(1):61-8.
93. Chen B-M, Xia L-W, Zhao R-Q. Determination of NG, NG-dimethylarginine in human plasma by high-performance liquid chromatography. Journal of Chromatography B: Biomedical Sciences and Applications. 1997;692(2):467-71.
94. Pi J, Kumagai Y, Sun G, Shimojo N. Improved method for simultaneous determination of L-arginine and its mono-and dimethylated metabolites in biological samples by high-performance liquid chromatography. Journal of Chromatography B: Biomedical Sciences and Applications. 2000;742(1):199-203.
95. van der Greef J, Davidov E, Verheij E, Vogels J, van der Heijden R, Adourian AS, et al. The role of metabolomics in systems biology. Metabolic profiling: Its role in biomarker discovery and gene function analysis: Springer; 2003. p. 171-98.
96. Wishart DS. Metabolomics for investigating physiological and pathophysiological processes. Physiological reviews. 2019;99(4):1819-75.

97. Johnson CH, Ivanisevic J, Siuzdak G. Metabolomics: beyond biomarkers and towards mechanisms. Nature reviews Molecular cell biology. 2016;17(7):451-9.
98. Zhang A, Sun H, Wang P, Han Y, Wang X. Recent and potential developments of biofluid analyses in metabolomics. Journal of proteomics. 2012;75(4):1079-88.
99. Rubert J, Righetti L, Stranska-Zachariasova M, Dzuman Z, Chrpova J, Dall'Asta C, et al. Untargeted metabolomics based on ultra-high-performance liquid chromatography–high-resolution mass spectrometry merged with chemometrics: A new predictable tool for an early detection of mycotoxins. Food chemistry. 2017;224:423-31.
100. Su Q, Guan T, He Y, Lv H. Siderophore biosynthesis governs the virulence of uropathogenic Escherichia coli by coordinately modulating the differential metabolism. Journal of proteome research. 2016;15(4):1323-32.
101. Beger R, Dunn W, Schmidt M, Gross S, Kirwan J, Cascante M, et al. for "Precision Medicine and Pharmacometabolomics Task Group"-Metabolomics Society Initiative. Metabolomics enables precision medicine:"A white paper, community perspective". Metabolomics. 2016;12(9):149.
102. Nicholson JK, Lindon JC. Metabonomics. Nature. 2008;455(7216):1054-6.
103. Naviaux RK, Naviaux JC, Li K, Bright AT, Alaynick WA, Wang L, et al. Metabolic features of chronic fatigue syndrome. Proceedings of the National Academy of Sciences. 2016;113(37):E5472-E80.
104. Danik M, Champagne D, Petit-Turcotte C, Beffert U, Poirier J. Brain lipoprotein metabolism and its relation to neurodegenerative disease. Critical Reviews™ in Neurobiology. 1999;13(4).
105. Mamas M, Dunn WB, Neyses L, Goodacre R. The role of metabolites and metabolomics in clinically applicable biomarkers of disease. Archives of toxicology. 2011;85(1):5-17.
106. Nicholson JK, Lindon JC, Holmes E. 'Metabonomics': understanding the metabolic responses of living systems to pathophysiological stimuli via multivariate statistical analysis of biological NMR spectroscopic data. Xenobiotica. 1999;29(11):1181-9.
107. Tuyiringire N, Tusubira D, Munyampundu J-P, Tolo CU, Muvunyi CM, Ogwang PE. Application of metabolomics to drug discovery and understanding the mechanisms of action of medicinal plants with anti-tuberculosis activity. Clinical and translational medicine. 2018;7(1):1-12.
108. Beale DJ, Pinu FR, Kouremenos KA, Poojary MM, Narayana VK, Boughton BA, et al. Review of recent developments in GC–MS approaches to metabolomics-based research. Metabolomics. 2018;14(11):1-31.
109. Aliferis KA, Jabaji S. Metabolomics–a robust bioanalytical approach for the discovery of the modes-of-action of pesticides: a review. Pesticide Biochemistry and physiology. 2011;100(2):105-17.
110. Markley JL, Brüschweiler R, Edison AS, Eghbalnia HR, Powers R, Raftery D, et al. The future of NMR-based metabolomics. Current opinion in biotechnology. 2017;43:34-40.
111. Farazi PA, DePinho RA. Hepatocellular carcinoma pathogenesis: from genes to environment. Nature Reviews Cancer. 2006;6(9):674.
112. El–Serag HB, Rudolph KL. Hepatocellular carcinoma: epidemiology and molecular carcinogenesis. Gastroenterology. 2007;132(7):2557-76.
113. Llovet JM, Burroughs A, Bruix J. Hepatocellular carcinoma. Lancet (London, England). 2003;362(9399):1907.

114. El-Serag HB. Epidemiology of viral hepatitis and hepatocellular carcinoma. Gastroenterology. 2012;142(6):1264-73. e1.
115. Yang JD, Roberts LR. Hepatocellular carcinoma: a global view. Nature reviews Gastroenterology & hepatology. 2010;7(8):448.
116. Huang Q, Tan Y, Yin P, Ye G, Gao P, Lu X, et al. Metabolic characterization of hepatocellular carcinoma using nontargeted tissue metabolomics. Cancer research. 2013;73(16):4992-5002.
117. Thomas MB, Zhu AX. Hepatocellular carcinoma: the need for progress. Journal of Clinical Oncology. 2005;23(13):2892-9.
118. El-Serag HB, Marrero JA, Rudolph L, Reddy KR. Diagnosis and treatment of hepatocellular carcinoma. Gastroenterology. 2008;134(6):1752-63.
119. Zhu AX, Duda DG, Sahani DV, Jain RK. HCC and angiogenesis: possible targets and future directions. Nature reviews Clinical oncology. 2011;8(5):292.
120. Folkman J. Opinion: Angiogenesis: an organizing principle for drug discovery? Nature reviews Drug discovery. 2007;6(4):273.
121. Chen C, Wang G. Mechanisms of hepatocellular carcinoma and challenges and opportunities for molecular targeted therapy. World journal of hepatology. 2015;7(15):1964.
122. Pang RW, Poon RT. From molecular biology to targeted therapies for hepatocellular carcinoma: the future is now. Oncology. 2007;72(Suppl. 1):30-44.
123. Iacovides DC, O'Shea CC, Oses-Prieto J, Burlingame A, McCormick F. Critical role for arginine methylation in adenovirus-infected cells. Journal of virology. 2007;81(23):13209-17.
124. Li Y-J, Stallcup MR, Lai MM. Hepatitis delta virus antigen is methylated at arginine residues, and methylation regulates subcellular localization and RNA replication. Journal of virology. 2004;78(23):13325-34.
125. Lubyova B, Hodek J, Zabransky A, Prouzova H, Hubalek M, Hirsch I, et al. PRMT5: A novel regulator of Hepatitis B virus replication and an arginine methylase of HBV core. PLoS One. 2017;12(10):e0186982.
126. Jiang H, Zhu Y, Zhou Z, Xu J, Jin S, Xu K, et al. PRMT 5 promotes cell proliferation by inhibiting BTG 2 expression via the ERK signaling pathway in hepatocellular carcinoma. Cancer medicine. 2018;7(3):869-82.
127. Zhu K, Peng Y, Hu J, Zhan H, Yang L, Gao Q, et al. Metadherin–PRMT5 complex enhances the metastasis of hepatocellular carcinoma through the WNT–β-catenin signaling pathway. Carcinogenesis. 2020;41(2):130-8.
128. Jaffee EM, Van Dang C, Agus DB, Alexander BM, Anderson KC, Ashworth A, et al. Future cancer research priorities in the USA: a Lancet Oncology Commission. The Lancet Oncology. 2017;18(11):e653-e706.
129. Wu H, Xue R, Dong L, Liu T, Deng C, Zeng H, et al. Metabolomic profiling of human urine in hepatocellular carcinoma patients using gas chromatography/mass spectrometry. Analytica chimica acta. 2009;648(1):98-104.
130. Dunn WB, Ellis DI. Metabolomics: current analytical platforms and methodologies. TrAC Trends in Analytical Chemistry. 2005;24(4):285-94.
131. Beckonert O, Keun HC, Ebbels TM, Bundy J, Holmes E, Lindon JC, et al. Metabolic profiling, metabolomic and metabonomic procedures for NMR spectroscopy of urine, plasma, serum and tissue extracts. Nature protocols. 2007;2(11):2692.

132. Chafey P, Finzi L, Boisgard R, Caüzac M, Clary G, Broussard C, et al. Proteomic analysis of β-catenin activation in mouse liver by DIGE analysis identifies glucose metabolism as a new target of the Wnt pathway. Proteomics. 2009;9(15):3889-900.
133. Wu CC, MacCoss MJ, Howell KE, Matthews DE, Yates JR. Metabolic labeling of mammalian organisms with stable isotopes for quantitative proteomic analysis. Analytical chemistry. 2004;76(17):4951-9.
134. Mayr M, Madhu B, Xu Q. Proteomics and metabolomics combined in cardiovascular research. Trends in cardiovascular medicine. 2007;17(2):43-8.
135. Barallobre-Barreiro J, Chung Y-L, Mayr M. Proteomics and metabolomics for mechanistic insights and biomarker discovery in cardiovascular disease. Revista Española de Cardiología (English Edition). 2013;66(8):657-61.
136. Wettersten HI, Hakimi AA, Morin D, Bianchi C, Johnstone ME, Donohoe DR, et al. Grade-dependent metabolic reprogramming in kidney cancer revealed by combined proteomics and metabolomics analysis. Cancer research. 2015;75(12):2541-52.
137. Mayr M, Yusuf S, Weir G, Chung Y-L, Mayr U, Yin X, et al. Combined metabolomic and proteomic analysis of human atrial fibrillation. Journal of the American College of Cardiology. 2008;51(5):585-94.
138. Hajduk J, Klupczynska A, Dereziński P, Matysiak J, Kokot P, Nowak DM, et al. A combined metabolomic and proteomic analysis of gestational diabetes mellitus. International journal of molecular sciences. 2015;16(12):30034-45.
139. Chen J-H, Hales CN, Ozanne SE. DNA damage, cellular senescence and organismal ageing: causal or correlative? Nucleic acids research. 2007;35(22):7417-28.
140. López-Otín C, Blasco MA, Partridge L, Serrano M, Kroemer G. The hallmarks of aging. Cell. 2013;153(6):1194-217.
141. Khosla S, Farr JN, Tchkonia T, Kirkland JL. The role of cellular senescence in ageing and endocrine disease. Nature Reviews Endocrinology. 2020;16(5):263-75.
142. Sacitharan P, Vincent T. Cellular ageing mechanisms in osteoarthritis. Mammalian Genome. 2016;27(7):421-9.
143. Barbosa MC, Grosso RA, Fader CM. Hallmarks of aging: an autophagic perspective. Frontiers in endocrinology. 2019;9:790.
144. Stouth DW, Manta A, Ljubicic V. Protein arginine methyltransferase expression, localization, and activity during disuse-induced skeletal muscle plasticity. American Journal of Physiology-Cell Physiology. 2018;314(2):C177-C90.
145. Li S, Yang P, Tian E, Zhang H. Arginine methylation modulates autophagic degradation of PGL granules in C. elegans. Molecular cell. 2013;52(3):421-33.
146. Ferrucci L, Giallauria F, Guralnik JM. Epidemiology of aging. Radiologic Clinics of North America. 2008;46(4):643-52.
147. Wang JC, Bennett M. Aging and atherosclerosis: mechanisms, functional consequences, and potential therapeutics for cellular senescence. Circulation research. 2012;111(2):245-59.
148. Chang AM, Halter JB. Aging and insulin secretion. American Journal of Physiology-Endocrinology And Metabolism. 2003;284(1):E7-E12.
149. De Lau LM, Breteler MM. Epidemiology of Parkinson's disease. The Lancet Neurology. 2006;5(6):525-35.

150. Brookmeyer R, Gray S, Kawas C. Projections of Alzheimer's disease in the United States and the public health impact of delaying disease onset. American journal of public health. 1998;88(9):1337-42.
151. Yazdanyar A, Newman AB. The burden of cardiovascular disease in the elderly: morbidity, mortality, and costs. Clinics in geriatric medicine. 2009;25(4):563-77.
152. Guasch-Ferré M, Hruby A, Toledo E, Clish CB, Martínez-González MA, Salas-Salvadó J, et al. Metabolomics in prediabetes and diabetes: a systematic review and meta-analysis. Diabetes care. 2016;39(5):833-46.
153. Suhre K, Meisinger C, Döring A, Altmaier E, Belcredi P, Gieger C, et al. Metabolic footprint of diabetes: a multiplatform metabolomics study in an epidemiological setting. PloS one. 2010;5(11):e13953.
154. Trushina E, Dutta T, Persson X-MT, Mielke MM, Petersen RC. Identification of altered metabolic pathways in plasma and CSF in mild cognitive impairment and Alzheimer's disease using metabolomics. PloS one. 2013;8(5):e63644.
155. Berg J, Tymoczko J, Stryer L, Clarke N. DNA replication, recombination and repair. Biochemistry 5th edition New York, WH Freeman & Co, pp1119-1120. 2002.
156. Houtkooper RH, Argmann C, Houten SM, Cantó C, Jeninga EH, Andreux PA, et al. The metabolic footprint of aging in mice. Scientific Reports. 2011;1(1):134.
157. Houtkooper RH, Argmann C, Houten SM, Cantó C, Jeninga EH, Andreux PA, et al. The metabolic footprint of aging in mice. Scientific reports. 2011;1:134.
158. Lee J, Sayegh J, Daniel J, Clarke S, Bedford MT. PRMT8, a new membrane-bound tissue-specific member of the protein arginine methyltransferase family. J Biol Chem. 2005;280(38):32890-6.
159. Niewmierzycka A, Clarke S. S-Adenosylmethionine-dependent methylation in Saccharomyces cerevisiae. Identification of a novel protein arginine methyltransferase. J Biol Chem. 1999;274(2):814-24.
160. Scorilas A, Black MH, Talieri M, Diamandis EP. Genomic organization, physical mapping, and expression analysis of the human protein arginine methyltransferase 1 gene. Biochem Biophys Res Commun. 2000;278(2):349-59.
161. Tee WW, Pardo M, Theunissen TW, Yu L, Choudhary JS, Hajkova P, et al. Prmt5 is essential for early mouse development and acts in the cytoplasm to maintain ES cell pluripotency. Genes Dev. 2010;24(24):2772-7.
162. Pawlak MR, Scherer CA, Chen J, Roshon MJ, Ruley HE. Arginine N-methyltransferase 1 is required for early postimplantation mouse development, but cells deficient in the enzyme are viable. Mol Cell Biol. 2000;20(13):4859-69.
163. Boffa LC, Karn J, Vidali G, Allfrey VG. Distribution of NG, NG,-dimethylarginine in nuclear protein fractions. Biochem Biophys Res Commun. 1977;74(3):969-76.
164. Esse R, Imbard A, Florindo C, Gupta S, Quinlivan EP, Davids M, et al. Protein arginine hypomethylation in a mouse model of cystathionine beta-synthase deficiency. FASEB J. 2014;28(6):2686-95.
165. Matsuoka M. [Epsilon-N-methylated lysine and guanidine-N-methylated arginine of proteins. 3. Presence and distribution in nature and mammals]. Seikagaku. 1972;44(8):364-70.
166. Paik WK, Paik DC, Kim S. Historical review: the field of protein methylation. Trends Biochem Sci. 2007;32(3):146-52.

167. Bremang M, Cuomo A, Agresta AM, Stugiewicz M, Spadotto V, Bonaldi T. Mass spectrometry-based identification and characterisation of lysine and arginine methylation in the human proteome. Mol Biosyst. 2013;9(9):2231-47.
168. Yang M, Vousden KH. Serine and one-carbon metabolism in cancer. Nature Reviews Cancer. 2016;16(10):650-62.
169. Locasale JW. Serine, glycine and one-carbon units: cancer metabolism in full circle. Nat Rev Cancer. 2013;13(8):572-83.
170. Larsen SC, Sylvestersen KB, Mund A, Lyon D, Mullari M, Madsen MV, et al. Proteome-wide analysis of arginine monomethylation reveals widespread occurrence in human cells. Science signaling. 2016;9(443):rs9-rs.
171. Lee YH, Stallcup MR. Minireview: protein arginine methylation of nonhistone proteins in transcriptional regulation. Mol Endocrinol. 2009;23(4):425-33.
172. Bhatter N, Roy R, Shah S, Sastry SP, Parbin S, Iyappan R, et al. Arginine methylation augments Sbp1 function in translation repression and decapping. Febs j. 2019;286(23):4693-708.
173. Stryeck S, Horvath A, Leber B, Stadlbauer V, Madl T. NMR spectroscopy enables simultaneous quantification of carbohydrates for diagnosis of intestinal and gastric permeability. Scientific reports. 2018;8(1):1-8.
174. Paik WK, Kim S. Enzymatic methylation of protein fractions from calf thymus nuclei. Biochem Biophys Res Commun. 1967;29(1):14-20.
175. Dhar S, Vemulapalli V, Patananan AN, Huang GL, Di Lorenzo A, Richard S, et al. Loss of the major Type I arginine methyltransferase PRMT1 causes substrate scavenging by other PRMTs. Sci Rep. 2013;3:1311.
176. Ye T, Zheng C, Zhang S, Gowda GN, Vitek O, Raftery D. "Add to subtract": a simple method to remove complex background signals from the 1H nuclear magnetic resonance spectra of mixtures. Analytical chemistry. 2012;84(2):994-1002.
177. Fan TW-M. Metabolite profiling by one-and two-dimensional NMR analysis of complex mixtures. Progress in nuclear magnetic resonance spectroscopy. 1996;28(2):161-219.
178. Nagayama K, Wüthrich K, Bachmann P, Ernst RR. Two-dimensional J-resolved 1H n.m.r. spectroscopy for studies of biological macromolecules. Biochem Biophys Res Commun. 1977;78(1):99-105.
179. Viant MR, Rosenblum ES, Tieerdema RS. NMR-based metabolomics: a powerful approach for characterizing the effects of environmental stressors on organism health. Environ Sci Technol. 2003;37(21):4982-9.
180. Wang Y, Bollard ME, Keun H, Antti H, Beckonert O, Ebbels TM, et al. Spectral editing and pattern recognition methods applied to high-resolution magic-angle spinning 1H nuclear magnetic resonance spectroscopy of liver tissues. Anal Biochem. 2003;323(1):26-32.
181. Hartel NG, Chew B, Qin J, Xu J, Graham NA. Deep protein methylation profiling by combined chemical and immunoaffinity approaches reveals novel PRMT1 targets. Molecular & Cellular Proteomics. 2019;18(11):2149-64.
182. Gary JD, Lin WJ, Yang MC, Herschman HR, Clarke S. The predominant protein-arginine methyltransferase from Saccharomyces cerevisiae. J Biol Chem. 1996;271(21):12585-94.
183. Henry MF, Silver PA. A novel methyltransferase (Hmt1p) modifies poly(A)+-RNA-binding proteins. Mol Cell Biol. 1996;16(7):3668-78.

184. Miranda TB, Sayegh J, Frankel A, Katz JE, Miranda M, Clarke S. Yeast Hsl7 (histone synthetic lethal 7) catalyses the in vitro formation of omega-N(G)-monomethylarginine in calf thymus histone H2A. Biochem J. 2006;395(3):563-70.
185. Young BD, Weiss DI, Zurita-Lopez CI, Webb KJ, Clarke SG, McBride AE. Identification of methylated proteins in the yeast small ribosomal subunit: a role for SPOUT methyltransferases in protein arginine methylation. Biochemistry. 2012;51(25):5091-104.
186. Plank M, Fischer R, Geoghegan V, Charles PD, Konietzny R, Acuto O, et al. Expanding the yeast protein arginine methylome. Proteomics. 2015;15(18):3232-43.
187. Erce MA, Abeygunawardena D, Low JK, Hart-Smith G, Wilkins MR. Interactions affected by arginine methylation in the yeast protein-protein interaction network. Mol Cell Proteomics. 2013;12(11):3184-98.
188. Sayegh J, Clarke SG. Hsl7 is a substrate-specific type II protein arginine methyltransferase in yeast. Biochemical and biophysical research communications. 2008;372(4):811-5.
189. Chia SZ, Lai YW, Yagoub D, Lev S, Hamey JJ, Pang CNI, et al. Knockout of the Hmt1p Arginine Methyltransferase in Saccharomyces cerevisiae Leads to the Dysregulation of Phosphate-associated Genes and Processes. Mol Cell Proteomics. 2018;17(12):2462-79.
190. Li L, Zhang Z, Ma T, Huo R. PRMT1 regulates tumor growth and metastasis of human melanoma via targeting ALCAM. Molecular medicine reports. 2016;14(1):521-8.
191. Bulau P, Zakrzewicz D, Kitowska K, Wardega B, Kreuder J, Eickelberg O. Quantitative assessment of arginine methylation in free versus protein-incorporated amino acids in vitro and in vivo using protein hydrolysis and high-performance liquid chromatography. Biotechniques. 2006;40(3):305-10.
192. Goulet I, Gauvin G, Boisvenue S, Côté J. Alternative splicing yields protein arginine methyltransferase 1 isoforms with distinct activity, substrate specificity, and subcellular localization. Journal of Biological Chemistry. 2007;282(45):33009-21.
193. Herrmann F, Pably P, Eckerich C, Bedford MT, Fackelmayer FO. Human protein arginine methyltransferases in vivo–distinct properties of eight canonical members of the PRMT family. Journal of cell science. 2009;122(5):667-77.
194. Litt M, Qiu Y, Huang S. Histone arginine methylations: their roles in chromatin dynamics and transcriptional regulation. Biosci Rep. 2009;29(2):131-41.
195. Musiani D, Giambruno R, Massignani E, Ippolito MR, Maniaci M, Jammula S, et al. PRMT1 is recruited via DNA-PK to chromatin where it sustains the senescence-associated secretory phenotype in response to Cisplatin. Cell reports. 2020;30(4):1208-22. e9.
196. Afman LA, Blom HJ, Drittij M-J, Brouns MR, van Straaten HW. Inhibition of transmethylation disturbs neurulation in chick embryos. Developmental brain research. 2005;158(1-2):59-65.
197. Fedoriw A, Rajapurkar SR, O'Brien S, Gerhart SV, Mitchell LH, Adams ND, et al. Anti-tumor activity of the type I PRMT inhibitor, GSK3368715, synergizes with PRMT5 inhibition through MTAP loss. Cancer Cell. 2019;36(1):100-14. e25.
198. Dhar S, Vemulapalli V, Patananan AN, Huang GL, Di Lorenzo A, Richard S, et al. Loss of the major Type I arginine methyltransferase PRMT1 causes substrate scavenging by other PRMTs. Scientific reports. 2013;3(1):1-6.
199. Ducker GS, Rabinowitz JD. One-carbon metabolism in health and disease. Cell metabolism. 2017;25(1):27-42.

200. Partridge L, Fuentealba M, Kennedy BK. The quest to slow ageing through drug discovery. Nature Reviews Drug Discovery. 2020:1-20.
201. Wang Y, Wysocka J, Sayegh J, Lee YH, Perlin JR, Leonelli L, et al. Human PAD4 regulates histone arginine methylation levels via demethylimination. Science. 2004;306(5694):279-83.
202. Chang B, Chen Y, Zhao Y, Bruick RK. JMJD6 is a histone arginine demethylase. Science. 2007;318(5849):444-7.
203. Liu F, Cheng G, Hamard P-J, Greenblatt S, Wang L, Man N, et al. Arginine methyltransferase PRMT5 is essential for sustaining normal adult hematopoiesis. The Journal of clinical investigation. 2015;125(9):3532-44.
204. Balint BL, Szanto A, Madi A, Bauer U-M, Gabor P, Benko S, et al. Arginine methylation provides epigenetic transcription memory for retinoid-induced differentiation in myeloid cells. Molecular and cellular biology. 2005;25(13):5648-63.
205. Uhlen M, Fagerberg L, Hallstrom BM, Lindskog C, Oksvold P, Mardinoglu A, et al. Proteomics. Tissue-based map of the human proteome. Science. 2015;347(6220):1260419.
206. Ludikhuize MC, Meerlo M, Gallego MP, Xanthakis D, Burgaya Julia M, Nguyen NTB, et al. Mitochondria Define Intestinal Stem Cell Differentiation Downstream of a FOXO/Notch Axis. Cell Metab. 2020;32(5):889-900 e7.
207. Haber AL, Biton M, Rogel N, Herbst RH, Shekhar K, Smillie C, et al. A single-cell survey of the small intestinal epithelium. Nature. 2017;551(7680):333-9.
208. Hong E, Lim Y, Lee E, Oh M, Kwon D. Tissue-specific and age-dependent expression of protein arginine methyltransferases (PRMTs) in male rat tissues. Biogerontology. 2012;13(3):329-36.
209. Wang Y-C, Wang C-W, Lin W-C, Tsai Y-J, Chang C-P, Lee Y-J, et al. Identification, chromosomal arrangements and expression analyses of the evolutionarily conserved prmt1 gene in chicken in comparison with its vertebrate paralogue prmt8. Plos one. 2017;12(9):e0185042.
210. Lim Y, Hong E, Kwon D, Lee E. Proteomic identification and comparative analysis of asymmetrically arginine-methylated proteins in immortalized, young and senescent cells. Electrophoresis. 2010;31(23-24):3823-33.
211. Kuilman T, Michaloglou C, Vredeveld LC, Douma S, van Doorn R, Desmet CJ, et al. Oncogene-induced senescence relayed by an interleukin-dependent inflammatory network. Cell. 2008;133(6):1019-31.
212. Woodsmith J, Casado-Medrano V, Benlasfer N, Eccles RL, Hutten S, Heine CL, et al. Interaction modulation through arrays of clustered methyl-arginine protein modifications. Life science alliance. 2018;1(5).
213. Kusevic D, Kudithipudi S, Jeltsch A. Substrate specificity of the HEMK2 protein glutamine methyltransferase and identification of novel substrates. Journal of Biological Chemistry. 2016;291(12):6124-33.
214. Fulton MD, Brown T, Zheng YG. The biological axis of protein arginine methylation and asymmetric dimethylarginine. International journal of molecular sciences. 2019;20(13):3322.
215. Low JK, Wilkins MR. Protein arginine methylation in Saccharomyces cerevisiae. The FEBS journal. 2012;279(24):4423-43.
216. Hsieh CH, Huang SY, Wu YC, Liu LF, Han CC, Liu YC, et al. Expression of proteins with dimethylarginines in Escherichia coli for protein–protein interaction studies. Protein science. 2007;16(5):919-28.

217. Tang J, Frankel A, Cook RJ, Kim S, Paik WK, Williams KR, et al. PRMT1 is the predominant type I protein arginine methyltransferase in mammalian cells. Journal of Biological Chemistry. 2000;275(11):7723-30.
218. Hamamoto R, Nakamura Y. Dysregulation of protein methyltransferases in human cancer: An emerging target class for anticancer therapy. Cancer Science. 2016;107(4):377-84.
219. Stopa N, Krebs JE, Shechter D. The PRMT5 arginine methyltransferase: many roles in development, cancer and beyond. Cellular and Molecular Life Sciences. 2015;72(11):2041-59.
220. Mentch SJ, Locasale JW. One carbon metabolism and epigenetics: understanding the specificity. Annals of the New York Academy of Sciences. 2016;1363(1):91.
221. Curi R, Lagranha CJ, Doi SQ, Sellitti D, Procópio J, Pithon-Curi TC, et al. Molecular mechanisms of glutamine action. Journal of cellular physiology. 2005;204(2):392-401.
222. Vander Heiden MG, DeBerardinis RJ. Understanding the Intersections between Metabolism and Cancer Biology. Cell. 2017;168(4):657-69.
223. Counihan JL, Grossman EA, Nomura DK. Cancer Metabolism: Current Understanding and Therapies. Chem Rev. 2018;118(14):6893-923.
224. Gary JD, Clarke S. RNA and protein interactions modulated by protein arginine methylation. Progress in nucleic acid research and molecular biology. 61: Elsevier; 1998. p. 65-131.
225. Luka Z, Mudd SH, Wagner C. Glycine N-methyltransferase and regulation of S-adenosylmethionine levels. Journal of Biological Chemistry. 2009;284(34):22507-11.
226. Liu YJ, Janssens GE, McIntyre RL, Molenaars M, Kamble R, Gao AW, et al. Glycine promotes longevity in Caenorhabditis elegans in a methionine cycle-dependent fashion. PLoS genetics. 2019;15(3):e1007633.
227. Lee BC, Kaya A, Gladyshev VN. Methionine restriction and lifespan control. Annals of the New York Academy of Sciences. 2016;1363:116.
228. Grandison RC, Piper MD, Partridge L. Amino-acid imbalance explains extension of lifespan by dietary restriction in Drosophila. Nature. 2009;462(7276):1061-4.
229. Bárcena C, Quirós PM, Durand S, Mayoral P, Rodríguez F, Caravia XM, et al. Methionine restriction extends lifespan in progeroid mice and alters lipid and bile acid metabolism. Cell reports. 2018;24(9):2392-403.
230. Low JK, Im H, Erce MA, Hart-Smith G, Snyder MP, Wilkins MR. Protein substrates of the arginine methyltransferase Hmt1 identified by proteome arrays. Proteomics. 2016;16(3):465-76.
231. Gelens L, Saurin AT. Exploring the function of dynamic phosphorylation-dephosphorylation cycles. Developmental cell. 2018;44(6):659-63.
232. Lee Y-J, Chang W-W, Chang C-P, Liu T-Y, Chuang C-Y, Qian K, et al. Downregulation of PRMT1 promotes the senescence and migration of a non-MYCN amplified neuroblastoma SK-N-SH cells. Scientific reports. 2019;9(1):1-14.
233. Gittings LM, Boeynaems S, Lightwood D, Clargo A, Topia S, Nakayama L, et al. Symmetric dimethylation of poly-GR correlates with disease duration in C9orf72 FTLD and ALS and reduces poly-GR phase separation and toxicity. Acta Neuropathol. 2020;139(2):407-10.
234. Suarez-Calvet M, Neumann M, Arzberger T, Abou-Ajram C, Funk E, Hartmann H, et al. Monomethylated and unmethylated FUS exhibit increased binding to Transportin and distinguish FTLD-FUS from ALS-FUS. Acta Neuropathol. 2016;131(4):587-604.

235. Dormann D, Madl T, Valori CF, Bentmann E, Tahirovic S, Abou-Ajram C, et al. Arginine methylation next to the PY-NLS modulates Transportin binding and nuclear import of FUS. EMBO J. 2012;31(22):4258-75.
236. Baker Brachmann C, Davies A, Cost GJ, Caputo E, Li J, Hieter P, et al. Designer deletion strains derived from Saccharomyces cerevisiae S288C: a useful set of strains and plasmids for PCR-mediated gene disruption and other applications. Yeast. 1998;14(2):115-32.
237. Lindeboom RG, van Voorthuijsen L, Oost KC, Rodríguez-Colman MJ, Luna-Velez MV, Furlan C, et al. Integrative multi-omics analysis of intestinal organoid differentiation. Molecular systems biology. 2018;14(6):e8227.
238. Bourgeois B, Hutten S, Gottschalk B, Hofweber M, Richter G, Sternat J, et al. Nonclassical nuclear localization signals mediate nuclear import of CIRBP. Proceedings of the National Academy of Sciences. 2020;117(15):8503-14.
239. Martinez A, Bourdreux F, Riguet E, Nuzillard JM. High-resolution and high-sensitivity 2D homonuclear J-resolved NMR spectroscopy. Magn Reson Chem. 2012;50(1):28-32.
240. Nuzillard J-M. Time-reversal of NMR signals by linear prediction. application to phase-sensitive homonuclear J-resolved spectroscopy. Journal of Magnetic Resonance. 1996;118(1):132-5.
241. Sakhaii P, Bermel W. Improving the sensitivity of conventional spin echo spectra by preservation of initial signal-to-noise ratio. Journal of Magnetic Resonance. 2014;242:220-3.
242. Meinitzer A, Puchinger M, Winklhofer-Roob BM, Rock E, Ribalta J, Roob JM, et al. Reference values for plasma concentrations of asymmetrical dimethylarginine (ADMA) and other arginine metabolites in men after validation of a chromatographic method. Clinica chimica acta. 2007;384(1-2):141-8.
243. Farazi PA, DePinho RA. Hepatocellular carcinoma pathogenesis: from genes to environment. Nat Rev Cancer. 2006;6(9):674-87.
244. Llovet JM, Burroughs A, Bruix J. Hepatocellular carcinoma. Lancet. 2003;362(9399):1907-17.
245. Kulik L, El-Serag HB. Epidemiology and Management of Hepatocellular Carcinoma. Gastroenterology. 2019;156(2):477-91 e1.
246. Forner A, Llovet JM, Bruix J. Hepatocellular carcinoma. Lancet. 2012;379(9822):1245-55.
247. Colli A, Fraquelli M, Casazza G, Massironi S, Colucci A, Conte D, et al. Accuracy of ultrasonography, spiral CT, magnetic resonance, and alpha-fetoprotein in diagnosing hepatocellular carcinoma: a systematic review. Am J Gastroenterol. 2006;101(3):513-23.
248. Lencioni R. Surveillance and early diagnosis of hepatocellular carcinoma. Dig Liver Dis. 2010;42 Suppl 3:S223-7.
249. Forner A, Bruix J. Biomarkers for early diagnosis of hepatocellular carcinoma. Lancet Oncol. 2012;13(8):750-1.
250. Chen L, Ho DW, Lee NP, Sun S, Lam B, Wong KF, et al. Enhanced detection of early hepatocellular carcinoma by serum SELDI-TOF proteomic signature combined with alpha-fetoprotein marker. Ann Surg Oncol. 2010;17(9):2518-25.
251. Huang S, Huang GQ, Zhu GQ, Liu WY, You J, Shi KQ, et al. Establishment and Validation of SSCLIP Scoring System to Estimate Survival in Hepatocellular Carcinoma Patients Who Received Curative Liver Resection. PLoS One. 2015;10(6):e0129000.

252. Ang SF, Ng ES, Li H, Ong YH, Choo SP, Ngeow J, et al. The Singapore Liver Cancer Recurrence (SLICER) Score for relapse prediction in patients with surgically resected hepatocellular carcinoma. PLoS One. 2015;10(4):e0118658.
253. Shim JH, Jun MJ, Han S, Lee YJ, Lee SG, Kim KM, et al. Prognostic nomograms for prediction of recurrence and survival after curative liver resection for hepatocellular carcinoma. Ann Surg. 2015;261(5):939-46.
254. Gao Q, Zhu H, Dong L, Shi W, Chen R, Song Z, et al. Integrated Proteogenomic Characterization of HBV-Related Hepatocellular Carcinoma. Cell. 2019;179(2):561-77 e22.
255. Schulze K, Nault JC, Villanueva A. Genetic profiling of hepatocellular carcinoma using next-generation sequencing. J Hepatol. 2016;65(5):1031-42.
256. Xing X, Liang D, Huang Y, Zeng Y, Han X, Liu X, et al. The application of proteomics in different aspects of hepatocellular carcinoma research. J Proteomics. 2016;145:70-80.
257. Wang Y, Liu H, Liang D, Huang Y, Zeng Y, Xing X, et al. Reveal the molecular signatures of hepatocellular carcinoma with different sizes by iTRAQ based quantitative proteomics. J Proteomics. 2017;150:230-41.
258. Satoh K, Yachida S, Sugimoto M, Oshima M, Nakagawa T, Akamoto S, et al. Global metabolic reprogramming of colorectal cancer occurs at adenoma stage and is induced by MYC. Proc Natl Acad Sci U S A. 2017;114(37):E7697-E706.
259. Chae YC, Vaira V, Caino MC, Tang HY, Seo JH, Kossenkov AV, et al. Mitochondrial Akt Regulation of Hypoxic Tumor Reprogramming. Cancer Cell. 2016;30(2):257-72.
260. Wang X, Zhang A, Sun H. Power of metabolomics in diagnosis and biomarker discovery of hepatocellular carcinoma. Hepatology. 2013;57(5):2072-7.
261. Yang Y, Li C, Nie X, Feng X, Chen W, Yue Y, et al. Metabonomic studies of human hepatocellular carcinoma using high-resolution magic-angle spinning 1H NMR spectroscopy in conjunction with multivariate data analysis. J Proteome Res. 2007;6(7):2605-14.
262. Megger DA, Naboulsi W, Meyer HE, Sitek B. Proteome Analyses of Hepatocellular Carcinoma. J Clin Transl Hepatol. 2014;2(1):23-30.
263. Llovet JM, Brú C, Bruix J, editors. Prognosis of hepatocellular carcinoma: the BCLC staging classification. Seminars in liver disease; 1999: © 1999 by Thieme Medical Publishers, Inc.
264. Amin MB, Greene FL, Edge SB, Compton CC, Gershenwald JE, Brookland RK, et al. The Eighth Edition AJCC Cancer Staging Manual: Continuing to build a bridge from a population-based to a more "personalized" approach to cancer staging. CA Cancer J Clin. 2017;67(2):93-9.
265. Wang Y, Liu H, Liang D, Huang Y, Zeng Y, Xing X, et al. Reveal the molecular signatures of hepatocellular carcinoma with different sizes by iTRAQ based quantitative proteomics. Journal of proteomics. 2017;150:230-41.
266. Stryeck S, Gastrager M, Degoricija V, Trbusic M, Potocnjak I, Radulovic B, et al. Serum Concentrations of Citrate, Tyrosine, 2- and 3- Hydroxybutyrate are Associated with Increased 3-Month Mortality in Acute Heart Failure Patients. Sci Rep. 2019;9(1):6743.
267. Zhang F, Kerbl-Knapp J, Akhmetshina A, Korbelius M, Kuentzel KB, Vujić N, et al. Tissue-specific landscape of metabolic dysregulation during ageing. Biomolecules. 2021;11(2):235.
268. Chong J, Soufan O, Li C, Caraus I, Li S, Bourque G, et al. MetaboAnalyst 4.0: towards more transparent and integrative metabolomics analysis. Nucleic Acids Res. 2018;46(W1):W486-W94.

269. Royston P, Altman DG. External validation of a Cox prognostic model: principles and methods. BMC Med Res Methodol. 2013;13:33.
270. Harrell FE, Jr., Lee KL, Mark DB. Multivariable prognostic models: issues in developing models, evaluating assumptions and adequacy, and measuring and reducing errors. Stat Med. 1996;15(4):361-87.
271. Steyerberg EW, Vickers AJ, Cook NR, Gerds T, Gonen M, Obuchowski N, et al. Assessing the performance of prediction models: a framework for traditional and novel measures. Epidemiology. 2010;21(1):128-38.
272. Phan LM, Yeung SC, Lee MH. Cancer metabolic reprogramming: importance, main features, and potentials for precise targeted anti-cancer therapies. Cancer Biol Med. 2014;11(1):1-19.
273. Kornberg MD, Bhargava P, Kim PM, Putluri V, Snowman AM, Putluri N, et al. Dimethyl fumarate targets GAPDH and aerobic glycolysis to modulate immunity. Science. 2018;360(6387):449-53.
274. Qian X, Li X, Lu Z. Protein kinase activity of the glycolytic enzyme PGK1 regulates autophagy to promote tumorigenesis. Autophagy. 2017;13(7):1246-7.
275. Qu J, Ko CW, Tso P, Bhargava A. Apolipoprotein A-IV: A Multifunctional Protein Involved in Protection against Atherosclerosis and Diabetes. Cells. 2019;8(4).
276. Didiasova M, Wujak L, Wygrecka M, Zakrzewicz D. From plasminogen to plasmin: role of plasminogen receptors in human cancer. Int J Mol Sci. 2014;15(11):21229-52.
277. Subramaniam S, Kelley RK, Venook AP. A review of hepatocellular carcinoma (HCC) staging systems. Chinese clinical oncology. 2013;2(4).
278. Liu PH, Su CW, Hsu CY, Hsia CY, Lee YH, Huang YH, et al. Solitary Large Hepatocellular Carcinoma: Staging and Treatment Strategy. PLoS One. 2016;11(5):e0155588.
279. Cloarec O, Dumas ME, Craig A, Barton RH, Trygg J, Hudson J, et al. Statistical total correlation spectroscopy: an exploratory approach for latent biomarker identification from metabolic 1H NMR data sets. Anal Chem. 2005;77(5):1282-9.
280. Huang Z, Hua D, Hu Y, Cheng Z, Zhou X, Xie Q, et al. Quantitation of plasma circulating DNA using quantitative PCR for the detection of hepatocellular carcinoma. Pathol Oncol Res. 2012;18(2):271-6.
281. Mezzalira S, De Mattia E, Guardascione M, Dalle Fratte C, Cecchin E, Toffoli G. Circulating-Free DNA Analysis in Hepatocellular Carcinoma: A Promising Strategy to Improve Patients' Management and Therapy Outcomes. Int J Mol Sci. 2019;20(21).
282. Gao R, Cheng J, Fan C, Shi X, Cao Y, Sun B, et al. Serum metabolomics to identify the liver disease-specific biomarkers for the progression of hepatitis to hepatocellular carcinoma. Scientific reports. 2015;5:18175.
283. Di Poto C, He S, Varghese RS, Zhao Y, Ferrarini A, Su S, et al. Identification of race-associated metabolite biomarkers for hepatocellular carcinoma in patients with liver cirrhosis and hepatitis C virus infection. PLoS One. 2018;13(3):e0192748.
284. Muir K, Hazim A, He Y, Peyressatre M, Kim D-Y, Song X, et al. Proteomic and lipidomic signatures of lipid metabolism in NASH-associated hepatocellular carcinoma. Cancer research. 2013;73(15):4722-31.
285. Anstee QM, Reeves HL, Kotsiliti E, Govaere O, Heikenwalder M. From NASH to HCC: current concepts and future challenges. Nature reviews Gastroenterology & hepatology. 2019;16(7):411-28.

286. Nakagawa H, Hayata Y, Kawamura S, Yamada T, Fujiwara N, Koike K. Lipid metabolic reprogramming in hepatocellular carcinoma. Cancers. 2018;10(11):447.
287. Younossi ZM, Koenig AB, Abdelatif D, Fazel Y, Henry L, Wymer M. Global epidemiology of nonalcoholic fatty liver disease—meta-analytic assessment of prevalence, incidence, and outcomes. Hepatology. 2016;64(1):73-84.
288. Bruix J, Sherman M, Practice Guidelines Committee AAftSoLD. Management of hepatocellular carcinoma. Hepatology. 2005;42(5):1208-36.
289. Inoue K, Takayama T, Higaki T, Watanabe Y, Makuuchi M. Clinical significance of early hepatocellular carcinoma. Liver Transpl. 2004;10(2 Suppl 1):S16-9.
290. Chan AW, Zhong J, Berhane S, Toyoda H, Cucchetti A, Shi K, et al. Development of pre and post-operative models to predict early recurrence of hepatocellular carcinoma after surgical resection. Journal of hepatology. 2018;69(6):1284-93.
291. Zhang X, Li J, Shen F, Lau WY. Significance of presence of microvascular invasion in specimens obtained after surgical treatment of hepatocellular carcinoma. J Gastroenterol Hepatol. 2018;33(2):347-54.
292. Cancer Genome Atlas Research Network. Electronic address wbe, Cancer Genome Atlas Research N. Comprehensive and Integrative Genomic Characterization of Hepatocellular Carcinoma. Cell. 2017;169(7):1327-41 e23.
293. Berretta M, Cavaliere C, Alessandrini L, Stanzione B, Facchini G, Balestreri L, et al. Serum and tissue markers in hepatocellular carcinoma and cholangiocarcinoma: clinical and prognostic implications. Oncotarget. 2017;8(8):14192-220.
294. Faubert B, Solmonson A, DeBerardinis RJ. Metabolic reprogramming and cancer progression. Science. 2020;368(6487).
295. Tzartzeva K, Obi J, Rich NE, Parikh ND, Marrero JA, Yopp A, et al. Surveillance imaging and alpha fetoprotein for early detection of hepatocellular carcinoma in patients with cirrhosis: a meta-analysis. Gastroenterology. 2018;154(6):1706-18. e1.
296. Van Deursen JM. The role of senescent cells in ageing. Nature. 2014;509(7501):439-46.
297. Liu J, Wang L, Wang Z, Liu J-P. Roles of telomere biology in cell senescence, replicative and chronological ageing. Cells. 2019;8(1):54.
298. Chapman J, Fielder E, Passos JF. Mitochondrial dysfunction and cell senescence: deciphering a complex relationship. FEBS letters. 2019;593(13):1566-79.
299. Childs BG, Baker DJ, Kirkland JL, Campisi J, Van Deursen JM. Senescence and apoptosis: dueling or complementary cell fates? EMBO reports. 2014;15(11):1139-53.
300. Farr JN, Xu M, Weivoda MM, Monroe DG, Fraser DG, Onken JL, et al. Targeting cellular senescence prevents age-related bone loss in mice. Nature medicine. 2017;23(9):1072-9.
301. Roos CM, Zhang B, Palmer AK, Ogrodnik MB, Pirtskhalava T, Thalji NM, et al. Chronic senolytic treatment alleviates established vasomotor dysfunction in aged or atherosclerotic mice. Aging cell. 2016;15(5):973-7.
302. Catic A. Cellular metabolism and aging. Progress in molecular biology and translational science. 155: Elsevier; 2018. p. 85-107.
303. Zhang L. Progress in Molecular Biology and Translational Science: Academic Press; 2008.
304. Wilkinson DJ, Rodriguez-Blanco G, Dunn WB, Phillips BE, Williams JP, Greenhaff PL, et al. Untargeted metabolomics for uncovering biological markers of human skeletal muscle ageing. Aging (Albany NY). 2020;12(13):12517.

305. Kuehne A, Hildebrand J, Soehle J, Wenck H, Terstegen L, Gallinat S, et al. An integrative metabolomics and transcriptomics study to identify metabolic alterations in aged skin of humans in vivo. BMC genomics. 2017;18(1):169.
306. Ivanisevic J, Stauch KL, Petrascheck M, Benton HP, Epstein AA, Fang M, et al. Metabolic drift in the aging brain. Aging (Albany NY). 2016;8(5):1000.
307. Bandeen-Roche K, Xue Q-L, Ferrucci L, Walston J, Guralnik JM, Chaves P, et al. Phenotype of frailty: characterization in the women's health and aging studies. The Journals of Gerontology Series A: Biological Sciences and Medical Sciences. 2006;61(3):262-6.
308. Yuan R, Peters LL, Paigen B. Mice as a mammalian model for research on the genetics of aging. ILAR journal. 2011;52(1):4-15.
309. Loria JP, Rance M, Palmer AG. A relaxation-compensated Carr− Purcell− Meiboom− Gill sequence for characterizing chemical exchange by NMR spectroscopy. Journal of the American Chemical Society. 1999;121(10):2331-2.
310. Raja G, Jung Y, Jung SH, Kim T-J. 1H-NMR-based metabolomics for cancer targeting and metabolic engineering–A review. Process Biochemistry. 2020.
311. Bingol K. Recent advances in targeted and untargeted metabolomics by NMR and MS/NMR methods. High-throughput. 2018;7(2):9.
312. Park DC, Reuter-Lorenz P. The adaptive brain: aging and neurocognitive scaffolding. Annual review of psychology. 2009;60:173-96.
313. Yin F, Boveris A, Cadenas E. Mitochondrial energy metabolism and redox signaling in brain aging and neurodegeneration. Antioxidants & redox signaling. 2014;20(2):353-71.
314. Lesnefsky EJ, Chen Q, Hoppel CL. Mitochondrial metabolism in aging heart. Circulation research. 2016;118(10):1593-611.
315. Epstein M, editor Effects of aging on the kidney. Federation proceedings; 1979.
316. Sato Y, Yanagita M. Immunology of the ageing kidney. Nature Reviews Nephrology. 2019;15(10):625-40.
317. Gong Z, Tas E, Yakar S, Muzumdar R. Hepatic lipid metabolism and non-alcoholic fatty liver disease in aging. Molecular and cellular endocrinology. 2017;455:115-30.
318. Brandenberger C, Mühlfeld C. Mechanisms of lung aging. Cell and tissue research. 2017;367(3):469-80.
319. Turner VM, Mabbott NA. Influence of ageing on the microarchitecture of the spleen and lymph nodes. Biogerontology. 2017;18(5):723-38.
320. Larsson SC, Markus HS. Branched-chain amino acids and Alzheimer's disease: a Mendelian randomization analysis. Scientific reports. 2017;7(1):1-4.
321. Segovia G, Porras A, Del Arco A, Mora F. Glutamatergic neurotransmission in aging: a critical perspective. Mechanisms of ageing and development. 2001;122(1):1-29.
322. Kaiser LG, Schuff N, Cashdollar N, Weiner MW. Age-related glutamate and glutamine concentration changes in normal human brain: 1H MR spectroscopy study at 4 T. Neurobiology of aging. 2005;26(5):665-72.
323. Hashimoto M, Fukamizu A, Nakagawa T, Kizuka Y. Roles of protein arginine methyltransferase 1 (PRMT1) in brain development and disease. Biochimica et Biophysica Acta (BBA)-General Subjects. 2020:129776.
324. Huang Y, Zhou M, Sun H, Wang Y. Branched-chain amino acid metabolism in heart disease: an epiphenomenon or a real culprit? Cardiovascular research. 2011;90(2):220-3.

325. Nicklin P, Bergman P, Zhang B, Triantafellow E, Wang H, Nyfeler B, et al. Bidirectional transport of amino acids regulates mTOR and autophagy. Cell. 2009;136(3):521-34.
326. Uddin GM, Zhang L, Shah S, Fukushima A, Wagg CS, Gopal K, et al. Impaired branched chain amino acid oxidation contributes to cardiac insulin resistance in heart failure. Cardiovascular diabetology. 2019;18(1):86.
327. Tobias DK, Lawler PR, Harada PH, Demler OV, Ridker PM, Manson JE, et al. Circulating branched-chain amino acids and incident cardiovascular disease in a prospective cohort of US women. Circulation: Genomic and Precision Medicine. 2018;11(4):e002157.
328. DeFeudis F. γ-Aminobutyric acid and cardiovascular function. Experientia. 1983;39(8):845-9.
329. Pauwels L, Maes C, Swinnen SP. Aging, inhibition and GABA. Aging (Albany NY). 2018;10(12):3645.
330. Patterson JM, Keevil N, McHenry E. Choline and the prevention of hemorrhagic kidneys in the rat. 2. Phospholipid turnover determined with radioactive phosphorus. Journal of Biological Chemistry. 1944;153:489-93.
331. Ossani G, Dalghi M, Repetto M. Oxidative damage lipid peroxidation in the kidney of choline-deficient rats. Front Biosci. 2007;12:1174-83.
332. Zhang H, Zhang G, Gonzalez FJ, Park S-m, Cai D. Hypoxia-inducible factor directs POMC gene to mediate hypothalamic glucose sensing and energy balance regulation. PLoS Biol. 2011;9(7):e1001112.
333. Pan C, Locasale JW. Targeting metabolism to influence aging. Science. 2021;371(6526):234-5.
334. Johmura Y, Yamanaka T, Omori S, Wang T-W, Sugiura Y, Matsumoto M, et al. Senolysis by glutaminolysis inhibition ameliorates various age-associated disorders. Science. 2021;371(6526):265-70.
335. Kannan L, Knudsen J, Jolly CA. Aging and acyl-CoA binding protein alter mitochondrial glycerol-3-phosphate acyltransferase activity. Biochimica et Biophysica Acta (BBA)-Molecular and Cell Biology of Lipids. 2003;1631(1):12-6.
336. Sastre J, Pallardo FV, Plá R, Pellín A, Juan G, O'Connor JE, et al. Aging of the liver: age-associated mitochondrial damage in intact hepatocytes. Hepatology. 1996;24(5):1199-205.
337. Chen C-F, Wang D, Hwang CP, Liu HW, Wei J, Lee RP, et al. The protective effect of niacinamide on ischemia-reperfusion-induced liver injury. Journal of biomedical science. 2001;8(6):446-52.
338. Mármol F, Sánchez J, López D, Martínez N, Xaus C, Peralta C, et al. Role of oxidative stress and adenosine nucleotides in the liver of aging rats. Physiological research. 2010;59(4).
339. Woods JA, Wilund KR, Martin SA, Kistler BM. Exercise, inflammation and aging. Aging and disease. 2012;3(1):130.
340. Lu G, Ren S, Korge P, Choi J, Dong Y, Weiss J, et al. A novel mitochondrial matrix serine/threonine protein phosphatase regulates the mitochondria permeability transition pore and is essential for cellular survival and development. Genes & development. 2007;21(7):784-96.
341. Cornu M, Albert V, Hall MN. mTOR in aging, metabolism, and cancer. Current opinion in genetics & development. 2013;23(1):53-62.
342. Nishio S-I, Negoro S, Hosokawa T, Hara H, Tanaka T, Deguchi Y, et al. The effect of taurine on age-related immune decline in mice: the effect of taurine on T cell and B cell

proliferative response under costimulation with ionomycin and phorbol myristate acetate. Mechanisms of ageing and development. 1990;52(2-3):125-39.
343. Bircan FS, Balabanli B, Turkozkan N, Ozan G. Effects of taurine on nitric oxide and 3-nitrotyrosine levels in spleen during endotoxemia. Neurochemical research. 2011;36(11):1978-83.
344. Hunsberger HC, Greenwood BP, Tolstikov V, Narain NR, Kiebish MA, Denny CA. Divergence in the metabolome between natural aging and Alzheimer's disease. Scientific reports. 2020;10(1):1-15.
345. Delfarah A, Parrish S, Yang J, Seo F, Li S, Wang P, et al. Inhibition of nucleotide synthesis mediates replicative senescence of human mammary epithelial cells. bioRxiv. 2018:423665.
346. Xia X, Chen W, McDermott J, Han J-DJ. Molecular and phenotypic biomarkers of aging. F1000Research. 2017;6.
347. Zhu Y, Tchkonia T, Pirtskhalava T, Gower AC, Ding H, Giorgadze N, et al. The Achilles' heel of senescent cells: from transcriptome to senolytic drugs. Aging cell. 2015;14(4):644-58.
348. Baar MP, Brandt RM, Putavet DA, Klein JD, Derks KW, Bourgeois BR, et al. Targeted apoptosis of senescent cells restores tissue homeostasis in response to chemotoxicity and aging. Cell. 2017;169(1):132-47. e16.
349. Chang J, Wang Y, Shao L, Laberge R-M, Demaria M, Campisi J, et al. Clearance of senescent cells by ABT263 rejuvenates aged hematopoietic stem cells in mice. Nature medicine. 2016;22(1):78-83.
350. Fuhrmann-Stroissnigg H, Ling YY, Zhao J, McGowan SJ, Zhu Y, Brooks RW, et al. Identification of HSP90 inhibitors as a novel class of senolytics. Nature Communications. 2017;8(1):1-14.
351. LeBrasseur NK, Tchkonia T, Kirkland JL. Cellular senescence and the biology of aging, disease, and frailty. Frailty: Pathophysiology, Phenotype and Patient Care. 83: Karger Publishers; 2015. p. 11-8.
352. Ruckenstuhl C, Netzberger C, Entfellner I, Carmona-Gutierrez D, Kickenweiz T, Stekovic S, et al. Lifespan extension by methionine restriction requires autophagy-dependent vacuolar acidification. PLoS Genet. 2014;10(5):e1004347.
353. Harrison DE, Strong R, Sharp ZD, Nelson JF, Astle CM, Flurkey K, et al. Rapamycin fed late in life extends lifespan in genetically heterogeneous mice. nature. 2009;460(7253):392-5.
354. Hensley CT, Wasti AT, DeBerardinis RJ. Glutamine and cancer: cell biology, physiology, and clinical opportunities. The Journal of clinical investigation. 2013;123(9):3678-84.
355. Antwi SO, Petrick JL, Campbell PT, Norez DA, Stevens VL, Liao LM, et al. One-carbon metabolism-related micronutrients intake and risk for hepatocellular carcinoma: a prospective cohort study. International journal of cancer. 2020;147(8):2075-90.
356. Ward PS, Thompson CB. Metabolic reprogramming: a cancer hallmark even warburg did not anticipate. Cancer cell. 2012;21(3):297-308.
357. Long J, Lang Z-W, Wang H-G, Wang T-L, Wang B-E, Liu S-Q. Glutamine synthetase as an early marker for hepatocellular carcinoma based on proteomic analysis of resected small hepatocellular carcinomas. Hepatobiliary Pancreat Dis Int. 2010;9(3):296-305.
358. DeBerardinis RJ, Lum JJ, Hatzivassiliou G, Thompson CB. The biology of cancer: metabolic reprogramming fuels cell growth and proliferation. Cell metabolism. 2008;7(1):11-20.
359. Qin Y, Hu Q, Xu J, Ji S, Dai W, Liu W, et al. PRMT5 enhances tumorigenicity and glycolysis in pancreatic cancer via the FBW7/cMyc axis. Cell Communication and Signaling. 2019;17(1):1-15.

360. Han H-S, Jung C-Y, Yoon Y-S, Choi S, Choi D, Kang G, et al. Arginine methylation of CRTC2 is critical in the transcriptional control of hepatic glucose metabolism. Science signaling. 2014;7(314):ra19-ra.
361. Choi D, Oh KJ, Han HS, Yoon YS, Jung CY, Kim ST, et al. Protein arginine methyltransferase 1 regulates hepatic glucose production in a FoxO1-dependent manner. Hepatology. 2012;56(4):1546-56.
362. Yang L, Venneti S, Nagrath D. Glutaminolysis: a hallmark of cancer metabolism. Annual review of biomedical engineering. 2017;19:163-94.
363. Jeyapalan JC, Ferreira M, Sedivy JM, Herbig U. Accumulation of senescent cells in mitotic tissue of aging primates. Mechanisms of ageing and development. 2007;128(1):36-44.
364. Messineo L, Denko CW, Petricevic M. Age-related changes in total DNA and RNA and incorporation of uridine and thymidine in rat liver, kidney and spleen. The International journal of biochemistry. 1983;15(9):1103.
365. Boisvert F-M, Déry U, Masson J-Y, Richard S. Arginine methylation of MRE11 by PRMT1 is required for DNA damage checkpoint control. Genes & development. 2005;19(6):671-6.
366. Gao Y, Zhao Y, Zhang J, Lu Y, Liu X, Geng P, et al. The dual function of PRMT1 in modulating epithelial-mesenchymal transition and cellular senescence in breast cancer cells through regulation of ZEB1. Scientific reports. 2016;6(1):1-13.

8 Appendix

Licenses for adapting figures and tables

1. Thandapani P, O'Connor TR, Bailey TL, Richard S. Defining the RGG/RG motif. Molecular cell. 2013;50(5):613-23. (Figure 1 on page 19)

License Number	5075291254663
License date	May 24, 2021
Licensed Content Publisher	Elsevier
Licensed Content Publication	Molecular Cell
Licensed Content Title	Defining the RGG/RG Motif
Licensed Content Author	Palaniraja Thandapani,Timothy R. O'Conı Bailey,Stéphane Richard
Licensed Content Date	Jun 6, 2013
Licensed Content Volume	50
Licensed Content Issue	5
Licensed Content Pages	11
Start Page	613
End Page	623
Type of Use	reuse in a thesis/dissertation
Portion	figures/tables/illustrations

37. Jarrold J, Davies CC. PRMTs and arginine methylation: cancer's best-kept secret? Trends in molecular medicine. 2019;25(11):993-1009. (Table 1 on page 23)

License Number	5075300392435
License date	May 24, 2021
Licensed Content Publisher	Elsevier
Licensed Content Publication	Trends in Molecular Medicine
Licensed Content Title	PRMTs and Arginine Methylation: Cancer's Best-Kept Secret?
Licensed Content Author	James Jarrold,Clare C. Davies
Licensed Content Date	Nov 1, 2019
Licensed Content Volume	25
Licensed Content Issue	11
Licensed Content Pages	17
Start Page	993
End Page	1009
Type of Use	reuse in a thesis/dissertation
Portion	figures/tables/illustrations